LIÈGE université
Gembloux
Agro-Bio Tech

REMOTE SENSING APPLICATIONS FOR THE CHARACTERIZATION AND MANAGEMENT OF RIPARIAN VEGETATION IN SOUTHERN BELGIUM

Leo Huylenbroeck

COMMUNAUTÉ FRANÇAISE DE BELGIQUE
UNIVERITÉ DE LIÈGE – GEMBLOUX AGRO-BIO-TECH

REMOTE SENSING APPLICATIONS FOR THE CHARACTERIZATION AND MANAGEMENT OF RIPARIAN VEGETATION IN SOUTHERN BELGIUM

Leo Huylenbroeck

Dissertation originale présentée en vue de l'obtention du grade de docteur en sciences agronomiques et ingénierie biologique

Promoteur : Pr. Philippe Lejeune
Co-promoteur : Dr. Adrien Michez
Année civile : 2024

Copyright

Auteur : Leo Huylenbroeck

Dépôt de la thèse : Décembre 2023

Crédits photographiques: Les photos sont de l'auteur, sauf mention explicite dans leur légende.

Citation: Huylenbroeck Leo, 2024. Remote sensing applications for the characterization and management of riparian vegetation in southern Belgium. Thèse de doctorat, Gembloux Agro-Bio Tech – Université de Liège, Gembloux, 233 p.

Résumé

La végétation qui se développe dans les zones riveraines des cours d'eau a une influence importante sur de nombreux processus au sein de l'hydrosystème. Dès lors, elle est souvent au cœur des pratiques de gestion visant à influencer le fonctionnement écologique et hydraulique de la rivière. La mise en place d'actions de gestion cohérentes, intégrant les différents enjeux et acteurs liés à la rivière, nécessite un diagnostic et une planification adéquate à l'échelle du bassin versant. La télédétection peut être utilisée pour obtenir de données à jour sur l'état de la végétation riveraine sur des surfaces importantes et à moindre coût. Cette thèse a pour objectifs de développer des outils de cartographie de la végétation riveraine et d'évaluer leur intérêt pour la gestion de cette dernière.

Premièrement, une revue de bibliographie a été réalisée pour obtenir une vue d'ensemble de l'utilisation de la télédétection pour l'étude de la végétation riveraine. Les résultats mettent en évidence une relation étroite entre les outils utilisés, les caractéristiques de la végétation riveraine étudiées et l'étendue cartographiée. Les données à haute résolution sont rarement utilisées pour les rivières sur plus de 100 km ou pour la cartographie de la composition en espèces. Une partie importante des études réalisées s'intéressent à la dynamique des écosystèmes riverains, et les images aériennes et satellitaires sont appréciées en raison de la disponibilité de séries temporelles. Nous avons identifié les opportunités qui peuvent être saisies avec la disponibilité accrue de données à haute résolution dans des régions peu étudiées, pour de grandes étendues et sous forme de séries temporelles. Certaines approches ont atteint un niveau opérationnel et sont désormais utilisées à des fins de gestion. Pour transférer les approches de télédétection aux gestionnaires des zones riveraines, nous suggérons de mutualiser les réalisations en produisant des outils robustes et open source, qui pourront être adaptées à chaque projet spécifique.

Deuxièmement, nous nous sommes intéressés à la cartographie de la biomasse aérienne des forêts riveraines, dont dépendent plusieurs fonctions clés des systèmes riverains. Concrètement, des données LiDAR ont été utilisées dans une approche à l'échelle de l'arbre pour cartographier la biomasse aérienne dans les forêts riveraines le long de 200 km de rivières et dans leur plaine alluviale associée, sur les bassins versants de la Semois et de la Chiers. Deux approches ont été testées, s'appuyant sur un modèle numérique de hauteur LiDAR seul ou en conjonction avec un nuage de points LiDAR. Les erreurs quadratiques moyennes relatives de la biomasse pour des parcelles de 0,3 ha étaient respectivement de 27 % et 22 % pour les deux approches. La cartographie a été utilisée pour mettre en lumière les facteurs environnementaux structurant cette biomasse riveraine à l'échelle du bassin versant étudié. Le régime de perturbations, surtout anthropiques, y explique en grande partie la distribution spatiale de la biomasse.

Troisièmement, nous avons exploité un jeu de données LiDAR à haute densité de points pour cartographier la composition en espèces des forêts riveraines sur 155 km de la Semois et sur sa plaine alluviale. Nous avons utilisé une approche à l'échelle

de l'arbre, un algorithme Random Forest et des variables issues du nuage de points et d'images multispectrales. Les arbres ont été classés selon quatre groupes aux caractéristiques écologiques similaires (saules, aulnes, autres feuillus et résineux) avec une précision globale de l'ordre de 80%. Nous avons ensuite évalué la précision de la classification lors de l'agrégation de l'information obtenue à l'échelle de l'arbre sur des unités de plus grande taille. La précision obtenue sur des unités de 900 m² est de 85 % pour la présence d'une espèce et de 89 % sur l'espèce dominante. Cette précision est encore améliorée pour des unités de plus grande dimension et est suffisante pour de nombreuses applications. Comme pour la biomasse, la distribution des espèces dans l'espace a été analysée par rapport à des facteurs tels que l'occupation du sol, la proximité à la rivière ou l'engorgement en eau du sol. La cartographie de la distribution spatiale de la composition spécifique confirme les patrons pressentis : les saules occupent les zones ouvertes et humides dans la plaine alluviale, les aulnes sont particulièrement présents dans les zones humides et à proximité des berges, et les feuillus à bois dur occupant les parties plus hautes de la zone riveraine.

Quatrièmement, nous avons évalué le potentiel de données 3D pour décrire la morphologie des berges et leur évolution. En effet, ces caractéristiques ont un intérêt direct pour la gestion de la végétation présente sur les berges des cours d'eau. Nous avons d'abord comparé les performances et les limites des approches de description de la géométrie du lit mineur basées d'une part sur la photogrammétrie d'images acquises à l'aide de drones et d'autre part sur des données LiDAR aériennes. Bien que la photogrammétrie permette une meilleure description des parties immergées de la rivière, le LiDAR offre des performances convenables dans les parties émergées et un potentiel de montée en échelle plus important. Ensuite, une méthodologie simple de cartographie de la mobilité latérale des berges à l'aide de MNT LiDAR multi-temporels a été développée. Cette dernière montre des résultats cohérents avec ceux obtenus par photointerprétation d'images aériennes.

Enfin, les approches de cartographie de la biomasse, de la composition spécifique et de l'érosion latérale ont été déployées sur un bassin versant comprenant 50 km de cours d'eau, en vue d'illustrer comment ces informations peuvent être croisées pour planifier et prioriser les interventions sur la végétation dans le lit mineur. L'accessibilité des méthodes de télédétection au plus grand nombre est discutée à l'aune des volumes de données à traiter et de la technicité des approches développées. Le manuscrit discute également de l'agrégation d'informations issues d'approches « à l'échelle de l'arbre » et de la montée en échelle. Enfin, des perspectives de recherche sont proposées pour améliorer l'interprétation des trajectoires de la végétation riveraine, la modélisation de processus et le suivi et l'évaluation de la végétation riveraine.

Summary

The vegetation that develops in the riparian zone has an important influence on many processes within the hydrosystem. As a result, it is often at the heart of management practices designed to influence the river's ecological and hydraulic functioning. The implementation of coherent management actions, integrating the various river-related issues and stakeholders, requires diagnosis and appropriate planning at basin scale. Remote sensing can be used to obtain up-to-date data on the state of riparian vegetation over large areas at low cost. The aim of this thesis is to develop tools for mapping riparian vegetation and to assess their value for riparian management.

Firstly, a literature review was carried out to obtain an overview of the use of remote sensing for the study of riparian vegetation. The results show a close relationship between the tools used, the riparian vegetation characteristics studied and the extent mapped. High-resolution data are rarely used for rivers over 100 km in length, or for mapping species composition. A significant proportion of the studies carried out relate to the dynamics of riparian ecosystems, and aerial and satellite images are valued for their availability as time series. We identified opportunities to seize with the increased availability of high-resolution data in little-studied regions, for large areas and as time series. Some approaches have reached an operational level and are now being used for management purposes. To transfer remote sensing approaches to riparian managers, we suggest mutualizing achievements by producing robust, open-source tools that can be adapted to each specific project.

Secondly, we focused on mapping the above-ground biomass of riparian forests, on which several key functions of riparian systems depend. Specifically, LiDAR data were used in a tree-centric approach to map above-ground biomass in riparian forests along 200 km of rivers and their associated floodplains, in the Semois and Chiers watersheds. Two approaches were tested, based on a LiDAR digital height model alone or in conjunction with a LiDAR point cloud. Relative root-mean-square biomass errors for 0.3 ha plots were 27% and 22% respectively for the two approaches. The map was used to highlight the environmental factors structuring riparian biomass at the scale of the watershed studied. The disturbance regime, mainly anthropogenic, largely explains the spatial distribution of biomass.

Thirdly, we used a high-density LiDAR dataset to map the species composition of riparian forests along 155 km of the Semois river and its floodplain. We used a tree-centric approach, a Random Forest algorithm and variables derived from the point cloud. Trees were classified into four groups with similar ecological characteristics (willows, alders, other hardwoods and conifers) with an overall accuracy of around 80%. We then assessed the accuracy of the classification when aggregating the information obtained at tree level onto larger units. The accuracy obtained on 900 m² units is 85% for the presence of a species and 89% for the dominant species. This accuracy is further improved for larger units and is sufficient for many applications.

As with biomass, the spatial distribution of species was analyzed in relation to factors such as land use, proximity to the river and soil moisture. Tree species spatial distribution confirms the expected patterns: willows occupy open, wet areas in the floodplain, alders are particularly present in wet areas and near riverbanks, and other hardwoods occupy the higher parts of the riparian zone.

Fourthly, we assessed the potential of 3D data to describe riverbank morphology and evolution. Indeed, these characteristics are of direct interest for the management of riparian vegetation. We began by comparing the performance and limitations of approaches for describing minor bed geometry based on aerial photogrammetry and on aerial LiDAR data. While photogrammetry provides a better description of the submerged parts of the river, LiDAR offers decent performance in the emergent parts and greater upscaling potential. We then developed a simple methodology for mapping bank lateral mobility using multi-temporal LiDAR DTMs. The results obtained are consistent with those obtained using photointerpretation of aerial images.

Finally, approaches for mapping biomass, specific composition and lateral erosion were deployed on a catchment comprising 50 km of watercourse. We assessed how this information can be used to plan and prioritize interventions on vegetation in the minor bed. The availability of remote sensing methods to non-specialists is discussed regarding the volumes of data to be processed and the technicity of the approaches developed. The manuscript also discusses the aggregation of information from "tree-scale" approaches, and upscaling to watersheds. Finally, research perspectives are proposed to improve the interpretation of riparian vegetation trajectories, process modeling and the monitoring and assessment of riparian vegetation.

Remerciements

Si une thèse représente un volume de travail important pour le doctorant, il faut souligner l'ampleur des contributions extérieures nécessaires à l'accomplissement de chacune de ses étapes. J'ai eu le privilège de collaborer avec de nombreuses personnes à la fois bienveillantes et soucieuses de réaliser un travail de qualité, à qui j'essaierai de rendre justice dans cette section.

Mes premiers remerciements vont à mes co-promoteurs Adrien Michez et Philippe Lejeune. Philippe, merci pour ta fiabilité, ton soutien et d'avoir toujours trouvé des solutions pour que je puisse travailler sereinement. Ton énergie est décoiffante. Adrien, merci de m'avoir transmis cette fascination pour les rivières qui ne me quitte plus. Plus prosaïquement, les développements de cette thèse s'inscrivent principalement dans la continuité de tes travaux. J'aurais pu replacer ton nom dans la majorité des paragraphes de remerciements qui suivent mais tu es déjà cité près de trente fois au sein de ce manuscrit. Une preuve d'amour suffisante?

Merci aux membres de mon comité de thèse pour votre confiance régulièrement renouvelée. Un merci tout particulier à Simon Dufour pour la qualité de ton écoute et la hauteur de tes analyses. Merci à Hugues Claessens pour ton investissement et ta bienvieillance dès le début de mon parcours. Merci à Aurore Degré pour ta perspicacité et pour avoir accepté la présidence du jury. Merci à Jérôme Lejot et Jean-François Bastin pour votre participation au jury et votre relecture attentive qui a permis d'améliorer le manuscrit après la défense privée. Je remercie également les cinq reviewers anonymes qui ont aidé à améliorer les deux chapitres publiés de cette thèse.

Les travaux de recherche menés dans le cadre de cette thèse ont été notamment rendus possibles par la participation des Provinces de Luxembourg et de Liège. Je suis reconnaissant à Bruno Khuat Duy et Pierre Clément pour votre bienveillance et pour avoir ancré ce travail dans le réel. Merci également au personnel des deux Provinces pour votre intérêt et votre application lors des journées de formation aux SIG et à l'acquisition d'images drones.

Je remercie l'ensemble des co-auteurs des deux articles publiés de cette thèse. Je pense tout particulièrement à Marianne Laslier avec qui j'ai co-écrit la revue de bibliographie proposée en chapitre 2. La rédaction d'une review n'est pas l'aspect le plus rock & roll de la recherche mais c'était un plaisir de le faire avec toi, et elle n'aurait pas abouti sans ta persévérance. Un second merci à Simon Dufour et aux porteurs du COST CONVERGES, vous avez rendu possible de telles collaborations et m'avez aidé à inscrire mes travaux dans ceux d'une communauté de chercheurs.

Merci à Michael Ronse de m'avoir accordé ta confiance pour la co-promotion de ton TFE. Ta persévérance et ta rigueur dans le traitement de données LiDAR pour la classification d'espèces a considérablement accéléré la réalisation du chapitre 4 de cette thèse.

Je n'oublie pas que mon parcours dans les rivières a commencé avec un mémoire passionant, réalisé en 2017 sous la promotion d'Adrien et d'Hugues Claessens et

largement retravaillé dans le chapitre 3 de cette thèse. Les tarifs de cubage pour le saule et l'aulne présentés dans ce chapitre ont été calibrés sur un chantier de la Direction des cours d'eau non navigables, avec l'appui de Pierre Otte et de Virginie Cuvelier. Je remercie au passage Coralie Mengal et les nombreux amis qui se sont succédé pour m'aider à mesurer ces nombreux arbres.

Merci au SPW qui acquiert et met à disposition de nombreuses données de télédétection, notamment des levés LiDAR dont j'ai fait un usage important. Merci à la Direction des Cours d'eau non navigables et en particulier à Didier Deglin et Jean-Charles Horlait pour la mise à disposition du jeu de données LiDAR à haute densité utilisé dans le chapitre 4.

Je suis reconnaissant à tous mes collègues, camarades, amis de l'unité. Vous avez été le sel des quatre premières années de cette thèse et avez créé un environnement stimulant et plus qu'agréable au quotidien. Chloé, je me demande ce qui t'a donné l'idée de me rejoindre en premier lieu dans ce si petit bureau. Et par quelle magie nous avons pu nous y sentir « chez nous » pendant deux hivers polaires ? Blandine, nous avons fait des thèses parallèles et je tiens la tienne pour référence. Je suis sûr que ta spontanéité et ta capacité à faire paraître simple des choses qui ne le sont pas en inspireront encore bien d'autres que moi. Romain, merci pour ta convivialité et tes inépuisables passions. Nicolas, je te remercie particulièrement pour tes conseils pour la rédaction du chapitre 3, ton aide dans le traitement des données de télédétection et la production des images multispectrales utilisées dans le chapitre 4. Merci Corentin de m'avoir fait bénéficier de ton expérience dans le traitement de données de télédétection (Chapitre 4), et Sébastien et Gauthier, pour vos conseils, données et codes concernant la compilation des équations allométriques du chapitre 3. Merci à Sam pour la gestion de l'infrastructure informatique, essentielle notamment pour le traitement de gros volumes de données. Alain, Cédric, Allan, Thibaut: merci pour votre contribution dans la bonne humeur à l'acquisition des données de terrain ou aux acquisitions d'images drones (Chapitre 4 et 5). Marie, Marie-Ange, merci pour votre souci de chacun et, Marie, pour ta disponibilité et ta rigueur dans le suivi administratif de mes projets. Je remercie enfin tous mes camarades de fêtes, de pauses cafés, de temps de midi qui me laisseront un tendre souvenir de ces années passées dans l'unité et à la Faculté.

Enfin, je remercie ma famille et mes amis de m'avoir encouragé à terminer ce projet. Emilie, je te suis reconnaissant de ton soutien de chaque jour et de m'avoir laissé consacrer le temps nécessaire à la finalisation de cette thèse. Je ne l'oublie pas !

Table of Contents

List of figures

List of tables

List of abbreviations and acronyms

- AGB: Aboveground Biomass
- AGL: Above Ground Level
- CHM: Canopy Height Model
- DBH: Diameter at Breast Height
- DHM: Digital Height Model
- DLC: Delineation Land Cover
- DSM: Digital Surface Model
- DTM: Digital Terrain Model
- FP: Floodplain
- GIS: Geographical Information system
- GNSS: Global Navigation Satellite System
- HD (to river): Horizontal Distance (to river)
- LC: Land Cover
- LiDAR: Light Detection And Ranging
- LWD: Large Woody Debris
- MAE: Mean Absolute Error
- MLS: Multiple Linear Regression
- MPS: Mean Producer Score
- MS: Mean Score
- MUS: Mean User Score
- NErA: Normalized Eroded Area
- NErV: Normalized Eroded Volume
- NIR: Near Infra-Red
- PARIS: Programmes d'Actions sur les Rivières par une Approche Intégrée et Sectorisée
- MSHS: Multispectral/Hyperspectral
- RADAR: Radio Detection And Ranging
- RGB: Red-Green-Blue
- GS: Grey Scale
- RMSE: Root Mean Square Error
- RMSEr: Relative Root Mean Square Error
- Sathi: Satellite image with high resolution
- Satlow: Satellite image with low resolution
- SFM-MVS: Structure From Motion – Multi-View Stereo
- UAV: Unmanned aerial vehicle
- VD (to river): Vertical Distance (to river)
- VEF: Volume Expansion Factor
- VU: Vegetation Unit
- WFD: Water Framework Directive

1

General introduction

1.1 Riparian vegetation: definitions, stakes and management

1.1.1 Riparian zones definition and ecology

The concept of a river hydrosystem is used to describe the river as an eco-complex, made up of interacting ecosystems or compartments. These compartments are subject to flows of matter and energy that are longitudinal (such as the flow of water from upstream to downstream), lateral (such as runoff from slopes and overflow into the floodplain) and vertical (such as exchanges with the aquifer). These flows are variable over time, and their main vector is water. The river hydrosystem is a dynamic system, whose structure reflects processes operating on multiple time scales (Petts and Amoros, 1996).

A distinction is generally made between the riverbed, occupied by the river for a flow rate lower than its mean flow rate, and the floodplain, occupied by the river during floods (Bren, 1993). Valley sides have a major influence on the hydrosystem, for example through sediment supply (Benda *et al.*, 2005). Numerous fluvial forms in the riverbed and floodplain such as oxbows, meanders and islands bear witness to past and present river activity (Figure 1).

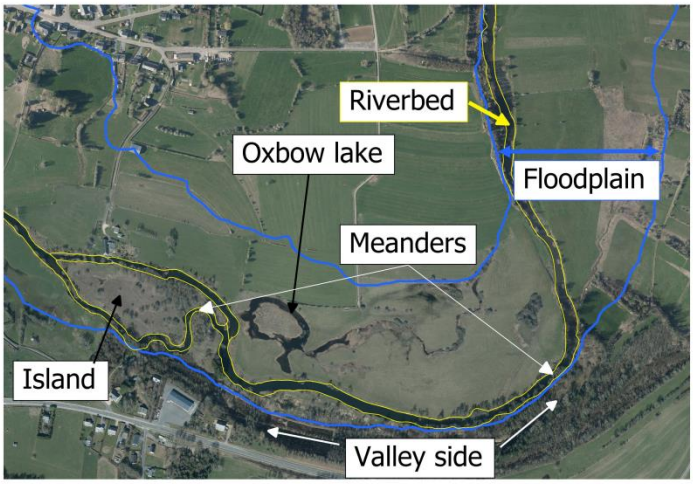

Figure 1: Constitutive elements of a riparian landscape

Original plant communities develop within the hydrosystem under the influence of the processes taking place there. These communities are structured by gradients and processes linked to water flows, such as the frequency, depth or duration of submersion (Beumer *et al.*, 2008; Deiller *et al.*, 2001), sedimentary processes (Hortobágyi *et al.*, 2018), propagule transfer (Nilsson *et al.*, 2010) or proximity to the aquifer (Bendix, 1999). The dynamic nature of riparian environments translates into significant spatial complexity, itself associated with high biodiversity (Naiman *et al.*, 1993).

Conversely, vegetation influences many processes within the hydrosystem. As illustrated in Figure 2, vegetation can control sediment processes through the rapid fixation of sediment bars or bank stabilization (Corenblit *et al.*, 2009). Vegetation roughness modifies flow velocities in the channel and floodplain (Curran and Hession, 2013). The production of dead wood associated with vegetation development also has significant geomorphological consequences, with a slowing of flows, an increase in the frequency of overflows leading to more intense sedimentation in the floodplain, and a complexification of fluvial forms following local disturbances to flow velocity (Wohl, 2017). Vegetation has an important influence on stream temperature (Wondzell *et al.*, 2019) or evapotranspiration phenomena in arid systems (Dahm *et al.*, 2002), the complexity of aquatic habitats (Thévenet *et al.*, 2003), trophic chains (Lobón-Cerviá *et al.*, 2016), physico-chemical water quality (Dosskey *et al.*, 2010) and carbon storage in hydrosystems (Sutfin *et al.*, 2016).

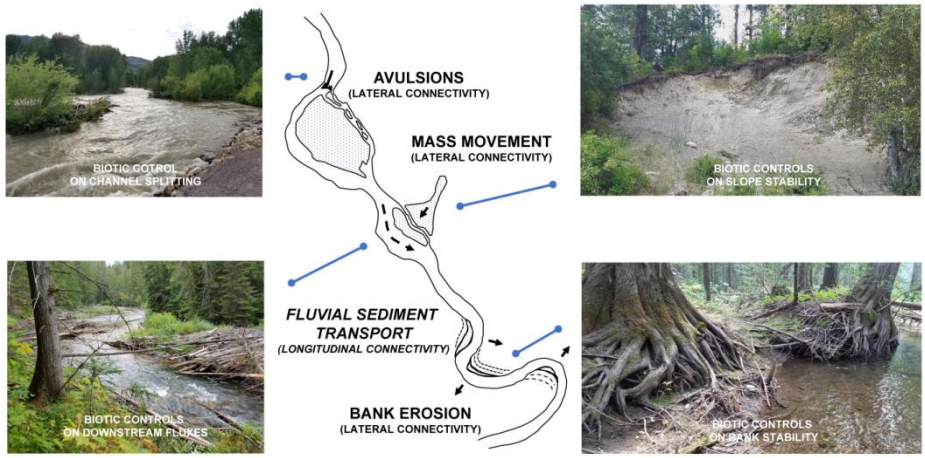

Figure 2: Riparian vegetation can control sediment processes by promoting the creation of new channels, stabilizing slopes and banks, or slowing water velocity and sediment transfer downstream. This figure was reproduced from Cienciala (2021).

Riparian vegetation can be broadly defined as any vegetation growing in the zone of influence of a watercourse, or having an influence on the watercourse. Since the many processes associated with riparian vegetation take place at different spatial scales or are expressed differently depending on the geographical context, its delimitation will often depend on the process or region being studied (Dufour *et al.*, 2019). For example, with regard to processes, direct shading by vegetation generally concerns a narrow band around the watercourse, whereas processes relating to exchanges with the water table are preferentially studied at floodplain scale. In terms of geographical context, in low-energy rivers, the geomorphological impact of vegetation is concentrated in areas immediately adjacent to the channel, whereas this

impact can extend further into the floodplain for torrential systems (Gurnell *et al.*, 2016).

There are many nuances in the terms used to designate and define riparian vegetation. These may reflect the interests of the authors, the structural characteristics or landscape organization of the vegetation (e.g. alluvial corridors vs floodplain forests), or its position in the floodplain. For example, riparian forests refer to the woody nature of the vegetation. The widely used French term “ripisylve” is associated with the woody character and the presence of typical native species, whose ecology is linked to the presence of the watercourse.

1.1.2 **Riparian vegetation: a management issue**

Given its influence on the hydrosystem, riparian vegetation is the source of numerous ecosystem services, useful to human societies, as well as disamenities, also known as disservices. For example, the presence of luxuriant vegetation and dead wood in the channel locally increases its roughness, causing the water line to rise. An overflow caused by this rise in water level can be beneficial in less sensitive areas upstream of populated areas, which will see their flood peak delayed (Dixon *et al.*, 2016). However, it will not be beneficial if this rise occurs in a sensitive area or immediately downstream. Moreover, dead wood can migrate downstream to sensitive areas during floods, causing damage to human infrastructure such as bridges. Similarly, while tree roots generally stabilize banks, high tree stems can increase the risk of the tree uprooting itself, dragging the bank with it. For these reasons, vegetation is actively managed in many river systems. In Western countries, the priority has long been to maintain the free flow of water, and many laws require vegetation maintenance for this purpose. Maintenance is sometimes entrusted to private individuals, sometimes to the community (Le Lay and Piégay 2007). Nevertheless, it is increasingly recognized that the full range of riparian vegetation functions needs to be integrated into its management. To achieve this, policies and regulations related to different issues (e.g. flood control, agriculture and nature conservation) need to be coordinated and take into account issues related to riparian ecosystems (Urbanič *et al.*, 2022).

Moreover, riparian ecosystems are subject to numerous pressures and threatened worldwide. In densely populated countries, urbanization and agricultural practices are often incompatible with the proper ecological functioning of riparian areas (Tockner and Stanford, 2002). Riparian zones are under pressure from river engineering (disconnection from the floodplain and flow regulation), which has profoundly altered processes essential to the functioning of these ecosystems (Hughes *et al.*, 2012). In other regions, such as the southwestern USA, riparian ecosystems are threatened by insufficient flows caused by water use and biological invasions (Poff *et al.*, 2011). Many riparian vegetation restoration programs aim to improve the biological quality of riparian zones or the associated ecosystem services. These may involve reconnecting the channel with its floodplain (Gumiero *et al.*, 2013), fencing off livestock (Forget *et al.*, 2013), planting (Salinas and Guirado, 2002), controlling invasive species (Claeson and Bisson, 2013),

introducing wood into the channel (Norbury *et al.*, 2021), land-use change (Burmeier *et al.*, 2011) or flow management in regulated systems (Hall *et al.*, 2011).

The implementation of coherent management plans that integrate the various issues and stakeholders linked to the river requires diagnosis and adequate planning on a watershed scale (Piégay and Landon, 1997; González *et al.*, 2015). The effectiveness of these actions must also be monitored and assessed. Nevertheless, such an approach implies having up-to-date data on the condition of rivers and riparian areas at the watershed scale.

Due to the dynamic nature of riparian zones and their often difficult accessibility, it is costly to obtain such data. Remote sensing techniques can provide an alternative to field inventories. Remotely sensed data are becoming increasingly available, including high-resolution or LiDAR products, which are of particular relevance to river management.

For example, remote sensing techniques have been used to map fluvial forms and floodplain topography (Szabó *et al.*, 2017), sedimentary processes (Lallias-Tacon *et al.*, 2014), riparian vegetation characteristics (Michez *et al.*, 2016b) or dynamics (Laslier *et al.*, 2019b), the presence of invasive species (Martin *et al.*, 2020). The use of remote sensing to study riparian vegetation will be discussed in greater detail in Chapter 2 and will not be developed further here.

1.2 Remote sensing: basic principles

The aim of this section is to briefly address the main principles of remote sensing that will be used in this manuscript.

1.2.1 **Definitions**

1.2.1.1 GIS

A geographic information system (GIS) is a system designed to handle spatially-referenced data. Its essential functions include the collection or production of such information (e.g. from databases or sensor-acquired information), its processing and analysis, and finally its representation (e.g. in the form of maps or tables) (Peuquet and Marble, 1990).

The first operational geographic information systems were put into service in the early 70s, and the first commercial software products took off in the 80s and 90s thanks to the democratization of computers (Maliene *et al.*, 2011). In four decades, GIS has undergone major developments, notably with the increase in processing possibilities (Lü *et al.*, 2019), the advent of the internet and server-stored data (Agrawal and Gupta, 2017) and the growing interoperability between systems and available databases (Sondheim *et al.*, 1999), evidenced by the current success of Open Source solutions (Löwe *et al.*, 2022). Among the most widely used geographic information systems are QGIS, Arcgis, Google Earth and the GDAL library.

Many problems have a spatial dimension. And as a result, GIS is used by a wide variety of professionals. For example, public authorities can use them to understand the impact of creating a new road, find the best location for a hospital or assess the

damage caused by a natural disaster. Managers of natural areas or forests can use them to plan management in a spatially differentiated way. Companies can use them to optimize their logistics or for marketing purposes. More recently, GIS is being used for precision agriculture (Longley *et al.* 2015).

1.2.1.2 Remote sensing

Remote sensing can be defined as the discipline of extracting information about a target from a distance, using sensors that exploit the electromagnetic spectrum and are mounted on mobile platforms (Fussell *et al.*, 1986).

In a remote sensing system, we need to differentiate between the vector and the sensor. The vector is the platform that carries the sensor. We can distinguish aerial platforms (airplane, helicopter, drone, balloon, etc.), which are rather flexible and inexpensive to deploy on a particular mission, and space platforms (satellites), deployed for longer missions and enabling information to be obtained regularly over a large part of the earth's surface.

The sensor is the instrument that collects the scene's radiative energy to derive a measurable electrical signal. First of all, we can distinguish analog and digital sensors. Analog sensors use film to record electromagnetic radiation. The images produced are then used for photo-interpretation or photogrammetry (see below). Digital sensors offer greater possibilities in terms of spectral richness and automatic processing, and have undergone greater methodological development since the 1970s (Congalton, 2010). These sensors record electromagnetic field information in the form of numbers, corresponding to the received signal intensity in a given frequency range.

Among digital sensors, a distinction can be made between passive and active sensors. Passive sensors exploit the electromagnetic radiation reflected by the target under the effect of solar radiation. Active sensors (e.g. LiDAR or RADAR) emit their own electromagnetic radiation in the direction of the target, and measure the properties of the reflected signal.

Remote sensing systems are often described in terms of their spectral, radiometric, spatial and temporal resolutions. A digital sensor often records information in several regions of the electromagnetic spectrum. A sensor recording information in four or more bands is generally described as "multispectral", while a sensor recording a large number of bands (several dozen or even several hundred according to Dian *et al.* (2021)) is generally described as "hyperspectral". Spectral resolution refers to the sensor's ability to differentiate between radiation emitted at two nearby wavelengths. High spectral resolution is generally associated with a large number of narrow spectral bands (ElMasry and Sun, 2010). Radiometric resolution, on the other hand, corresponds to the sensor's sensitivity to differences in the intensity of radiation emitted by the target (Ose *et al.*, 2016). Temporal resolution is often used to designate the time interval between two data collections. For satellite platforms, this return time is often determined by trajectory and swath (the width covered by an image during one pass around the Earth). For aerial platforms and satellite platforms operating "on demand", this temporal resolution can be modulated by the data

producer (Ose *et al.*, 2016). Spatial resolution corresponds to the footprint of a pixel on the ground, or the elementary unit at which spectral properties are measured. It depends on both the sensor and the platform used. For a given sensor, the greater the distance to the target, the lower the spatial resolution. As the number of pixels in an image is generally an intrinsic characteristic of the sensor, high spatial resolution is achieved at the cost of a smaller image footprint. The adjectives "high", "very high" or "low" resolution are relative to the object of study: images can be considered high resolution when the objects of study are represented by a large number of pixels. For low-resolution images, the objects of study are smaller than the pixels (Strahler *et al.*, 1986). In the case of riparian vegetation, we consider the boundary between high and low resolution to be of the order of 10 m, corresponding to the size of a mature tree crown. This limit is also taken up by White *et al.* (2016), although the latter also considers other classes of lower or higher resolution. For small rivers or studies related to bank morphology for example, this limit could be set lower.

It is impossible to produce remote sensing data with high spatial, temporal, spectral and radiometric resolution over large areas at an affordable cost. It is therefore necessary to make a compromise according to the needs of the considered application (Figure 3).

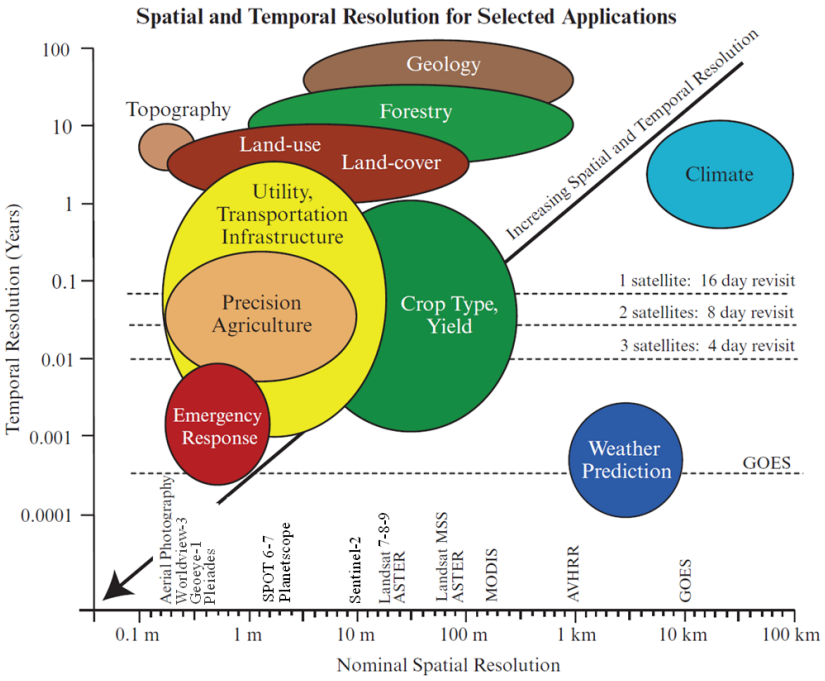

Figure 3: Spatial and temporal resolution required for a set of applications and corresponding data. This figure was originally produced by Jensen (2015) and updated by Vandendaele (2022).

Aerial platforms have been used for longer than satellite images and have long been the only means of obtaining high spatial resolution information (Toth and Jóźków, 2016). They were widely used to describe western rivers during the 20th century and are still widely used for their flexibility and for obtaining information at high spatial resolution. The first operational satellite platforms for monitoring natural resources came into service in the 1970s with the Landsat-1 satellites (80 m spatial resolution, 18-day revisit time, 4 spectral bands). Images from Landsat 7-8-9, commissioned in 1999, have a resolution of 30 m, four spectral bands and a revisit time of 16 days. The Sentinel-2 A and B satellites, commissioned in 2015 and 2017, offer 13 spectral bands, a resolution ranging from 60 to 10 m, and a revisit time of around 5 days. In parallel with government programs, numerous private satellites have been put into orbit with resolutions of a few meters with the Ikonos, Quickbird, RapidEye, Pléiades or WorldView satellite series. More recently, the use of small satellite constellations (PlanetLabs, SkySat) has become more common (Toth and Jóźków, 2016). For example, the PlanetScope constellation comprises more than four hundreds of satellites at the time of the writing of this thesis. Each satellite has a spatial resolution of 3 to 4 meters and carries a sensor that records 4 to 8 bands. The revisit time is about 1 day. While image quality (for example georeferencing, spectral or radiometric homogeneity) does not match that of other larger satellites, the quality of on-board sensors and image correction techniques are being gradually improved (Frazier & Hemingway, 2021).

1.2.2 **Focus on a sensor: LiDAR**

1.2.2.1 Definition

LiDAR (Light Detection And Ranging) technology is an active remote sensing technique used to model the relief of the earth's surface. During a LiDAR acquisition, a light beam (generally infrared) is emitted towards the Earth and reflected by the various obstacles encountered (vegetation, buildings, soil). The properties of the reflected beam (return time and intensity) can then be analyzed. Often, the returns are discretized to build a point cloud, where each point corresponds to an obstacle encountered (Chazette *et al.*, 2016). As the LiDAR beam is not completely stopped by vegetation, this technology provides information on the ground surface beneath the vegetation. LiDAR sensors can be mounted on aerial platforms (airplanes, microlights, helicopters or drones) or space platforms (GLAS or GEDI satellites, for example) (Sun *et al.*, 2022).

Point clouds are often processed to produce three types of raster products (Figure 4). Schematically, a DSM (digital surface model) is obtained by extracting the altitude of the highest point (surface relief) for each pixel. The DTM (digital terrain model) is obtained by extracting the altitude of the lowest point (ground relief). Finally, the DHM (digital height model) is obtained by subtracting the elevation of a DSM and a DTM (Guth *et al.*, 2021). It can be called a CHM (canopy height model) in forested areas. Other information can be extracted from the LiDAR signal, relating to the number, spatial distribution and intensity of returns.

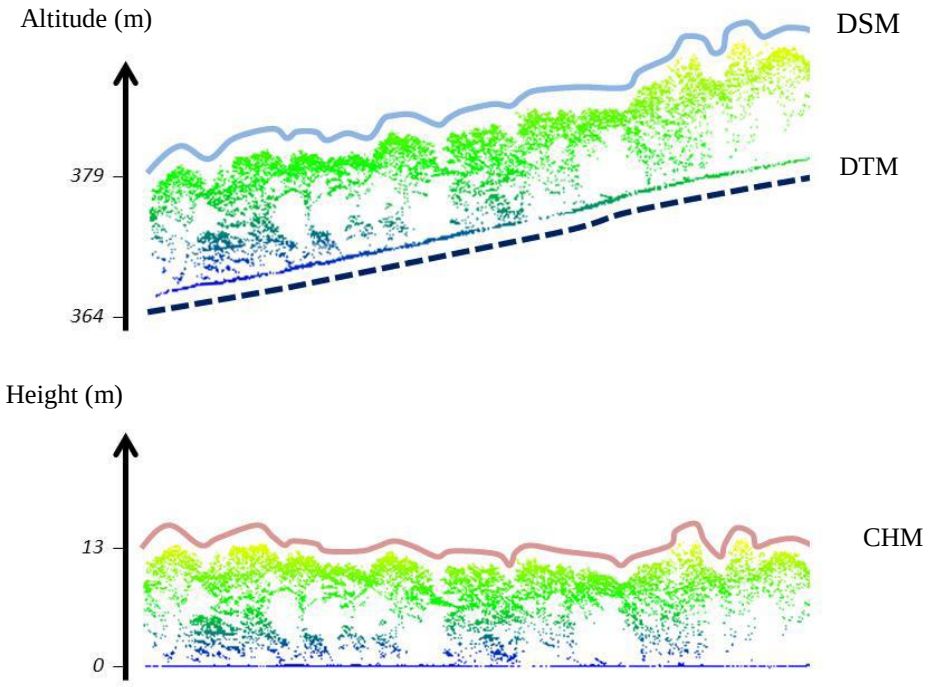

Figure 4 : Construction of the main raster products obtained using a LiDAR sensor. DSM = Digital surface model; DTM = Digital terrain model; CHM = Canopy height model. This figure was reproduced from Michez (2016).

1.2.2.2 Applications

These properties make LiDAR a useful tool for research and environmental management. According to Hyyppä *et al.* (2008), there are two main approaches to using LiDAR data for forestry applications: "area-based" and "object-based" approaches (Figure 5). The surface approach consists in extracting variables describing the LiDAR signal within a defined surface, such as a 12 m radius disk or a 30 m pixel. The object-based approach is implemented in two stages. First, objects are created by segmenting the point cloud or the CHM. These objects may correspond to trees, in which case the approach is referred to as individual tree crown approach or tree-centric approach. Variables related to the distribution of returns or the shape of tree crowns are then calculated at the scale of segmented tree crowns. Such approaches offer a clear advantage in fragmented landscapes such as riparian zones, where edge effects make it difficult to build fixed-area calibration units (Dalponte and Coomes, 2016). Other approaches based on deep learning, which don't fit into any of these boxes, have recently been deployed in forest research (Bolyn *et al.*, 2022).

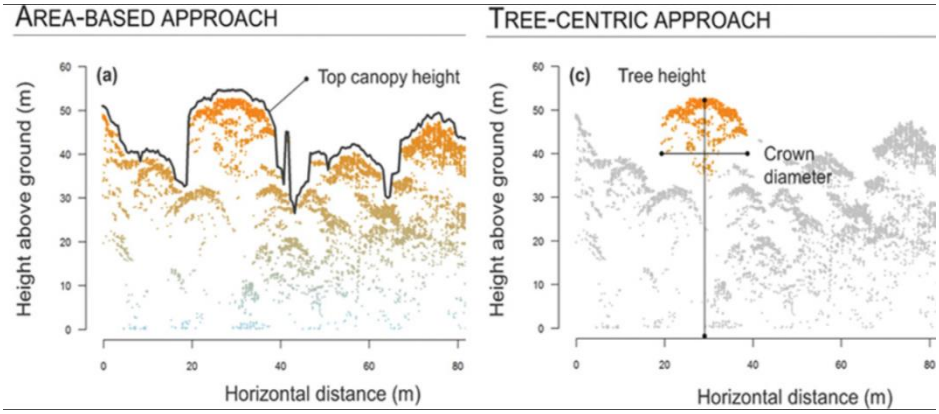

Figure 5 : Comparison of the "area-based" approach, which exploits LiDAR variables at the canopy scale, with a "tree-centric" approach, which exploits LiDAR variables at the scale of a tree crown. This figure was reproduced from Coomes *et al.* (2017).

In the riparian context, LiDAR data are used to extract basic information about a river such as its position, width or longitudinal slope (Biron *et al.*, 2013). LiDAR DTM are widely used in hydraulic modelling (Mandlburger *et al.*, 2009) or to map flood vulnerability (Muhadi *et al.*, 2020). The ability of LiDAR to describe both topography and vegetation (in this case, its hydrodynamic properties), has been exploited by several authors to parameterize terrain roughness according to the vegetative cover (Straatsma and Baptist, 2008; Zahidi *et al.*, 2018). Topographic data from a LiDAR dataset can also be exploited by geomorphologists to identify the floodplain, oxbow lakes, terraces and drainage ditches (Notebaert *et al.*, 2009), or to measure the height of sediment banks (Caponi *et al.*, 2019). When several surveys spaced over time are available, sedimentary phenomena can sometimes be quantified (Lallias-Tacon *et al.*, 2014). Applications for mapping riparian vegetation, at the crossroads of remote sensing applied to rivers and terrestrial vegetation, will be discussed in Chapter 2. The use of LiDAR data for describing the riverbed itself will be discussed in Chapter 5.

1.2.3 **Focus on aerial photogrammetry**

1.2.3.1 Definition and applications

Images acquired from a camera are two-dimensional and distorted. As a result, they cannot be directly precisely referenced in space and measures cannot be directly performed on them. Photogrammetry is a technique for measuring distances and angles, by exploiting the parallax of images acquired from different viewpoints.

Although photogrammetry has been around for over a century, it has undergone a revolution since the 2000s. This evolution is linked to the advent of digital photography and increased computing power. Older photogrammetry, based on analog photos, required expensive metric cameras and considerable know-how for image acquisition and processing. More recent techniques mobilize large numbers of

images, powerful and largely automated computer vision and computing algorithms (Pierrot-Deseilligny and Clery 2011).

Aerial photogrammetry is the application of photogrammetry to images acquired using airborne sensors. While aerial photogrammetry has long been used in many fields, the increasing, low-cost availability of drones with on-board cameras has created renewed interest in the technique (Lisein *et al.*, 2013).

Products derived from aerial photogrammetry are used for a wide range of applications. These include the use of photogrammetric 3D models as a substitute for LiDAR point clouds in forestry (Michez *et al.*, 2020), the use of photogrammetric point clouds to describe the geometry of a river's minor bed or the evolution of its morphology (Woodget *et al.*, 2019), or even more simply, the use of time series of aerial images to describe the evolution of riparian landscapes.

1.2.3.2 Image acquisition

Photogrammetry relies on redundant images, on which a sufficient number of homologous points (points taken with different shots) can be found. The aerial platform (e.g. a plane or drone) follows parallel lines of flight and takes images at regular intervals, so as to achieve sufficient lateral and longitudinal overlap (Figure 6). The camera is generally oriented at right angles to the ground: this is known as NADIR photography.

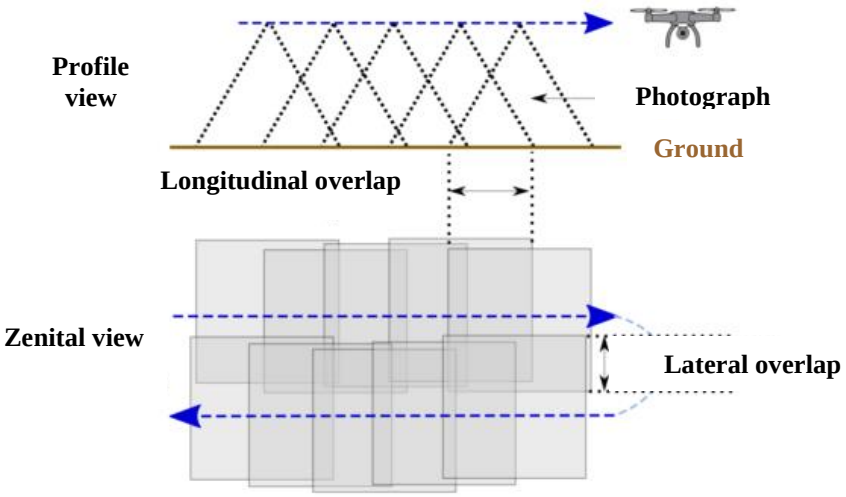

Figure 6: Flight and image acquisition scheme for an aerial platform for subsequent photogrammetric processing.

Figure 7 summarizes the most important camera parameters. Focal length is a fundamental characteristic of the camera lens. A long focal length (telephoto) produces detailed photos over a small area, while a short focal length (wide-angle) produces less detailed photos over a larger area. The number of pixels on the sensor is equal to the number of pixels that will be present on the photograph. All things

being equal, a higher pixel count leads to greater resolution. Swath depends on sensor dimensions (the wider the sensor, the larger the swath), focal length (the shorter the focal length, the larger the swath) and height (the higher the flight altitude, the larger the swath).

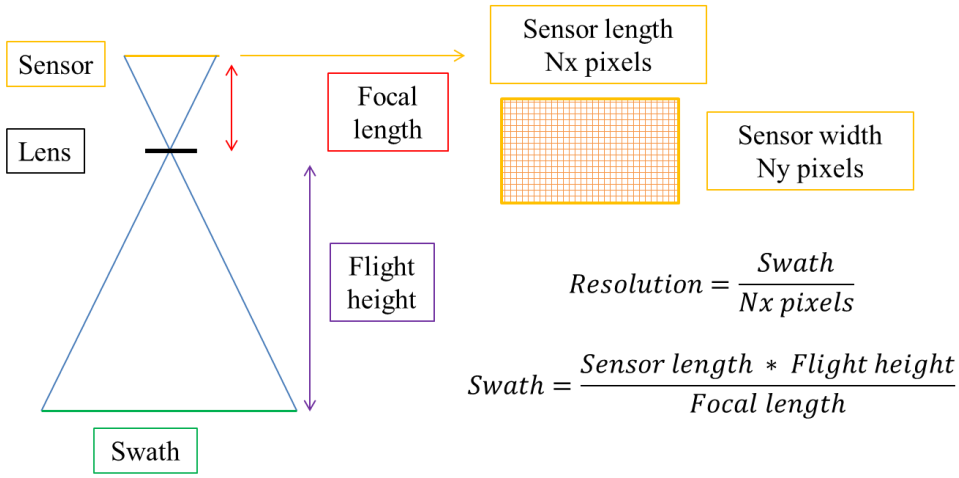

Figure 7: Diagram showing the main parameters of a camera used in photogrammetry.

1.2.3.3 Overview of a processing chain

An overview of an SFM-MVS (Stucture from motion - Multi-view stereo) processing chain is shown in Figure 8. The first step is to detect characteristic points visible in several images: homologous points, also known as tie points. This search is often carried out using SIFT (scale invariant feature transform) algorithms. These algorithms analyze images locally to find landmarks that remain visible despite changes in viewpoint from one image to the next.

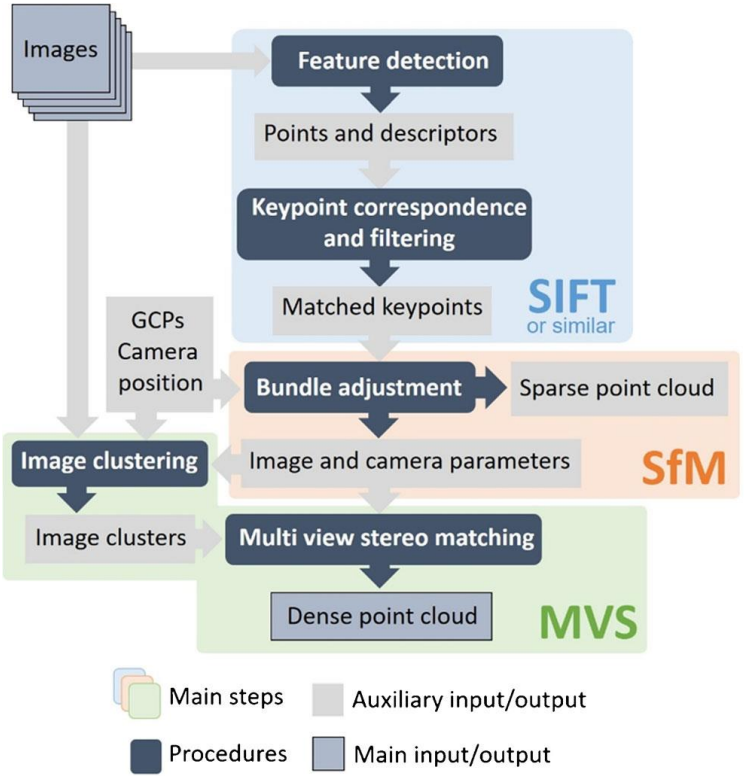

Figure 8 : Schematic diagram of an SFM-MVS processing chain. This figure was reproduced from Iglhaut *et al.* (2019).

Tie points, camera and geographic information (platform and sensor position and orientation, points with known coordinates on images) are used to estimate and refine shot positions and orientations. Geometric distortions in the images are sometimes also modeled at this stage, known as camera calibration. Image calibration and the estimation of shot orientations (aerotriangulation) are carried out iteratively to minimize the error of reprojecting a tie point from one image to another, or the error of positioning on points with known coordinates (Egels, 2011). The result is a sparse point cloud that forms the skeleton of the 3D model.

In the densification stage (dense matching or dense correlation), the pixels around the homologous points are added to the model, using the positions of the shots and the model optimized for the camera. This step results in the creation of a denser point cloud. This cloud is used to produce an orthophotomosaic (also known as an orthophoto, orthophotoplan or orthomosaic). An orthophoto is a two-dimensional image whose distortions have been corrected, so that it can be overlaid on a plane at any point (Figure 9). A digital surface model (DSM) can also be produced.

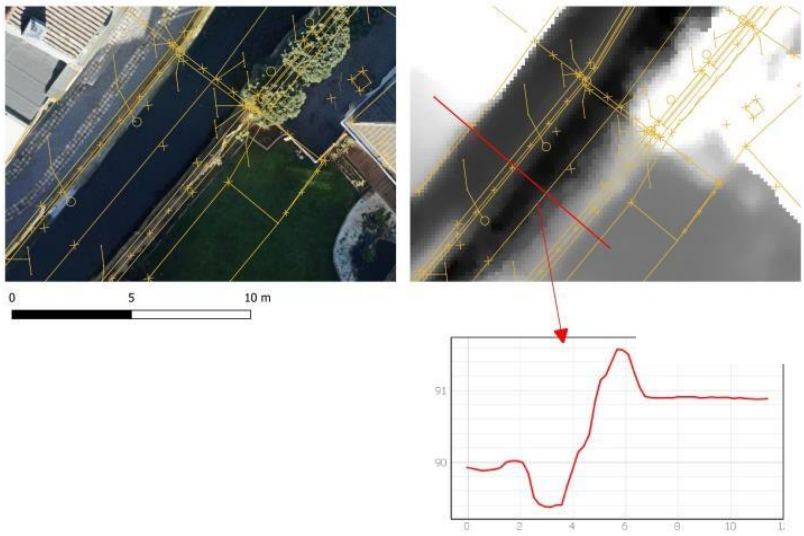

Figure 9: An orthophoto and a DSM are overlaid on a topographic survey. A profile is also extracted from the DSM to estimate the height of a wall.

1.2.3.4 Geometric quality and georeferencing

In the absence of geographic information, photogrammetry produces scale-free 3D models in an arbitrary geographic reference system. Absolute position information can be obtained from the GNSS positions of the platform in flight and the orientation of the sensor (accuracy of a few centimeters to a few meters, depending on the equipment used), or from points on the ground visible on the images and whose absolute position is known (Figure 10).

Figure 10 : Control point surveyed with precision GNSS (left) and visible on a photograph taken with a drone (right)

Accuracy is a measure of the geometric quality of the photogrammetric model. The absolute error corresponds to the positioning error of an object between its

representation in the model and in reality. It is calculated using a representative sampling of the area. The position of check points visible on the orthophoto is precisely measured in the field and compared with the position of the same point on the orthophoto. The relative error corresponds to the error in the dimension of an object between its representation in the model and in reality. Indeed, it is possible to obtain a model whose geometric properties are correct, but whose absolute position in space is offset (Meinen and Robinson, 2020).

1.3 Objectives and manuscript organization

The aim of this thesis is to propose new mapping tools to support riparian vegetation management. These tools are based on high-resolution airborne remote sensing techniques. The first sub-objective is to develop innovative approaches for describing riparian vegetation at watershed scale. The second sub-objective aims to identify the applicative potential of remote sensing tools to support the management of riparian ecosystems. Figure 11 illustrates how these two sub-objectives relate to the chapters of the thesis.

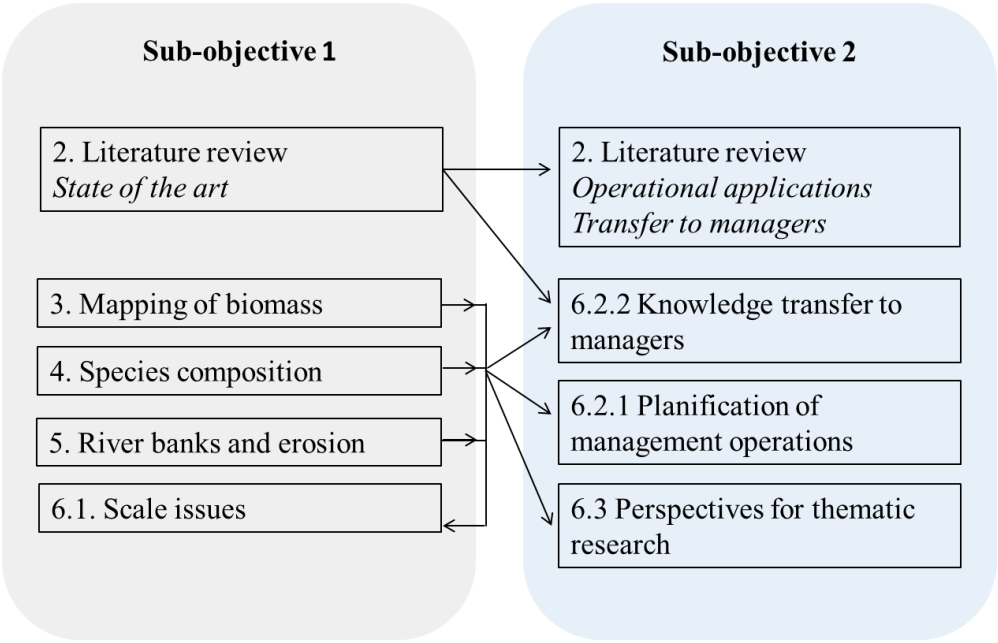

Figure 11: Schematic view of sub-objectives and chapters of the thesis

A review of the literature (Chapter 2, published article) provides an overview of the state of the art and identifies research prospects. Based on a detailed review of the literature, we identify operational applications and the challenges faced by researchers in transferring the approaches developed to riparian ecosystem managers. This chapter relates to the two sub-objectives of the thesis.

Three approaches to mapping riparian vegetation using remote sensing are then deployed on the Semois and Chiers river basins in southern Belgium. The following three chapters relate to the first sub-objective of the thesis and address mapping of biomass, specific composition and bank erosion. These indicators relate to flood risk (production of large woody debris influenced by these three indicators) and nature conservation (vegetation type and diversity, maturity and dynamic character), which are the main stakes addressed by managers of riparian areas located in western countries with a temperate climate (Dufour *et al.*, 2020).

Chapter 3 (published article) presents a method for estimating woody biomass at the scale of 230 km of rivers and their floodplains, based on LiDAR data. Biomass is a variable of interest for riparian vegetation management. It summarizes the state of the vegetation and is associated with numerous functions within the hydrosystem. The spatial structuring of this biomass is then analyzed with regard to factors linked to geomorphology, history or human activity.

Chapter 4 (original unpublished work) presents an approach to mapping the species composition of riparian forests at the scale of 155 km of rivers and their floodplains, based on LiDAR data. The spatial structuring of species composition is also analyzed.

Chapter 5 (original unpublished work) deals more specifically with the description of riverbanks using LiDAR data and UAV images. Bank morphology and mobility have a direct influence on riparian vegetation and its management. The accuracy and limitations of both techniques are analyzed. To illustrate the potential application of the techniques presented, lateral bank erosion is mapped at the scale of a small watershed.

Chapter 6 is structured into three subsections. Section 6.1 relates to the first sub-objective of the thesis and discusses methodological issues relating to scale, which run through all the work presented in this thesis. Section 6.2 relates to the second sub-objective of the thesis and discusses the application of remote sensing methods for the benefit of river management. The concrete use of the techniques developed in this thesis in the context of river management is illustrated in section 6.2.1. In this section, the bank erosion data produced in Chapter 5 are combined with biomass and specific composition data to prioritize riparian management over the watershed. Section 6.2.2 focuses on the transfer of simplified remote sensing methods, which can be deployed directly by river managers. Section 6.3 discusses perspectives for thematic research on riparian vegetation.

2

Using remote sensing to characterize riparian vegetation: A review of available tools and perspectives for managers

Foreword

This chapter provides an introduction to the use of remote sensing to characterize and support vegetation management. It begins with a quantitative analysis of the scientific literature. This is structured according to the riparian vegetation characteristics studied, the scale of observation, the multi-temporal nature and the type of data used. Secondly, operational applications are presented and challenges related to knowledge transfer are discussed. This chapter is adapted from an article published in the Journal of Environmental Management.

Reference (Chapter adapted from publication)

Huylenbroeck, L., Laslier, M., Dufour, S., Georges, B., Lejeune, P., & Michez, A. (2020). Using remote sensing to characterize riparian vegetation: A review of available tools and perspectives for managers. *Journal of environmental management*, *267*, 110652.

Abstract

Riparian vegetation is a central component of the hydrosystem. As such, it is often subject to management practices that aim to influence its ecological, hydraulic or hydrological functions. Remote sensing has the potential to improve knowledge and management of riparian vegetation by providing cost-effective and spatially continuous data over wide extents. The objectives of this review were twofold: to provide an overview of the use of remote sensing in riparian vegetation studies and to discuss the transferability of remote sensing tools from scientists to managers. We systematically reviewed the scientific literature (428 articles) to identify the objectives and remote sensing data used to characterize riparian vegetation. Overall, results highlight a strong relationship between the tools used, the features of riparian vegetation extracted and the mapping extent. Very high-resolution data are rarely used for rivers longer than 100 km, especially when mapping species composition. Multi-temporality is central in remote sensing riparian studies, but authors use only aerial photographs and relatively coarse resolution satellite images for diachronic analyses. Some remote sensing approaches have reached an operational level and are now used for management purposes. Overall, new opportunities will arise with the increased availability of very high-resolution data in understudied or data-scarce regions, for large extents and as time series. To transfer remote sensing approaches to riparian managers, we suggest mutualizing achievements by producing open-access and robust tools. These tools will then have to be adapted to each specific project, in collaboration with managers.

2.1 Introduction

At the interface between terrestrial and aquatic biota, riparian vegetation is a central element in the hydrosystem, where it plays many ecological roles and interacts with all hydrosystem components (Naiman *et al.*, 2005). In a broad sense, riparian vegetation corresponds to all vegetation types that grow within the area influenced by a river network (Naiman and Décamps, 1997).

Despite covering a relatively small area, riparian vegetation provides many ecosystem services related to river flow (Dixon *et al.*, 2016), sedimentary processes (Zaimes *et al.*, 2004), biodiversity (Naiman and Décamps, 1997), water quality (Honey-Rosés *et al.*, 2013, Brogna *et al.*, 2018), cultural value (Décamps, 2001, Klein *et al.*, 2015, Vollmer *et al.*, 2015). However, riparian ecosystems experience multiple pressures (e.g. land use, water diversion, modified flood regime) (Stella and Bendix, 2019) and have been severely altered in many regions of the world, for example in Western Europe (Hughes *et al.*, 2012), southwestern North America (Poff *et al.*, 2011), in the Murray-Darling Basin in Australia (Mac Nally *et al.*, 2011) or in South Africa (Holmes et al, 2005). Consequently, riparian vegetation is often the focus of management practices, including restoration or rehabilitation measures (Dufour and Piégay, 2009; González *et al.*, 2015; Capon and Pettit, 2018), buffer implementation (Lee *et al.*, 2004) or repeated maintenance operations such as wood removal (Piégay and Landon, 1997; Wohl *et al.*, 2016).

In this context, management practices must be based on accurate and up-to-date information about the state of riparian vegetation (National Research Council, 2002). Regional or national programs have thus been established in many countries to monitor the health of riparian ecosystems. Examples include southern Belgium (Debruxelles et al, 2009), Spain and more generally the European Union in the frame of the Water Framework Directive (Munné *et al.*, 2003, Willaarts *et al.*, 2014), Australia with the South East Queensland Healthy Waterways Partnership (Bunn *et al.*, 2010) or the monitoring of riparian condition in several National Parks in North America (Starkey, 2016). Dense sampling schemes can help target and implement management practices (Landon *et al.*, 1998; Beechie *et al.*, 2008) or assess their effectiveness (González *et al.*, 2015). However, due to the spatial arrangement, dynamism and inaccessibility of riparian ecosystems, data acquisition in the field can be labor-intensive, especially for large areas (i.e. more than 100 km of a river) (Johansen *et al.*, 2007). It is thus difficult to sample densely in the field, and the density or the extent of observations must be reduced. This can be problematic, because river scientists argue that small scale or discontinuous observations are inadequate to understand spatially continuous processes that occur at large spatial scales (Fausch *et al.*, 2002; Marcus and Fonstad, 2008; see also Tabacchi *et al.*, 1998 or Palmquist *et al.*, 2018 for examples related to riparian vegetation).

Remote sensing provides the ability to acquire continuous data over large extents. In the past few decades, the continued development of sensors, vectors and computational power has fueled the development of applications in environmental

science (Anderson and Gaston, 2013; Wulder *et al.*, 2012). The positive contribution of remote sensing to the management of natural resources is addressed by many articles related to river or riparian management (Carbonneau and Piégay, 2012, Dufour *et al.*, 2012). This is not only a theoretical issue as is it regularly raised by riparian managers in the grey literature (Vivier *et al.*, 2018, Fédération des Conservatoires d'espaces naturels, 2018). However, it is difficult for managers to know whether and which remote sensing methods are relevant to a particular situation (Dufour *et al.*, 2012).

The use of remote sensing to study riparian vegetation raises specific challenges. These challenges are linked to the vegetation's relative structural complexity and spatial organization (Naiman and Décamps, 1997), or to the difficulty to extract specific features or processes related to riparian vegetation functions (e.g. surface roughness by Straatsma and Baptist (2008), shading of streams by Loicq *et al.*, 2018). In a recent literature review, remote sensing emerged as a particularly dynamic subject in riparian studies (Dufour *et al.*, 2019). Remote sensing of riparian vegetation was mentioned in several reviews addressing the remote sensing of rivers (Muller *et al.*, 1993; Goetz, 2006, Tomsett and Leyland, 2019, Piégay *et al.*, 2020). Specific aspects were also reviewed such as the mapping of roughness coefficients with remote sensing (Forzieri *et al.*, 2012) or the use of satellite images to map riparian vegetation in New Zealand (Ashraf *et al.*, 2010). Dufour *et al.* (2012) and Dufour *et al.* (2013) summarized and discussed several examples of remote sensing applications to map riparian vegetation. However, none of the aforementioned articles comprehensively reviewed the use of remote sensing to map riparian vegetation across regions, scales and researcher's interests. Indeed, the latter are fragmented among several fields of knowledge (e.g. ecology, geomorphology or hydraulics) (Dufour *et al.*, 2019).

The aims of this article are 1) to provide a comprehensive overview of the relevance of remote sensing to support the study of riparian vegetation and 2) to discuss how remote sensing approaches can be valued as operational tools for managing riparian vegetation. To these ends, we first systematically review the different types of data used to study major features, functions and processes related to riparian vegetation across scales (section 2.3). The second part of the article (section 2.4) is based on expert judgment. We provide concrete examples where remote sensing is used in management contexts, in order to identify the challenges of conveying remote sensing tools from scientists to managers.

2.2 Materials and methods

Our approach was structured as following: we first selected relevant articles in the Scopus database. Second, relevant information was extracted for each article, and summarized into graphs. Our results were discussed in terms of trends and perspectives for research, and in terms of operationality and transferability to riparian managers. The Figure 12 synthesizes our approach. Major steps are further detailed in the following sections.

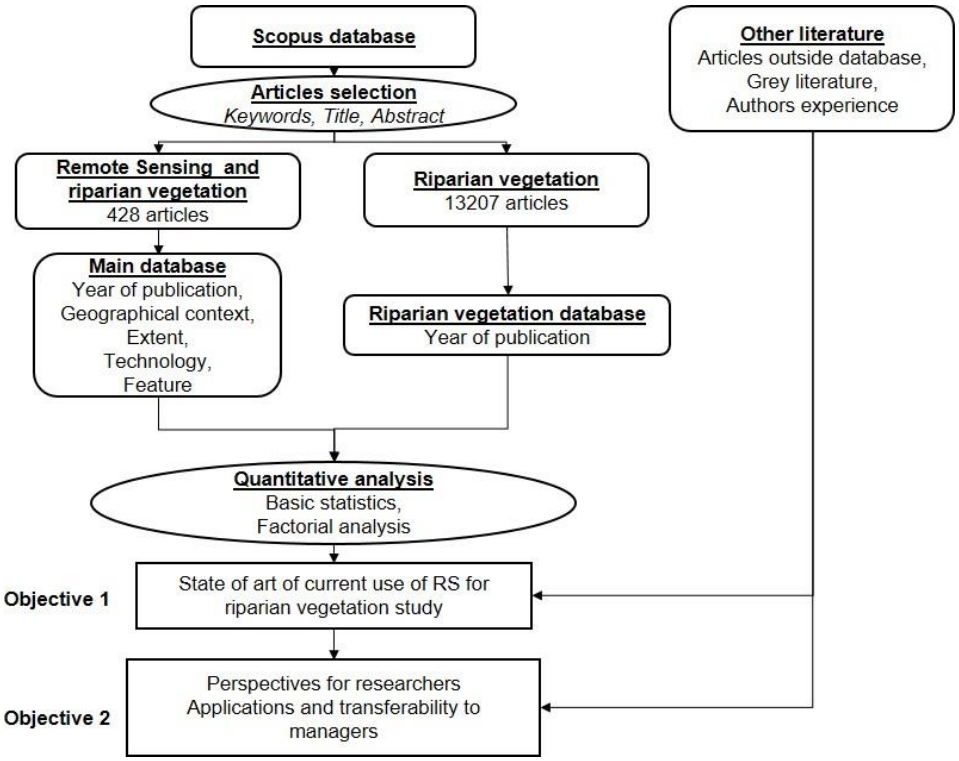

Figure 12: General workflow for the reviewing process.

2.2.1 **Database collection**

Relevant articles were selected from the Scopus database (www.scopus.com) for the period 1980 - April 2018, when the database was queried. We searched the title, abstract and the keywords for words related both to riparian vegetation and to remote sensing technologies. More precisely, we used the request described in the Figure 13.

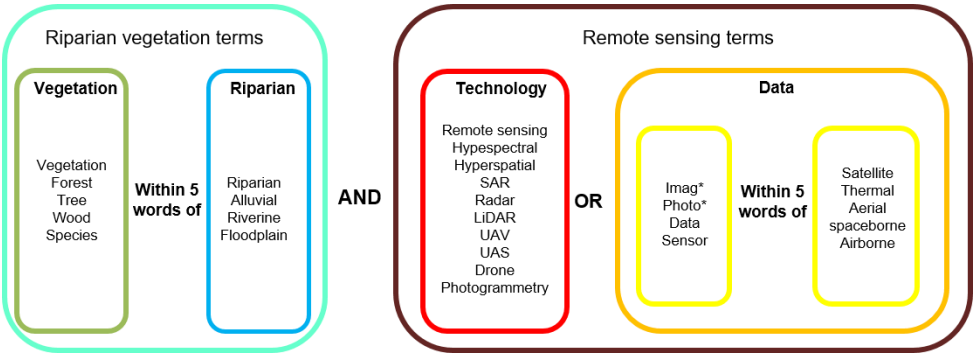

Figure 13: Keywords used for database collection

Our choice of keywords excluded articles that mentioned riparian zones, but not specifically riparian vegetation. While some of these articles could have been relevant for this review, including keywords related to riparian zones would have resulted in unmanageable noise.

This request yielded 791 articles. We first filtered out irrelevant articles based on their title (672 articles kept). Then, we sorted through the remaining articles based on their abstracts (428 articles kept). During these two filtering steps, we removed mainly articles in which riparian vegetation was not an essential part of the study. For example, we removed geomorphological articles in which riparian vegetation was mentioned in the abstract but was not actually studied. Articles that used GIS but no remote sensing data were also removed (e.g. those using cadastral archives).

We also built a second database using only keywords related to riparian vegetation, excluding those related to remote sensing. This second database was solely used to estimate the proportion of remote sensing studies among riparian vegetation studies, and was not analyzed using the analysis grid described in the following section.

2.2.2 **Analysis grid**

We searched for features that characterized the articles collected to perform quantitative analysis and statistics. We built our analysis grid (Table 1) around five groups of variables: “general information”, “remote sensing technology”, “study extent”, “type of indicator” and “multi-temporality”. In this paragraph, when not obvious, we highlight in bold the codes (used in figures) associated with the variables. ”General information” included variables such as the publication year and location of study area. “Remote sensing technology” described the type of remote sensing data used. To simplify interpretation, we recorded this information as common combinations of sensors and vectors. We distinguished the following: airplane with a RGB/GS (red-green-blue or panchromatic), digital or analog sensor (**Plane_RGB**); airplane with a multispectral or hyperspectral sensor (**Plane_MSHS**); UAV with any sensor (**UAV**); any vector with a LiDAR sensor (**LiDAR**); any vector with a RADAR sensor (**RADAR**) and satellite with a multispectral or hyperspectral sensor. This last variable was coded according to image resolution: medium (> 10 m, **Satlow**) or high (≤ 10 m, **Sathi**). Such a limit was also used in White *et al.* (2016) in forest ecosystems and separates images where trees or small groups of trees can be distinguished from images where they cannot. ”Study extent” described the extent of the study area as the **length** of studied river or **area** of the study area. These two variables were recorded in categories and then summarized into a single category to simplify interpretation: **study extent.** “Type of indicator” described the type of features extracted with remote sensing data to describe riparian vegetation. Delineation of riparian vegetation among other land cover types (**DLC**) is the first feature extracted for managing riparian vegetation. Species composition is a major feature of riparian plant formations. It is related to habitat provision, bank stabilization and flood regulation functions; for example, willow is a pioneer species that helps to stabilize banks (Hupp, 1992). We

distinguished studies that differentiate groups of species (**Communities**) and studies that differentiate species (**SP**). We also distinguished studies in which the target species were invasive (**SP_invasive**), since riparian zones are particularly prone to invasions (Richardson *et al.*, 2007). We distinguished studies in which the target communities were **succession stages**, since riparian systems are pulsed systems in which succession is regularly reinitiated, leading to a mosaic of succession stages (Kalliola and Puhakka, 1988). The structure of riparian vegetation is related to many ecological functions. We recorded general descriptors of vegetation structure such as vegetation **height**, **density**, **biomass** and **landscape** structure. We also recorded studies interested in hydraulic properties of vegetation (**Roughness**), since riparian vegetation has tremendous effects on the hydraulic regime of rivers, especially by slowing river flow (Curran and Hession, 2013). Riparian **shade** (or overhang) influences fish habitats and is a major factor regulating stream temperature (Poole and Berman, 2001). Large woody debris (**LWD**) has many effects on provision of aquatic habitats, river morphology and flood risk prevention (Wohl, 2017). Features related to physiological processes, including **phenology** and **health statuts** (e.g. tree dieback), are a major concern for managers (Cunningham *et al.*, 2018). Riparian **evapotranspiration** has often been studied in arid or semi-arid systems because it has a major effect on providing water for human use (Dahm *et al.*, 2002). "Multi-temporality" included only one variable (**Diachronic**), which corresponded to a special type of study – diachronic analysis – that uses a temporal series of images to describe vegetation dynamics. We recorded all variables as presence/absence data to capture the use of several types of data or the mapping of several indicators in the same article.

Table 1: Analysis grid used for each article in the database

Group of variables		Variable	Values	Description
General information		Year		Publication year
		X1		Longitude of the study area
		Y1		Latitude of the study area
		Biome		World Wildlife Fund Biome of the study area (extracted from the geographical coordinates of the study area)
Type of remote sensing data		Plane_RGB	0/1	Use of black and white or true-color aerial images (except images acquired from UAVs)
		Plane_MSHS	0/1	Use of aerial images with 4 or more spectral bands (except those from UAVs)
		Satlow	0/1	Use of satellite images with resolution > 10 m
		Sathi	0/1	Use of satellite images with resolution ≤ 10 m
		UAV	0/1	Use of images acquired from UAVs
		LiDAR	0/1	Use of LiDAR data
		RADAR	0/1	Use of RADAR data
Extent of the study area		Length	1 to 5	Length of the river studied (for studies at the scale of the minor bed or floodplain)
		Area	1 to 5	Area of the study area (for studies at the watershed scale)
		Study extent	1 to 5	Combination of Length and Area: • Local: Length < 10 km • River segment: Length 10-100 km OR Area < 100 km² • Subregional: Length 100-1000 km OR Area 100-1000 km² • Regional: Length > 10,000 km OR Area 1000-10,000 km² • Very large scale: Area > 10,000 km²
Type of indicator	Delimitation	DLC	0/1	Mapping of riparian vegetation (including land cover studies)

	Species composition	Communities	0/1	Mapping of several distinct riparian plant communities
		Succession stages	0/1	Mapping of several succession stages
		SP	0/1	Mapping of riparian vegetation at the species level
		SP_invasives	0/1	Mapping of invasive species
	Vegetation structure	Height	0/1	Mapping of vegetation height
		Landscape	0/1	Calculation of landscape metrics (e.g. continuity)
		Density	0/1	Mapping of vegetation density
		Shade	0/1	Mapping of shade cast by vegetation
		Biomass	0/1	Mapping of biomass
		LWD	0/1	Large woody debris (wood in rivers)
		Roughness	0/1	Mapping of vegetation hydraulic properties
	Physiological processes	Evapo-transpiration	0/1	Estimate of vegetation evapotranspiration
		Health status	0/1	Mapping of vegetation health status (e.g. tree dieback, defoliation)
		Phenology	0/1	Mapping of vegetation phenology
Multi-temporality		Diachronic	0/1	Diachronic analysis

2.2.3 **Statistical analysis**

We computed the annual number of published studies using remote sensing of riparian vegetation. We also computed for each year the proportion of studies that used remote sensing among all riparian vegetation studies. To do so, we compared the number of articles in the database related to remote sensing and riparian vegetation with the number of articles in the database related to riparian vegetation in general.

The data collected with the analysis grid were summarized and plotted. We computed the number of articles for each WWF biome, the use of different remote sensing technologies through time. We then compared the use of different technologies according to the scale of observation, the indicator extracted and the multi-temporal character of studies.

Finally, we performed a multiple correspondence analysis in order to highlight relationships between the type of data and the type of feature extracted. We used the package FactoMineR of R software. All variables were recorded as categorical variables. Variables related to study extent and multi-temporality were added as supplementary variables.

2.2.4 **Interpretation of results**

Results were discussed in two phases. First (section 2.3), we use our quantitative review of the literature to establish the state of the art and main perspectives in the use of remote sensing to map riparian vegetation. Second (section 2.4), we discuss how remote sensing can be used in real management contexts. We first discuss the added value of remote sensing in such contexts using concrete examples from the grey literature and personal experience. Then, we use these examples to discuss the challenges that must be overcome in order to promote the use of remote sensing by riparian managers. Therefore, while the section 2.3 of this article is based on a rigorous review of the scientific literature, the section 2.4 of this article is rather based on expert judgment.

2.3 Results and discussion of the systematic review

2.3.1 **Location of the studies**

Most studies in the 428 selected layed in the Northern Hemisphere (79%), especially in North America (40% of studies) and Europe (20% of studies) (Figure 14). South America, Oceania, Asia (mostly Japan) and Africa represented respectively 9%, 9%, 11% and 5% of studies. Most represented biomes (Figure 15) were hardwood and mixed temperate forests (28%), temperate coniferous forests (14%), and deserts and xeric bushes (13%). Mediterranean biomes (10%) and temperate open biomes (8%) were also well represented. Well-represented biomes generally corresponded to those in developed countries. Conversely, boreal forests and tundra were least represented (< 1% of studies), though they cover a large area globally (> 10% of emerged land area). In addition, despite the large extent of tropical biomes (tropical and equatorial forests or open vegetation, ca. 30% of emerged land area), few studies focused on them.

Figure 14: Locations of the study areas of the studies reviewed.

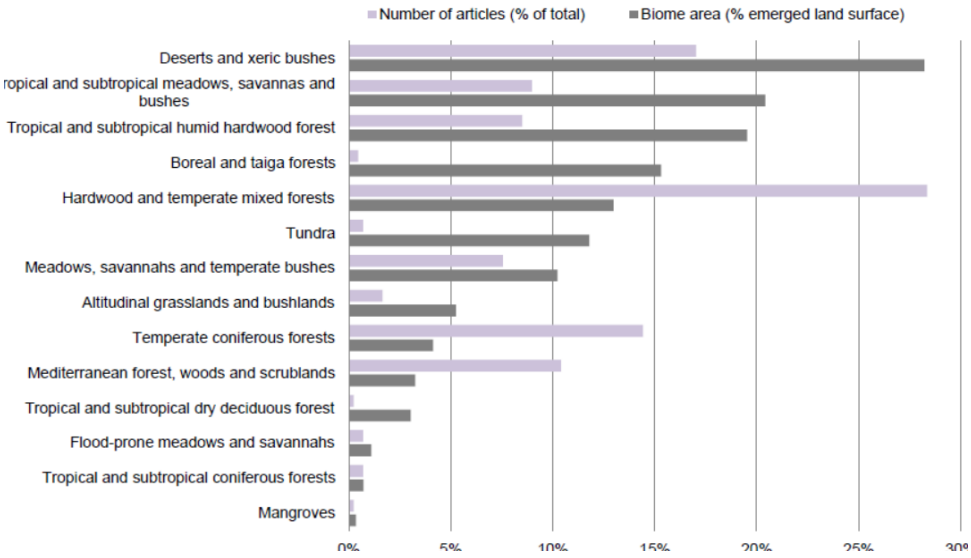

Figure 15: Locations of studies reviewed, by World Wildlife Fund biome.

This result highlights the lack of knowledge and studies about tropical and boreal riparian forests, perhaps due to the location of laboratories, which are often located in developed countries and temperate climates. Our results are similar to those of Dufour *et al.* (2019) for all riparian vegetation studies and those of Bendix and Stella (2013) for studies of vegetation/hydromorphology relationships.

However, we suggest that the increasing quality of remote sensing data has great potential for research in understudied areas and at the global scale. One condition is that these data must be available to their potential users. Open or free remotely sensed data, such as Landsat, MODIS or, more recently, Sentinel images, allow researchers to overcome the issue of the prohibitive cost of data acquisition. This is particularly true for researchers in developing countries for data that are produced in wealthier countries (Sá and Grieco, 2016). However, to broaden the user base, it is also necessary to facilitate access to these data (Turner *et al.*, 2015). Access can be facilitated by providing higher-level (e.g. atmospherically corrected) or derived products, such as global land cover maps (Gong *et al.*, 2013), global floodplain models (Nardi *et al.*, 2019) and maps of riparian zones (Weissteiner *et al.*, 2016, at the European scale). Access can also be made easier by developing an open, free or user-friendly environment to find, visualize and process data (Turner *et al.*, 2015).

2.3.2 Changes over time in the number of studies that used remote sensing to study riparian vegetation

Most of the 428 studies (89%) that used remote sensing to study riparian vegetation from 1980-2018 were published after 2000 (Figure 16A), when the number of studies began to increase greatly. Before 1990, few studies used remote sensing to study riparian vegetation. The percentage of studies using remote sensing among studies studying riparian vegetation increased in the 2000s (Figure 16B). Each year after 2000, 2-6% of all studies of riparian vegetation used remote sensing. Thus, even recently, relatively few studies use remote sensing data to study riparian vegetation, and field-based approaches dominate riparian vegetation studies despite the development of remote sensing and modeling approaches. This could be due to three main reasons. First, field-based approaches have traditionally been used and are straightforward. Some aspects of riparian vegetation, such as biogeochemical functioning and soil properties, cannot realistically be studied with remote sensing (Dufour *et al.*, 2012). Second, the spatial structure of riparian vegetation makes it difficult to study using remote sensing. Its complexity (Naiman *et al.*, 2005) and narrow shape is difficult to observe with low resolution satellite images (Johansen *et al.*, 2010). Additionally, the linear shape of riparian corridors requires acquiring images over large areas (to cover sufficient corridor length), only to focus on small areas (near the river, rather than other land cover classes). For example, Weissteiner *et al.* (2016) estimated that Europe's riparian area represented ca. 1% of its total continental area. Third, we removed duplicate and irrelevant articles from our database, but did not do so when identifying all articles describing studies of riparian vegetation in general, which may have led us to underestimate the percentage of all riparian studies that used remote sensing.

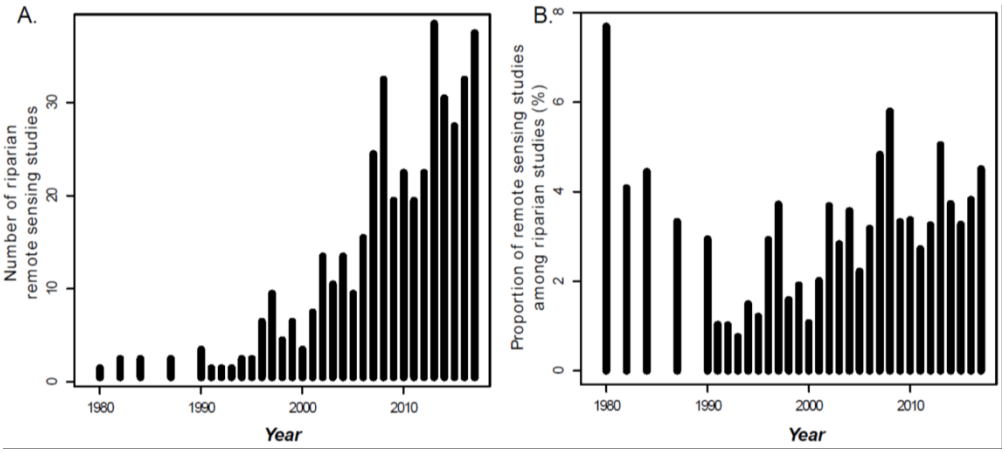

Figure 16: A) Number of studies from 1980-2018 that used remote sensing to study riparian vegetation. B) Percentage of studies from 1980-2018 that used remote sensing, out of all studies concerning riparian vegetation (see section 2.2.3).

2.3.3 **Changes in remote sensing data over time**

The remote sensing data used most were aerial RGB/GS images (44% overall) and medium-resolution satellite images (> 10 m resolution, and ≤ 50 m for most studies) (Figure 17). Aerial multispectral images appeared in the 1990s and peaked during the 2000s. The use of high resolution satellite data (≤ 10 m such as IKONOS, SPOT 5 and WorldView) started in the late 1990s and reached a plateau around 2010. The use of LiDAR data consistently increased during the 2000s, accounting for 20% of studies using remote sensing for riparian vegetation in 2017. The use of UAV images sharply increased in the 2010s. As the use of these technologies increased, the percentage of studies using RGB/GS aerial images and low resolution satellite images decreased slightly. Overall, less than 2% of studies used RADAR data. Their use peaked in the early 2000s and then decreased.

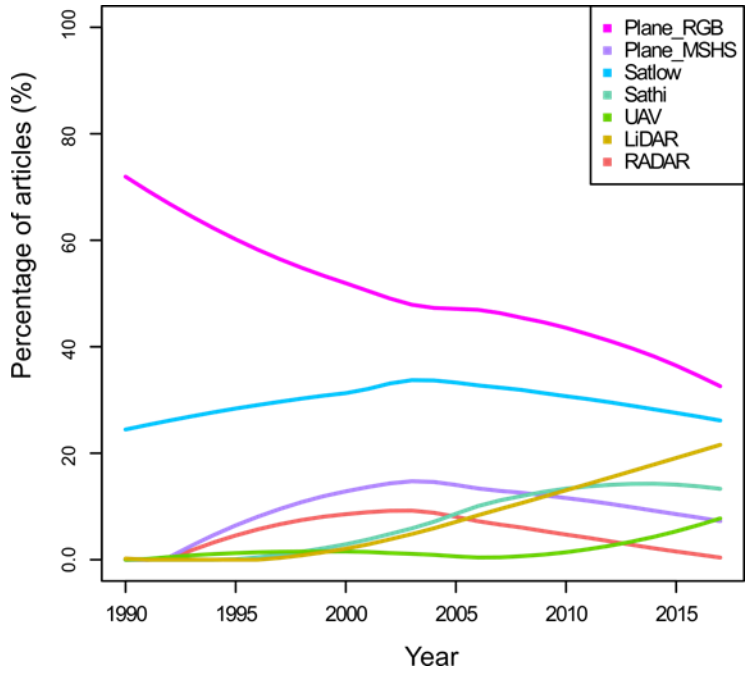

Figure 17: Percentage of studies that used a given technology per year. The curve was smoothed using a loess regression.

The popularity of RGB/GS aerial and low resolution satellite images can be explained by their low cost and wide availability, including as time series. Other data have been used as they became available (e.g. LiDAR and high resolution satellite images in the 2000s, UAVs in the 2010, with earlier appearances corresponding to captive balloons that were assimilated to UAVs). The relative decrease in the use of multispectral aerial images could be due to their replacement by high resolution satellite images. Finally, the low percentage in the use of RADAR data could be due to the relative difficulty of interpretation of such data, especially as water surfaces can modify RADAR signals. Most studies in our database that used RADAR data focused on the interaction between water and riparian vegetation, mapping flooding events or roughness coefficients (Townsend, 2002). The early decrease in the use of RADAR data coincides with the increase in the use of LiDAR data, which also provide structural information.

2.3.4 **Which technology for which study scale?**

There was a strong relationship between the scale of the study (local to very large scale) and the type of remote sensing data used (Figure 18). In general, aerial images were used more at relatively local scales (i.e. local and river segment), while medium-resolution satellite images were used more at larger scales (i.e. regional or very large scale). There is often a tradeoff between resolution and coverage: UAVs

can produce images with centimetric resolution but struggle to cover large areas, while satellites such as Landsat and MODIS provide images at a lower resolution (30 m for Landsat, 250 m for MODIS) but can cover large areas.

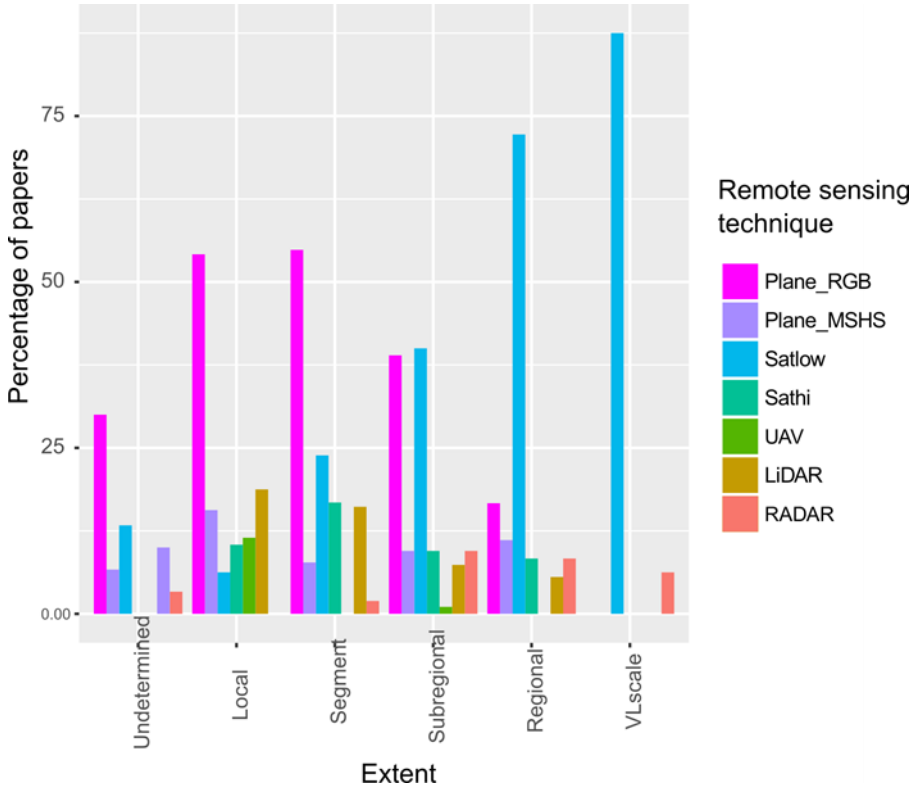

Figure 18: Percentage of studies that used a given remote sensing technology, by spatial extent of the study.

2.3.4.1 Use of UAVs at the local scale

At the local scale (< 10 km long), 86% of studies were based on airborne remote sensing (of which 79% used airplanes and 11% used UAVs). This scale of study lies within the range of action of relatively inexpensive UAVs that can carry RGB and multispectral cameras. While most UAVs were used at the local scale, the low percentage of local scale studies that used UAVs was surprising. This can be explained by the recent availability of these platforms: of studies published in the 2010s, 20% of those at the local scale used UAVs. UAVs are considered more versatile than planes, and a growing number of "ready-to-fly" platforms allow end-users to perform their own acquisitions (Anderson and Gaston, 2013). Moreover, UAV imagery provides very high spatial resolution imagery (up to centimetric), which is ideal for operator photointerpretation, which is frequently used at this scale.

However, most developed countries have established regulations that restrict the potential and spread of UAV technology (Stöcker *et al.*, 2017).

2.3.4.2 Use of airplanes and satellites at the segment and subregional scales

Both airborne and spaceborne sensors were used at the segment (10-100 km) and subregional scales (100-1000 km). RGB/GS aerial images were used in 55% and 39% of studies at respectively the river-segment and subregional scale (Figure 18). Most researchers photointerpret these images to describe riparian vegetation features. This method is long-standing, but remains a relevant and effective approach to map riparian vegetation over small watersheds or along dozens (more rarely hundreds) of km of rivers (Jansen and Backx, 1998; Matsuura and Suzuki, 2013; Carli and Bayley, 2015; González del Tánago *et al.*, 2015; Solins *et al.*, 2018). However, photointerpretation of hundreds of km of river can become tedious. In this case, one would use more automated approaches, such as object-based approaches, which can decrease the time required for photointerpretation (Belletti *et al.*, 2015).

The effectiveness of automated techniques is strongly correlated with the homogeneity of spectral signatures within a single feature class (Cushnie, 1987). Homogeneity in spectral signatures requires homogeneous atmospheric and illumination conditions within the dataset. To this end, airplanes equipped with multispectral cameras can be used over long river segments in a short period to avoid variations in weather and illumination conditions (Forzieri *et al.*, 2013; Bucha and Slávik, 2013). However, this approach remains challenging for large river networks, which decreases the possibility of automation at these scales (Dauwalter *et al.*, 2015).

In this context, the wider swath of satellite imagery would be an advantage. High-resolution satellite images were often used to map vegetation automatically (16% and 9% of studies at respectively the river-segment and subregional scale) (Figure 18). For example, Strasser and Lang (2015), Riedler *et al.* (2015) and Doody *et al.* (2014) used WorldView-2 data to map riparian vegetation along a few dozen km. Tormos *et al.* (2011) and Macfarlane *et al.* (2017) used SPOT images and GeoEye-1 images to map vegetation along corridors respectively 60 and 90 km long. However, it may be difficult to acquire high-quality datasets for larger areas, for which several high-resolution satellite images must be combined (Goetz, 2002; Johansen *et al.*, 2010b; Zogaris *et al.*, 2015).

The percentage of studies based on LiDAR surveys decreased with scale: 19%, 16%, 7% and 6% of studies at respectively the local, river-segment, subregional and regional scale (Figure 18). However, some authors were able to use LiDAR data to monitor narrow riparian corridors over large areas (Johansen *et al.*, 2010; Michez *et al.*, 2017). One advantage of tri-dimensional LiDAR data is that they are less subject to changing atmospheric and lightning conditions during the survey than spectral data. Moreover, LiDAR coverage is becoming more frequent at the regional/national scale (Parent *et al.*, 2015; Wasser *et al.*, 2015; Shendryk *et al.*, 2016; Tompalski *et al.*, 2017). When an initial nationwide LiDAR survey is performed, digital aerial photogrammetry (DAP) can be used to further update LiDAR canopy height models

(CHMs). DAP CHMs can be produced from aerial images acquired on a regular basis by national or regional mapping agencies in several countries and can potentially provide vegetation height data at low additional cost (Michez *et al.*, 2017).

2.3.4.3 Large scale: satellite images

The use of satellite images with medium to coarse resolution (> 10 m) increased as the extent increased. For studies at the regional or very large scale, satellite images were used in respectively 72% and 82% of cases (Figure 18). Coarse-resolution images (> 100 m) were not used to study riparian vegetation, which often appears as linear or fragmented features (Gergel *et al.*, 2007). Medium-resolution images such as Landsat TM, ETM+ or OLI images are preferred. The use of these data to map riparian vegetation cover has yielded satisfying results in wide riparian corridors (Lattin *et al.*, 2004, Yousefi *et al.*, 2018). However, their resolution often becomes limiting in the case of narrow riparian corridors or small vegetation units that are a few Landsat pixels wide (Congalton *et al.*, 2002, Henshaw *et al.*, 2013). Although aerial images (multispectral, RGB and panchromatic) were used in 25% of studies at the regional scale, they were always used with medium-resolution satellite images (Fullerton *et al.*, 2006; Groeneveld and Watson, 2008; Claggett *et al.*, 2010). High-resolution satellite images, which were used in 8% of studies at the regional scale, were used mostly with pansharpening methods to enhance lower resolution satellite images (Seddon *et al.*, 2007; Staben and Evans, 2008; Scott *et al.*, 2009).

2.3.5 **Which technology for which riparian feature?**

The features of interest extracted from remote sensing data to describe riparian vegetation were strongly related to the type of remote sensing data (Figure 19). Four major trends emerged. First, the study of physiological processes (e.g. phenology, evapotranspiration and, to a lesser extent, health status) was strongly associated with the use of medium-resolution satellite images and large study extents. Second, the study of features or processes related to vegetation structure (shade, roughness, height) was strongly associated with the use of LiDAR data. Third, the study of features related to species composition was associated with the use of high-resolution multispectral images (acquired from satellites, planes or UAVs) or RGB/GS aerial images (especially for successional stages) and with small study extents. Fourth, the delineation of riparian vegetation was weakly associated with the use of RGB/GS aerial images or medium-resolution satellite images. These four trends are discussed in the following four sections.

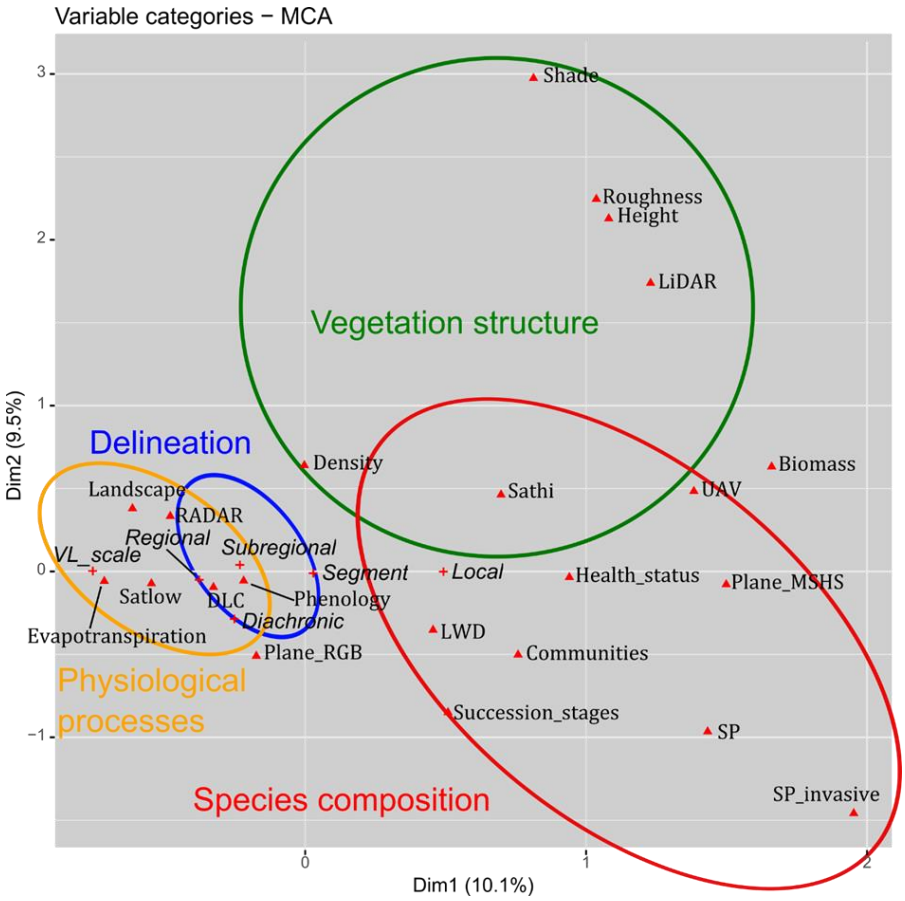

Figure 19: Results of the multiple correspondence analysis (see section 2.2.3 for the methods). Supplementary variables (i.e. variables related to study extent and multi-temporality) are represented as crosses with text in italics. The first two axes explain 19.6% of total variance. Ellipses were drawn arbitrarily to simplify interpretation. See Table 1 for code definitions.

2.3.5.1 Delineation of riparian vegetation

How riparian vegetation is delineated depends on how it is defined (Verry *et al.*, 2004). In general, riparian vegetation is defined based on its specific characteristics (e.g. spectral signature, texture) and on contextual information (e.g. topographic position, proximity to a river) (Weissteiner *et al.*, 2016). Photointerpretation of RGB/GS aerial images is a traditional approach in which the operator uses both types of information (Morgan *et al.*, 2010). It was used in 53% of studies that delineated riparian vegetation (Figure 20). Multispectral images (airborne or spaceborne, accounting for 45% of studies) are often used to delineate riparian vegetation in an automated way (Alaibakhsh *et al.*, 2017; Johansen *et al.*, 2010b; Bertoldi *et al.*, 2011). Contextual information can be provided by ancillary data (e.g.

hydrographic network, as in Claggett *et al.* (2010) or Yang (2007)), a LiDAR digital terrain model (DTM) (Arroyo *et al.*, 2010; Wagner-Lücker *et al.*, 2013), or a Shuttle RADAR Topography Mission DTM (Maillard and Alencar-Silva, 2013; Weissteiner *et al.*, 2016). Congalton *et al.* (2002) indicate that medium-resolution satellite data (used in 29% of studies) are not adapted for delineating narrow riparian corridors because the corridors do not contain enough pixels (see section 2.3.4.3).

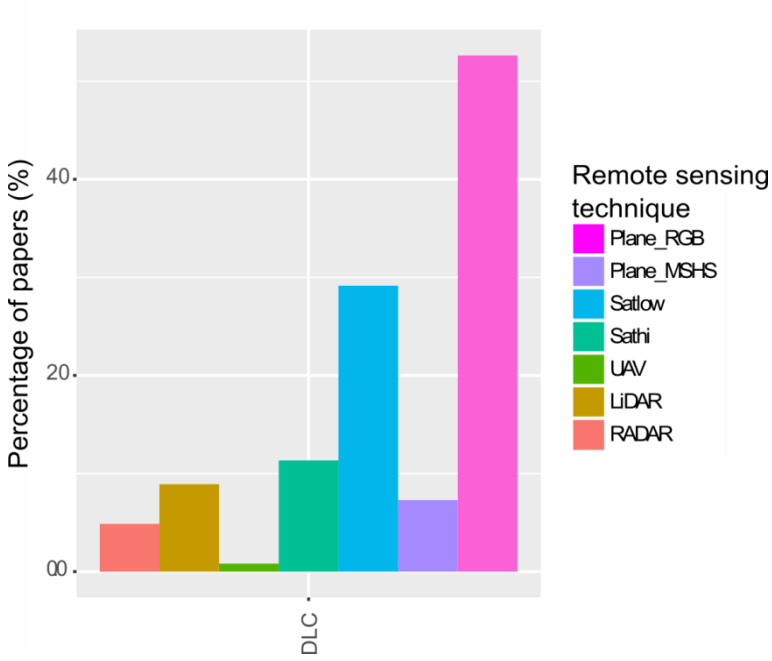

Figure 20: Percentage of studies that used given remote sensing data to delineate riparian vegetation (i.e. Distinguish riparian vegetation from other land-cover types)

2.3.5.2 Species composition

Species composition is a recurrent subject that was studied in 42% of studies. Photointerpretation of RGB/GS aerial images concerned 51%, 47% and 45% of studies that differentiated respectively communities, species, and invasive species (Figure 21). This approach is widely used to describe successional stages or changes in their distribution (86% of such studies). Indeed, RGB/GS aerial images have been available since before the 1950s (González *et al.*, 2010; Rood *et al.*, 2010; Varga *et al.*, 2013; Wan *et al.*, 2015). However, manual interpretation of images is time-consuming, and the discriminating power of RGB/GS aerial images is limited by their low spectral range (Narumalani *et al.*, 2009; Fernandes *et al.*, 2014). Medium-resolution satellite images were used in 21% of studies that differentiated communities. These images were used mainly when vegetation patches were larger than the image resolution (Vande Kamp *et al.*, 2013; Hamandawana and Chanda, 2013; Maruthi Sridhar *et al.*, 2010; Groeneveld and Watson, 2008; Townsend and

Walsh, 2001), although spectral unmixing can, to some extent, resolve this issue (Gong *et al.*, 2015; Wang *et al.*, 2013).

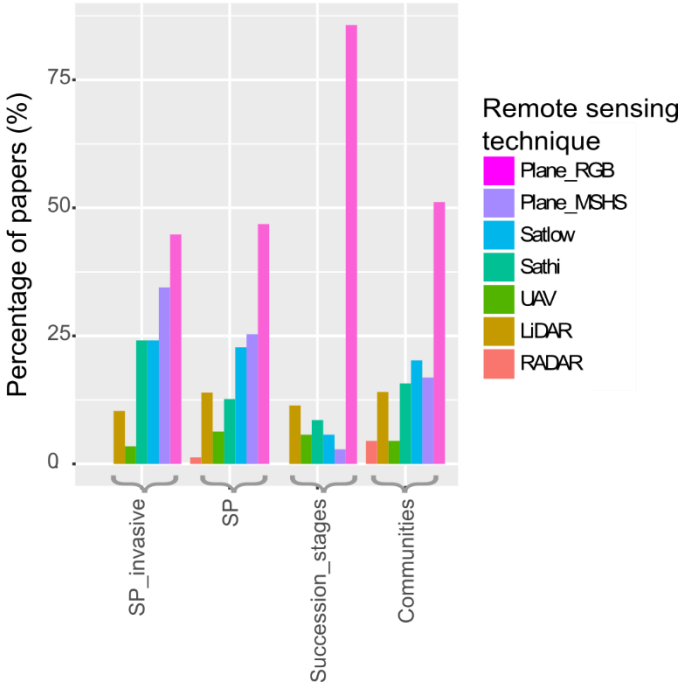

Figure 21: Percentage of studies that used given remote sensing data to map indicators related to species composition.

The most promising approaches to address this issue are based on high-resolution, aerial or spaceborne, multispectral or hyperspectral images. These images were used in 30%, 33% and 45% of studies that differentiated respectively communities, species and invasive species (Figure 21). The accuracy of a particular project depends on the context, objectives, available data and methods used to evaluate it. Therefore, we present recent studies that mapped species in the Table 2. In general, a large number of narrow spectral bands increases the ability to distinguish species. However, in mature, species-rich floodplain forests, it remains challenging to obtain classification accuracy that is satisfactory for operational use, even when using hyperspectral imagery (Richter *et al.*, 2016). The use of multi-temporal images, which reveal the succession of phenological stages, can sometimes replace the spectral range. For example, Rapinel *et al.* (2019) used Sentinel-2 time series to classify grassland plant communities in a temperate floodplain using the relationship between inundation, grassland management and vegetation composition. Similarly, Michez *et al.* (2016b) used UAV time series to distinguish riparian tree species using images acquired during several phenological stages (from spring to fall). It is

also possible to acquire images at a single but appropriate date to take advantage of the singular aspect of one species at a particular phenological stage. This approach is especially effective when a single species has to be mapped, such as the invasive species *Arundo donax* (Fernandes *et al.*, 2013b) or *Heracleum mantegazzianum* (Michez *et al.*, 2016a). The spatial resolution of images must be sufficiently high to limit the occurrence of mixed pixels that hinder the performance of automated classifications (Belluco *et al.*, 2006; Narumalani *et al.*, 2009). However, small mixture of species remains a source of difficulty, even with a cm resolution (Michez *et al.*, 2016a). LiDAR data, also used to classify species, can supplement multispectral data with vegetation height data (Forzieri *et al.*, 2013). They can also be used to segment trees before classifying them (Dutta *et al.*, 2016). They have also been used as the sole source of data by relating species identity to the structure of the point cloud (Laslier *et al.*, 2019a).

Table 2: Examples of remote sensing methods used to classify riparian species in different settings and their accuracy

Reference	Data	Classes	Accuracy	Comment
Mature riparian forests				
Fernandes *et al.* (2013a)	RGB-NIR aerial imagery (0.5 m resolution)	3 types of mature, temperate/Mediterranean riparian forests	61 (small) - 78% (large river)	
Dunford *et al.* (2009)	RGB imagery acquired with UAV (0.13 m resolution)	4 tree species (*Populus*, *Salix* and 2 *Pinus*) in a riparian Mediterranean forest	91% (for an image) - 71% (for a mosaic)	
Michez *et al.* (2016b)	RGB-NIR imagery acquired with UAV (0.1 m resolution)	5 tree species in a temperate, riparian forested/agricultural landscape	84 (forested) - 80% (agricultural)	Multi-temporal dataset
Richter *et al.* (2016)	Hyperspectral aerial imagery (367 bands, 2 m resolution)	10 tree species in a mature temperate floodplain forest	74% (single-date survey) - 78% (two-date survey)	
Dutta *et al.* (2016)	Hyperspectral aerial imagery (48 bands, 1 m resolution)	4 groups of tree species in a mature, temperate riparian forest	86%	LiDAR is used to segment the trees
Laslier *et al.* (2019a)	High density (> 45 points/m²) LiDAR point cloud	8 tree species in a temperate riparian agricultural/forested landscape	67%	
Pionneer/species-poor riparian settings				
Macfarlane *et al.* (2017)	Pansharpened GeoEye-1 imagery (RGB-NIR, 0.5 m resolution)	Pioneer (*Salix*, *Populus*) and invasive (*Tamarix*) species in an arid context	80%	

Forzieri *et al.* (2013)	RGB-NIR aerial imagery (0.2 m resolution); hyperspectral aerial imagery (102 bands, 3 m resolution) and LiDAR data (DSM/DTM with 1 m resolution)	Pioneer (*Salix*, *Populus*) and invasive (*Arundo donax*) species in a temperate context	93%	
Invasive species				
Narumalani *et al.* (2009	Hyperspectral aerial imagery (62 bands, 1.5 m resolution)	*Tamarix*, *Elaeagnus angustifolia*, *Cirsium arvense*, *Carduus nutans* and mixed classes	74%	Mixed classes are not well classified and decrease overall accuracy
Fernandes *et al.* (2014)	RGB-NIR aerial imagery (0.5 m resolution)	Arundo donax	97%	Choice of the best date for aerial survey
	WorldView 2 imagery (8 bands, 2 m resolution)	Arundo donax	95%	
Michez *et al.* (2016a)	RGB-NIR imagery acquired with UAV (0.05-0.1 m resolution)	Impatiens glandulifera	72%	Mixture with native species hinders accurate classification
		Heracleum mantegazzianum	97%	
		Fallopia japonica	68%	
Peerbhay et al (2016)	WorldView 2 imagery (8 bands, 2 m resolution)	Solanum mauritanum	68%	
Miao *et al.* (2011)	Hyperspectral aerial imagery (227 bands, 1 m resolution)	Prosopis glandulosa and Tamarix	92%	
Doody *et al.* (2014)	WorldView 2 imagery (8 bands, 2 m resolution)	Salix	93%	

These approaches based on high resolution data, although powerful, are mainly used at the local scale. We showed in the section 2.3.4.2 that upscaling such data was challenging beyond a few dozen km of river. However, at this scale, remote sensing would be a particularly useful alternative to field campaigns or photointerpretation. Species classification methods that are more robust to upscaling still need to be developed, as indicated by Fassnacht *et al.* (2016) in a review of forest tree species classification.

2.3.5.3 Physiological processes

Medium-resolution satellite images (> 10 m resolution and ≤ 50 m for most studies) were the most popular type of data used to assess physiological processes of riparian vegetation (100%, 73% and 54% of studies concerning respectively evapotranspiration, phenology and health status) (Figure 22). One advantage of using these images in this context is that they are often available as dense series, which is useful for studying cyclic processes. For example, Wallace *et al.* (2013) used AVHRR images (return period < 1 day) to detect variations in the timing of greening up/scenescing of vegetation. Nagler *et al.* (2012) used MODIS (return period 1-2 days) to study phases of the life cycle of the tamarix leaf beetle (*Diorhabda carinulata*) throughout the year. Cadol and Wine (2017) and Nagler *et al.* (2016) used long-term records (several years) of satellite images along with flow data to investigate relationships between hydrology and physiological processes in riparian vegetation. Zaimes *et al.* (2019) used a 27-year time series of Landsat images to study the impact of dam construction on vegetation health status. Sims and Colloff (2012) used MODIS images over several years to assess responses of riparian vegetation during and after flooding events. However, the low resolution often means that pixels in the image aggregate greater heterogeneity in ground features. Accuracy thus decreases, making it more complicated to study different types of vegetation separately (Tillack *et al.*, 2014; Cunningham *et al.*, 2018). The health status of vegetation is often studied with higher resolution data, occasionally with a single image (Tillack *et al.*, 2014; Michez *et al.*, 2016b; Bucha and Slávik, 2013; Shendryk *et al.*, 2016; Sankey *et al.*, 2016).

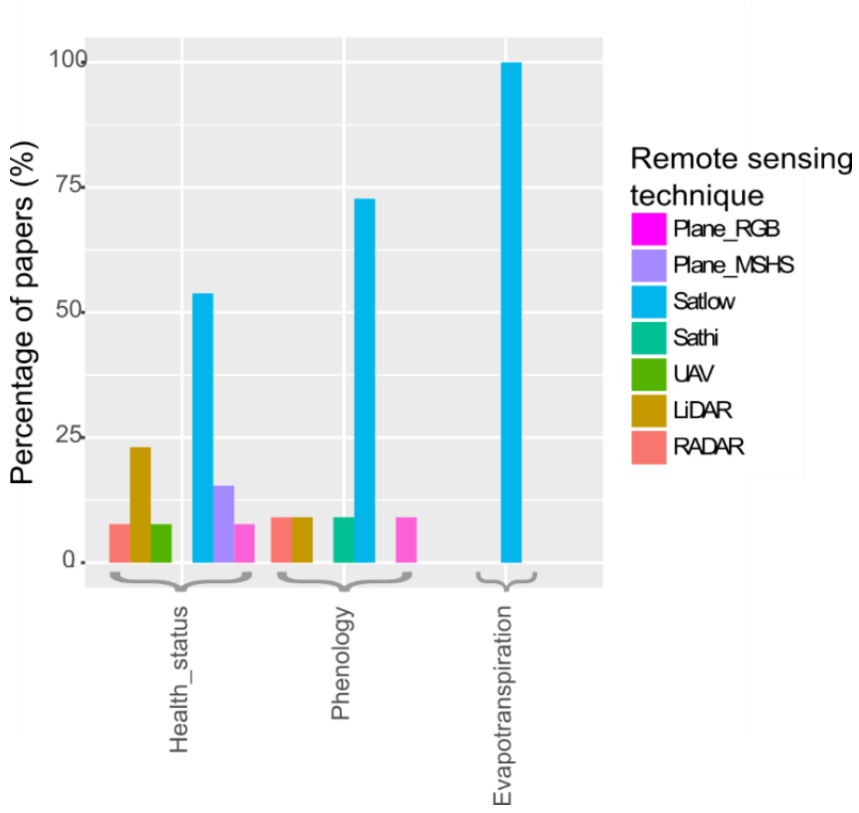

Figure 22: Percentage of studies that used given remote sensing data to describe physiological indicators.

2.3.5.4 Vegetation structure

LiDAR appears to be the most used technology for describing vegetation structure features, except for Large Woody Debris, landscape metrics and vegetation cover (Figure 23). LiDAR appears therefore to be the most promising technology for describing vegetation structure and related functions such as shading or surface roughness. The LiDAR signal can penetrate the canopy and the water surface, and provides information about topography under dense canopies, the internal structure of canopies and bathymetry.

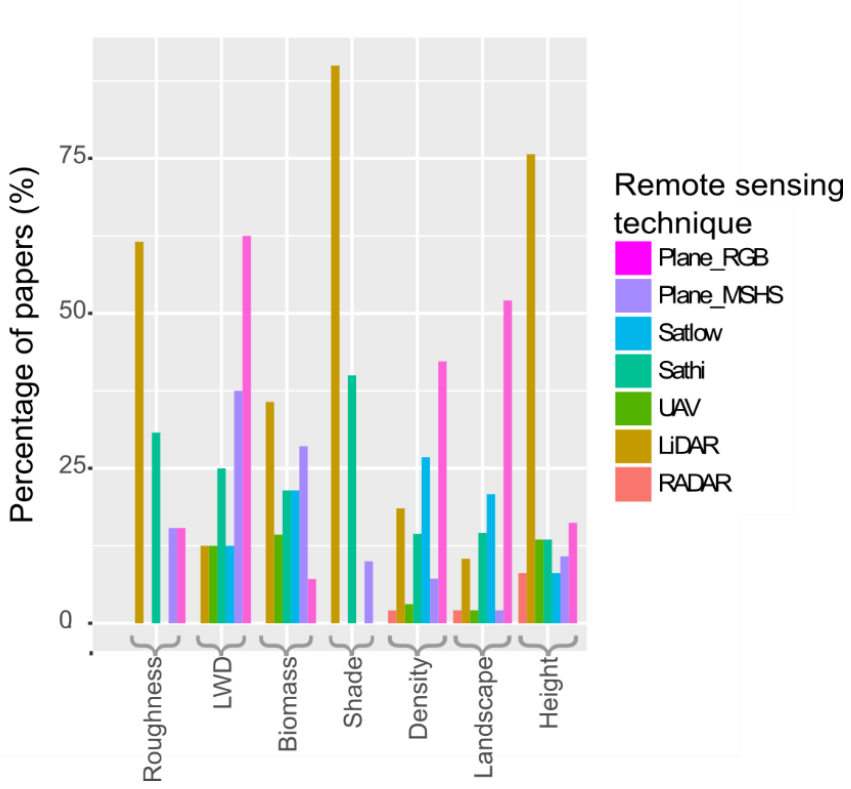

Figure 23: Percentage of studies that used given remote sensing data to map structural features of riparian vegetation.

Retrieving simple structural attributes of vegetation (e.g. height, continuity, overhanging character) is straightforward, since they can be extracted from DTMs, DSMs or CHMs delivered by LiDAR data producers. These applications have reached an operational level. However, further methodological developments for processing the 3D point cloud and new generations of full-waveform LiDAR data must be explored before they can be transferred to management operations. For example, full-waveform LiDAR data have shown promising results in forestry applications (e.g. Koenig and Höfle, 2016), but there are few examples for riparian vegetation (Shendryk *et al.*, 2016).

LiDAR data have been used in 90% of studies (Figure 23) to map riparian shade, which is a major parameter that influences stream water temperature (Poole and Berman, 2001). Temperature regulates the habitat of aquatic species such as the brown trout (*Salmo trutta fario* L.) (Caissie, 2006; Georges *et al.*, 2020), and the effect of riparian shade on stream water temperature is strong enough to affect aquatic communities significantly (Bowler *et al.*, 2012). Field methods used to measure stream shade are expensive and time-consuming (Rutherford *et al.*, 2018).

LiDAR data appears to be the most promising alternative because they can describe shade at a fine scale (Richardson *et al.*, 2019). Several methods for using LiDAR data to measure riparian shade have been described in the literature. Richardson *et al.* (2009) calculated light penetration index raster products as a predictor of light conditions. LiDAR data can describe shadowing properties using a simple CHM derived from point clouds (Michez *et al.*, 2017; Loicq *et al.*, 2018; Wawrzyniak *et al.*, 2017). Other studies have used 3D point clouds to retrieve the finest-scale information about vegetation structure. For example, Akasaka *et al.* (2010) used a LiDAR point cloud to estimate biomass overhanging the river, while Tompalski *et al.* (2017) used one to model solar shading on a given summer day. Recently, Shendryk *et al.* (2016) used full-waveform LiDAR data to estimate the dieback of individual riparian trees, which was related to their shadowing properties.

LiDAR data have also been used in 61% of studies to map floodplain roughness in a spatially continuous manner (Figure 23). Forzieri *et al.* (2012) distinguished two main approaches for mapping floodplain roughness using remote sensing: classification-derived mapping and hydrodynamic modeling. In the former, thematic maps of land cover or vegetation classes are produced with remote sensing data. A roughness coefficient (often Manning's coefficient) is then assigned to each class using a lookup table. In the latter, hydrodynamic properties of vegetation are estimated using an indicator of vegetation structure (e.g. leaf area index, stem or crown diameter, vegetation height). LiDAR technology has several advantages in this case: it measures structural attributes directly and can account for complex, multilayered structures (Manners *et al.*, 2013; Jalonen *et al.*, 2015). Hydrodynamic modeling is often combined with classification-derived mapping, with separate modeling of hydrodynamic properties of each vegetation class (Straatsma and Baptist, 2008; Zahidi *et al.*, 2018). Development of restoration and multi-objective management practices (to promote ecosystem health while protecting people and goods) has increased demand for models that represent effects of vegetation on flow more accurately (Rubol *et al.*, 2018). However, research on hydrodynamic properties of vegetation and how to measure them in the field is ongoing (Shields *et al.*, 2017).

2.3.6 **Multi-temporality of remote sensing riparian studies**

Overall, 54% of studies in the database were multi-temporal (i.e. studies where data acquired at several dates are used to understand the dynamics of riparian vegetation). RGB/GS aerial images were used in more than 60% of the multi-temporal studies (Figure 24B), such as those of Dufour *et al.* (2015) or Lallias-Tacon *et al.* (2017). Such studies usually focus on decadal time scales. It can be explained by the fact that this type of images is simple to use and has been available over a large extent since the 1950s (Dufour *et al.*, 2012). In most of the countries previously highlighted as active in riparian research, public administrations have performed long-term and systematic national aerial surveys for general purposes (e.g. urban planning) that researchers can use at low cost. Most multi-temporal studies that included aerial photographs used photointerpretation to describe riparian

vegetation features. Medium resolution satellite images were often used in multi-temporal studies, notably for the study of physiological processes (see section 2.3.5.3).

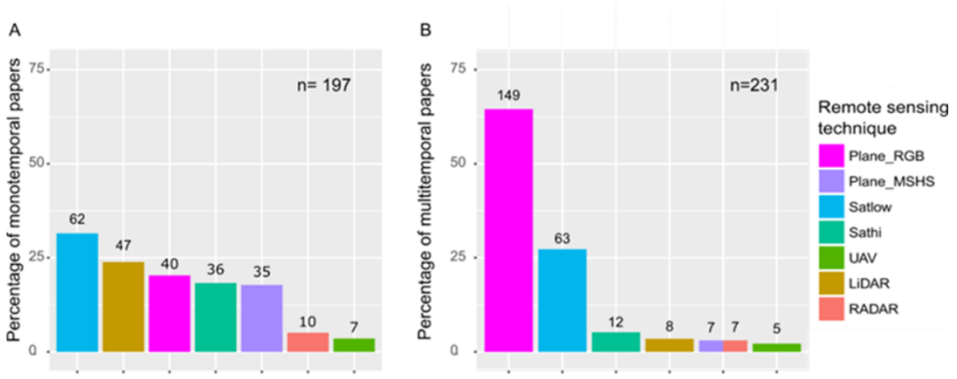

Figure 24: Use of remote sensing data in (A) mono-temporal and (B) multi-temporal studies (respectively 46% and 54% of the studies).

Conversely, more recent technologies (e.g. high-resolution satellite images, LiDAR data) were far more common in studies that focused on one period than in multi-temporal studies (Figure 24A). For example, LiDAR and high-resolution satellite data were used in respectively 24% and 18% of mono-temporal studies against 4% and 5% of multi-temporal studies. In mono-temporal studies, the methods developed to map riparian forest attributes were more complex and mostly automated, such as supervised classifications (Michez *et al.*, 2016b; Antonarakis *et al.*, 2008) and calculation of metrics (Riedler *et al.*, 2015).

We predict that diachronic analyses will be renewed by the increasing quality and availability of remote sensing data. Indeed, data acquired from new sensors, such as LiDAR and hyperspectral sensors, become more and more available as time series. For example, a LiDAR survey covers the entire region of Wallonia (southern Belgium) every six years. In France, in the framework of the Litto3D program, ca. 45,000 km² of coast (bathymetry included) will be regularly covered with a dense LiDAR survey, in order to monitor sediment dynamics and erosion processes. These new data provide the opportunity to monitor changes in specific features of riparian vegetation, such as canopy height, species composition or fine scale physiological processes. In addition, acquisition frequency has increased. For example, UAVs can acquire dense time series easily. High-resolution satellite images such as Sentinel-1 and Sentinel-2 (four bands at 10 m resolution) provide images of the Earth's entire surface every few days. More recently, CubeSat constellations provide higher resolution and higher frequency. For example, the Dove constellation (Planet Labs, Inc., San Francisco, CA, USA) provides resolution up to 3 m and daily coverage. This increased frequency of image acquisition provides new opportunities to study

rapid riparian vegetation processes, including intra-annual ones such as phenology and impacts of flood events.

2.4 Perspectives for riparian vegetation management

The second objective of this review was to discuss how remote sensing approaches developed by scientists can be used by riparian managers. Research in remote sensing of riparian vegetation often has an applied perspective, and 38% of the abstracts in our database contained the words "management", "restoration" or their derivatives. However, scientific articles usually do not describe how remote sensing developments are made available to managers, and how they can be implemented in management situations.

Therefore, we completed our systematic review of the literature with an approach based on expert judgment, focusing on how remote sensing developments can be valued as operational tools available to managers. In section 2.4.1, we selected five examples of applications for riparian management. For each example, we highlight how remote sensing approaches can be embedded in operational tools, and how scientific developments (previously discussed in section 2.3) can contribute to these tools. In section 2.4.2, we further discuss the challenges of knowledge transfer from scientists to managers, illustrated by the five selected examples.

2.4.1 **Examples of near-operational applications**

We chose three contrasting fields of applications that we considered as particularly relevant for the riparian context: eradication of invasive plant species, monitoring ecological integrity at the regional scale and maintenance of hydraulic conveyance.

2.4.1.1 Example 1: Managing invasive plant species at the local scale

Riparian managers often conduct programs to eradicate invasive plant species. These programs require identifying and locating individuals prior to eradication measures and subsequent monitoring of invasive cover (i.e. to ensure that practices were effective and that the species do not re-emerge) (Vaz *et al.*, 2018). These actions can be performed with UAVs that combine high spatial resolution (useful for detecting invasive plant species at an early stage, before they form large clumps) and high temporal resolution (invasive plant species are often more distinct from the background during a particular phenological phase, according to Manfreda *et al.* (2018)). Many studies have shown that detecting invasive plant species using a UAV could outperform ground surveys in terms of cost, effectiveness and risk mitigation for operators (Martin *et al.*, 2018; Michez *et al.*, 2016a). The detection of invasive plants can be performed using photo-interpretation (most simple method) or a supervised classification (most scalable method) of orthoimages (Hill *et al.*, 2017). In the future, real-time or onboard processing (i.e. analysis of streamed imagery) will enable detection and eradication steps to be performed at the same time (Hill and Babbar-Sebens, 2019).

In order to implement this approach, river managers must have access to skilled staff who are able to pilot the UAV and process the images based on the needs of

riparian managers. The staff can be recruited and trained within the organization, or work for an exterior contracting organization. For invasive species, work is often concentrated in time, and skilled staff must be available at that time.

2.4.1.2 Examples 2 and 3: Monitoring ecological integrity at the regional scale

Managers of riparian vegetation at the regional or national scale sometimes need information about the entire river network to assess effects of policies or define management strategies (e.g. to prioritize which zones should be restored). For example, all EU member states must monitor the state of riparian ecosystems to comply with the Water Framework Directive (WFD), which promotes a good health status of European rivers. These assessments have historically been performed during field visits to sites sampled throughout each river network (Hering *et al.*, 2010; Munné *et al.*, 2003). They can include remote sensing techniques in different ways. We briefly present two contrasting approaches to include remote sensing in ecological assessments: a sampling- and photointerpretation-based approach using aerial images, or the use of regional LiDAR data to map riparian structural attributes automatically.

In the first approach (hereinafter referred to as example 2), aerial images can be integrated with minor adaptations into a traditional field-based, sampling approach. Aerial images are used to target sampling sites (e.g. where riparian vegetation is present) and to perform certain aspects of the assessment, especially those that require less specific information at a larger scale. For example, the Riparian Quality Index, initially developed for Iberian rivers, includes measurements of width, continuity, strata, composition, regeneration, bank condition, lateral connectivity and substratum (González del Tánago and García de Jalón, 2011). Width, continuity and strata can be described using aerial imagery, while other attributes are assessed in the field.

In the second approach (hereinafter referred to as example 3), regional LiDAR data can be used to assess riparian features in a spatially continuous manner. In this case, the strength of LiDAR data is that the 3D component is homogenous at the regional scale unlike spectral data (see section 2.3.4.2). Moreover, it can extract attributes of the channel even when it is hidden by vegetation. Riparian attributes are calculated with a high level of automation and can be updated at the same frequency as the actualization frequency of the LiDAR cover. For example, in Wallonia (southern Belgium), Michez *et al.* (2017) used LiDAR and photogrammetric point clouds to map riparian buffer attributes along 12,000 km of rivers (vegetation continuity, height and overhang; channel width and sinuosity; and lateral connectivity, indicated by emerged channel depth). The results are meant to be used as decision making tools by river managers. They are made available on an online platform, where river managers must plan their management practices for a six year period.

2.4.1.3 Examples 4 and 5: Improving flood modeling with better estimates of floodplain roughness

Many regions of the world must address significant and increasing threats of flooding, as well as the need to conserve riparian ecosystems (Straatsma *et al.*, 2019). Floodplain vegetation can influence flood risk by increasing hydraulic roughness (Curran and Hession, 2013). In the Netherlands, where these challenges are particularly acute, several remote sensing applications integrate riparian vegetation management more into flood mitigation strategies.

One example (hereinafter referred to as example 4) includes a legal map produced to describe the maximum roughness of vegetation cover allowed within the floodplains of major Dutch rivers. The legal map uses a historical situation as a target reference (Rijkswaterstaat, 2014). To support use of this legal map, Deltares (an independent applied research institute) and the Rijkswaterstaat (the administration responsible for river management) developed an online vegetation-mapping tool based on free multispectral, high-resolution satellite images. In the Google Earth Engine environment, users can easily classify the vegetation cover observed on recent Sentinel-2 images to ensure that it complies with the legal standard. The tool is available on smartphones and can be used in the field. Actual vegetation can be compared to the map before each winter, when most floods occur. The tool provides information about the areas on which management practices should focus, following a dialogue with the landowners concerned (Penning, 2018).

Modeling approaches are also useful to support decisions. To prevent flood damage in Dutch deltas, multiple practices, such as raising dikes or removing riparian vegetation, must be implemented in a coordinated manner. Straatsma and Kleinhans (2018) developed the RiverScape toolbox. This tool models the effects of riparian cutting on flow using hydrological and spatial data (including a DTM, a vegetation map and its associated roughness coefficients). The RiverScape toolbox (hereinafter referred to as example 5) can optimize the location of cutting operations to reduce water levels during floods.

2.4.2 **Challenges of conveying tools to managers**

The five examples given in the previous section illustrate that remote sensing approaches can be embedded in operational tools for riparian managers. In this section, we discuss more generally how scientists and managers can collaborate to produce and implement such tools for the management of riparian vegetation.

We distinguish three main steps in this process (Figure 25). First, managers and remote sensing experts must work together to define clear **objectives**. Second, the **development** step implies a technological phase. Third, thorough **assessment** must be performed for accuracy, reliability and relevance for managers. **Critical thinking** is required throughout this process because the choice of a remote sensing approach is not neutral and has implications for how riparian vegetation is managed.

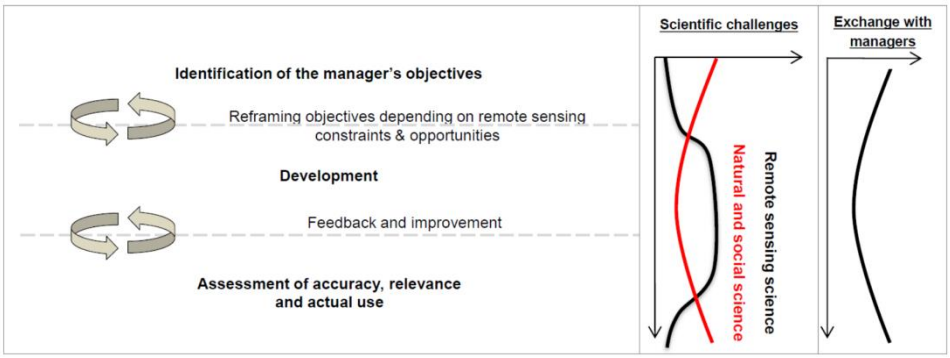

Figure 25: Conceptual framework of the transfer of remote sensing tools from scientists to managers. On the graphics to the right, the horizontal axes represent scientific challenge and exchange degree to be planned between managers and researchers (from low to high), while the vertical axes represent their dynamics from start to finish.

2.4.2.1 Identifying the issues/needs of riparian vegetation managers

The first step in implementing a remotely sensed application is to define the needs and objectives of riparian vegetation managers. Key issues must be addressed, such as the features to be mapped, the scale of observation, the time required to obtain usable information and the frequency of updating. Objectives can be refined during the development step, depending on the tradeoffs between costs and image quality. Nevertheless, thoroughly defining the objectives beforehand is clearly a factor of success (Kennedy *et al.*, 2009). In the example 1 (use of UAVs to help eradicate invasive species, section 2.4.1.1), it is often easier to detect plants at a particular phenological phase. For instance, *H. Mantegazzianum* is easier to detect while flowering, thanks to its characteristic white umbels (Michez et al, 2016a). While this detection period might be appropriate for scientific purposes, it does not fully satisfy eradication requirements, since individuals must be removed before they form fruit, which leaves little time for eradicators to remove them. One must consider that kind of details when developing operational tools for management.

The thorough definition of objectives is not straightforward. To translate monitoring objectives into a remote sensing approach requires an explicit space for collaboration between remote sensing specialists and managers (Kennedy *et al.*, 2009). Managers are often unsure about the operational potential of remote sensing approaches (Vanden Borre *et al.*, 2011). This is increasingly true, since new technologies (e.g. satellites, UAVs) seem to be developed very quickly, and even faster than the applications for using them. Therefore, realistic monitoring objectives must be defined along with remote sensing specialists. Moreover, field and remote sensing approaches often are not perfectly interchangeable (Dufour *et al.*, 2012). Challenging the work routine of managers might be required to fully benefit from remote sensing approaches. The collaborative process should thus be open enough to

consider adapting work routines. Similarly, when relevant, managers and scientists from different fields must be involved. It is important to combine a variety of scientific perspectives (e.g. geomatic, landscape planning, riparian ecology) to avoid too narrow or inappropriate solutions.

In many cases at this stage, riparian vegetation is not the center of management operations. Many studies and management operations focus on the river channel and its hydrological and geomorphological components. In the example 5 (modeling the impact of management practices on flood hazard, section 2.4.1.3), the RiverScape toolbox does not only consider riparian cuttings but also raising dykes or lowering floodplain level.

2.4.2.2 Developing applications that use remote sensing data

Once the objectives have been clearly identified, the next step is to develop the solution to use remote sensing data to pursue the manager's objectives. Several stakeholders are involved in this process. We artificially distinguish "data producers" from the "developers".

We consider "data producers" the stakeholders who provide rough datasets, such as raw satellite images or raw ancillary data (e.g. national space agencies such as NASA and CNES, UAV constructors). While they do not interact closely with riparian vegetation managers, their role is important in the long run since they set the agenda for the main future developments of new remote sensing technologies. More directly, they can promote the use of remote sensing data for natural resource managers by making the data affordable and easier to use, as mentioned in section 2.3.1. In the example 4 (floodplain roughness monitoring with Google Earth Engine, section 2.4.1.3), the classification of vegetation in the floodplain is made possible by the availability of free temporal series of Sentinel-2 images.

We consider "developers" the stakeholders who develop tools that use raw remote sensing data. They may interact more closely with riparian vegetation managers and provide solutions that are tailored to the latter's needs through the previously mentioned space for collaboration. The main stakeholders in this category are academic and research institutes, as well as commercial or non-academic organizations, which use remote sensing data. In theory, the needs identified define the type of stakeholders involved. For example, if the manager's issue has scientific relevance (e.g. understanding the spread of an invasive species not studied before), academics would logically be involved. If no scientific issue is identified, however, then commercial or non-academic organizations are more appropriate.

Simple remote sensing approaches can be sometimes be deployed with only minor investment, such as the monitoring of riparian quality attributes with aerial images described in the example 2 (section 2.4.1.2). However, the fixed costs of implementing a remote sensing approach are often relatively high and can be prohibitive for many local managers, even though free solutions increasingly appear on the market. These costs include designing the method, deploying the platform or acquiring the minimum number of satellite images and possibly training personnel. Moreover, performing certain analyses requires technical skills (e.g. object-based

image analysis, machine learning approaches, LiDAR full waveform analysis). Therefore, remote sensing could have greater relevance when the area to be mapped is large and/or the operation must be repeated several times (Johansen *et al.*, 2007). The approach deployed in the example 3 (monitoring river networks with LiDAR data) is efficient because it concerns 12.000 km of rivers and it is to be repeated every 6 years. However, many stakeholders with different objectives are generally involved, since riparian vegetation covers large geographical areas. This can reduce the potential for economies of scale, whether for river managers trying to develop their own expertise or for businesses offering their services. This narrow market provides relatively limited opportunities for companies to develop specific tools adapted for this vegetation type. Indeed, we do not expect specific UAV applications to become as developed for managing invasive species in riparian areas (see example 1 in section 2.4.1.1) as they are for precision agriculture.

To address the challenge of attaining "critical mass" for riparian vegetation, we suggest a more collaborative approach, as described by Steiniger and Hay (2009). Processing routines developed by remote sensing scientists could be embedded into OpenAccess toolboxes. To benefit a large audience, these tools must be robust by having little sensitivity to situations that differ slightly from those for which they were created. For managers to use them, they need to be flexible and integrate easily with other processing routines or platforms (e.g. GIS platforms) (Vanden Borre *et al.*, 2011). Finally, they should be based on widely available data: the tool presented in the example 4 (floodplain roughness monitoring using Sentinel images in the Netherlands, section 2.4.1.3) could potentially be replicated in many regions since Sentinel-2 images are available worldwide. OpenAccess tools for river or ecosystem management could be collected in community repositories along with other tools for river or ecosystem management, along with freely available datasets, as suggested by Tomsett and Leyland (2019) or Piégay et al (2020). These tools could form a foundation that commercial companies, researchers and managers could adapt to specific projects.

2.4.2.3 Assessment and feedback

The final step in conveying remote sensing tools to riparian managers involves accurate and effective assessment of the maps produced and the potential for future monitoring. Accuracy involves the statistical validity of the product, which is the conformity of the map to reference data (e.g. thematic accuracy, in the case of classification). This step is crucial because it indicates the extent to which the map can be trusted. Remote sensing specialists usually consider it a central element, although controversy remains on the reliability of popular accuracy assessment methods (Pontius and Millones, 2011). Moreover, users must be cautious when reproducing the method at another site, since accuracy is often assessed for small test sites, and robustness is often not assessed sufficiently (Fassnacht *et al.*, 2016).

However, the relevance of a remote sensing approach cannot be reduced to its accuracy. The relevance of the information for management purposes must consider the costs and benefits of obtaining such information (Kennedy *et al.*, 2009). We

argue that temporality should be considered when addressing this aspect. The true effectiveness of a tool is often observed long after it is first produced. Moreover, the issue of using remote sensing data in future monitoring (or not) must be considered. For example, after a restoration action, vegetation must be monitored in the short term (i.e. after one year) and the long term (i.e. after 5-10 years). Consequently, it is important to define which stakeholders are involved in this future monitoring (the initial producer of the map, the managers themselves or an external stakeholder) and which methods will be used. If managers are in charge of future monitoring, training should be provided. The example 2 (monitoring of riparian quality attributes with aerial images, see section 2.4.1.2) only requires basic training in GIS and photo-interpretation. However, for the example 3 (monitoring river networks with LiDAR data), training courses that include programming must be provided to river managers, in order to enable them to update riparian indicators based on future regional LiDAR coverage.

The ease of use of the tools developed and their integration into existing workflows are also central aspects determining whether a manager will adopt remote sensing tools (Vanden Borre *et al.*, 2011). We argue that it is crucial to obtain feedback from managers about the real use of the maps and features produced using remote sensing data. This feedback would help to develop tools that are more adapted to the managers' needs.

2.4.2.4 Issues beyond the remote sensing discipline

The development and use of remote sensing tools to manage riparian vegetation is not only a technical issue. It raises at least two particular issues that must be addressed in an interdisciplinary or even transdisciplinary manner. First, the information must be scientifically relevant from a thematic perspective. In the example 3 (section 2.4.1.2), LiDAR data make it possible to measure vegetation height or continuity. However, whether this information is sufficient or relevant to assess a particular function of riparian vegetation must be discussed with experts from different disciplines (e.g. ecologists, hydrologists). Second, critical feedback about the use of remote sensing tools is also needed afterwards. Using these tools to assess environmental patterns and processes or to map natural resources is clearly not neutral. In some cases, these methods exclude certain stakeholders who do not have access to the technology, limit the understanding of certain complex phenomena and generate controversial data (e.g. Fairhead and Leach, 1998; Harwell, 2000; Turner and Taylor, 2003; Rajão, 2013). In the example 5 (section 2.4.1.3), the RiverScape tool helps managers finding the best location for practices that aim to reduce flood hazard. However, the tool is not meant to be used alone to make decisions. Within a larger governance system, it can help stakeholders find a common ground through providing a large scale perspective, and through highlighting tradeoffs between stakes and stakeholders (Straatsma et al, 2019). More generally, sociological and cultural effects must be understood, and adverse effects of using remote sensing for natural resource management should be properly handled. Social scientists should be involved throughout the process to address these issues.

2.5 Conclusion

We found a substantial body of literature in which remote sensing was used to study riparian vegetation. Remote sensing became considerably popular at the turn of the millennium, but its relative use in riparian vegetation studies remains limited (ca. 4%), and mostly in developed countries. In order to increase the user base, scientists can develop approaches that are robust to slight context changes and that take advantage of widely available data. These approaches can be embedded in Open Access or easy-to-use tools. The production, dissemination and use of large or global datasets concerning rivers, floodplains or land cover should also be promoted.

Development of new sensors and platforms has improved remote sensing approaches. However, most studies that use newer sensors and platforms focus on the local-to-river segment scale. Large-scale studies are based on medium-resolution satellite images. Algorithms are needed to process high-resolution data that is robust to upscaling. Spectral heterogeneity makes upscaling the study of species composition using spectral data more challenging than upscaling the study of vegetation structure using 3D data.

Riparian vegetation is highly dynamic, and the multi-temporal nature of riparian remote sensing studies is central (54 % of studies are multi-temporal). To date, diachronic analyses have relied essentially on aerial photographs, and it is clear that these data will remain popular given their availability and simplicity of use. However, other data time series become increasingly available. Scientists should test using these data to study complex and subtle phenomena, beyond changes in the extent of riparian forests or plant succession. For example, temporal series of LiDAR data should be tested to map subtle changes in vegetation structure such as growth, regeneration or senescence. Higher resolution or more frequent satellite images could help understand physiological or community responses of riparian vegetation to environmental stress over large extents, yet at a finer spatial or temporal scale than before.

It is often suggested that remote sensing approaches can contribute to management of riparian vegetation by providing objective, continuous and up-to-date data for a large area. This contribution was difficult to determine via a review of the scientific literature, and an extensive review of the gray literature could provide further insight into this subject. However, there are many examples of operational or near-operational applications, not only with aerial images but also with more recent data (LiDAR, UAVs and satellite images). We suggest that a collaborative effort is required to make remote sensing approaches more robust and available, both in terms of cost and ease of use. However, implementing a remote sensing approach in actual management context still requires a tailored approach. It must include managers and scientists (thematicians and remote sensing scientists), be structured around well-defined objectives and include sufficient feedback.

Acknowledgement

The collaboration that led to the writing of this article was initiated during a short term scientific mission financed by the Converges COST action (CA16208). This work received financial support from the Province of Liège, the Province of Luxembourg and the Agence de l'eau Seine Normandie.

3

What factors shape spatial distribution of biomass in riparian forests? Insights from a LiDAR survey over a large area.

Foreword

This chapter presents a method for mapping woody biomass in riparian forests using LiDAR data. The method is deployed at the scale of 230 km of rivers and their floodplain (Semois-Chiers basin, which will also be studied in Chapters 4 and 5). The spatial organization of this biomass is also analyzed in relation to variables such as time since last disturbance, land use, topographical position or pedology.

Biomass is a quantitative and synthetic indicator of riparian vegetation. It is one of the main characteristics of riparian vegetation alongside specific composition (a qualitative indicator), which will be discussed in Chapter 4. The joint use of these indicators to prioritize management operations will be discussed in chapter 6 (section 6.2.1).

Reference (Chapter adapted from publication)

Huylenbroeck, L., Latte, N., Lejeune, P., Georges, B., Claessens, H., & Michez, A. (2021). What factors shape spatial distribution of biomass in riparian forests? Insights from a LiDAR survey over a large area. *Forests*, *12*(3), 371.

Abstract

Riparian ecosystems are home to a remarkable biodiversity, but have been degraded in many regions of the world. Vegetation biomass is central to several key functions of riparian systems. It is influenced by multiple factors, such as soil waterlogging, sediment input, flood, and human disturbance. However, knowledge is lacking on how these factors interact to shape spatial distribution of biomass in riparian forests. In this study, LiDAR data were used in an individual tree approach to map the aboveground biomass in riparian forests along 200 km of rivers in the Meuse catchment, in southern Belgium (Western Europe). Two approaches were tested, relying either on a LiDAR Canopy Height Model alone or in conjunction with a LiDAR point cloud. Cross-validated biomass relative mean square error for 0.3 ha plots were, respectively, 27% and 22% for the two approaches. Spatial distribution of biomass patterns were driven by parcel history (and particularly vegetation age), followed by land use and topographical or geomorphological variables. Overall, anthropogenic factors were dominant over natural factors. However, vegetation patches located in the lower parts of the riparian zone exhibited a lower biomass than those in higher locations at the same age, presumably due to a combination of a more intense disturbance regime and more limiting growing conditions in the lower parts of the riparian zone. Similar approaches to ours could be deployed in other regions in order to better understand how biomass distribution patterns vary according to the climatic, geological or cultural contexts.

3.1 Introduction

Riparian ecosystems are ecotones where rivers and upland areas influence one another. They host specific plant communities related to water proximity and availability, soil anoxia or flood disturbance. They are home to an exceptional biodiversity (Naiman *et al.*, 1993), and riparian vegetation produces numerous ecosystem services concerning water quality, flow regulation or erosion mitigation (Riis *et al.*, 2020). However, they are subject to multiple pressures and have been degraded in many regions of the world (Stella and Bendix, 2019). Consequently, there has been a particular interest for several decades in the conservation or restoration of these ecosystems (Gonzàlez *et al.*, 2015).

Dybala *et al.* (2019b) and Matzek *et al.* (2018) pointed out that carbon storage for climate change mitigation could be a co-benefit of conservation or restoration policies that promote biodiversity. Indeed, vegetation biomass, which is one of the largest compartments for carbon storage in riparian ecosystems (Sutfin *et al.*, 2016), is related to other key biophysical functions of riparian ecosystems. For example, vegetation biomass drives the production of large woody debris, which is a key process influencing habitat complexity, hydraulic and sedimentary processes (Balian and Naiman, 2005; Keeton *et al.*, 2007). Vegetation biomass also has tremendous effects on nutrient cycling in the ecosystem (Dosskey *et al.*, 2010; Tufekcioglu *et al.*, 2003). More generally, biomass is a component of forest structure, which itself influences sediment stabilization (Matzek *et al.*, 2020), hydraulic roughness (Forzieri *et al.*, 2012) or habitat provisioning (Dybala *et al.*, 2019a).

The amount of biomass in riparian vegetation depends primarily on productivity, vegetation type (e.g., tree longevity or wood density) and disturbance regime. Productivity of riparian vegetation is notably influenced by the interplay between water availability (Dufour *et al.*, 2008), soil anoxia occurring as a result of flooding or proximity to the water table (Megonigal *et al.*, 1997, Rodriguez-Gonzàlez *et al.*, 2010) or nutrient-rich sediment brought in during floods (Marks *et al.*, 2020). Disturbances related to flooding and erosion (Kramer *et al.*, 2008), beavers (Wohl *et al.*, 2012), livestock (Lucas *et al.*, 2014), or anthropogenic disturbances related to agriculture and forestry (Michez *et al.*, 2017; Wasser *et al.*, 2015; da Silva *et al.*, 2017) notably reduce vegetation biomass. The aforementioned factors also influence the type of vegetation that establishes in one place, which in turn determines potential biomass storage, for example through tree longevity (Marks *et al.*, 2020). However, knowledge is lacking on how these factors interact to shape vegetation biomass distribution, and few studies have been carried out in Europe (Riis *et al.*, 2020; Matzek *et al.*, 2018; Dybala *et al.*, 2019b). Moreover, there is a lack of allometric equations for estimating tree biomass in riparian forests (Fernandes *et al.* 2020).

Remote sensing is widely used for estimating biomass over wide areas in a spatially continuous manner (Lu, 2006; Goetz and Dubayah, 2011). However, most studies in the riparian context have been limited to reaches a few kilometers long

(Huylenbroeck *et al.*, 2020), and used spectral data in classification-based approaches (Fernandes et al, 2020; Mendez-Estrella *et al.*, 2017; Husson *et al.*, 2014). Such approaches do not take into account the great spatial variability and continuum between different vegetation types in riparian systems. LiDAR (light detection and ranging) data have several advantages over spectral data for biomass estimation. They are less subject to saturation (Mitchard *et al.*, 2012; Filippi *et al.*, 2014; Forzieri, 2012; Suchenwirth *et al.*, 2014), and are suitable for direct biomass modeling (Fassnacht *et al.*, 2014). LiDAR data can be used to build digital terrain models (DTMs), which allow the heterogeneous topography of the riparian zone under the canopy to be observed, unlike spectral data. They are increasingly available, and have a strong potential for upscaling biomass estimates over hundreds to thousands kilometers of rivers (Huylenbroeck *et al.*, 2020). LiDAR data are often used as point clouds, where each point corresponds to a LiDAR return. This method requires some skills and is computationally intensive, but it enables studying the internal structure of the canopy (Laslier *et al.*, 2019a). For simplicity, LiDAR data are often preprocessed as a raster format CHM (Canopy Height Model), where each pixel represents the height of the canopy top. LiDAR data have proven to be effective for estimating biomass in different forest types (Zolkos *et al.*, 2013) and in a riparian context (Cartisano *et al.*, 2013). As compared to other forests, riparian forests have an original structure with multi-stemmed trees and shrubs (Karrenberg *et al.*, 2002), high species diversity (Naiman *et al.*, 2005), and a complex landscape organization with many linear patches. In this context, the high 2D and 3D resolution of LiDAR is a definite advantage, and biomass is preferably estimated using object-based approaches (with objects corresponding to trees or groups of trees), which are expected to improve performance and simplify field sampling in fragmented landscapes (Dalponte and Coomes, 2016).

Although promising, to our knowledge, object-oriented approaches based on LiDAR data have not been used to estimate biomass in riparian forests. Moreover, remote sensing has not been used to improve understanding of spatial distribution of biomass patterns in riparian ecosystems according to geomorphic and anthropogenic factors (related studies include Mendez-Estrella *et al.* (2017) and Cadol and Wine (2016), who used satellite data to map vegetation greenness in relation to geomorphic factors). The objectives of this article were as follows:

- To propose an approach to estimate aboveground biomass at tree level, and to compare two biomass estimates based on variables from a raster-format LiDAR CHM or from the original LiDAR point cloud;
- To highlight environmental factors structuring biomass distribution in riparian forests at a sub-regional scale (200 km of river and their riparian zone) in the context of low-energy temperate rivers (Meuse catchment, Western Europe).

3.2 Materials and Methods

3.2.1 **Study Area and Available Data**

The study area is located in Wallonia (southern Belgium), within the Meuse catchment area (Figure 26). It is a publicly managed area, comprising about 200 km of rivers mapped from the point where their catchment area reaches 50 km2. The studied rivers drain an area of about 1200 km2. Public management in the study area is limited to the bankfull channel of rivers, as well as vegetation or other structures in the channel. It encompasses all actions needed in the channel to promote its hydraulic, ecological and social functions such as logjam removal, bank reinforcement, riparian planting, etc. The study area can be divided into two main sub-basins. In the northern part of the study area, the Semois and its tributaries have a gravel bed, a gentle slope and frequently overflow in winter. Downstream, the Semois produces broad, steeply sloping meanders (Gob *et al.*, 2005). In the southern part, the Ton and its tributaries have sandy beds, flow into clayey plains and have a hydrological regime dominated by base flow. On the whole, these rivers have little activity and flow in a landscape of forests and meadows, where riparian forests are often reduced to a row of trees along the river. The most frequent tree species are alders (*Alnus glutinosa* (L.) Gaertner) and willows (including *Salix alba x fragilis* L., *S. viminalis* L., *S. caprea* L. and *S. aurita* L.), which are often multi-stemmed. Maple (*Acer pseudoplatanus* L.), ash (*Fraxinus excelsior* L.), oak (*Quercus robur* L.) and hornbeam (*Carpinus betulus* L.) are also common. Finally, even-aged spruce plantations (*Picea abies* (L.) Karst) can be found in the valley bottoms.

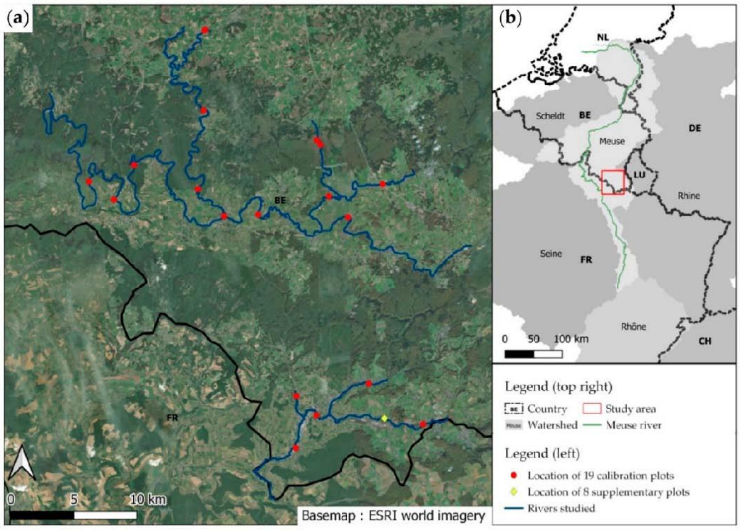

Figure 26: (a) Study area and inventory plots. (b) Location of study area within the Meuse catchment area.

The area was covered during the winter of 2014 by an aerial LiDAR survey. The survey was ordered by the Walloon administration over the entire Wallonia. The initial aim was to produce a DTM (Digital Terrain Model) that could then be used for multiple purposes. The acquisition was performed with a Riegl Litemapper 6800i, with a pulse repetition rate of 150 kHz and a maximum scan angle of 60◦. The flight altitude ranged from 1200 to 1500 m AGL and the flight speed was 75 m/s. Average point density was 0.8 to 1 ground return/m2. Point positions were corrected during post-processing using ground references, and the mean absolute error in planimetry was 0.12 m. The point cloud was classified using full wave and morphological analysis. One-meter-resolution DTM and DSM (digital surface model) were created using a Natural Neighbor interpolation, using points classified as "ground" and points with maximum altitude, respectively. Data were provided as a point cloud with a non-normalized intensity and as 1-m-resolution DTM and DSM. A CHM was created by subtracting the DTM to the DSM. Data can be obtained on request to the Walloon public service (Service Public de Wallonie, 2014).

The zone was also covered by recent (2012, 2015 and 2016) or old (several coverages since 1971) high-resolution orthophotos (<1 m). Finally, data from 17 gauging stations and models of the area flooded with a recurrence of 25 years were available throughout the area (Service Public de Wallonie, 2020). These models were produced by the regional administration using hydraulic models, hydrological statistics or field surveys, and cover the submerged areas approximately once every 25 years.

3.2.2 **Biomass Field Data and Equations**

The first step of the methodology aimed to obtain reliable biomass estimates for trees whose crown could be delineated on a LiDAR CHM. These estimates were subsequently used to calibrate a model based on LiDAR variables (see Section 3.2.3).

Nineteen plots were visited in 2016. Each plot was about 0.3 ha in size and located in the immediate vicinity of a river (Figure 26). While in the field, tree crowns were delineated on an orthophoto (year 2016, 25 cm in resolution) and the LiDAR CHM. Each delineated crown corresponded to the smallest unit that could be distinguished on images and linked to stems measured on the ground. A crown usually covered several stems (trees were often multi-stemmed). Species and diameter at breast height were described for all stems (DBH > 12 cm) under each crown. Stems that were not visible on aerial images were included in the crown that covered them. A total of 355 crowns were delineated, including 162 alders, 76 willows, 32 ashes, 25 maples, 18 oaks, 12 hornbeams and 32 other species.

The total wood volume of trees was estimated using volume equations for each stem separately (Figure 27). Volume equations relied on species, diameter and height data. Species and diameter were described in the field. The heights of dominant stems (whose canopies were visible from above) were estimated with the maximum height of the LiDAR CHM. The heights of suppressed stems or stems with aberrant LiDAR heights were modeled with Diameter-Height relationships,

computed on other riparian trees of known height. The Diameter-Height relationship was modeled for each tree species separately using a Chapman Richards curve, which is regularly used in this context (Corral-Rivas *et al.*, 2014; Ahmadi *et al.*; 2017). A different procedure was used to estimate total volume for alders and willows on one hand, and other species on the other.

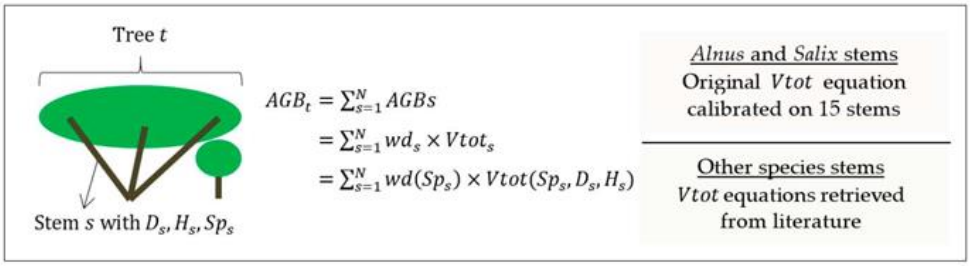

Figure 27: Diagram of the field estimation of tree biomass. t = tree index, s = stem index within the tree t, N = number of stems within the tree t, AGB = aboveground biomass, wd = wood density retrieved from Zanne *et al.* (2009), Vtot = total wood volume, Sp = species, D = diameter, H = tree height. A new total volume equation was developed in this study for Alnus and Salix. For other species, volume equations were retrieved from Dagnelie *et al.* (2013) and Longuetaud *et al.* (2013).

Alders and willows were the two most frequently encountered genera. However, volume equations for these genera are rare and, in the case of alders, mostly limited to single-stemmed trees growing in forests managed for wood production. To estimate the total volume of these two genera, specific equations were developed on trees felled for the study. The total volume was measured by dividing the stem into two compartments: the trunk and big branches down to 12 cm in diameter on one hand, and the trunk and branches beyond the 12 cm crosscut on the other hand (see Figure S1 in Supplementary Material). Wood volume within the first compartment was measured in a traditional way, with successive diameter measures along the stem. To estimate the volume of the trunk and branches less than 12 cm in diameter, the wood contained in this compartment was shredded and the volume of shredded wood was measured. An expansion coefficient was estimated by shredding a batch of wood of known solid volume. The total volume was thus measured for 15 stems. The volume within the trunk and branches down to 12 cm in circumference was measured on 54 supplementary stems to ensure that the 15 stems selected for the total volume measurements were representative. The Equation (1), which is commonly used in tree allometry (Zianis *et al.*, 2005), was fitted using the method of least squares:

$$\ln Vtot = a + b \times \ln D + c \times \ln H \quad (1)$$

where Vtot is the total wood volume, D the diameter at breast height (130 cm) and H the total height. The predictive bias associated with the log transformation was corrected by the coefficient of Baskerville (1972).

To estimate the total wood volume of other species, we used regional forest trunk and stump volume equations (Dagnelie *et al.*, 2013) and the volume expansion factors of Longuetaud *et al.* (2013) to estimate the total wood volume, which includes the volume of the stump, trunk and branches, following Equation (2):

$$Vtot = (Vd7 \times VEF + Vstump) \quad (2)$$

where Vd7 is the volume of the trunk until 7 cm in diameter (Dagnelie *et al.* 2013), Vstump the volume of the stump (Dagnelie *et al.*, 2013), and VEF the volume expansion factor Longuetaud *et al.* (2013). We systematically used double - entry equations (diameter and height), because the use of single-entry forest equations significantly overestimates the volume of riparian trees, which have a lower height than upland forest trees.

The conversion of total volume to biomass was carried out using the specific infra-density values presented in the database of Zanne *et al.* (2009), using the equation AGB = Vtot × wd, where AGB is the tree aboveground biomass and wd the wood infra-density.

In addition, aboveground biomass was estimated in eight additional plots about 0.3 ha each, using the same methods except that tree crowns were not delineated. These eight plots were used as complementary data for validation (see Section 3.2.5).

Figure 28 illustrates the ecosystems encountered throughout the study area with their associated aboveground biomass.

Figure 28: In order to better visualize the diversity of vegetation structure in the study area, examples of encountered ecosystems and associated biomasses are presented in this figure. From left to right and from top to bottom: Riparian strip mainly composed of willow shrubs (27 t/ha); riparian strip composed of willows and alder of diverse age classes (45 t/ha); mature riparian strip mainly composed of willow (88 t/ha); open hardwood forest composed of ash, maple, alder and oak (130 t/ha); mature alder forest (180 t/ha), hardwood forest mainly composed of hornbeam, alder and oak (200 t/ha).

3.2.3 **Biomass Prediction from LiDAR Data at Tree Level**

A tree-level allometric relationship was then adjusted between the biomass calculated in the field (in Section 3.2.2) and the LiDAR variables. A total of 39 trees were removed from the dataset at this stage because their crowns could not be accurately delineated. A further 23 trees were removed for other reasons, mainly because they had lost a significant part of their crown between the LiDAR and the field survey, or because they were highly distorted, and the validity of volume equations was doubtful. In the end, 293 (out of 355) trees remained. The LiDAR variables presented in Table 3 were extracted at the scale of the digitized tree crowns from the CHM and from the point cloud using the std.metrics function of the lidR R package (Roussel *et al.*, 2020).

Table 3: Summary of the different variables extracted from the CHM and LiDAR point cloud.

Source	Variable	Definition	Interest for Biomass Prediction
CHM	H90 (m)	90th height percentile within the canopy	Tree size
	Area (m^2)	Tree crown area (digitized or automatically segmented)	Tree size
Point cloud (std.metrics)	Zq30 (m)	30th height percentile within the canopy	Crown shape: trees located inside forests have more branches at the top of the crown
	Pground (%)	Proportion of returns classified as "ground"	Crown porosity: heliophilous species have less dense branching

Two parametric models were adjusted using least squares regression method. Since tree biomass can differ by several orders of magnitude, a logarithmic transformation was applied to the explanatory and response variables in order to minimize the relative error on the biomass estimate rather than the absolute error. This procedure is common for tree allometry (Zianis *et al.*, 2005). The first model m1 (Equation (3)) was based solely on variables derived from the CHM: the area of the crown digitized by the operator (Area) and the tree height (H90) on the CHM. Several combinations of variables were tested, and the best one was chosen.

$$\ln AGB = a + b \times \ln Area + c \times \ln H90 \quad (3)$$

The second model (m2) was based on variables from a CHM and from the LiDAR point cloud. After several attempts, the selected model takes the first model and adds a correction factor (Equation (4)). The first component of this correction factor is Pground, which corresponds to the proportion of returns classified as "ground"

within the crown. This component has a high value for crowns that are porous to the LiDAR signal. The second component is the ratio of the height of the 30th percentile of the point cloud (Zq30) to the total crown height (H90) (Table 3). When returns are concentrated in the upper part of the canopy, this component has a high value. Together, these two factors help distinguish shade tolerant trees growing in dense forest (dense foliage concentrated in the upper crown area) from sun-demanding trees growing in full light (light foliage distributed over the entire crown). These ecological traits are worth considering because crown structure and wood density are very different along this gradient. The correction factor may also be influenced by other factors such as health status, social status or understory vegetation.

$$\ln AGB = a + b \times \ln Area + c \times \ln H90 + d \times \ln\left(1 + \frac{Pground}{100}\right) + e \times \ln(1 + \frac{Zq30}{H90}) \quad (4)$$

These tree-level allometric models were evaluated using a leave-one-out approach, where tree crowns from 18 plots were used to calibrate a model which was then validated on the digitized tree crowns of the last plot.

3.2.4 **Individual Tree Segmentation**

Tree crowns were segmented using the algorithm of Dalponte and Coomes (2016), implemented in the lidR package (Roussel *et al.*, 2020) and working only with a CHM. The segmentation parameters were adjusted by trial and error on a representative area. Segmentation accuracy was assessed on the 19 inventory plots by analyzing the overlaps between reference and segmented tree crowns. Two crowns corresponded when more than 50% of a reference crown was included in a segmented crown and the reference crown included more than 50% of the segmented crown (Lamar *et al.*, 2005). The overall accuracy of the segmentation was calculated using the equation $Global\ accuracy = \frac{2 \times N\ accurate}{N\ reference + N\ segmented}$, where N accurate is the number of corresponding tree crowns, N reference the number of manually digitized tree crowns and N segmented the number of segmented tree crowns.

3.2.5 **Validation at Plot Level**

The allometric models m1 and m2 were validated at the scale of each inventoried plot. This validation was different from the assessment carried out at the tree level because it integrated error aggregation over several crowns and the error related to segmentation (Figure 29). A leave-one-out approach was deployed. For each of the 19 plots, we adjusted the m1 and m2 allometric models based on the trees of the other 18 plots Figure 29A). On the validation plot, the trees were automatically segmented (Figure 29B) and the model built with the trees of the 18 other plots was applied to the segments Figure 29C). Tree biomasses were aggregated at plot scale (Figure 29D). The biomass estimated by remote sensing was then compared to the total biomass of the trees measured on the plot, including those that were not selected to calibrate the allometric relationship (Figure 29E). Only segments with more than half of the area within the plot were selected. A total of 8 independent

plots of about 0.3 ha in which total woody biomass was known were also used for validation (see Section 3.2.2). The model was thus validated on a total of 27 plots.

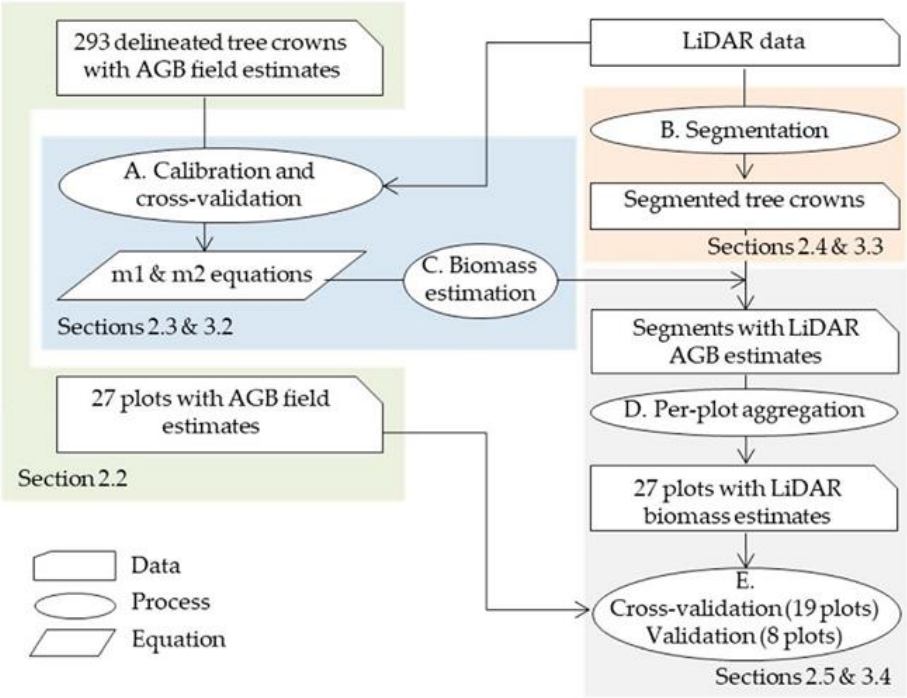

Figure 29: General workflow for the validation of biomass remote sensing estimates. (A–E). Processes are described in the text of Section 3.2.5.

3.2.6 Riparian Forest Delineation and Upscaling of Biomass Prediction

The riparian zone was delineated as the area that is flooded every 25 years. This outer limit corresponds to that of zone 4 defined by Gurnell *et al.* (2016) under a temperate climate. Beyond this limit, flooding no longer has a marked impact on ecosystem functioning. A map of the flooded area for a 25-year period was available for the entire study area (see Section 3.2.1). On rivers that are confined in narrow valleys, the flooded area does not always include vegetation patches that interact intensively with the river, without being periodically submerged (Clerici *et al.*, 2013). Therefore, a fixed buffer of 30 m was delimited on both sides of the river banks. The riparian zone consists of the sum of the two envelopes: a variable buffer corresponding to the flooded area and a fixed buffer of 30 m on either side of the banks (Figure 30a). A dilation followed by an erosion of 30 m were applied to this envelope in order to eliminate small holes in the riparian zone, which have little meaning from an ecological point of view.

In this study, riparian forests were defined as native woody plant formations within the riparian zone. Segmented tree crowns were used as a starting point to delineate

riparian forests (Figure 30b). Coniferous plantations (non-native to the region) and buildings, which are sometimes segmented as trees by watershed algorithms, were filtered out using an auxiliary layer at 2 m resolution previously produced at the scale of the region (Radoux *et al.*, 2019). Tree crowns were then used to generate a "riparian forest" envelope by applying a 10-m dilation followed by a 10-m erosion. This procedure enabled the inclusion of areas that were not covered by a tree crown in plant formations where canopy is not continuous (willow thickets for example). This "riparian forest" envelope was divided into zones of homogeneous age based on historical aerial orthophotos (Figure 30c; see also Section 3.2.7).

It was then arbitrarily divided into vegetation units (VUs) of about 0.3 ha using the "Polygon divider" tool, implemented in QGIS (Figure 30d) (Huck, 2020). This area corresponds to a compromise between the finesse of the analysis (the environmental factors must be as homogeneous as possible within a VU), representativeness and validity of biomass estimates, which were validated on plots of similar size. The surface biomass of each VU (in Mg/ha) is equal to the sum of the biomasses of segmented crowns whose centroid lies within the VU, divided by the surface area of the VU. VUs less than 1000 m2 that could not be merged with another adjacent VU of similar age were excluded from the analysis to give equal weights to VUs with similar areas.

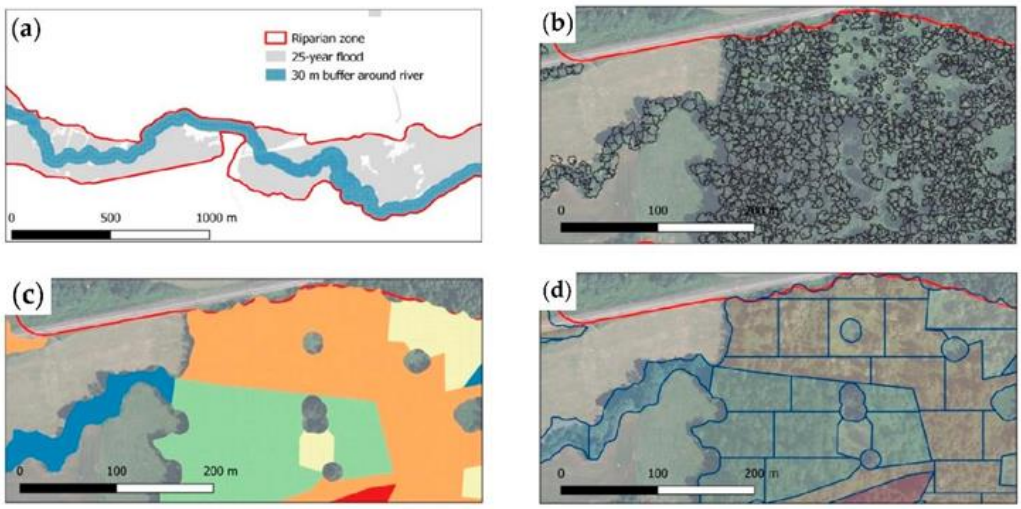

Figure 30: (a) Delineation of riparian zone as the sum of two envelopes: area flooded every 25 year and 30-m buffer on either side of the river. (b) Segmentation of tree crowns within the riparian zone. (c) Morphological filtering on the segmented tree crowns and first division into zones of similar age (each color corresponds to a different age). (d) Division of this envelope into vegetation units (VUs) of approximately 0.3 ha.

3.2.7 **Analysis of Environmental Factors Structuring the Spatial Distribution of Biomass**

To understand what environmental factors shape the spatial distribution of biomass, different explanatory variables were computed for each VU at two different scales (Table 4). At the VU scale, environmental variables were extracted at the scale of the 0.3 ha VU polygon. At the floodplain (FP) scale, the riparian zone was cut 250 m upstream and downstream of the VU, and environmental variables were extracted and summarized at the scale of the resulting polygon. Variables can be grouped into three main thematic groups: historical, land use and geomorphological variables.

Table 4: Explanatory variables used to analyze VU biomass distribution.

Thematic Group	Scale	Name	Detail	Source
History	Vegetation unit (0.3 ha)	Age (years)	Age estimated by photo-interpretation of historical aerial images	Historical orthophotos
		Planted	Regeneration type (1 = planting, 0 = natural regeneration or undescribed). Described only for VUs less than 40 years old	
Geomorphology	Vegetation unit (0.3 ha)	Horizontal distance (m)	Horizontal distance to the main channel	Hydrographic Network
		Vertical distance (m)	Vertical distance to river mean water level.	LiDAR digital terrain model (DTM)
		Relative vertical distance	Vertical distance to river mean water level, divided by the relative altitude of the 25-year flood stage. A value less than 1 means that the VU is located in the 25-year floodplain, while a value superior to 1 corresponds to valley slopes. Values higher than 2 were thresholded at 2.	
		Slope (%)	Terrain slope	
		Waterlogging	Waterlogging classes. Anoxia traces are found beyond 125 cm deep (class 1), between 80 and 125 cm (class 2), between 80 and 50 cm (class 3), between 30 et 50 cm (class 4), before 30 cm deep (class 5).	Regional soil map (Service Public de Wallonie, 2015)

	Floodplain (250 m upstream and downstream of VU)	Width (m)	Floodplain width (25-year flood)	25-year flood map (Service Public de Wallonie, 2021)
		Sinuosity	River sinuosity	Hydrographic network
		Catchment area (m^2)	Catchment area	LiDAR digital terrain model (DTM)
Land use	Vegetation unit (0.3 ha)	Artificial in VU (%)	% artificial areas	Regional land use map (Service Public de Wallonie, 2008)
		Agriculture in VU (%)	% agricultural areas	
		Forest in VU (%)	% forest and other natural areas	
	Floodplain (250 m upstream and downstream of VU)	Artificial in FP (%)	% artificial areas	
		Agriculture in FP (%)	% agricultural areas	
		Forest in FP (%)	% forest and other natural areas	

Vegetation Age is presumed to be an essential variable, because many VUs in the study area result from recent colonization of agricultural areas, or have been cut down at least once during the last fifty years. Age was estimated by photo-interpretation using available orthophotos for the years 2012, 2009, 2006, 1995–1999 (several partial covers), 1983–1987 (several partial covers) and 1971. This step was performed before the final division into VUs (Figure 30c). We identified groups of contemporary trees that regenerated at the same time on historical orthophotos. The minimum size for a group of trees to be differentiated from its neighbors was 300 m^2. For each group of trees, the date of vegetation regeneration was chosen as follows: when the young recruits corresponding to contemporary trees were visible on an orthophoto at a particular date, this date was retained. Otherwise, when contemporary trees appeared between two dates, the median date was chosen. As the time between two successive coverages was not constant through time, the precision was higher for young VUs (e.g., less than 3 years for trees regenerated around 2009) than for old VUs (e.g., about 14 years for trees regenerating around 1975). For trees that were already present in 1971, an age of 60 years was assigned when the trees appeared to be less than 20 years old on the 1971 orthophoto. When the vegetation seemed to already be well established, an age of 100 years was arbitrarily assigned. The trees within each VU had the same age, except for recruitment over less than 300 m^2 following thinning. The type of regeneration (Planted or naturally regenerated) influences productivity in the early years, and is an important variable for managers (Dybala *et al.*, 2019b). It was therefore also described for VUs when possible, i.e., for those that regenerated after 1971.

In riparian zones, many processes related to the proximity of a river can influence biomass production. Soil Waterlogging leads to anoxia, which inhibits tree growth (Kreuzwieser *et al.*, 2004). It was characterized using a regional soil map with five classes of waterlogging corresponding to the depth at which traces of oxidation-reduction were observed (Service Public de Wallonie, 2015). A low altitudinal position may be linked to waterlogging due to the proximity of the water table or flooding, but also increases tree growth due to water availability (Singer *et al.*, 2013; Schifman *et al.*, 2012) and sediment input during floods (Marks *et al.*, 2020). It was characterized by the Vertical distance variable, which corresponds to the difference between the altitude of the VU and the altitude of the river. It was calculated following the method of Alber and Piegay (2011), which was implemented in the QGIS Fluvial Corridor Toolbox (Dunesme *et al.*, 2020). The Relative vertical distance corresponds to the Vertical distance divided by the 25-year flood stage. The horizontal distance to the river (Horizontal distance) differentiates between VUs close to the current river course and subject to its direct influence, and VUs located on the old channels, where the sediments are generally finer. A high Sinuosity implies that a larger area is subject to the direct influence of the watercourse (Camporeale and Ridolfi, 2010), and characterizes the past activity and complexity of the channel (Sutfin *et al.*, 2016). The Width of the floodplain differentiates between open, humid plains and the more shaded, steeper valleys. Catchment area is a commonly used variable that characterizes the size of the river. Finally, the terrain Slope essentially differentiates the alluvial floor from the valley slopes.

Land use is a proxy for the direct impacts of human activity on riparian vegetation. It also has an influence on light conditions or the supply of propagules. It was described using a regional land use layer from 2007, with three thematic classes: artificial areas, agricultural areas, forest areas (Service Public de Wallonie, 2008). The proportion of each land-use class was expressed in percentage area at the scale of the VU (Artificial in VU, Agriculture in VU, Forest in VU) and at the scale of the floodplain (Artificial in FP, Agriculture in FP, Forest in FP).

Explanatory variables were standardized prior to statistical analyses. A PCA (principal component analysis) was first realized in order to explore relationships between explanatory variables. A variance partition was carried out using the vegan package (Oksanen *et al.*, 2020) in order to explain the share of variance in VU biomass explained by each thematic group (history, land use and geomorphology). All variables were used at this stage. A set of variables that were poorly correlated with one another (i.e., whose absolute Pearson's correlation coefficient with other selected variables was less than 0.5) was then constituted. A MLR (multiple linear regression) model predicting VU biomass was then adjusted with the following equation:

$$AGB = K \times Age + \sum(K_i \times X_i) + \sum(k_i \times Age \times X_i) \quad (5)$$

where *Xi* are explanatory variables excluding *Age*. The interactions of each variable with age were integrated because it was expected that the effect of the

variables influencing productivity or mortality evolves with the age of vegetation. The best model was selected using a stepwise procedure based on the AIC (Akaike information criterion). The relative importance of each selected variable was computed by decomposing the explained variance into non-negative contributions, using the method of Lindeman *et al.* (1980) implemented in the R package "relaimpo" (Groemping and Lehrkamp, 2018).

3.3 Results

3.3.1 Volume Equations for Alnus and Salix

The selected model for estimating the total volume of alder and willow stems in the field is presented in Equation (6) (corresponding to the fitting of Equation (1) presented in Section 3.2.2). The conditions of null mean and normality of residuals, and the condition of homoscedasticity were verified respectively by a Student (p = 1), Shapiro-Wilk (p = 0.31) and Breusch Pagan test (p = 0.77). The total volume was therefore retrieved according to Equation (7), which incorporates the Baskerville correction (Baskerville, 1972).

$$\ln Vtot = -10.8469 + 2.4079 \times \ln D + 0.7703 \times \ln H \quad (6)$$

(R^2 = 0.98, RMSE = 0.16)

$$Vtot = 1.9721 \times 10^{-5} \times D^{2.4079} \times H^{0.7703} \quad (7)$$

where *Vtot* is the total volume in cubic meters, *D* the diameter at breast height (1.3 m) in centimeters and *H* the tree height in meters.

3.3.2 Biomass Prediction from LiDAR Data at Tree Level

The two linear models fitted with variables from CHM (Equation (8)) and the CHM and point cloud (Equation (9)) have the following equations:

$$\ln AGB = -9.0796 + 0.9157 \times \ln Area + 1.8354 \times \ln H90 \quad (8)$$

(R^2 = 0.79, RMSE = 0.63)

$$\ln AGB = -8.3445 + 0.8979 \times \ln Area + 1.4880 \times \ln H90 - 0.7951 \times \ln\left(1 + \frac{Pground}{100}\right) + 1.5534 \times \ln(1 + \frac{Zq30}{H90}) \quad (9)$$

(R^2 = 0.81, RMSE = 0.61)

Deviations from application conditions were limited, and biomass was recovered by introducing a Baskerville correction. M1 and m2 estimates are retrieved using Equations (10) and (11), respectively:

$$AGB = 1.383 \times 10^{-4} \times Area^{0.9157} \times H90^{1.8354} \quad (10)$$

$$AGB = 2.834 \times 10^{-4} \times Area^{0.8979} \times H90^{1.4880} \times (1 + \frac{Pground}{100})^{-0.7951} \times (1 + \frac{Zq30}{H90})^{1.5534} \quad (11)$$

As expected, the m2 model (1.57 log-average error, corresponding to a 57% overestimation or a 36% underestimation) was slightly but significantly better than

the m1 model (1.59 log-average error, corresponding to a 59% overestimation or a 37% underestimation) (Table 5).

Table 5: Performance of m1 and m2 log-transformed models. The error was evaluated by a leave-one-out approach, in which a model calibrated on 18 plots is validated on the trees of the remaining plot. Mean absolute error (MAE) was significantly higher for m1 (letter a) than for m2 (letter b) according to a sign test. Errors are expressed in logarithmic units. In brackets: the back-transformed error (also called log-average error).

Model	R^2	Mean error	MAE
m1	0.79	0.0029 (1.0029)	0.4644 [a] (1.5911)
m2	0.81	0.0022 (1.0022)	0.4513 [b] (1.5703)

3.3.3 Individual Tree Segmentation

The overall median segmentation accuracy on the reference plots was 52% (see Section 3.2.4 for a definition). Often several crowns were aggregated into one segment or a crown was divided into several segments, which was expected as many trees were multi-stemmed. The distribution of crowns areas was not significantly different (p = 0.82 in a Wilcoxon test) between segmented and reference (i.e., manually delineated). This close similarity justified our choice to apply calibrated allometric relationships to segments for upscaling to the whole study area.

3.3.4 Validation at Plot Level

The accuracy of biomass estimation at plot level was assessed using the 27 plots for m1 and m2 (Table 6 and Figure 31). As a reminder, plot aboveground biomass is equal to the sum of the biomass of all trees in the plot. Neither of the two models delivered a significantly biased biomass mean. Despite a clear improvement in R2 in m2, the models did not differ significantly in terms of absolute error (p-values of 0.44 and 0.27, respectively, for MAE (mean absolute error) and RMSE). Nevertheless, the m2 model appeared to be better than m1 for the set of criteria studied, and it was thus retained for the spatial analysis of biomass in relation to environmental factors.

Table 6: Evaluation of biomass predictions at plot level (27 plots studied) using a leave-one-out approach. For the mean error, a negative value corresponds to an underestimation of the prediction. n.s = not significant. The RMSEr (relative root mean square error) was calculated using $\text{RMSEr} = \frac{\text{RMSE}}{\text{Mean(Field AGB)}}$. The letters correspond to the groups identified by a paired test of Student comparing the means of signed errors per plot (for the mean error) and a paired test of Wilcoxon comparing the medians of errors (for the mean absolute error MAE and the root mean square error RMSE).

Model	R^2	Mean Error (Mg/ha)	MAE (Mg/ha)	RMSE (Mg/ha)	RMSEr
m1	0.83	1.75 a (n.s.)	12.79 a	19.44 a	0.27
m2	0.90	1.70 a (n.s.)	11.26 a	15.52 a	0.22

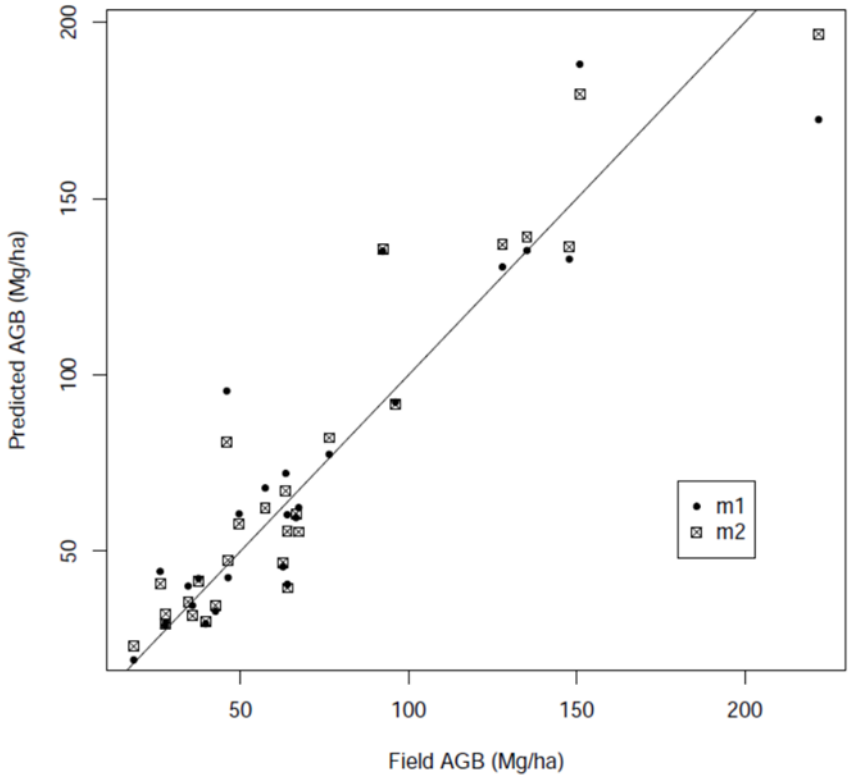

Figure 31: Predicted AGB (Mg/ha) according to field AGB for the 27 plots studied and for the two models m1 (based on CHM) and m2 (based on CHM and point cloud).

3.3.5 Analysis of Environmental Factors Structuring Spatial distribution of biomass

A total of 3162 VUs were selected for analysis. The results of a principal component analysis on explanatory variables are shown in Figure 6. Positive values on the first axis are associated with VUs occupying a higher altitudinal position, located in narrow, forested valleys, where the vegetation is older and more biomass accumulates in vegetation (high values for Vertical distance, Relative vertical distance, Slope, Age, Forest in FP and Forest in VU). Negative values are associated with VUs occupying a lower altitudinal position, located in wide, humid and predominantly agricultural valleys (high values for Agriculture in FP, Agriculture in VU, Width and Waterlogging). The second axis distinguishes the most humid VUs located in marginal depressions, in semi-open landscapes (high values for Horizontal distance, Waterlogging, Forest in FP and Forest in VU) and on the upper left the units located in more inhabited agricultural landscapes (high values for Artificial in VU and Artificial in FP).

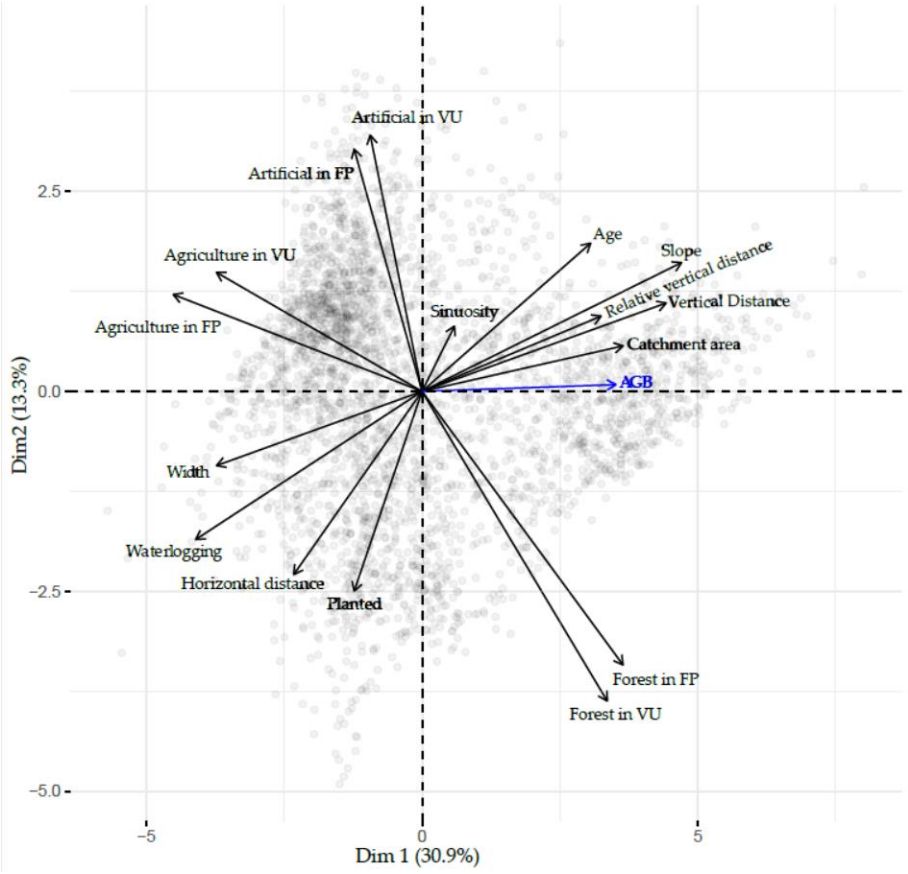

Figure 32: Results of principal component analysis on all explanatory variables. AGB was plotted as a supplementary variable.

Biomass within the VUs ranged from 3 to 515 Mg/ha (Figure 33). The average biomass for all VUs was 121 Mg/ha, and 148 Mg/ha in forested VUs (i.e., where forest land use class occupied more than 50% of the VU area). In the oldest VUs (already well established on the 1971 aerial images), the median biomass was 174 Mg/ha and 205 Mg/ha for forested VUs only. Biomass was consistently higher on valley slopes (i.e., in VUs where the relative vertical distance to the river was superior to 1) than in the floodplain (Relative vertical distance < 1).

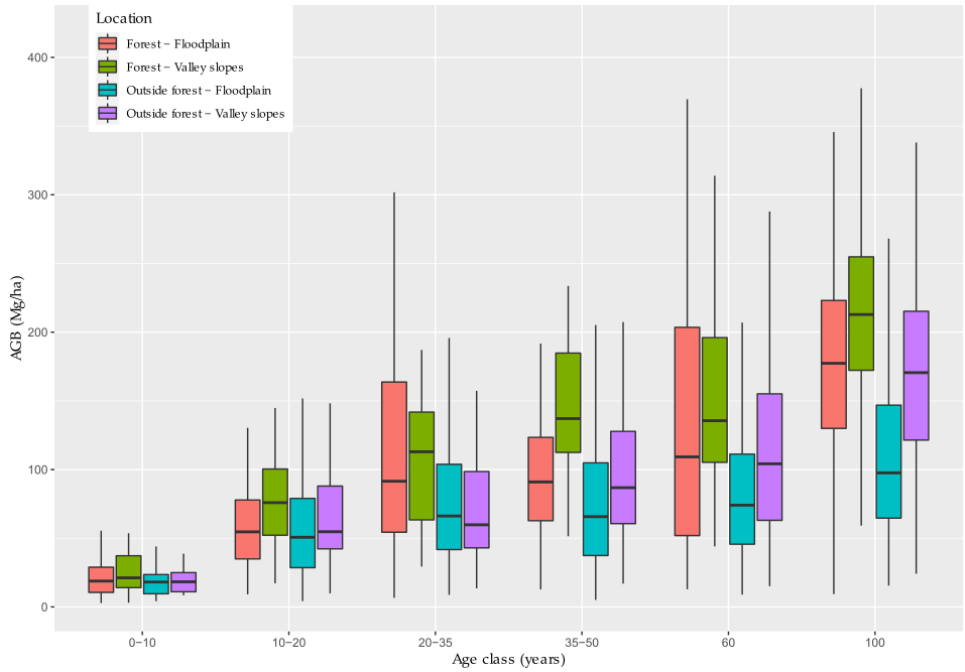

Figure 33: Aboveground biomass of VU depending on their age and location inside (Forest in VU > 50%) or outside forest, in the floodplain (Relative vertical distance < 1) or on valley slopes. Age classes “60” and “100” are indicative values, see section 3.2.7.

The variance partitioning carried out with all the variables explained 48% of the variance of the biomass (Figure 34). VU history (age and regeneration type) explained 34% of the variance, present land use 25% and geomorphology 26%. Nevertheless, a large part of the variance was shared between two or all three groups of variables. The variance explained exclusively by history, land use and geomorphology were 15, 4 and 2%, respectively. VU history was thus by far the first driver of biomass accumulation in riparian forests.

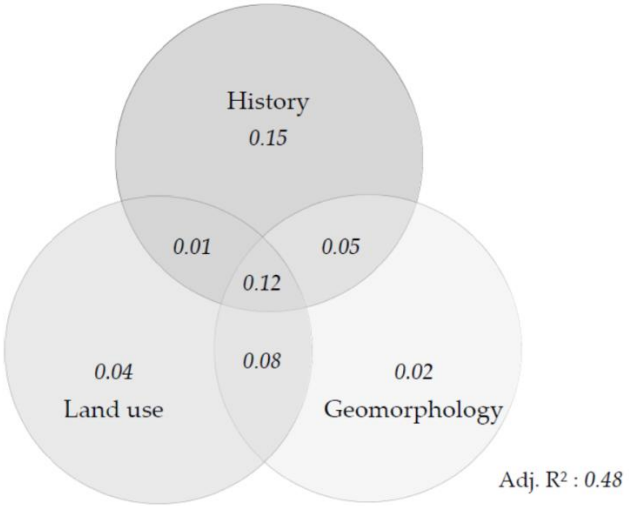

Figure 34: Venn diagram showing the contribution of each thematic group of variables to explain the distribution of biomass. The values shown correspond to the adjusted R2.

Vertical and horizontal distances to the river (Vertical distance and Horizontal distance), VU Age, Sinuosity, land use (Artificial in VU, Forest in VU, Agriculture in FP), type of regeneration (Planted) and Waterlogging variables presented Pearson's correlation coefficients below 50%. They were thus integrated with their interactions with Age into a MLR (multiple linear regression) model predicting VU biomass. However, it must be kept in mind that variables that were removed at this stage will be accounted for by remaining, correlated variables. For example, Slope and Relative vertical distance were highly correlated with Vertical distance, and Width was highly correlated with Agriculture in FP and Horizontal distance.

The terms of the MLR model selected by a stepwise procedure are presented in Table 7. The age and the vertical distance to the river had a strong positive effect on the biomass. The percentage of forest in the VU had a strong positive effect which was strengthened by Age. Regeneration by plantation also had a positive effect strengthened by Age. It should be noted, however, that this variable always has a value of 0 for VUs older than 40 years, and therefore it has no effect on the oldest VUs. Conversely, the percentage of agriculture in the floodplain had a strong negative effect strengthened by Age. The percentage of artificialized areas in the VU and the horizontal distance to the river also had a negative impact on biomass. Finally, Sinuosity had a marginal, negative impact on biomass.

Table 7: Results of MLR with stepwise variable selection to predict VU biomass (following Equation (5)). Explanatory variables were standardized prior to regression. Relative importance corresponds to the proportion of variance explained by each term. The model had an R2 of 0.50.

Term	Estimate	Std.Error	Statistic	*p*-Value	Relative Importance (%)	Relative Importance (Rank)
(Intercept)	113.51	1.18	95.86	0		
Age	39.09	1.25	31.16	5.33×10^{-186}	25.17	1
Agriculture in FP	−15.33	1.37	−11.22	1.12×10^{-28}	9.53	2
Vertical distance	7.99	1.28	6.27	4.20×10^{-10}	4.8	3
Forest in VU	10.6	1.41	7.54	6.18×10^{-14}	4.26	4
Age:Forest in VU	10.93	1.26	8.69	5.67×10^{-18}	2.12	5
Horizontal distance	−5.19	1.13	−4.57	4.98×10^{-6}	1.04	6
Planted	25.78	4.66	5.53	3.38×10^{-8}	0.94	7
Age:Agriculture in FP	−5.84	1.27	−4.58	4.73×10^{-6}	0.96	8
Artificial in VU	−5.55	1.14	−4.85	1.29×10^{-6}	0.83	9
Age:Planted	15.57	4.31	3.62	3.04×10^{-4}	0.23	10

3.4 Discussion

3.4.1 LiDAR Biomass Estimates

The relative error on LiDAR biomass estimates (RMSEr of 22% on 0.3 ha plots for the m2 model) was in the lower range of the errors reported by Zolkos *et al.* (2013) for temperate deciduous forests. These estimates are thus satisfactory, especially considering other uncertainties resulting from field data and allometric equations.

Tree biomass is primarily influenced by height, diameter and wood density (related to tree species). Tree height is assumed to be well estimated with LiDAR data. However, stem diameter and wood density estimates are more difficult to measure. At the individual tree level, the addition of variables from the point cloud between m1 and m2 slightly improved the model. The addition of a shape and porosity factor for the crown limited the biases linked to the light conditions (that influences the relationship between stem diameter, tree height and crown area) and the species (which also influences wood density). For example, this correction factor was significantly different depending on the species (Figure 35), and can be considered as a proxy for the heliophilous character. In a riparian context, the heliophilous character of a tree is related to its growth rate and to the density of the wood. For example, in general, *Salix* spp. are heliophilous, have a fast growth rate and a low wood density. When tree biomass estimates were aggregated at plot level, the added value of the variables derived from point cloud was no longer significant.

However, m2 outperformed m1 in terms of R^2, MAE and RMSE, and the non-significance of differences could simply be due to the small number of plots considered. Our results are thus more nuanced than those of Garcia *et al.* 2017 and Chirici *et al.* (2016), who found no significant difference between biomass models based on CHM or point cloud. Despite a lower performance, there are several advantages to using a model based solely on tree height and crown area. First, the use of a CHM is straightforward and does not need high computational power. The influence of survey parameters (e.g., point density, flight altitude or scan angle) or ground conditions (e.g., phenology) on CHM properties or height estimates has been well studied (Roussel *et al.*, 2020; Holmgen *et al.*, 2003; Nasset, 2004; Zhao *et al.*, 2018). Therefore, when working simultaneously with several CHMs (e.g., multi-temporal or compiled from several locations), these effects can be accounted for or assumed to be negligible (Duncanson and Dubayah, 2018). In contrast, when using point clouds, it may be more difficult to do so with variables related to lower height percentiles, canopy closure or LAI (leaf area index) (Liu *et al.*, 2018). A third advantage of CHMs beyond ease of use and robustness is that it can be updated with photogrammetric point clouds once a first LiDAR survey has been done (Michez *et al.*, 2020). The m1 model could thus be better suited to the use of time series or to the comparison of sites covered by different datasets.

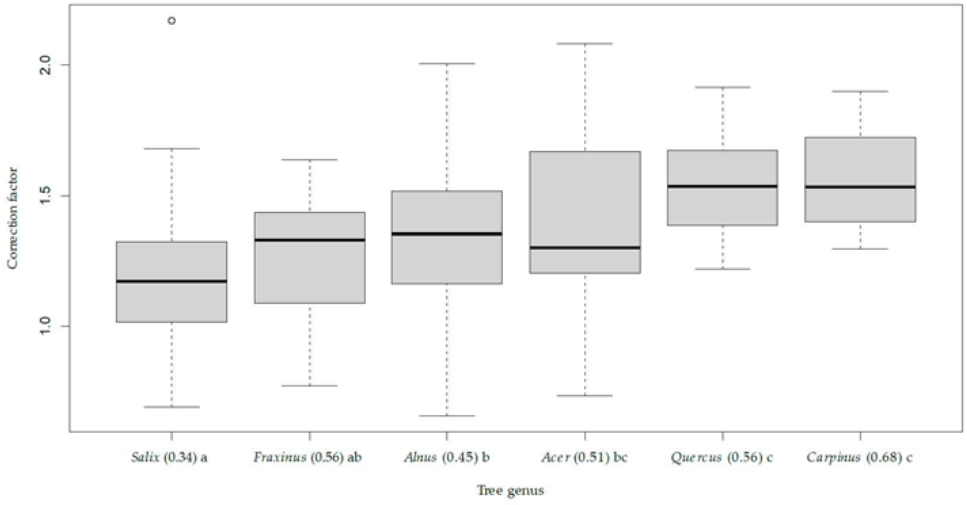

Figure 35: value of the correction factor of the m2 model $[(1+\frac{\text{Pground}}{100})^{-0.7951} \times (1+\frac{\text{Zq30}}{\text{H90}})^{1.5534}]$ depending on tree species. The thick line corresponds to the median correction factor. The species are ordered according to the average of the correction factor, and the letters abc correspond to the groups separated by a wilcoxon test. The values in brackets correspond to the wood densities for each species in Mg/m3.

3.4.2 **Spatial Distribution of Biomass and Influencing Factors**

Age was by far the most structuring variable for biomass. Moreover, as in the study of Dybala *et al.* (2019b), planting increases production in the early years compared to natural regeneration. This higher productivity of plantations was at least partially due to the choice of fast-growing species such as poplar for plantations. The median values obtained for standing biomass within forested VUs (205 Mg/ha for VUs older than 60 years, 122 Mg/ha for VUs aged 40–60 years) were within the range of values reported by for a temperate climate (Dybala *et al.*, 2019a; Giese *et al.*, 2003). The median value obtained here for all age classes combined for forest units was 121 Mg/ha. Some authors reported very high values for all age classes, such as 284 Mg/ha for alder forests (Fernandes *et al.*, 2020), or 199 Mg/ha for poplar forests and 281 Mg/ha for hardwood forests (Cierjacks *et al.*, 2010). Nevertheless, these studies were carried out in smaller or protected areas, whereas the present study includes actively managed and heavily disturbed areas. Finally, the values obtained within forest units were lower than the values of aboveground woody biomass stored within forests in general in Wallonia, which are about 200 Mg/ha for deciduous forests (Latte *et al.*, 2013). Our lower values may be related to the lower age of the forests within the floodplain than in upland areas.

Apart from age, land use variables had a significant impact on biomass distribution. The results of variance partitioning and especially those of the MLR tended to show that the effect of land use was more important than the effect of geomorphology. In agricultural or urban areas, some VUs are regularly thinned or pruned, which can limit the accumulation of biomass. Moreover, vegetation that develops spontaneously on abandoned agricultural plots does not regenerate as quickly as in forests: the recruitment of large trees can be blocked by pioneer shrubs and is not promoted by silvicultural practices. As a result, woody recruitment is often spatially uneven or even scattered. Wasser *et al.* (2015) also found a lower tree height in riparian corridors located in agricultural landscapes than in forested landscapes, related to higher disturbance (e.g., wind throw, mowing or plowing) and different species composition. Our results highlight the greater importance of human factors (land use and associated management practices, as well as vegetation age, which is related to human disturbance) over those of natural origin (geomorphology) in the study area. This stresses the relevance of taking into account the socio-cultural dimension of riparian ecosystems, as suggested by Dufour *et al.* (2019).

Vegetation units in the lower parts of the riparian zone (i.e., lower vertical distance to the river) had a lower biomass at the same age than those occupying a higher topographical position. Two factors may explain this distribution. First, VUs located in lower parts of the floodplains are more heterogeneous and are subject to a more intense disturbance regime. These disturbances include flooding, erosion, and the action of beavers, which are well established throughout the area of interest. Trees in the more humid parts of the plain may also be more exposed to diseases such as *Phytophtora alni* (Strnadovà *et al.*, 2010) or *Hymenoscyphus fraxineus* (Marçais *et al.*, 2016). Tree falls may also be promoted by waterlogging (Ferry *et al.*, 2010).

Apart from disturbance, waterlogging in the lower parts of the plain would have a greater impact on productivity than nutrients provided by sediment. In other studies, the balance between these two environmental variables was sometimes a dominance of the negative effect of waterlogging on productivity (Megonigal *et al.*, 1997; Cavalcanti and Lockaby, 2006; Jolley *et al.*, 2009), and sometimes a dominant positive effect of nutrients or water availability (Marks *et al.*, 2020, Clawson *et al.*, 2001). In particular, Rodriguez-Gonzalez *et al.* (2010) found lower radial wood growth in the wettest areas for *Alnus glutinosa* and *Salix atrocinerea* forests in the Iberian Peninsula, which are quite similar to those considered in our study. In our study, a combination of both factors—waterlogging stress and a more intense disturbance regime—explains the lower biomass found in the lower parts of the floodplain.

Finally, VUs located far from the main channel (i.e., higher horizontal distance to the river) had a lower biomass. This effect was most noticeable beyond the first fifty meters from the channel. In the study area, VUs far from the river were actually located in wide sections of the floodplain, in marginal depressions or in old channels disconnected from the river bed. These areas are enriched with fine sediments and are poorly drained. They are often occupied by shrubs such as *Salix aurita*, which have a low biomass.

The factors structuring riparian biomass distribution are not yet well known in most regions of the world (Sutfin *et al.*, 2016). The proposed approach could be replicated in other regions in order to compare biomass distribution patterns. For example, with a drier climate, water availability may be more limiting (Amlin and Rood, 2003). The response of biomass to the vertical distance to the river, which was monotonous in our study, could in these cases present a peak at intermediate altitudes as proposed by Odum *et al.* (1979). It would also be possible to compare areas receiving more or less rich sediments (Schilling and Lockaby, 2006), to study the distribution of biomass in other geomorphological contexts, such as in braided rivers where mortality due to erosion may be higher (Francalanci *et al.*, 2020), in larger catchment areas (by going further upstream or downstream), or in less anthropized areas.

3.4.3 **Perspectives for Generalization of the Approach**

Our method essentially exploits LiDAR data, which are increasingly available at regional scales (Michez *et al.*, 2017). Most of the auxiliary data used are available in many countries (land use, river network) or can be derived from a LiDAR dataset (vertical distance to the river, slope, floodplain boundaries). Most countries do not have soil maps as precise as those available in Belgium, where the map is based on about two survey plots per hectare. However, soil variables seemed to be accounted for by topographical variables, and were not kept in the final MLR model. The age and type of regeneration can nevertheless be costly or tedious to obtain, as they rely on photo-interpretation of historical orthophotos, whose accessibility is uneven from one country to another.

An advantage of the individual trees approach used in this study is its flexibility regarding spatial scale. For the needs of the study, segmented trees were grouped in 0.3 ha vegetation units. However, trees can easily be re-aggregated differently depending on pursued objectives. For example, one could study biomass in the immediate vicinity of the river (e.g., first 30 m from the water edge, where bio-geomorphic interactions are most intense) using the same delineated crowns and associated biomass estimates.

We estimated only one compartment of the carbon stored by riparian ecosystems: the aboveground woody biomass. This is justified because it is the most variable compartment at a fine spatial scale and the most dynamic on time scales of a few decades (Suchenwirth *et al.*, 2014; Cierjacks *et al.*, 2010). Storage within the other compartments (especially in roots, soil and dead wood) is more difficult to measure, but it can have a significant magnitude and spatial variation, as shown by Wohl *et al.* (2012). These compartments are difficult to study by remote sensing, but could be modeled using topographic or geomorphological data, as in Suchenwirth *et al.* (2014).

3.5 Conclusions

Our individual-tree, LiDAR-based approach enabled us to map aboveground biomass over 200 km of rivers with an error of 22% at the scale of 0.3 ha units. The addition of variables derived from the point cloud did not significantly improve CHM-based biomass estimates. For practitioners, the marginal improvement when working with point clouds must be balanced with the advantages of working with CHMs: robustness to varying survey conditions, ease of use, low computational requirements and possible update with photogrammetric point clouds.

The biomass map was used to better understand the patterns of biomass distribution within the riparian zone. In the study area, vegetation age was the most important variable. Present land use was second, followed by geomorphological variables. Over the study area, anthropogenic factors (land use and vegetation age, which are related to human practices) were more important than geomorphic factors concerning biomass accumulation within vegetation.

Surface biomass was higher inside forest, in higher topographical parts of the riparian zone and close to the river rather than in remnant patches in the agricultural landscape, and in low-lying areas further away from the river. The implementation of similar approaches in other catchments will be eased by the growing availability of LiDAR data at regional scales. Ultimately, remote sensing approaches could help understand how spatial biomass distribution patterns vary depending on the ecological context, and inform land use, conservation or restoration policies in riparian zones.

3.6 Additional information

Supplementary Materials: The following are available online at www.mdpi.com/xxx/s1, Figure S1: Estimation of total wood volume.

Author Contributions: Conceptualization, L.H., A.M., N.L. and P.L.; methodology, L.H., A.M. and N.L.; software, L.H. and A.M.; formal analysis, L.H.; data curation, L.H.; writing—original draft preparation, L.H.; writing—review and editing, L.H., A.M., N.L., P.L., H.C., B.G.; supervision, A.M. and P.L. All authors have read and agreed to the published version of the manuscript.

Funding: This work received financial support from the Province of Liège and the Province of Luxembourg.

Institutional Review Board Statement: Not applicable

Informed Consent Statement: Not applicable

Data Availability Statement: Original data created in this study including VUs with associated AGB and explanatory variables and calibration measures for alder/willow field volume equations are available at Mendeley Data (doi: 10.17632/ydrkfw9r84.1). Other data are available from the corresponding author upon reasonable request.

Acknowledgments: Measurements for *Alnus*/*Salix* field volume equations were made possible by the Service Public Wallonie—Direction des Cours d'eau non navigables.

Conflicts of Interest: The authors declare no conflict of interest.

4

Mapping species composition

4.1 Introduction

Riparian ecosystems are ecotones (transition zones between two ecosystems) where terrestrial and aquatic systems influence each other. In riparian areas, plant communities are linked to the proximity and availability of water, soil anoxia and flood disturbance (Naiman and Décamps 1997).

These plant communities, in particular riparian forests, provide numerous ecosystem services or disservices linked to water flow, sedimentary processes and habitat provision (Riis *et al.*, 2020). These services depend themselves on the species present and their ecological specificities. In Western Europe, floodplain forests are rich in woody species that may or may not be river-dependent. These species occupy a mosaic of environments in the floodplain created by ancient and recent sediment processes or flooding (Dufour and Piégay, 2006; Schnitzler, 1995). Among these, the salicaceae (willows and poplars) include fast-growing, short-lived pioneer species with a high potential for vegetative reproduction. They have a major influence on sedimentary processes in the active fringe of the riparian zone. Indeed, they are capable of rapidly colonizing and stabilizing sediment bars (Hortobágyi *et al.*, 2018; Politti *et al.*, 2018). Willows (*Salix* spp.) are also host to a large number of herbivorous insects, which through their role in the trophic chain can be considered founder species, at the base of characteristic ecosystems (Brändle and Brandl, 2001; Cronk *et al.*, 2015). Alder (*Alnus glutinosa*) is a heliophilous species with a root system that penetrates deep into waterlogged soils (Claessens *et al.*, 2010). It is a nitrogen fixer whose litter has a major influence on the trophic regime of rivers (Alonso *et al.*, 2021; Seena *et al.*, 2017). Ash (*Fraxinus exelsior*) is a key species of hardwood alluvial forests, which develop on the better-drained, rarely flooded soils of the alluvial plain. Host to a large number of species, including lichens and fungi, ash populations are threatened by severe dieback in Europe due to the pathogen *Hymenoscyphus fraxineus* (Pautasso *et al.*, 2013, Łubek *et al.*, 2020). Lastly, numerous species that are less tolerant of flooding and more tolerant of shade thrive on the higher parts of the alluvial plain, such as *Acer pseudoplatanus*, *Quercus robur* or *Carpinus betulus* (Dufour and Piégay, 2006).

The species composition of riparian forests is evolving in many regions as a result of changes in the hydrological regime of the river, themselves linked to climate change or flow regulation (Rivaes *et al.*, 2014, Tonkin *et al.*, 2018). Changes in bed morphology (bank stabilization, rectification or deepening) also alter species composition and successional trajectories (Janssen *et al.*, 2020). Riparian zones are also particularly sensitive to biological invasions (Stohlgren *et al.*, 1998), such as by *Robinia pseudoacacia* (Nadal-Sala *et al.*, 2019) or *Acer Negundo* (Saccone *et al.*, 2013). The species composition of riparian forests is also influenced more directly by silviculture (poplar plantations or, in the Ardenne valleys discussed in this study, spruce plantations) and agriculture. These alterations in species composition can in turn lead to biodiversity losses, changes in the trophic regime of rivers and alterations to the hydrological regime (Kominoski *et al.*, 2013).

Remote sensing provides information on the specific composition of riparian forests over large areas. Species composition is a key factor in the functioning of riparian forests, whose knowledge can be used to guide management actions (Huylenbroeck *et al.*, 2020). Concretely and in a non-exhaustive manner, maps of specific composition produced with remote sensing have been exploited to understand the distribution of invasive species (Martin *et al.*, 2020), to assess the biological quality of Natura 2000 habitats (Strasser *et al.*, 2013; Riedler *et al.*, 2015; Belcore *et al.*, 2021), to identify priority areas for restoration (Macfarlane *et al.*, 2017), to improve hydraulic models (Belcore *et al.*, 2021, Chaulagain *et al.*, 2022), to monitor the response of riparian vegetation following restoration (Laslier, 2018), climate change (Pace *et al.* 2021) or change in river dynamics (Durning *et al.*, 2021; Kui *et al.*, 2017; Lallias-Tacon *et al.*, 2017).

As explained in Chapter 2, mapping species composition in riparian forests is generally carried out using high-resolution data (< 10 m) and object-oriented approaches, due to its spatial organization (linear and fragmented formations) and specific richness (multi-species forests). Species mapping was mainly carried out on limited areas using multispectral data. The image acquisition period is important, and the use of images acquired on several dates often improves results (Huylenbroeck *et al.*, 2020). On-demand acquisition of high-resolution multispectral images over long linear distances and at a chosen date is costly. To obtain high-resolution satellite images over large areas at low cost, Latte and Lejeune (2020) and Bolyn *et al.* (2022) merged Planet and Sentinel-2 images. These images were then used to map the specific composition of mixed forests.

While LiDAR data has often been used to complement multispectral imagery (e.g. for object segmentation or to differentiate trees from low vegetation), it can also be used as a primary or sole source of data for species mapping (Korpela *et al.*, 2010; Heinzel and Koch, 2011; Cao *et al.*, 2016; Shi *et al.*, 2018; Budei *et al.*, 2018). Indeed, it provides information on both canopy structure (variables based on the position of returns) and leaf reflectance and orientation (variables based on the intensity of returns). However, variables linked to the intensity of returns are sensitive to acquisition conditions, and more or less complex intensity corrections must be made before data can be exploited (Kashani *et al.*, 2015).

LiDAR technology is particularly well-suited to the riparian context, as it also provides data on river topography. Moreover, this type of data is increasingly available on a regional or national scale, making it possible to consider operational applications for operators in charge of river management (Michez *et al.* 2017). Yet few studies have focused on mapping the specific composition of riparian forests using LiDAR data (Laslier *et al.*, 2019a; Ba *et al.*, 2020).

The objectives of this study were twofold:

- assess the potential of a high-density LiDAR dataset and multispectral satellite images (Sentinel-2 and PlanetScope fusion) for tree species classification in a riparian context at sub-regional scale (150 km of river and associated floodplain) ;

- highlight the spatial distribution and structuring environmental factors of riparian species composition over the study area.

4.2 Methods

4.2.1 **Study area**

The study area is located in Wallonia (southern Belgium), within the Meuse watershed (Figure 36). It comprises a 155 km stretch of the Semois. Within the study area, the Semois flows mainly through Ardenne, except upstream where it makes a few incursions into Lorraine. The Semois has a gravel bed and an average gradient of 0.1%. In the study area, it produces wide, steeply-sloping meanders, except in the Lorraine region where the alluvial plain widens and the landscape is more open. The river is not very active and regularly overflows its banks in winter. The Semois flows through a landscape composed mainly of forests and meadows. There are few large towns along the river, but numerous tourism infrastructures (campsites) are located in the downstream third of the area. At the study area's outlet (the border with France), the watershed has a total surface area of almost 13,000 km², mostly covered by forests and meadows. The mean flow at Membre (downstream of the study area) is 28.90 m³/s, the mean annual maximum flow is 245 m³/s (winter floods) and the low flow (p05) is 2.19 m³/s (Service Public de Wallonie, 2023).

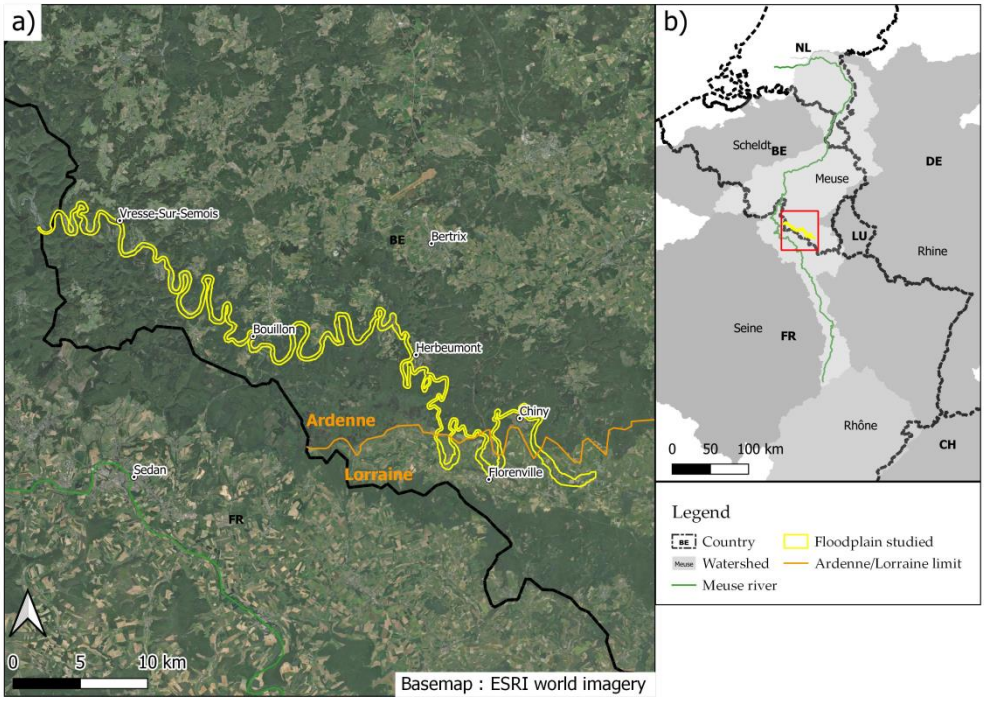

Figure 36: Location of study area

The main tree species are alders (*Alnus glutinosa*) and willows (mainly *S. aurita*, *Salix fragilis* x *alba* and *S. caprea*), which often have a multi-stemmed structure. Maple (*Acer pseudoplatanus*), ash (*Fraxinus exelsior*), oak (*Quercus robur*), hornbeam (*Carpinus betulus*) and birch (*Betulus pendula* and *B. pubescens*) are also common. Finally, there are numerous even-aged plantations of spruce (*Picea abies*) in the valley bottoms.

The riparian zone was defined as the area flooded with a 100-year return period, plus a 30-meter buffer zone. The extent of the 100-year flood was defined on the basis of the flood hazard map (Service Public de Wallonie, 2021). The study area thus constituted covers about 2,900 hectares.

4.2.2 **Data used and collected**

4.2.2.1 Field data

In order to calibrate a tree-centric predictive model of the species, 1,700 broadleaved tree crowns were delineated at 39 separate sites during the summers of 2019 and 2020 (Figure 37). Data collection was carried out in the field using a precision GNSS and a computer with access to mapping resources. These included orthophotos (Service Public de Wallonie, 2018) and a CHM created on the basis of the LiDAR dataset described in section 4.2.2.2. Species and crown diameter were described. The crowns were digitized as pure discs, containing a single tree species. Exact positioning was carried out on the CHM to limit positioning errors. Only dominant trees, whose crowns were visible on the ortophotos, were retained. Coniferous tree crowns were also digitized by photointerpretation, without a field visit.

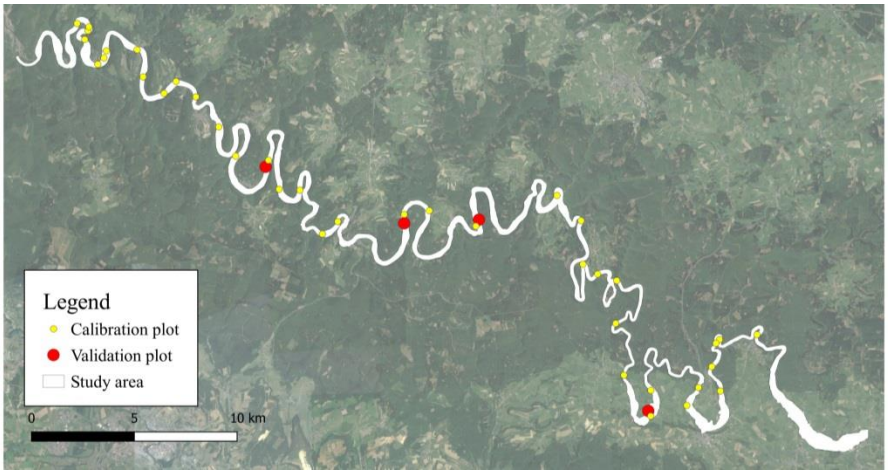

Figure 37: Location of inventory plots used for calibration and validation of tree species classification

A second field survey was carried out to validate the model at the scale of 30 m quadrats (Figure 38). This second campaign was carried out using an approach combining orthophotos based on drone images and a ground survey. Four sites were

flown over using a DJI Phantom 4 to produce orthophotos at 3 cm resolution. As it is not easy to distinguish species on the basis of an RGB orthophoto, these orthophotos were interpreted directly in the field, iteratively validating the photointerpretation result with field observations until a reliable interpretation of the images could be obtained. A total of 206 quadrats were photointerpreted on four distinct sites, representing 18.5 hectares. The use of a different dataset than that used for calibration has several advantages. First, it is completely independent from the dataset used for calibration, which limits overfitting or spatial auto-correlation between calibration and validation datasets. Second, data acquisition was faster for the validation dataset since trees were not individually and as precisely georeferenced as in the calibration dataset, and since only four species classes were distinguished. Therefore we were able to measure a large number of validation plots. Finally, this validation scheme allowed us to study the effect of VU size on classification accuracy, by merging adjacent quadrats (see section 4.2.3.3).

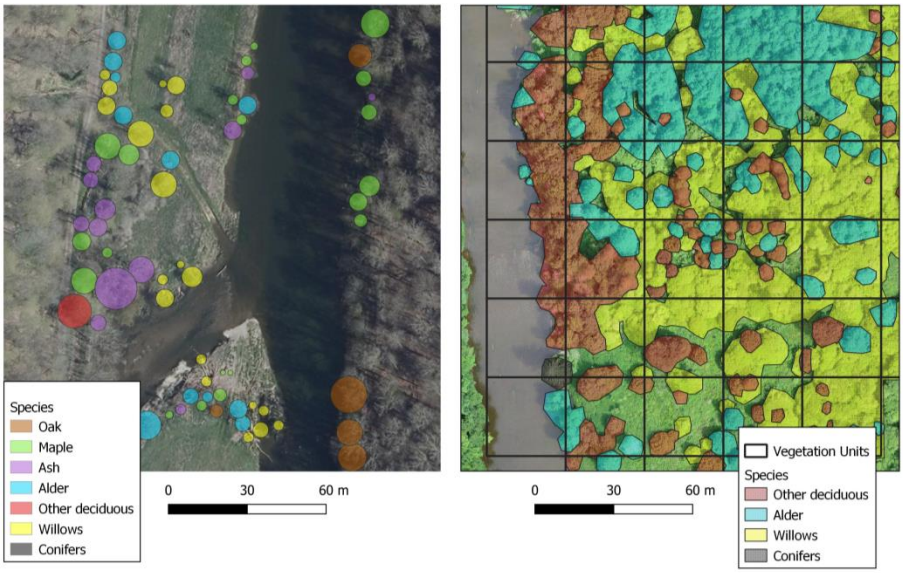

Figure 38: Reference data used for calibration (left) and validation (right). Calibration crowns were surveyed in the field as discs containing a single species. Validation data were obtained by delimiting areas containing a single species group (willows, alder, conifers, other deciduous) by photointerpretation of high-resolution orthophotos. Species proportions were then calculated on 30 m quadrats.

4.2.2.2 Remote sensing data

A LiDAR flight was carried out in May 2018 over the entire study area at an altitude of 400 meters. The sensor used was the Titan DualWave, which emits two beams at 532 nm (green) and 1064 nm (infrared).

Multispectral satellite images were obtained using a fusion of Sentinel-2 and PlanetScope data (the latter being used to improve resolution of the former). Two

multispectral images were produced for winter 2018-2019 and summer 2019. In order to obtain cloud-free images, winter images were produced using Sentinel images acquired between 17 November 2018 and 1st April 2019, with more weight given to dates close to the 23 January 2019. In practice, most used images were acquired in the second half of February 2019. PlanetScope images were acquired in three dates in February and March 2019. Summer images were produced using Sentinel images acquired between 12 July 2019 and 15 September 2019, with more weight given to dates close to the 16 July 2019. PlanetScope images were acquired on the 23 July 2019. Resulting images have 10 bands corresponding to the original 10 m and 20 m resolution bands of Sentinel-2 images, but with 2.5 m resolution. The production of these images is described in detail in Latte and Lejeune (2020) and in Bolyn *et al.* (2022) for the weighting of images acquired at different dates.

Several 30 cm resolution orthophotos are also available over the study area, but these were used only for photointerpretation during the calibration field survey.

4.2.3 **Tree species classification**

4.2.3.1 Data preparation

LiDAR data were received as a discretized point cloud with a maximum of four returns per pulse. The point cloud was processed using version 3.2.3 of the lidR package (Roussel *et al.*, 2020). For the sake of simplicity, to limit data volume and the number of features to compute for classification, and to maintain a reproducible approach with widely distributed datasets, only the infrared channel was used (40 pulses per m² on average). Indeed, most authors have pointed that the inclusion of features from the 532 nm channel did not significantly improved classification models (Yu *et al.*, 2017; Amiri *et al.*, 2018; Hakula *et al.*, 2023, Goodbody *et al.*, 2020), especially when multispectral images were integrated in models (Kukkonen *et al.*, 2019).

Intensity was corrected using the formula presented in Kukkonen *et al.* (2019):

$Icorr = Iraw * (\frac{Range}{Range\_ref})^f$ where *Icorr* is the corrected intensity, *Iraw* the raw intensity, *Range* the distance from the sensor to the target, *Range_ref* the median distance from the sensor to the target, and *f* a constant set at 2.

Height was normalized. Ground points were classified by the data provider using TerraScan software. Vegetation points were classified by considering points belonging to beams with several returns and a height greater than two meters. Only points classified as "ground" and "vegetation" were retained.

The point cloud was segmented using a watershed algorithm (segment_trees function, Dalponte2016 algorithm in the lidR package). The selection of the best parameters was carried out visually and qualitatively on a test area, so as to obtain segments of a similar size to the observed crowns.

A geometric relationship was empirically calibrated to link the digitized tree crowns in the field to the automatically segmented crowns. If a segment includes more than 30% of points intersecting reference discs corresponding to the same

species, the segment is considered to be belonging to that species. This tolerant threshold generates few attribution errors in practice.

Predictive variables were computed at the scale of segments. Variables derived from the LiDAR point cloud were computed using the tree_metrics function in the lidR package, with the stdtreemetrics parameter as input. The values of each band within the segments were also averaged for each multispectral satellite image (10 bands and three years, i.e. 30 multispectral variables). A summary of the variables selected in the model is shown in Table 8.

Table 8: Description of variables computed at the scale of each segment

Lidar metrics	**Description**
zmax, zmean	Maximum and mean of height of point cloud.
zsd, zskew, zkurt, zentropy	Standard deviation, skewness, kurtosis and entropy of height distribution.
pzabovezmean, pzabove2	Percentage of height distribution above zmean value and above 2 m
zq95, zq90, … , zq5	95th, 90th, …, 5th percentile of height distribution.
zpcumx	Cumulative percentage of points in x^{th} equal depth layer of 10, where x is 1 to 9.
itot	Sum of return intensity
imax, imean, isd, iskew, ikurt	Descriptive statistics of intensity distribution of point cloud.
ipcumzk	Percentage of intensity returned below the kth percentile of height, where k = 10, 30, 50, 70, 90.
ipground	Percentage of intensity from ground returns
p1th, p2th, ... , pground	Percentage of first, second,… , ground returns
Multispectral metrics	**Description**
ms[w/s][n]	Spectral band. The [w/s] letter corresponds to the season of acquisition during winter 2018-2019 or summer 2019, and [n] corresponds to the band's central wavelength (490, 560, 665, 705, 740, 783, 842, 865, 1610 and 2190 nm).

4.2.3.2 Tree species classification

The tree crowns were divided into four species groups: conifers, alders, willows and other deciduous species (Table 9). These four groups were separated according to their ecological characteristics and their interest in riparian ecosystem management, which were mentioned in section 4.1. The possibility of discrimination using the available dataset was also taken into account. The contrasting signatures of tree species in LiDAR and multispectral datasets will be further discussed in section 4.4.1.

Table 9: Species classes and number of reference crowns for each class

Classification	Species	Number of reference trees
Willow	*Salix* spp.	440
Alder	*Alnus glutinosa*	385
Other deciduous	*Acer pseudoplatanus*	247
	Fraxinus excelsior	227
	Quercus robur	253
	Other (mainly *Carpinus betulus*, *Betula* spp., *Corylus avellana*, *Populus* spp.)	326
Conifers	Not identified (mostly *Picea abies)*	809

The numbers of trees within classes were balanced by randomly removing trees the over-numbered classes in the training dataset. Variable selection was performed in a stepwise procedure using the R package VSURF (Genuer *et al.*, 2015). Random Forest classification was performed using the R Ranger package (Wright and Ziegler, 2017).

In order to assess the contribution of LiDAR and multispectral images for species classification, three models were built. The LiDAR model relies solely on LiDAR data, the Multispectral model relies solely on multispectral images and the LiDAR-Multispectral combines LiDAR data and multispectral images.

4.2.3.3 Spatial aggregation and validation

The classification into four species groups was applied to all segments in the study area. The proportion of cover for each species was then aggregated to the scale of 30x30 m units (i.e. 900 m²), that will be called vegetation units (VU). Only VUs with at least 200 m² of vegetation were retained.

The map was independently validated on 206 VUs using a field survey (section 4.2.2.1). To quantify the accuracy of predicting species mix, we used the method developed by Bolyn *et al.* (2022). A species was considered dominant when it occupied at least 60% of the canopy's surface. A species was considered present in a vegetation unit when it occupied more than 10% of the canopy's surface.

The Mean Score (MS) corresponds to the proportion of correct attributions (presence or absence) within a vegetation unit.

$$MS = \frac{1}{n}\sum_{i}^{n}\frac{c_i}{4}$$

Where n corresponds to the number of validation VU and for VUi, c_i corresponds to the number of correct attributions (presence or absence) among the four classes.

The *Mean Producer Score* (MPS) corresponds to the proportion of correct attributions (presence) in relation to the reference data.

$$MPS = \frac{1}{n}\sum_{i}^{n}\frac{t_i}{cr_i}$$

Where n corresponds to the number of validation VUs and, for VUi, t_i corresponds to the number of true positives among the cr_i number of species actually present in VUi.

The *Mean User Score* (MUS) is the proportion of correct attributions (presence) compared with the predicted data.

$$MUS = \frac{1}{n}\sum_{i}^{n}\frac{t_i}{cp_i}$$

Where n corresponds to the number of validation VU and, for VUi, t_i corresponds to the number of true positives among the cp_i number of species predicted in VUi.

A traditional confusion matrix was also produced for vegetation units where one class was dominant.

In order to assess the impact of VU size on classification quality, Mean Score and overall accuracy for vegetation units dominated by one class were also calculated for units of 225 m², 450 m², 1800 m², 3600 m², 8100 m² and 14400 m².

4.2.4 **Spatial analysis**

Variables were calculated 1) at VU scale or 2) at the floodplain scale. The latter scale is obtained by cutting the riparian zone 250 m upstream and downstream of the VU under consideration. Environmental variables are then extracted from the resulting polygon (Table 10). Variables can be grouped into two main families: variables relating to land use and variables relating to geomorphology, topographical position or soil conditions. Computed variables are described in more detail in section 3.2.7.

Table 10: Explanatory variables used to analyze VU species distribution

Thematic Group	Scale	Name	Detail	Source
Geomorphology	Vegetation unit (900 m²)	HD_to_river	Horizontal distance to river edge (m)	Hydrographic network (Service Public de Wallonie, 2020)
		VD_to_river	Vertical distance to river water altitude (m). Values greater than 10 m were replaced by 10 m.	LiDAR DTM
		Slope	Average terrain slope	

		Waterlogging	Drainage class: hydromorphy spots beyond 125 cm (class 1), between 80 and 125 cm (class 2), between 80 and 50 cm (class 3), between 30 and 50 cm (class 4) and before 30 cm depth (class 5).	Soil map (Service Public de Wallonie, 2015)
		Position	ValleySlope : outside floodplain River_Banks: in the floodplain, less than 30 m horizontally from the minor bed; Terrace: in flood zone but more than 3 m above the minor bed; Floodplain: in the floodplain, less than 3 m above the minor bed.	LiDAR DTM ; hydrographic network (Service Public de Wallonie, 2020) ; flood hazard map (Service Public de Wallonie, 2021)
	Floodplain (250 m upstream and downstream of the considered VU)	Sinuosity	River sinuosity (ratio between river length and euclidean distance between points located 250 m upstream and 250 downstream of VU)	Hydrographic network (Service Public de Wallonie, 2020)
Land use	Vegetation unit (900 m²)	S_vg	Area covered by tree vegetation (2 m MNH threshold)	LiDAR point cloud
	Floodplain (250 m upstream and downstream of the the considered VU)	LC_artif	% of built-up area	Land use maps (Radoux *et al.*, 2022)
		LC_agri	% of land occupied by agriculture	
		LC_forest	% of surface occupied by forest and other subnatural environments	
		LC_water	% of surface area occupied by water surfaces	

Two variance partitions were performed using the vegan package (Oksanen *et al.*, 2020) to explain the proportion of variance in alder and willow cover that were explained by the two thematic groups of variables. The significance of the

individualized fractions of the variable groups was assessed using the method of (Legendre *et al.*, 2011) implemented in the vegan package.

Finally, a canonical correlation analysis (CCA) was performed between the proportions of the four species groups and the environmental variables.

4.3 Results

4.3.1 **Classification quality at tree scale**

The three classification models were built on the basis of 1540 trees (385 per class). Following variable selection, 16, 8 and 17 predictors were retained respectively for the LiDAR model, the Multispectral model and the LiDAR-Multispectral model (Table 11).

The most important LiDAR variables in the LiDAR and LiDAR-Multispectral models were maximum height (zmax) and other height quantiles (notably zq50 and zq95) and proportion of fourth returns (p4th). Intensity metrics were selected in both models but had a lesser importance. The most important multispectral variables in the Multispectral and LiDAR-Multispectral models were winter spectral variables (msW490, msW665, msW842 and msW2190). Several summer spectral variables were also selected in both models, especially in the short wave infrared (msS2190 and msS1610) and near infra-red (msS740) regions of the spectrum.

Table 11: Presentation of selected variables for the three classification models, ranked by importance (Varimp function, VSURF r package). Feature definitions can be found in Table 8.

LiDAR Model		Multispectral Model		LiDAR-Multispectral Model	
Feature	Variable importance	Feature	Variable importance	Feature	Variable importance
zmax	105,2	msW490	183,1	msW490	123,7
p4th	97,0	msW665	160,5	zmax	105,8
zq50	92,0	msW842	153,0	p4th	102,8
zq45	86,6	msW2190	148,4	zq95	91,6
zq95	81,8	msS2190	143,0	msW665	86,0
zsd	77,1	msS1610	127,0	msW2190	79,2
area	77,0	msS560	124,7	msS2190	64,2
zmean	74,9	msS740	114,5	iskew	60,1
p3th	70,1			msW560	59,1
imean	69,3			msS1610	56,7
pzabov2	68,9			msW1610	51,6
isd	54,5			msW865	47,1
ipcmz70	52,0			msS490	47,1
iskew	50,8			msS740	46,5
ikurt	49,8			p2th	46,1
ipcmz50	47,3			msW783	45,1
				msW740	41,7

The internal accuracy at tree scale was respectively 76%, 73% and 82 % for the LiDAR, multispectral and LiDAR-Multispectral models. The addition of multispectral variables to the LiDAR model improved the accuracy for each class, especially for the “conifers” and “other deciduous” classes. The addition of LiDAR variables to the multispectral model improved the accuracy for each class, with a marked impact on the three deciduous classes (Table 12).

Table 12: Producer, user and global accuracy for each class of the three species classification models.

	Model 1 (LiDAR)		Model 2 (Multispectral)		Model 3 (LiDAR + Multispectral)	
	PA (%)	UA (%)	PA (%)	UA (%)	PA (%)	UA (%)
Other deciduous	58	66	60	63	72	72
Alder	74	70	57	59	74	77
Willows	82	74	78	72	85	80
Conifers	88	93	96	95	97	99
Global	**76**		**73**		**82**	

In the LiDAR-Multispectral model that was retained for further analysis, the "conifer" class was the best predicted, followed by willow, alder and other deciduous. The most frequent confusions concern alders with other deciduous or willows with other deciduous (Table 13).

Table 13: out-of-bag error matrix for the LiDAR-Multispectral model. This matrix was calculated on the basis of the 1,540 trees used to calibrate the classification.

	Other deciduous	*Alder*	*Willows*	*Conifers*	*Total*	*Producer accuracy (%)*
Other deciduous	**278**	66	39	2	385	72
Alder	57	**286**	41	1	385	74
Willows	39	18	**326**	2	385	85
Conifer	10	0	1	**374**	385	97
Total	384	370	407	379	1540	**82**
User accuracy (%)	72	77	80	99	**82**	

4.3.2 **Aggregation at VU scale**

The Mean Score at the VU scale (900 m²) is 84%, the Mean User Score is 94% and the Mean Producer Score is 78%. The analysis of attributions (presence within a plot) is presented in Table 14. The "Other deciduous" class is the best predicted (89 and 91% respectively for Producer and User accuracy), followed by the "Conifers" class (80 and 84%). The "Willows" and "Alder" classes have high user accuracies

(100 and 92% respectively for alder and willows), but low producer accuracies (68 and 61%).

Table 14: Results of the independent assessment of classification quality for "presence" values. The "True positives" column corresponds to the number of plots in which a species is present (> 10% cover) in both the reference data and the prediction. The "Present (reference)" and "Present (prediction)" columns correspond to the number of plots in which a species is present, in the reference and predicted data respectively. Producer and user accuracies are calculated from these values.

	True positives	Present (référence)	Present (prédiction)	Producer accuracy (%)	User accuracy (%)
Other deciduous	135	152	149	89	91
Alder	87	142	95	61	92
Willows	56	82	56	68	100
Conifers	33	41	39	80	85

As for the prediction of the dominant species, the overall accuracy is 89%. Most of the poorly predicted cells are alder, willow or conifer-dominated cells that are predicted to be dominated by other deciduous trees (Table 15).

Table 15: Dominant species confusion matrix, calculated on the 141 plots where one species accounted for more than 60% of the cover according to field data.

Reference/ predicted	Other deciduous	Alder	Willows	Conifers	Total	Producer accuracy (%)
Other deciduous	**58**	1	0	0	59	98
Alder	6	**25**	0	0	31	81
Willows	3	1	**25**	1	30	83
Conifers	3	0	0	**18**	21	86
Total	70	27	25	19	141	
User accuracy (%)	83	93	1	95		89

The impact of VU size on classification quality is shown in Figure 39. For small units, the Mean Score and overall accuracy on units with a dominant species is close to the accuracy of tree-scale classification. Classification performance improves with increasing size of aggregation units.

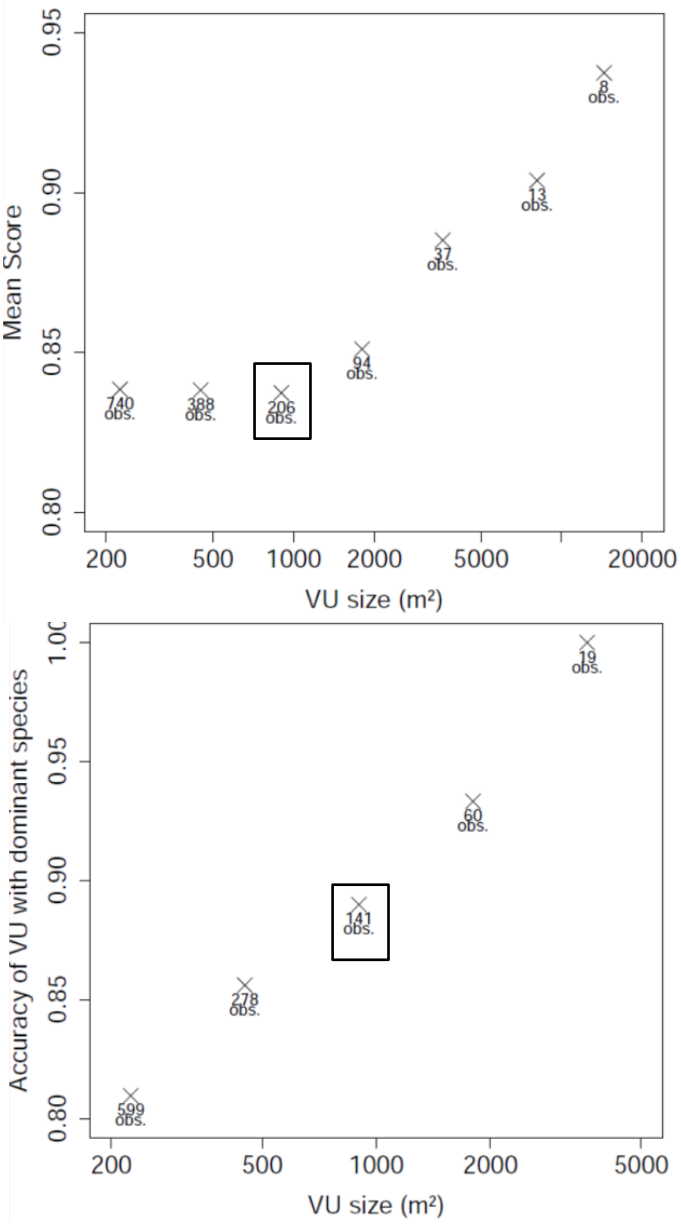

Figure 39: Mean score (top) and overall accuracy of plots with a dominant species (bottom) according to VU size (in square meters, logarithmic scale). The numbers below the points correspond to the number of plots considered for quality assessment. The number of plots with a dominant species is insufficient to assess the overall accuracy of the 8100 and 14400 m² units. The point corresponding to the selected VU size (900 m²) is framed.

An example of how species proportions can be represented on a map is shown in Figure 40.

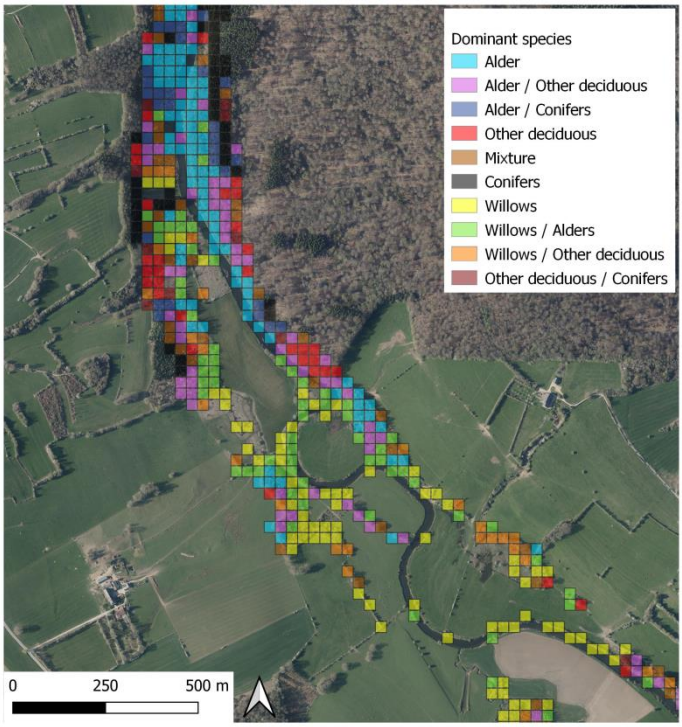

Figure 40: Sample from the species map. The symbology has been chosen so that all species covering more than 20% of the canopy area within a VU are represented. When more than two species each covered more than 20% of the canopy area, the class "Mixture" was assigned.

4.3.3 **Spatial distribution**

The results of the variance partition are shown in Figure 41. The variance of willow proportion explained by environmental variables is 21.5%, and 7.8% for alder. These low values indicate significant noise on canopy proportions, but the effect of environmental variables is significant. The proportion of willow is determined by land use and to a lesser extent by geomorphological factors. In comparison, the proportion of alder is also linked to geomorphological factors, and only weakly to land use.

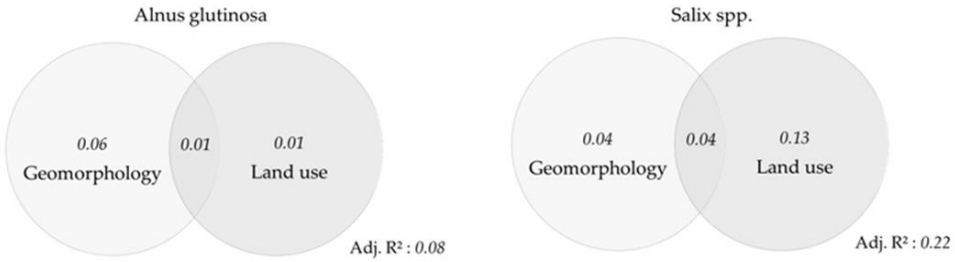

Figure 41: Venn diagram showing the contribution of each thematic group of variables in explaining the proportion of alder (left) and willow (right). The values shown correspond to the adjusted R². All fractions are significant.

The CCA results are shown in Figure 42. The proportion of willow is associated with the openness of the environment (positive association with *LC_agri* and *LC_artif*, negative association with *LC_forest* and *s_vg*), low topographic position and wet soils (positive association with *Waterlogging* and *Floodplain* position, negative association with *Valley_slopes* or *VD_river*). The proportion of alder is associated with soil waterlogging and low topographic position (positive association with *Waterlogging* and negative association with *VD_to_river*), and *River banks* position. The proportion of conifers is associated with the forest context (*LC_forest*). Finally, the proportion of other deciduous is associated with valley slopes (positive association with *Slope*, *Valley Slopes* position and *VD_to_river* and negative association with *Waterlogging*).

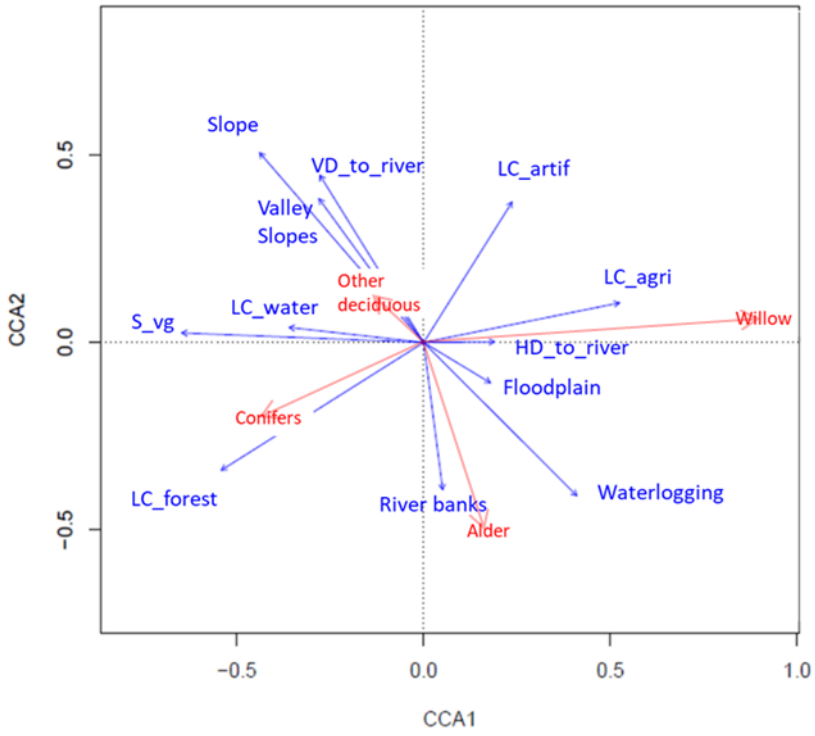

Figure 42: CCA results explaining the proportion of species groups according to environmental variables. Slope = Slope, VD_to_river = vertical distance to the river; HD_to_river = Horizontal distance to the river; River banks, Valley slopes and Floodplain refer to the position of the VU, Waterlogging = soil waterlogging, S_vg = area covered by woody vegetation within the VU, LC_artif, LC_agri, LC_forest, LC_water = proportion of land-use classes in the floodplain.

4.4 Discussion

4.4.1 Important variables and classification quality

LiDAR data were useful to differentiate between functional groups of trees with very different structures, coinciding with distinct ecological characteristics. In the temperate riparian context, LiDAR is particularly well suited to separating pioneer and heliophilous formations (willow stands, alder stands and probably cottonwood stands in other geographical contexts) from hardwood forests (oak-ash-elm stands, beech stands). The LiDAR model was driven by variables linked to height distribution and variables linked to signal penetration through the canopy (number of returns per beam and to a lesser extent distribution of intensity values). The response of alder was characterized by a large number of returns per beam (high values for p4th) with low intensity on average (low value for imean) and a skewed distribution

with many low intensity returns (Figure 43). These properties could be linked to the orientation of alder leaves in all directions, as opposed to sycamore maple or willow, whose foliage is planophilic (Pisek *et al.*, 2022). Indeed, horizontal leaves tend to generate higher intensity returns (Korpela *et al.*, 2010; Budei *et al.*, 2018). The low number of returns associated with willows (low p4th value) and the relatively high proportion of returns below 2 meters (low pzabov2) may be related to their light and single-layered foliage, which separates them from other deciduous that exhibit a higher number of returns. Ash shows an intermediate response between alder and other deciduous and was found to be frequently confused with the alder class. Ash has plagiophilic foliage, with inclined leaves (Pisek *et al.*, 2022). The low intensity of the returns (low value for imean) could also result from the presence of exposed branches, themselves linked to frequent defoliation by *Hymenoscyphus fraxineus*. Indeed, exposed branches have a lower reflectance for the wavelength used than branches with leaves (Fassnacht *et al.*, 2016). Finally, height (notably zmax) contributes to the classification of willows, which rarely exceed around fifteen meters, and conifers, whose height is often over thirty meters (Figure 43).

The Multispectral model relied both on winter and summer spectral signatures. Leaf-off images were helpful to distinguish coniferous and deciduous trees. Selected bands included blue (msW490), which is related to bare soil under leaf-off trees, and red/infrared bands (msW665, msW842 and msW2190) which are related to the presence or absence of foliage. The summer spectral signature was especially useful to distinguish willows from other deciduous species, which explains the relatively high classification accuracy for this species in the multispectral model (Figure 43).

The LiDAR-Multispectral model showed higher accuracies than models relying solely on LiDAR or multispectral data. Classification was primarily driven by winter spectral response (notably msW490) that helped distinguish conifers from deciduous species, height (zmax and zq95) that helped distinguished conifers from willows, and p4th that helped distinguish alders from willows. Intensity skewness, whose high values characterized the alder class, and summer spectral response, that helped distinguish willow from other species, were used to a lesser extent. The limited added value of summer multispectral images in the LiDAR-Multispectral model differed from the results obtained by other authors exploiting LiDAR and multispectral data with tree-centric approaches (Holmgren *et al.*, 2008; Deng *et al.*, 2016; Hartling *et al.*, 2019; Shi *et al.*, 2018; Michałowska and Rapiński, 2021). Several factors may explain the low presence of the summer spectral signature in our model. Firstly, images display significant noise linked to the shadows cast by trees on one another, particularly in a context of irregular forests. Additional noise is generated by ground spectral signature for trees located in zones with sparse canopy cover. Secondly, the fusion of images acquired at different times of the growing season may have led to a homogenization of the spectral signatures of different species. Finally, in our dataset, the summer spectral signature was particularly useful to separate conifers from willows, which were already well separated using LiDAR variables or the winter spectral response.

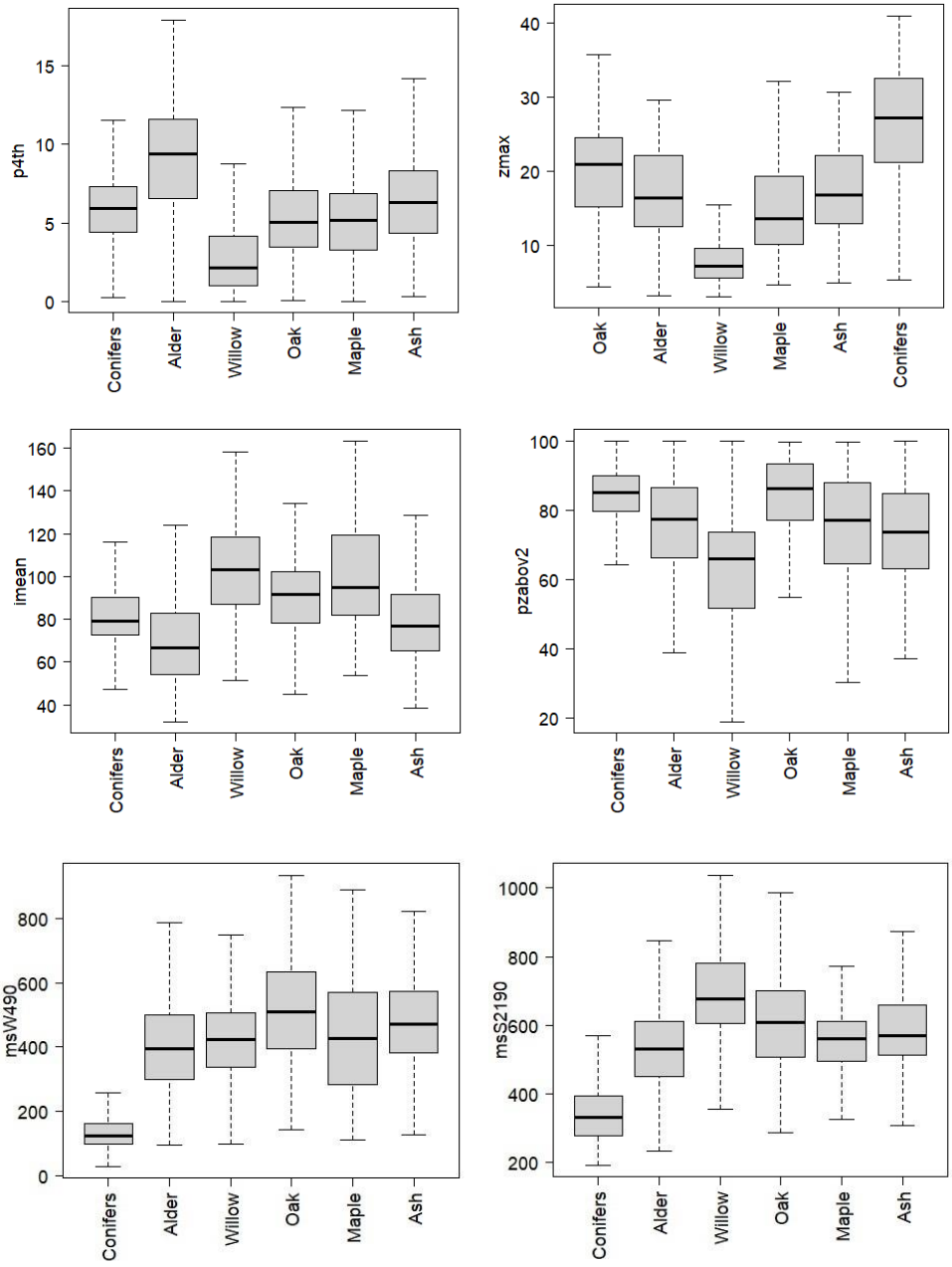

Figure 43: Distribution of six selected variables for each species. From left to right and top to bottom: p4th (proportion of fourth LiDAR returns), zmax (maximum height), imean (mean intensity of all returns), pzabov2 (proportion of returns above 2 meters), msW490 (winter reflectance, wavelength 490 nm) and msS2190 (summer reflectance, wavelength 2190 nm).

In view of these results, the model could probably be further improved by the use of multispectral images acquired at a single date, during spring or autumn where phenological differences between species are more important (Michez *et al.*, 2016b, Lisein *et al.*, 2015, Grabska *et al.*, 2019). A different computation of certain LiDAR variables could also enable an improvement in the proposed classification. For example, intensity variables could be calculated only on the first return, where the specific response is assumed to be the most original (Shi *et al.*, 2018). Using the undiscretized signal (full waveform) could also reveal new variables useful to distinguish species (Yu *et al.*, 2014). Finally, a more readable model could have been built by removing highly correlated variables and by using spatially separated folds during model calibration at the scale of individual trees, in order to reduce spatial autocorrelation which can be a source of overfitting in our setting according to Ploton *et al.* (2020).

The model's performance was enhanced by the spatial aggregation of tree crowns into vegetation units. We were unable to identify any saturation of accuracy with increasing unit size. As far as dominant species are concerned and for 900 m² units, the overall accuracy of almost 90% is satisfactory for many uses. As far as presence/absence prediction is concerned, the user's accuracy was satisfying: the model rarely detects species that are not present. However, alders and willows present in mixtures with other deciduous trees are more difficult to detect. On the one hand, mixed crowns can make classification more difficult. On the other hand, in a closed landscape, alder and some willow species may present a structure that makes them more difficult to differentiate from other deciduous, with foliage concentrated in the top of the tree. For example, Racine *et al.* (2021) have shown in monospecific forest plots that, for a given species, the distribution of points can be influenced by the proportion of tree cover.

4.4.2 **Species distribution**

These results confirm those obtained during field surveys carried out in the same region. Alder is present in strips along riverbanks and in clumps in valley bottoms. The presence of alder is associated with waterlogged soils. It is consistent with its autoecology as alder can tolerate anoxia (Claessens *et al.*, 2010). In riparian buffer strips in open areas, it is often found in association with willows. In forest environments, it is found with other deciduous trees such as ash, maple, oak or hornbeam. Thus, while alder is considered as a heliophilous species, it is relatively unaffected by variables related to ecosystem openness (land use variables or vegetation cover), probably because floodplain forests in the study area are relatively open and disturbed. In contrast, ecosystem openness is the primary factor explaining willow distribution. Indeed, willow species can thrive in a wide variety of hydric and trophic conditions. They are often dominant in buffer strips in open areas, as observed by Claessens *et al.* (2009). Eared willow (*Salix aurita*) is locally dominant in more closed areas, in marginal depressions of the floodplain, far from the river and on permanently waterlogged soils (Mertens, 2011). Although the factor was not included in the model, the natural region has an impact, with willows more

frequently encountered in the Lorraine part of the study area (Figure 36), as observed by Debruxelles and Claessens (2008). Finally, valley sides in the study area are steep. They are dominated by deciduous trees such as oak, hornbeam and maple, and even beech at the top of the valley slope.

Our results support the view that, as far as major functional groups of tree species are concerned, riparian vegetation is not structured along a simple gradient of inundation frequency (represented here by the vertical distance from river). It is also structured by other drivers. These drivers may vary longitudinally (e.g. land use, valley confinement, geologic region) or more locally under the influence of geomorphological or anthropogenic features that tend to define patches (e.g. position in the vicinity of river banks or in marginal depressions, direct human intervention), as proposed by Scown *et al.* (2016) or van Coller *et al.* (2000).

A multi-scale framework could be used to gain a better understanding of spatial distribution, as in Hough-Snee *et al.* (2014). Multiple pixel sizes or VU types could be used (e.g. longitudinal fractioning of floodplains which are expected to highlight larger scale longitudinal drivers, linear units along banks which are expected to be more influenced by fluvial processes). Environmental variables could also be produced at different scales in order to quantify explained variance in species proportions associated with these different scales. In addition, spatial auto-correlation could be included in the distribution model as local species abundance can be expected to influence recruitment of young trees.

4.5 Conclusion

Our object-oriented approach, based on a high-density LiDAR point cloud and multispectral satellite imagery, delivers tree-scale accuracy of 81% for a four-class model. This accuracy is improved when the data are aggregated, with an accuracy on the dominant species of the order of 89% at the scale of 900 m² vegetation units for the four-class model. LiDAR variables were most important for differentiating alder, willows and other deciduous, while multispectral data were most useful for distinguishing deciduous trees from conifers. With the increasing availability and improved quality of regional LiDAR datasets and of high resolution multispectral images, the mapping of key riparian tree species is becoming increasingly accessible, making it possible to envision operational applications.

Spatial distribution analysis confirms the expected patterns of tree distribution in riparian landscapes, which is structured as a mosaic influenced by lateral and longitudinal gradients. Alder is found in the wettest areas, both in forests and in more open landscapes, and along riverbanks. Willow is found in wet, open areas, and other deciduous in higher parts of the riparian zone.

5

Characterization of bank morphology and erosion with 3D data

5.1 Introduction

The previous three chapters have dealt with the use of remote sensing to characterize riparian vegetation. Nevertheless, the management of the latter cannot be dissociated from the management of the physical component of the minor bed (Urbanič *et al.*, 2022). Characterization of riparian zones as ecosystems often includes variables relating to stream sinuosity, morphology or bank stability (Tompalski *et al.*, 2017; Michez *et al.*, 2017; Johansen *et al.*, 2010). Thus, remote sensing techniques focused on the physical component of rivers are also tools that can support riparian vegetation management.

Longitudinal and cross-sectional profiles of rivers provide essential information for understanding their hydraulic and sedimentary functioning. These profiles are traditionally obtained by ground operators equipped with GNSS and total stations. Among the many remote sensing alternatives available today, approaches based on LiDAR data and photogrammetric processing of UAV images are becoming increasingly available. However, the presence of water poses a challenge for both technologies: light refraction through the water surface biases photogrammetric measurements, and the infrared beam used in LiDAR does not penetrate water (Woodget *et al.*, 2015).

Furthermore, sedimentary processes are an essential process in the hydrosystem, whose understanding is essential for planning the management of rivers and floodplains. In particular, bank erosion is one of the main mechanisms through which wood enters the river (Comiti *et al.*, 2016), and riparian vegetation has an important influence on sedimentary processes (Politti *et al.*, 2018). Field methods for quantifying erosion are only feasible for limited areas (Papanicolaou *et al.*, 2012; Stoffel *et al.*, 2013). For larger areas, aerial photographs are regularly used (Hughes *et al.*, 2006; Hooke and Yorke, 2010). However, this approach is difficult to automate, and cannot be implemented when vegetation shadows the banks on photographs. Furthermore, aerial photographs provide information limited to the lateral displacement of banks; they miss other phenomena and don't allow eroded volumes to be calculated (Grove *et al.*, 2013). Consequently, digital terrain models, field observations and cross-sectional profiles are sometimes used to complement aerial photographs and obtain more complete information on erosion phenomena (Spiekermann *et al.*, 2017; De Rose and Basher, 2011). At a local scale, photogrammetric techniques (often based on UAV images) can also be used (Hamshaw *et al.*, 2019). Photogrammetric approaches are based on the subtraction of diachronic digital terrain models and enable erosion-deposition phenomena to be visualized and quantified. Several authors have used multi-temporal LiDAR surveys to quantify or understand erosion phenomena, usually on a local scale or on river segments a few tens of kilometers long, on braided (Baggs Sargood *et al.*, 2015; Grove *et al.*, 2013; Lallias-Tacon *et al.*, 2014) or more rarely meandering (Kessler *et al.*, 2012) rivers. The growing availability of regional and multi-temporal LiDAR surveys is multiplying the possibilities for large-scale monitoring. The infrared beams generally used for LiDAR are absorbed by water surfaces, so there is no

information on submerged surfaces (Bailly *et al.*, 2012). As a result, incision or deposition phenomena are more difficult to study than the lateral displacement of banks (Nardi and Rinaldi, 2014), except when erosion or deposition heights are well above the height of the water surface (Scorpio *et al.*, 2018). Topo-bathymetric systems exploiting multiple wavelengths can be used to overcome this limitation (Lague and Feldmann, 2020). Nevertheless, these are not widely available compared with conventional LiDAR datasets, which many countries are acquiring on a large scale for use in a wide range of applications.

The aims of this chapter are as follows:

- Quantify the accuracy of two methods using remotely sensed data to extract information on riverbank morphology (LiDAR and aerial photogrammetry);
- Map lateral bank erosion in a small watershed using two LiDAR datasets acquired 7 years apart.

5.2 Methods

5.2.1 Accuracy assessement of 3D LiDAR and photogrammetric models for describing bank morphology

Two remote sensing approaches for topographic surveying were evaluated on two Ardenne rivers (Figure 44). The first site is the Lhomme in Bras (commune of Libramont). At the study site, the river is straight with a gradient of around 5‰, has a catchment area of 12 km² and has banks eroded by cattle trampling. The second site is the Sûre à Volaiville (commune of Léglise). On the study site, the Sûre has a catchment area of 114 km², an average gradient of around 4‰, and flows through a landscape of forests and meadows. Re-meandering had just been carried out at the time of the flight. The two stretches studied have no woody vegetation and a low sediment load.

For the Lhomme river, we used a DJI Phantom 4 Pro UAV flying at an altitude of 40 m, with the camera oriented at 80°. Flight lines followed the river in a longitudinal way, then crossed it transversally for each flight line (cross grid flight plan). For each flight line, longitudinal overlap was 85% and lateral overlap was 80%. Such a flight plan may not be the best configuration according to Meinen & Robinson (2020) or Manfreda *et al.* (2019) who recommend using both NADIR and convergent images. However, it was designed to collect images with a variety of perspectives in order to minimize model distortion, especially dome-like distortions that are frequent in linear settings (Tournadre *et al.*, 2015). 20 well-distributed control points were used to georeference and adjust the model, which covers around 400 m of the river (area of 40.000 m²) with around 600 images. Such a GCP density is in line with the recommendations of a minimum of 3 GCP for 100 images emitted by Sanz-Ablanedo *et al.* (2018). Average image resolution was 1.03 cm. Geometric accuracy was assessed with 10 independent check points. Planimetric RMSE was 2.1 cm and altimetric RMSE was 6.7 cm.

For the Sûre, we used a DJI mini flying at an altitude of 20 m, with the camera oriented at 90°. Flight plan was a single grid with lateral and longitudinal overlaps of 80%. 6 well-distributed control points were used for georeferencing and model adjustment. The study area covered a linear distance of around 100 m or 7.000 m², 216 images were used. The average resolution of the images was 0.5 cm. Geometric accuracy was assessed with 4 independent check points. Planimetric RMSE was 4.1 cm and altimetric RMSE was 3 cm.

The sites are covered by a 2021 LiDAR DTM (4 pulses/m²), whose altimetric accuracy was also quantified. A traditional topographic survey was carried out at each site to characterize the accuracy of the LiDAR and photogrammetric digital terrain models.

Figure 44: Two remote sensing approaches for topographic surveying (LiDAR and UAV image photogrammetry) were evaluated on two Ardennes rivers: the Sûre (left) and the Lhomme river (right).

Digital terrain models produced by photogrammetry are not correct on water surfaces. The tie points found on these surfaces are incorrectly positioned, notably due to the refraction of light as it passes from air to water (Figure 45). Several methods exist to correct the altitude at water surfaces. The most effective method has been developed by Dietrich (2017). It exploits the information contained in each tie point on the water surface: knowing the position of the water interface and the position of the incident rays for each tie point, the position of each tie point can be corrected. However, the method is computationally intensive (requiring the manipulation of point clouds and iterative photogrammetric processing). Another simpler method, developed by Woodget *et al.* (2015), was deployed on both study sites. If the images are acquired with a quasi-NADIR orientation and the rays are homogeneously distributed (an assumption not verified for the edges of the surveyed area), there is a constant relationship between apparent and actual depth. The

apparent depth is simply underestimated by a factor of 1.34 (refraction coefficient of water). The method of Woodget *et al.* (2015) requires the altitude of the water surface to be known at every point. The altitude read on the DSM is incorrect at the water surface, but it is correct at the land-water interface. Therefore, we need to extract the DSM elevation at points along the land-water interface and interpolate this elevation to create a raster with the local water elevation at each point. Real depth and bottom elevation can then be calculated by correcting the apparent depth with the water's refraction coefficient.

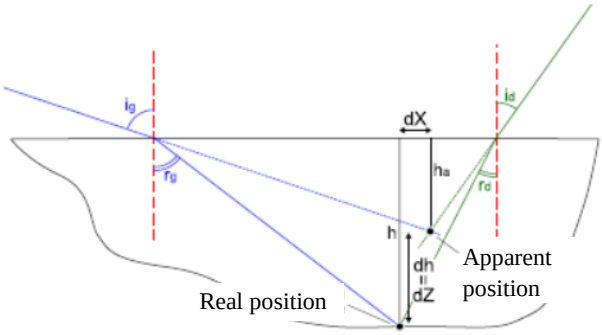

Figure 45 : Refraction of light as it crosses a water surface, and its impact on the photogrammetric process. The green and blue lines represent two drone shots. The apparent position corresponds to the position of the tie point in the photogrammetric model. It is located at a higher altitude than the actual position. The diagram was adapted from Feurer (2009).

The altimetric accuracy associated with the LiDAR and photogrammetric DTMs was first quantified using a network of independent validation points surveyed with precision GNSS (116 emerged points and 45 submerged points for the Lhomme, 10 emerged and 7 submerged points on the Sure). On five representative profiles of the Lhomme site, three parameters were calculated to synthetically describe the bank geometry: bankfull width, bankfull depth and bankfull cross-sectional area (Figure 46). The values of these three parameters were compared for the traditional, LiDAR and photogrammetric approaches.

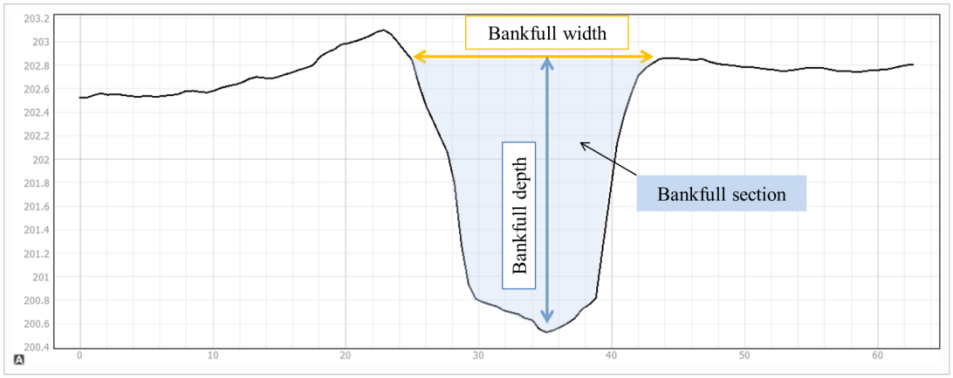

Figure 46: Schematic representation of the three parameters evaluated: bankfull width, bankfull depth and bankfull cross-sectional area.

5.2.2 **Using multi-temporal LiDAR data to quantify lateral bank erosion**

5.2.2.1 Study area and available data

The study area covers the Ton sub-basin. This has an area of around 300 km² and comprises 50 km of watercourses, taken from the point where their catchment area reaches 50 km² (Figure 47). The watershed includes the Ton, the Vire, the Chevratte and part of the Chiers (whose the Ton is a tributary). The watershed is mainly agricultural (livestock farming) and forested. The rivers have mostly natural banks, except where they cross the villages of Virton, Saint-Mard, Signeulx and Lamorteau. Rivers are low-gradient with banks composed of uncohesive sand. Le Ton, upstream of its confluence with the Vire, is a stream dominated by a base flow, like the Chevratte. The Vire has a more pronounced seasonal dynamic, which is reflected in the Ton downstream of its confluence with the Vire.

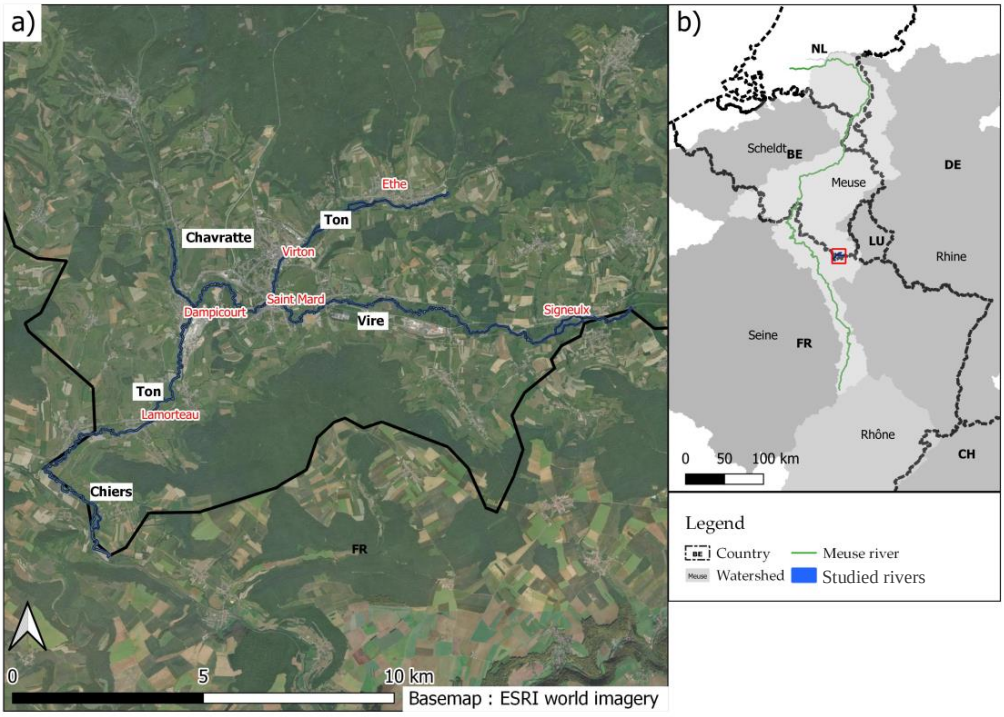

Figure 47: Location of study area (Ton sub-basin in Meuse basin, Wallonia)

Two LiDAR dataset cover the area. The first was completed in April 2014 with a density of around 0.8 pulses per square meter. The second was carried out in March 2021 with a density of around 4 pulses per square meter. Both campaigns were carried out under similar flow conditions. Data were supplied in the form of interpolated DTMs. The water surface was delineated in 2014 based on LiDAR return intensity in Michez *et al.* (2017), and manually edited.

5.2.2.2 Verification of water levels during LiDAR surveys

LiDAR point clouds provide little or no information on submerged river beds. The elevation read on an interpolated DTM does not correspond to the bottom elevation, as the LiDAR infrared beam is absorbed by water surfaces. This altitude can be expected to be close to the nearest emerged points on the river banks. Therefore, for a LiDAR dataset with a sufficiently high point density, the level should be close to the water level during the acquisition campaign.

This hypothesis was verified by comparing the elevation read on the 2014 and 2021 DTMs with the elevation of five water level gauges in the study area, where the water elevation during the survey was known (see section 5.3.2). This verification of water levels on both flight dates also ensures that water levels are similar on both dates, and that they are not too high. In the event of a difference in water levels, the conditions for detecting erosion presented in section 5.2.2.3 need to

be adapted. On the other hand, if water levels are high or overflowing during one of the flights, the possibilities of mapping bank erosion will be reduced.

5.2.2.3 Detection and quantification of erosion

The simple subtraction of two DTMs generates significant noise that must be removed in order to distinguish erosion phenomena (Lallias-Tacon *et al.*, 2014). Firstly, the elevation read over submerged surfaces is very different for the two surveys. The main reason is that, since the 2014 survey has a coarser resolution, the first visible emergent points are generally located higher up the bank than for 2021. Therefore, areas submerged in 2014 were masked on the differential DTM. On the other hand, an area emerged in 2014 and submerged in 2021 at an equal or lower altitude was considered as eroded. Only negative differences have been retained: depositional phenomena are explicitly ignored. Only pixels located at a distance of less than 12 meters from the surface submerged in 2014 were retained.

Three methods were then tested to remove noise on the differential DTM created (Figure 48). The Method 1 consisted in retaining only differences greater than 50 cm. Such a threshold visually removes much of the noise. Based on the estimated altimetric accuracy on flat surfaces of the LiDARs used, Baggs Sargood *et al.*, (2015) used a threshold of 44 cm for erosion detection, close to the threshold we used. Nevertheless, river banks are often steep and the altimetric error can be greater. This is why the following methods also filter differences according to the width of the erosion detected. The most aggressive Method 3 also includes a morphological filtering process that retains only pixel groups over 1.5 meters wide and 3 m² in area. For the Method 2, a buffer is applied to the selected pixel groups in the Method 3. The width of the buffer was chosen equal to the square root of the pixel group area. All pixels corresponding to a difference of more than 50 cm within this buffer were then retained. Compared with Method 3, which only retains the core of the erosion zones detected, Method 2 enables the shape and size of these zones to be retained. The volume eroded was also calculated by integrating the values of the differential DTM on the eroded surface.

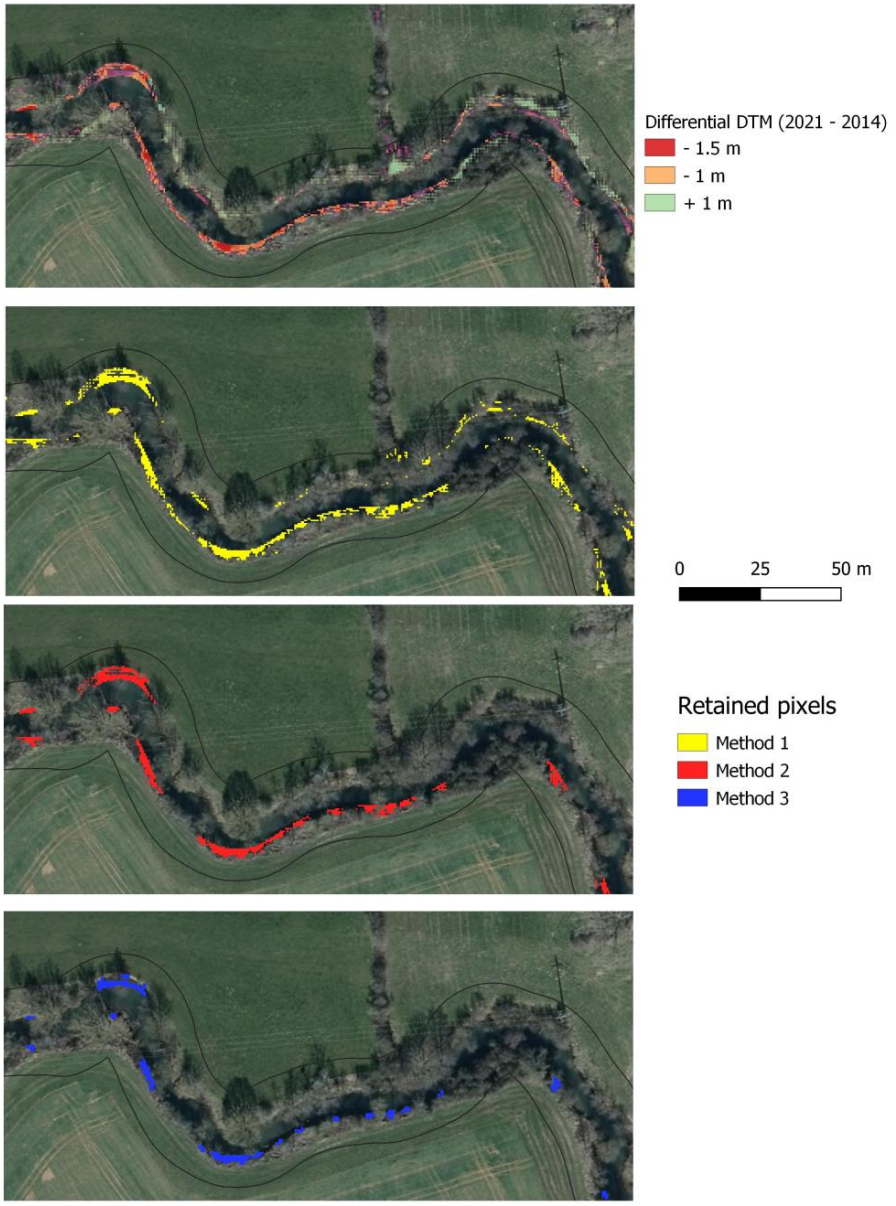

Figure 48: Noise elimination according to three methods. From top to bottom: zones of erosion (orange-red) and deposition (blue-green) on a differential DTM; erosion zones retained for filtering Method 1 (threshold of 50 cm difference in altitude); according to Method 2 (threshold of 50 cm difference in altitude and morphological filtering); according to Method 3 (threshold of 50 cm difference in altitude, 1.5 m wide and 3 m² area).

The total eroded area was normalized by the length of the stretch considered and the river width (2014 value). The three methods of calculating the eroded area were validated on twelve 300-meter stretches of watercourse, where the eroded areas were digitized manually on the basis of orthophotos contemporary with the LiDAR campaigns and field knowledge (Figure 49). The eroded volume has not been validated.

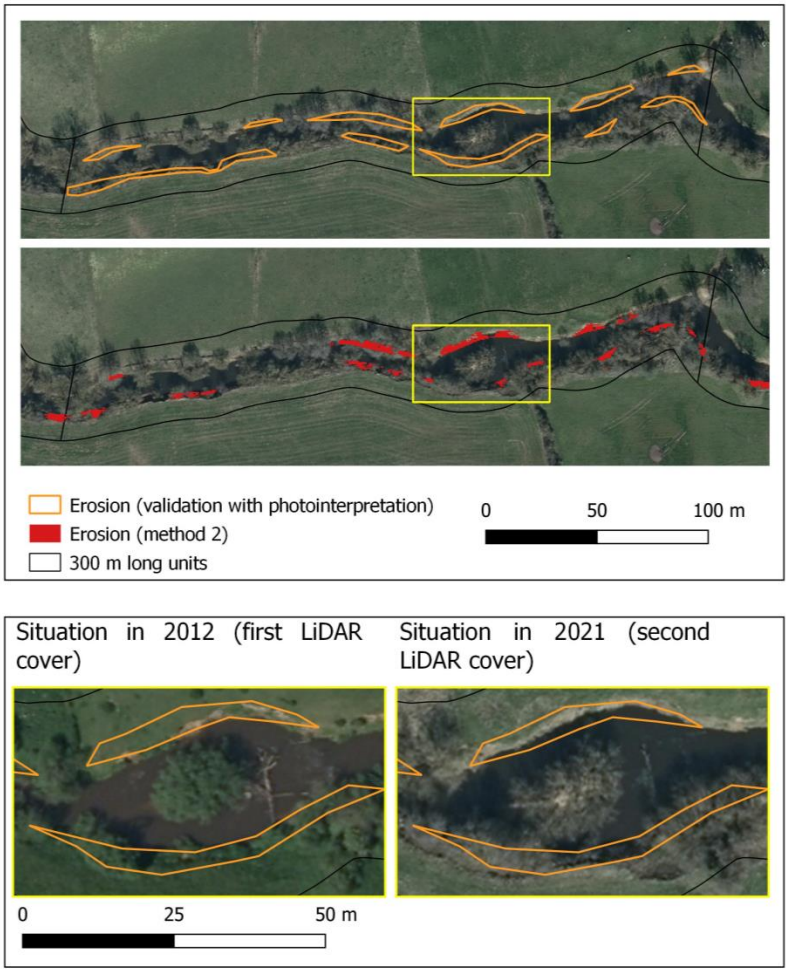

Figure 49: Validation of the eroded area by photointerpretation. Top: comparison between the area mapped by photointerpretation and the area mapped after filtering method 2 on the LiDAR differential DTM. Bottom: comparison of the situation in 2012 (corresponding to the LiDAR flight carried out in 2014) and in 2021 (corresponding to the LiDAR flight carried out in 2021) on an eroded area.

5.3 Results

5.3.1 **Assessing the accuracy of photogrammetric and LiDAR surveys compared with a conventional topographic survey**

The photogrammetric surveys carried out on the Sûre and Lhomme rivers show centimetric altimetric accuracy (Table 16). Bathymetric correction removes the bias associated with water refraction on both sites, confirming the results obtained by other authors (Woodget *et al.*, 2015; Dietrich, 2017). The use of a LiDAR DTM generates satisfactory results for emerged points, although altimetric accuracy is slightly lower. On the other hand, the elevation of submerged points is significantly overestimated on both sites.

Table 16: Overall error in elevation of corrected photogrammetric, uncorrected photogrammetric and LiDAR points in relation to the reference survey, according to their emerged or submerged position. The * in the "Mean error" column corresponds to the significance of the bias, verified by a Student's t test. The letters abc in the "Mean absolute errors" column correspond to the significance of the differences between the DSMs, assessed by Wilcoxon tests (conditions unmet for a Student test), paired in the case of the comparison of submerged points with or without bathymetric correction.

	Lhomme		Sûre	
	Mean error (cm)	Median absolute error (cm)	Mean error (cm)	Median absolute error (cm)
Emerged points (photogrammetric DSM)	-0,5	2[a]	2,5	3[a]
Submerged points (uncorrected photogrammetric DSM)	10,0*	7,9[c]	7,3*	5,6[a]
Points immergés (corrected photogrammetric DSM)	0,5	5,9[b]	-0,4	2,3[a]
Emerged points (LiDAR)	4.3*	5.0[b]	-1,6	5,1[a]
Submerged points (LiDAR)	34.4*	32.0[d]	51,9*	46,3[b]

Five representative cross-sectional profiles of the Lhomme site are shown in Figure 50. Measurements of bankfull width, depth and cross-sectional area and associated errors are presented in Table 17. Photogrammetric approaches yield cross-sections similar to a traditional approach when bathymetric correction is applied, with insignificant biases on cross-sectional area and width values, and a slight overestimation of depth. The main limitation of photogrammetric approaches

is that the cross-sections are not valid in the presence of vegetation, as in the case of cross-section N°1, for which the cross-sectional area is significantly underestimated (Figure 50). This limitation is particularly problematic for narrow rivers, where the presence of vegetation along the entire length prevents the extraction of valid cross-sections. In wider rivers, representative cross-sections can be extracted preferentially in open areas (without riparian vegetation), and the herbaceous vegetation present on the banks generates low relative errors on key profile parameters such as bankfull cross-sectional area. In comparison, LiDAR technology systematically overestimates the altitude of the river bed: infra-red beams are absorbed by water surfaces and the thalweg value must therefore be interpolated from the higher banks. As a result, the maximum depth and cross-sectional area are significantly underestimated. Measuring bankfull width only requires the use of emerged points, and LiDAR technology provides values that are close to reality. The longitudinal profile illustrated in Figure 51 shows that LiDAR elevations in the riverbed are close to the water surface elevations.

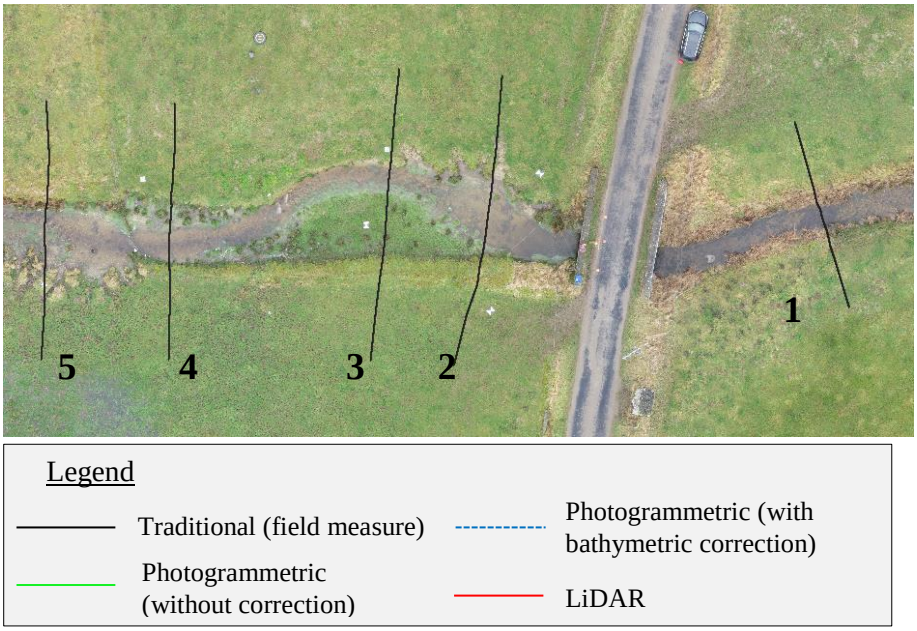

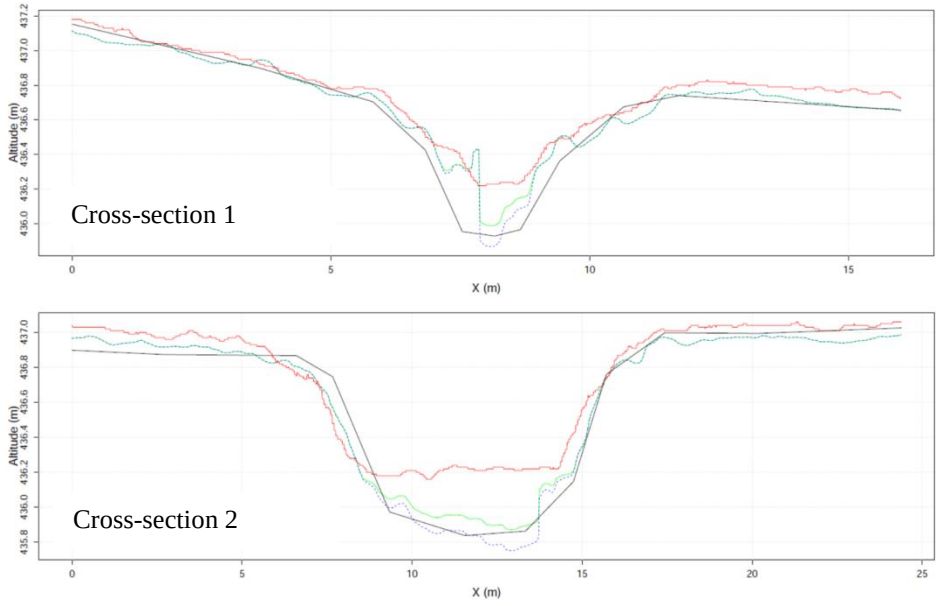

Figure 50: Representative cross-sections obtained with traditional, photogrammetric (uncorrected or corrected for refraction) and LiDAR methods.

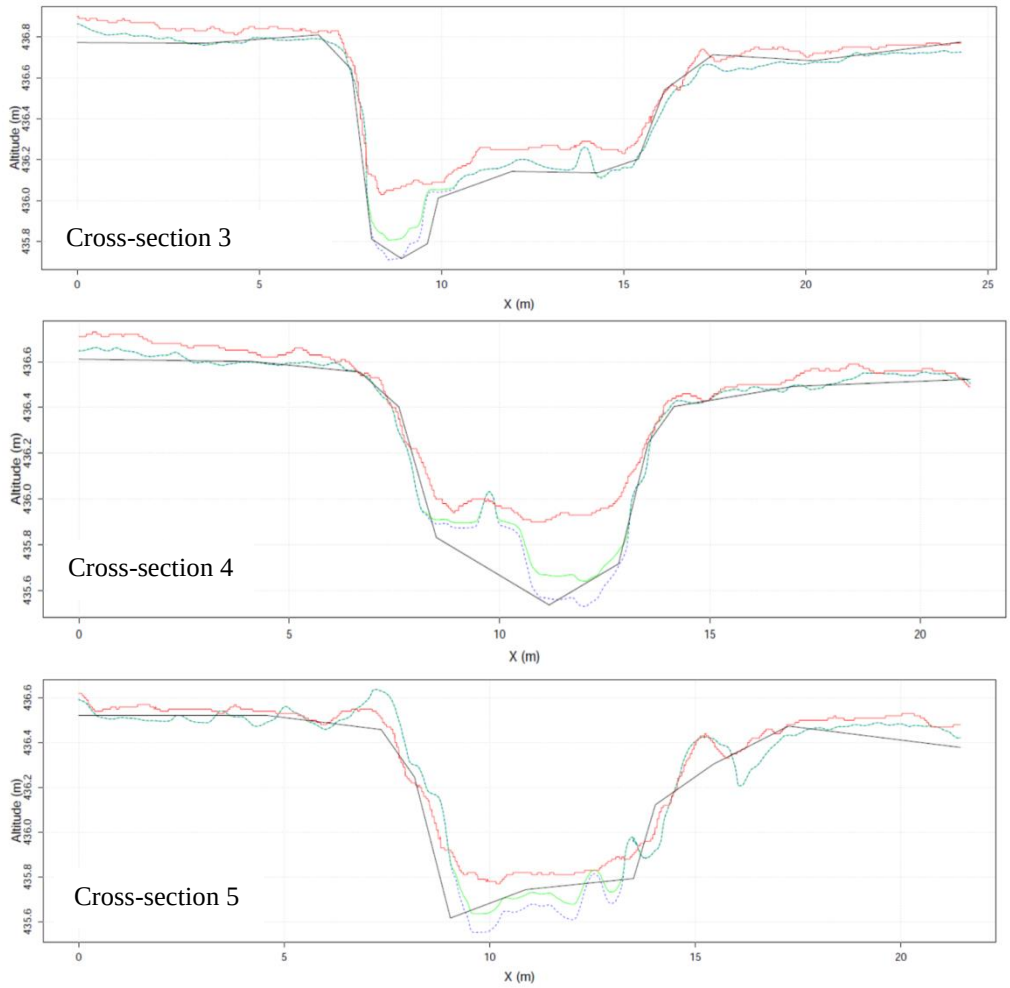

Figure 50 (continued): Representative cross-sections obtained with traditional, photogrammetric (uncorrected or corrected for refraction) and LiDAR methods.

Table 17: Measured values for bankfull cross-sectional area, maximum bankfull depth and bankfull width for 5 cross-sections representative of the Lhomme study site. Reference values were calculated from a field survey. The significance of the mean error was tested using a Wilcoxon signed-rank test (* p-value < 0.1, ** p-value < 0.05), and the error distributions for the photogrammetric and LiDAR methods were tested using a Wilcoxon paired-rank test (letters a and b, 10% probability threshold).

	Bankfull cross-sectional area (m²)						
	1	2	3	4	5	Mean error (m²)	Relative mean error
Reference	1,74	6,34	5,90	4,62	3,99		
Photogrammetric	1,35	6,67	5,82	4,35	4,01	-0,08 (a)	-2%
LiDAR	0,92	4,84	4,48	3,10	3,36	-1,18 (*) (b)	-26%

	Maximum depth (m)						
	1	2	3	4	5	Mean error (m²)	Relative mean error
Reference	0,77	1,01	1,01	0,96	0,78		
Photogrammetric	0,83	1,10	1,02	0,97	0,85	0,04 (*) (a)	5%
LiDAR	0,48	0,69	0,70	0,60	0,63	-0,29 (*) (b)	-32%

	Bankfull width (m)						
	1	2	3	4	5	Mean error (m²)	Relative mean error
Reference	5,23	9,90	14,72	9,82	8,96		
Photogrammetric	5,30	11,10	14,94	9,86	7,69	0,05 (a)	1%
LiDAR	4,77	10,01	12,78	9,49	7,22	-0,87 (b)	-9%

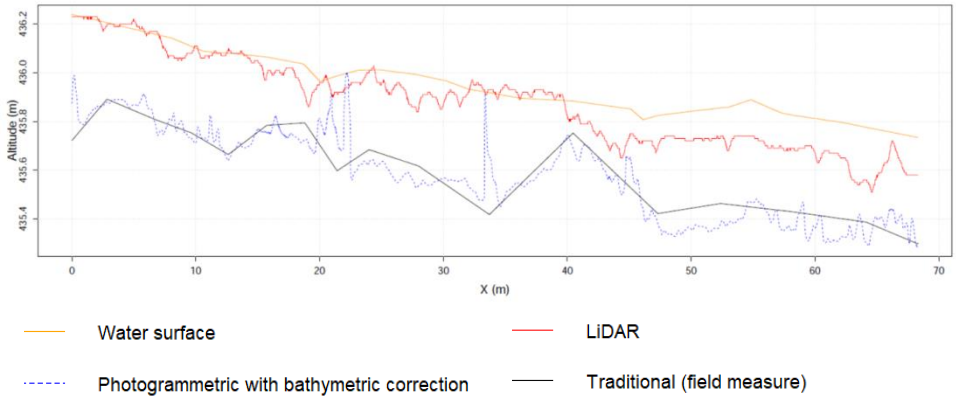

Figure 51: Illustration of a longitudinal profile of the Lhomme river, obtained with a traditional field survey, a LiDAR DTM and a photogrammetric DTM with bathymetric correction. The LiDAR elevation (in red) follows the water surface elevation (in orange).

5.3.2 Using multi-temporal LiDAR data to quantify lateral bank erosion

Water stages measured on the 2014 and 2021 LiDAR DTMs for five gauging stations in the Ton sub-basin are presented in Table 18. Water levels measured at the gauging stations during the 2014 flight were slightly lower than in 2021. The greatest difference in water level was observed on the Chiers, with 36 cm. As expected, the 2021 DTM delivers an altitude closer to the water level recorded during the survey than the 2014 DTM. For the latter, the altitude read on the DTM is systematically higher than the water level recorded at the station. According to these results, the hypothesis of equivalence of water levels during the two LiDAR surveys was considered valid.

Table 18: Comparison of altitudes extracted from LiDAR DTMs and limnimeter readings taken during the LiDAR flight, for the years 2014 and 2021.

	2021				2014			
Limnimetric station	Flight date	Alt. Limni. (m)	Alt. LiDAR (m)	Error (m)	Flight date	Alt. Limni. (m)	Alt. LiDAR (m)	Error (m)
L6440 Ton in Virton	01-03-21	207,70	207,68	-0,02	18-04-14	207,70	207,91	0,21
L6030 Vire in Latour	01-03-21	206,22	206,38	0,16	18-04-14	206,26	206,45	0,19
L5220 Ton in Harnoncourt	01-03-21	193,86	193,84	-0,02	18-04-14	193,68	194,01	0,33
L7660 Chavratte	01-03-21	201,48	201,48	0,00	18-04-14	201,41	201,6	0,19
9741 Chiers in Torgny	01-03-21	189,97	189,95	-0,02	18-04-14	189,61	190,34	0,73

The results of the validation of normalized eroded area on twelve 300 meters long stretches are shown in Figure 52. All filtering methods show a non-significant intercept. The second method, involving morphological filtering and extraction of erosion pixels in a buffer around the selected pixel groups, shows an R^2 of 0.84 that is higher than the other two methods. These characteristics indicate that this method effectively erases noise for stretches with little erosion, and yields a value correlated with that obtained by photointerpretation of orthophotos. This filtering method was therefore selected for the production of the erosion map. Nevertheless, the area estimated by method 2 is on average 1.85 times smaller than the area estimated by photointerpretation.

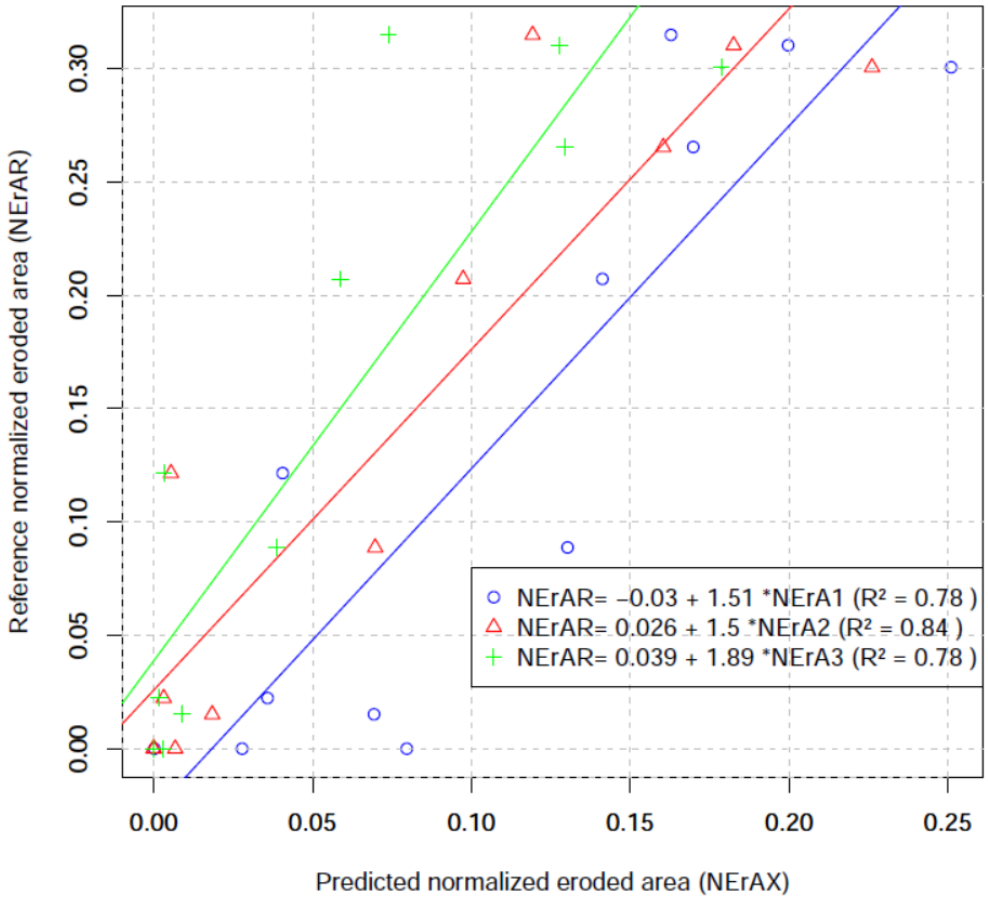

Figure 52: Comparison of normalized eroded areas estimated by photointerpretation (ordinate) and LiDAR (abscissa) according to three filtering methods.

Figure 53 shows the results for normalized eroded volume. This value is much less sensitive to the method used. The second filtering method is also the best in this case.

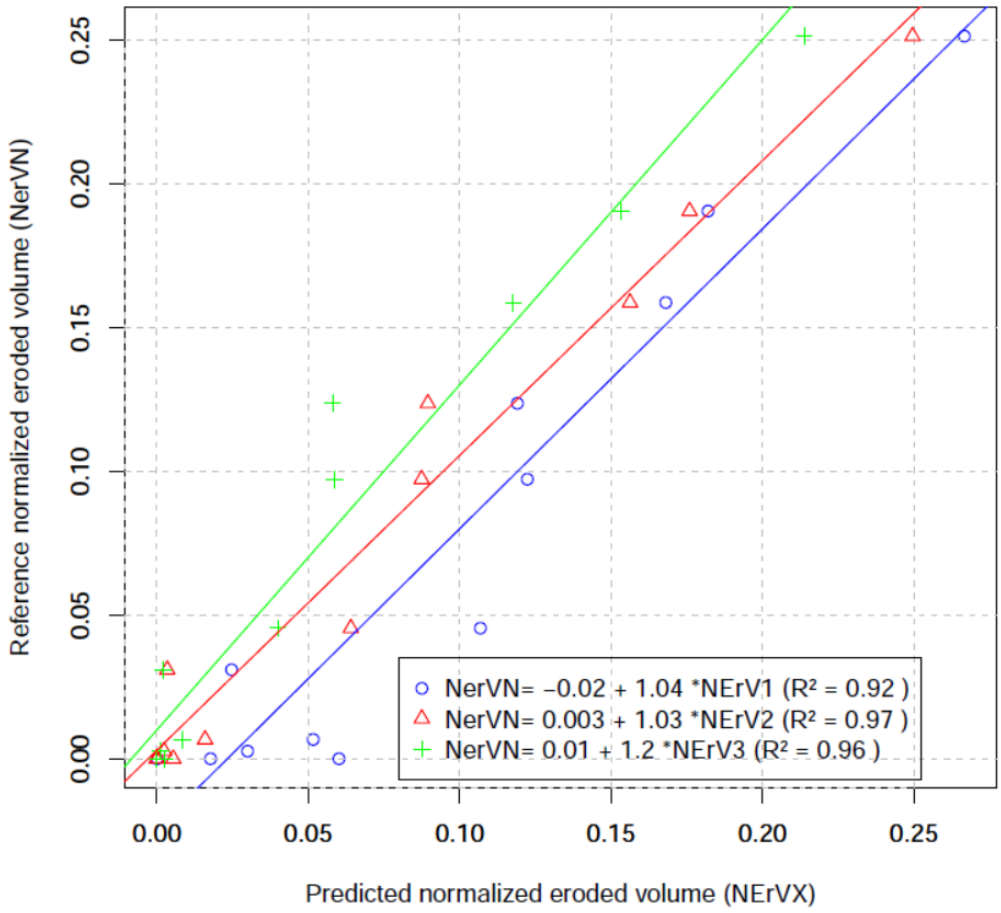

Figure 53: Comparison of normalized eroded volumes estimated by photointerpretation and LiDAR (ordinate) and using LiDAR (abscissa) according to three filtering methods.

5.3.3 **Mapping at basin scale**

The map of normalized eroded area is shown in Figure 54. The Ton is little active upstream of its confluence with the Vire (banks moved less than 2% of river width in 7 years). The Vire and the Chavratte show intermediate activity (2 to 5% of their width in 7 years). Finally, the Ton downstream of its confluence with the Vire and the Chiers is more active (over 10% of their width in 7 years). Activity is higher on the more sinuous stretches and lower on stretches that are straight or that flow through urban areas.

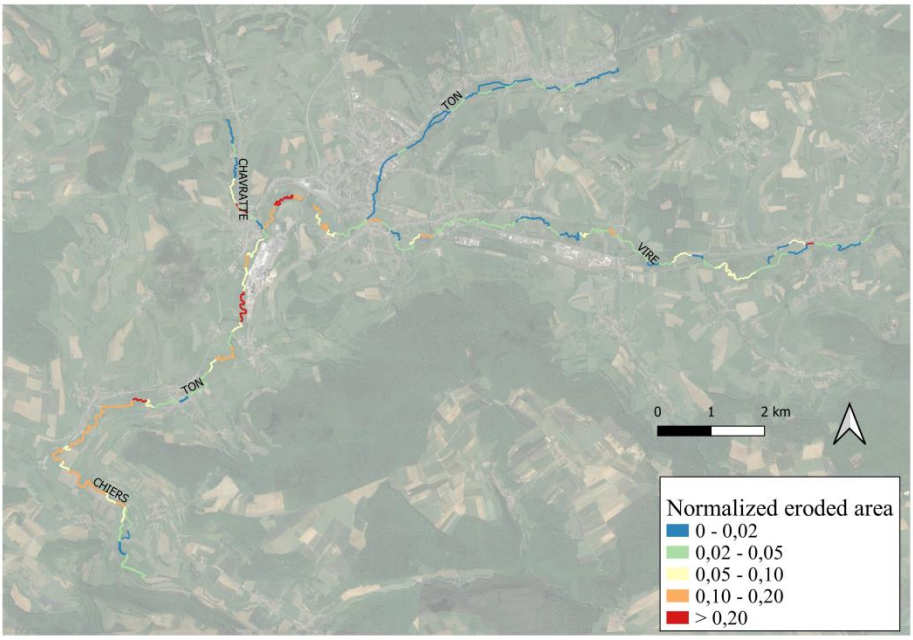

Figure 54: Map of normalized eroded area over the Ton basin, at the scale of 300 m long units.

5.4 Discussion

5.4.1 Comparison of photogrammetric and LiDAR surveys to describe bank morphology and erosion

Two sources of data have been used to describe bank morphology in this chapter. The following paragraphs summarize the strengths and limitations of each method.

When LiDAR surveys are available, they can be used to obtain information on the width of a river or bank mobility. The greater the point density, the more detailed the information. The data can be used over long linear distances, even in the presence of woody vegetation. Most of the processing is carried out by the data provider, and the use of digital terrain models is relatively straightforward: the presented method for mapping bank erosion essentially requires knowledge of GIS (see section 5.2.2). However, the submerged parts of the river are not described. Techniques have been developed to exploit LiDAR data on emerged parts and optical data for bathymetry, but these techniques are labor-intensive and difficult to deploy over large areas (see for example Legleiter (2012)).

Under the application conditions for photogrammetric surveys based on UAV images (little vegetation, shallow bed with visible bottom), these enable finer mapping of the minor bed and its evolution, including in its submerged parts. Our results confirm those of Woodget *et al.* (2019) and Woodget *et al.* (2015), and

complement them with a comparison with key parameters measured with traditional surveys (bankfull cross-sectional area, bankfull maximum depth and bankfull width). The very high-resolution orthophotos produced simultaneously with the 3D models are useful for interpretation. The main constraint is having the necessary equipment and know-how to carry out a good survey. Nevertheless, the marginal cost of acquisition is low. The river length that can be covered is limited by the amount of work required (surveying a stretch of one to a few kilometers takes a day, and data processing half a day) and by the conditions of application, which are rarely encountered on long stretches. Photogrammetric surveying is therefore an alternative or a complement to traditional topographic surveying, particularly for monitoring over time or when cross-sections are highly variable.

In all cases, sedimentation is more difficult to observe than erosion. Indeed, sedimentation results in increments of a few centimetres, which can be masked by the presence of vegetation or slight elevation biases linked to acquisition conditions. In addition, the results of these different methods need to be cross-checked and critically interpreted, as the 3D products generated are not free of artifacts.

5.4.2 **Prospect for erosion mapping over large areas**

Although bi-temporal LiDAR datasets have been used in other studies to quantify erosion phenomena, there has been little methodological development on this subject. Errors associated with the estimation of eroded volumes have notably been analyzed by Kessler *et al.* (2012) for lateral erosion in meandering rivers, and by Lallias-Tacon *et al.* (2014) who carried out the sediment budget of a braided river. Error assessment is not generally based on in situ erosion measurements, which are rarely available. It is mainly based on a calculation of error propagation on LiDAR DTMs and on sensitivity analyses. Lallias-Tacon *et al.* (2014) have shown that estimated erosion values can be highly sensitive in relation to the quality of LiDAR datasets and the method used (co-referencing of LiDAR coverages, whether or not submerged surfaces are taken into account and processed, thresholds set for elevation differences). Our study also shows that the noise filtering method has a significant influence on the absolute value of the eroded area. Eroded volume seems less affected by the noise filtering method. However, comparison with an approach based on photointerpretation is not a true evaluation of error; it merely ensures that our method accounts for the contrast between more and less eroded stretches.

In order to mobilize erosion maps within an institutional framework (for example, to support the definition of standards for land-use planning, or as part of watershed management plans), we need to be able to extend mapping to the scale of a region or larger watersheds, i.e. over thousands of kilometers of watercourses. This upscaling involves a number of challenges. Firstly, we used two LiDAR surveys carried out under similar limnimetric conditions, with average water levels. This assumption cannot be systematically verified. As a result, eroded area will be underestimated in basins with higher water levels, and will be positively or negatively influenced when the difference in water levels between the two LiDAR coverages is significant. Secondly, river width, bank height and bank mobility will also influence the

indicator value. In the watershed studied, some streams are five meter wide and show little activity. These streams often have values of normalized eroded area equal to zero, with no contrast from one stretch to another. The proportion of erosion contained in patches over 1.5 m wide is expected to be small in relation to total erosion in these stretches, and the underestimation of actual erosion is therefore expected to be significant. As far as bank height is concerned, it must be greater than the altimetric difference threshold selected (a condition met here with a threshold of 50 cm). Indeed, the higher the banks, the more aggressive filtering can be performed on the difference in elevation without significantly affecting eroded volumes according to Kessler *et al.* (2012). Nevertheless, we can expect bank erosion to be underestimated for streams with low bank heights. Generally speaking, the value of the bank lateral erosion indicator will be essentially comparable between different stretches of the same river or between several rivers in the same catchment area. Further comparisons could only be achieved by correcting the erosion value for the fraction of undetected erosion.

Further studies could focus on the improvement of the method (use of co-referenced datasets, improved and automated delimitation of water surface), as well as on the better characterization of accuracy and biases in contrasted river settings.

5.5 Conclusion

Two data sources were compared to describe cross-sections of a river. Under favorable conditions, a photogrammetric approach based on images acquired using UAVs and incorporating bathymetric correction provides cross-sections equivalent to those obtained by a traditional survey. The use of LiDAR provides a satisfactory description of the emerged part of the banks, although the resolution may be limiting.

Taking advantage of these properties, two LiDAR surveys spaced seven years apart were exploited to generate an indicator of bank lateral erosion over a watershed comprising 50 km of watercourse. Our estimates of eroded area are consistent with estimates made by photointerpretation and with field knowledge. Nevertheless, the method lacks sensitivity for smaller or less active streams. This sensitivity, which varies according to the river under consideration, as well as the different limnimetric conditions at the time of the LiDAR surveys, pose challenges for scaling up to larger watersheds.

6

General discussion

6.1 Scale considerations

When it comes to scale, we need to differentiate between the scale at which the results are represented (size and shape of the map's elementary units, be they pixels, objects or successive river stretches), and the area over which the results are produced (a section of river, a watershed or a region, for example). Considerations relating to these two scales are discussed in sections 6.1.1 and 6.1.2 respectively.

6.1.1 **Scale for displaying results**

When producing a vegetation map, it is necessary to choose the elementary unit for which the selected features will be calculated. The choice of these elementary units (their shape, size and boundaries) poses particular questions in the case of mapping riparian vegetation, and riparian ecosystems in general (Alber and Piégay, 2011). Riparian vegetation is fragmented and organized in the form of a network whose constituent elements vary in dimension according to the size of the river, the width of the floodplain or the degree of fragmentation. Moreover, variations can occur both longitudinally and laterally.

The "tree-centric" approaches deployed in chapters 3 and 4 give spatially fine results, which can then be re-aggregated. In the case of mapping woodland and herbaceous ecosystems, the tree-centric approach is compatible with "object-oriented" approaches regularly used in the riparian context (Rommel *et al.*, 2022; Macfarlane *et al.*, 2017). The aggregation scale must be defined in a way that is consistent with the objective pursued. Four examples of aggregation scales that were used in this manuscript are shown in Figure 55. In Chapter 3, the aim was to understand the distribution of biomass stored in riparian ecosystems within the floodplain, so patches of native vegetation of similar age (the main variable explaining biomass) were considered as reference units (Figure 55a). These were then re-cut so they had a similar size of 1000 to 3000 m². As determining the age of the patches was manual and therefore tedious, it was necessary to disregard the smallest vegetation patches. In Chapter 4, specific composition was mapped using square vegetation units, comparable to pixels and chosen for their ease of use (Figure 55b). These vegetation units do not require any assumption concerning riparian spatial structure and provide the best possible visualization of both longitudinal and lateral gradients, as well as local drivers (Scown *et al.*, 2016). If we are interested in mapping a narrow corridor along the watercourse (e.g. in order to support bank maintenance in a low-energy river), a riparian corridor of constant width can be divided into stretches of equal length (Figure 55c). This division has been used in the context of the use of remote sensing for minor bed management (Chapter 6, section 6.2.1). Such a division into stretches is also feasible for the entire floodplain (Figure 55d): it allows us to relate the riparian vegetation to a portion of the river and neutralize the effect of the width of the alluvial plain. However, it does not allow us to observe lateral gradients within the floodplain.

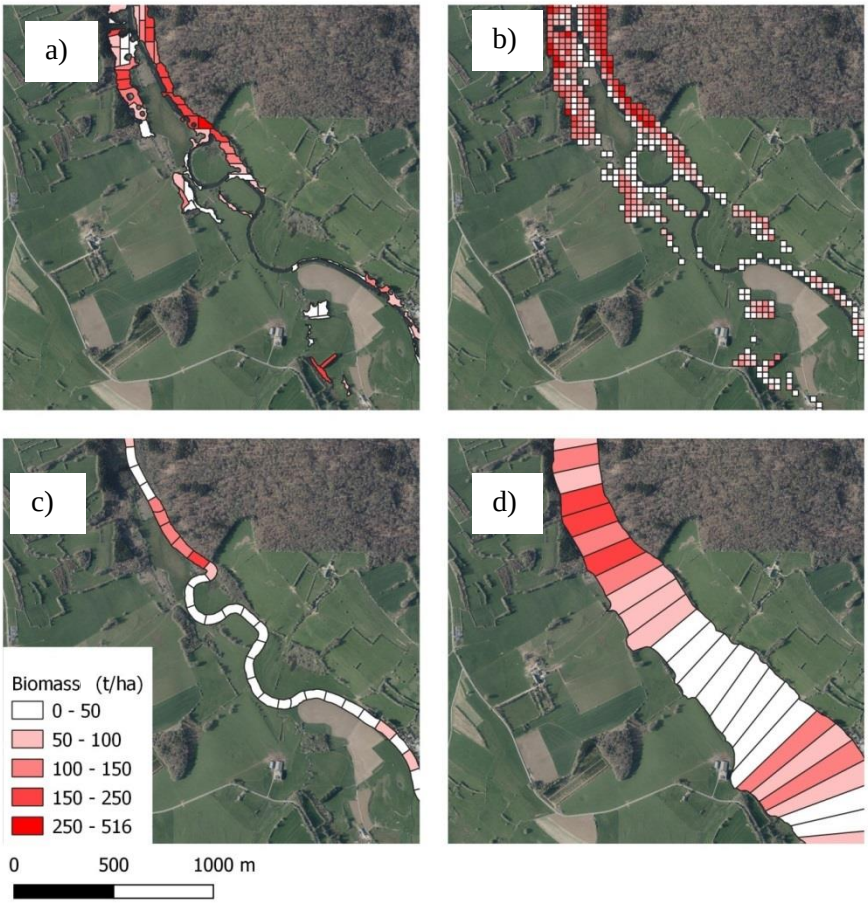

Figure 55: Four types of elementary units for characterization of riparian vegetation. The color levels indicate the areal biomass of riparian vegetation. A) Division into vegetation units of similar age and with a size between 1000 to 3000 m². B) Division into 30 m x 30 m vegetation units. C) Division of a 12 m wide riparian corridor on either side of the river into 100 m long stretches. D) Longitudinal division of the floodplain into 100 m-long units.

When aggregating tree-level information into larger spatial entities, an improvement in accuracy can be expected. In Chapter 4, a species classification model at tree scale is shown to have an overall accuracy of around 80%. When aggregated into 900 or 3600 m² vegetation units, accuracies can exceed 90%, with a more rapid increase for species dominance than for absence/presence predictions (that will intrinsically benefit less from error averaging). In Chapter 3, the aggregation into 3000 m² units reduces a relative error of the order of 40-60% for individual trees to a relative error of the order of 20-30% for 3000 m² units. Zolkos *et al.* (2013) observed similar improvements in a review of the accuracy of forest

biomass estimates with LiDAR data, and linked it to error averaging and a diminution of co-registration errors between field plots and LiDAR datasets. In our case, accuracy improvement can be assumed to be essentially linked to error averaging. Indeed, co-registration errors were limited as reference trees were directly delineated on the LiDAR dataset. It is to be noted however that segmentation errors were found to have a limited impact on biomass estimates. It can be explained by the fact that biomass followed a quasi-linear relationship with crown area. Therefore, when LiDAR pixels are wrongly attributed to a neighboring tree with similar height, the resulting impact on biomass estimates will be attenuated.

Our results show that it is essential to assess the quality of classifications not only at the tree level (which helps us to understand the model's functioning), but also and above all at the scale of the aggregated units that will be used as a decision-making tool or as basic data to answer research questions.

6.1.2 **Extent of area of interest**

Most of the methods presented in this manuscript (with the exception of the work based on UAV images presented in section 5.2.1) have been applied or are relevant on scales ranging from a few dozen to several hundred kilometers of watercourse. At these scales, airborne or satellite sensors are used (Figure 56). It can be difficult to obtain multispectral data with good spectral homogeneity and spatial resolution over such large areas. However, for the species classification model presented in Chapter 4, spectral data have limited weight (both for the high-resolution satellite images used in the model and for the four-band multispectral aerial images tested and not retained).

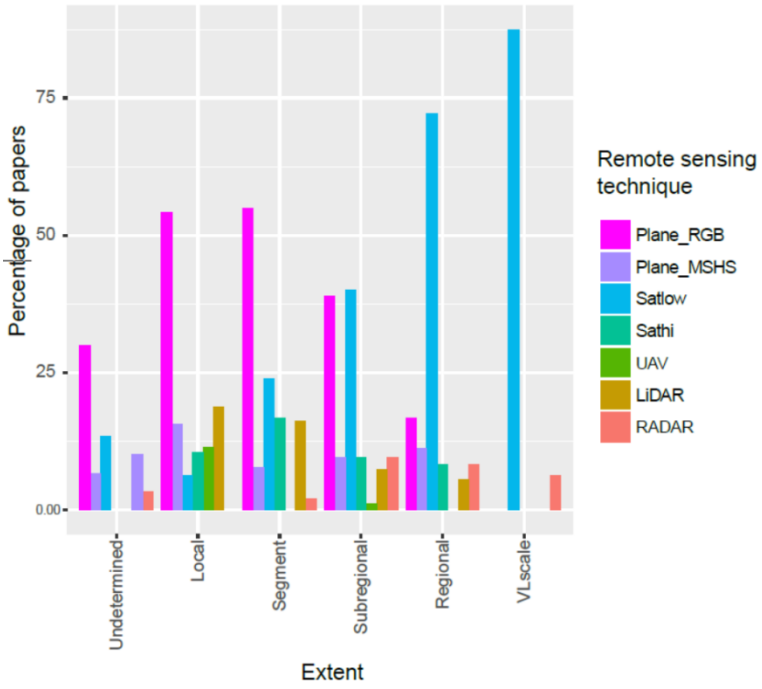

Figure 56: Percentage of use of different data sources according to the size of the study area, taken from the literature review (Chapter 2). For data sources : Plane_RGB = aerial images, plane_MSHS: multispectral aerial images (> 3 bands), Satlow: moderate resolution satellite images (> 10m), Sathi: high resolution satellite images (<= 10 m), UAV: aerial images acquired using a drone, LiDAR: LiDAR sensor, RADAR: RADAR sensor. For scales: Local: < 10 km, segment: 10 to 100 km or < 100 km², sub-regional: 100 to 1000 km or 100 to 1000 km², regional: > 10,000 km or 1000 to 10,000 km², VLscale: >10,000 km².

The algorithms used for species classification and biomass estimation are very different in nature, and this may have an impact on potential upscaling. Biomass is a quantitative variable for which a simple model is used, where the response variable is directly related to the explanatory variables (tree dimensions extracted from a LiDAR dataset). If equivalent variables can be extracted from a second dataset, the model can remain valid under certain conditions. This may be a nearby area with similar vegetation characteristics, or the same area covered by a second, more recent LiDAR survey. This potential is exploited in section 6.2.1 (see Appendix 1) to update biomass estimates using a new LiDAR dataset. In contrast, specific composition is a qualitative response, for which Machine learning and explanatory variables indirectly linked to the response variable are used. The large number of explanatory variables makes it very difficult to extract comparable variables, and a new training dataset has to be constituted each time the algorithm is applied for classification (see section 6.2.1 and Appendix 1).

Furthermore, the main challenges associated with upscaling are not necessarily to be found in the processes linked to the images, their processing or the allometric relationships defined. For example, while the bank erosion detection method proposed in section Chapter 5 is very simple in terms of algorithms and image processing, upscaling is complicated by the need to integrate the local specificities of each river, such as differences in flow between two acquisitions (not the same from one watershed to another), the type of section encountered (bank height influences the erosion detection threshold) or geomorphological characteristics (type of erosion encountered and possibility of detecting it with the method used). For riparian vegetation mapping, GIS operations or the delimitation of the floodplain and riparian zone may be limiting for upscaling. Indeed, it is often necessary to integrate various types of geographical information (hydrographic network, hydraulic or statistical flow models, soil maps, etc.), whose processing and compilation can become prohibitive over large areas. Finally, the interpretation of indicators is a challenge in its own right when they are available at the scale of entire hydrographic networks, as they are influenced by many factors other than those of interest, which act on the ecosystem at different scales (e.g. regional effect linked to geology and climate VS local alteration of anthropogenic origin in Michez *et al.* (2017)).

6.2 Using remote sensing tools to support riparian ecosystem management

This discussion is structured in three subsections. Section 6.2.1 puts biomass, specific composition and erosion mapping in the context of riparian management. The aim is to show how the approaches developed can be used to support riparian management planning. Section 6.2.2 discusses knowledge-transfer and the use of presented methods, sometimes simplified, by river managers themselves.

6.2.1 **Use of indicators for intervention planning**

6.2.1.1 A Walloon framework for planning interventions in riparian zones

In Wallonia, the minor bed and river banks whose catchment area exceeds 100 hectares are directly managed by the State, and the level of authority depends on the size of the river. The administration carries out maintenance work, such as vegetation cutting, removing logjams, dredging and bank stabilization. One effect of this low threshold of 100 hectares is that public authorities are responsible for a significant river length. Since 2016, PARIS programs (Programmes d'Actions sur les Rivières par une Approche Intégrée et Sectorisée) have aimed to evolve river management around several key principles (Figure 57). Greater planning is required for interventions. Managers set six-year objectives for each sector (river stretch), based on local stakes such as flood control or nature conservation. Actions consistent with these objectives are then planned and evaluated at the end of the period. The PARIS programs formalize consultation between the stakeholders

involved in various river management issues, and include monitoring of actions carried out at catchment scale (Service Public de Wallonie, 2022).

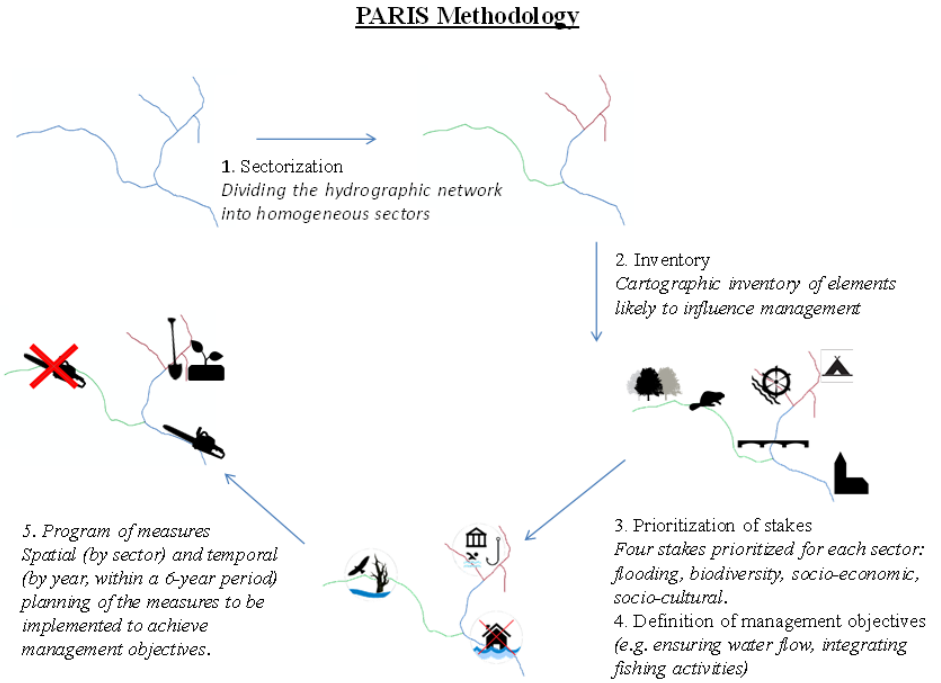

Figure 57: Steps in developing a PARIS action program (figure adapted from the Walloon region's riparian zone management guide (Huylenbroeck *et al.*, 2019)).

Planning, diagnosis and monitoring require up-to-date data on the condition of the river network and riparian areas. In rural watersheds, vegetation management and related phenomena can account for the majority of maintenance work carried out. Remote sensing can be used to assess the state of vegetation at basin scale, with a view to planning maintenance work.

6.2.1.2 A concrete example of the application of the tools developed in this thesis

The three indicators of riparian condition and bank mobility developed as part of this thesis were mapped at the scale of a small watershed, in order to target priority areas for vegetation maintenance in the context of flood prevention. The river network was divided into 300 m long stretches, on which biomass, species composition and normalized eroded area were described. This scale was chosen because it is comparable to the average length of an intervention on riparian vegetation. Species classification (willow, alder, poplar, other deciduous and coniferous) and biomass estimation were carried out according to the methods

presented in chapters 3 and 4 of this thesis. The method and results specific to this section are presented in Appendix 1. The normalized eroded area was calculated at the scale of the study area in Chapter 5.

The two main factors for the production of dead wood in the watershed considered are forest ageing and erosion-driven treefall. Ignoring the mobility of wood, which remains limited given the size of the considered rivers (river width is less than tree height, see Gurnell, 2003), we can consider that local wood production zones correspond to areas at risk of log jams. In order to target the areas where the risk of flow obstruction is greatest, we have highlighted the stretches verifying one of the criteria presented in Table 19. Treefall caused by erosion is favored by the presence of species with shallow roots or by the presence of a high above-ground biomass (high leverage effect). Regarding ageing, it occurs more rapidly in riparian forests composed of pioneer species.

Table 19: Grid for targeting areas of deadwood production

Variable	Criterion	Targeted mechanism
Species composition	Conifer and poplar cover > 20%	Treefall following lateral erosion
Erosion	Normalized eroded area > 5%	
Biomass	Biomass > 100 t/km	Treefall following lateral erosion
Erosion	Normalized eroded area > 5%	
Species composition	Willow cover > 50%	Tree ageing
Biomass	Biomass > 100 t/km	
Species composition	Mixed cover with more alders and willows than other deciduous or conifers	Tree ageing
Biomass	Biomass > 250 t/km	
Species composition	Mixed cover with more other deciduous or conifers than alders and willows	Tree ageing
Biomass	Biomass > 350 t/km	

Areas with increased risk of logjams were then intersected with areas of housing or other sensitive infrastructure in the floodplain, in order to target priority areas for intervention. The result of this intersection is shown in Figure 58. Thirty 300-meter stretches (out of the 154 studied) combine at least one of the risk factors identified in Table 19 with the presence of sensitive infrastructures. These thirty stretches are concentrated in around fifteen zones. The results of this selection are consistent with the vegetation management work planned or recently carried out in the watershed. The upstream part of the catchment is mainly affected by the ageing of well-developed riparian zones made up of alders and other deciduous. Downstream, erosion is more intense and plays a greater role in deadwood production.

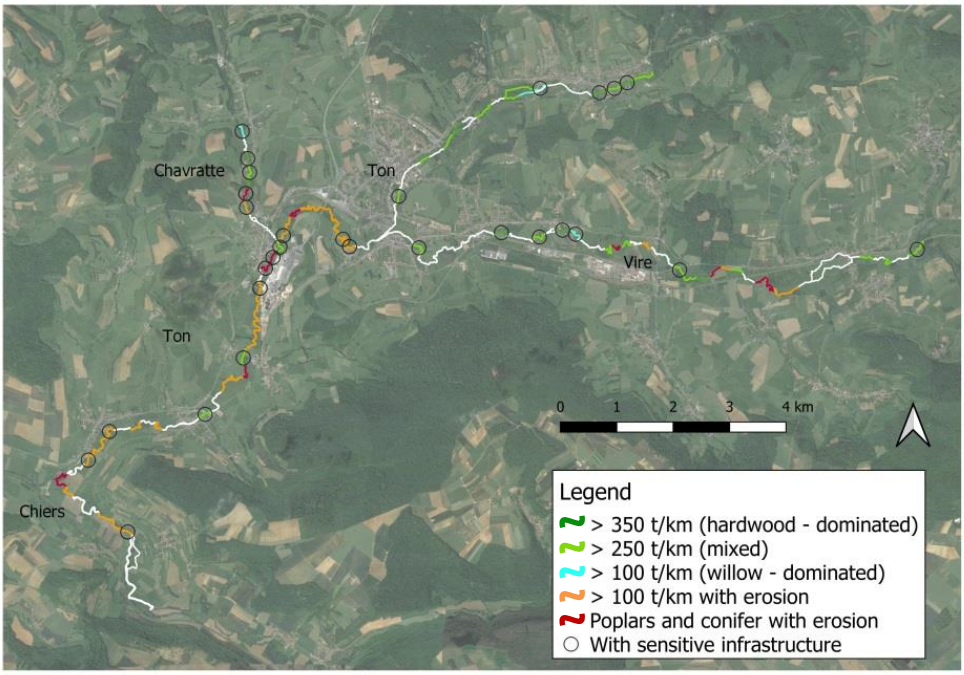

Figure 58: Identification of priority areas for riparian vegetation maintenance. The colors correspond to stretches with increased deadwood production, and the circled areas correspond to the thirty stretches combining sensitive infrastructures and a deadwood production factor.

6.2.1.3 Perspectives and operational application

The cartographic approach proposed for planning riparian interventions provides a synoptic representation of the state of the riparian forest at a given point in time. Targeted areas on the map can be visited to confirm the need for intervention. In addition to highlighting the zones most at risk of tree fall, this synoptic view can help authorities to adopt a readable management approach to riparian vegetation, based on objective data and consistent across the watershed. This approach can be fully integrated into a planning process such as the PARIS approach developed by the Walloon administration. The reference period for this approach is six years, which is comparable to the updating of LiDAR data in Wallonia.

The indicators produced can also be integrated into a broader database that also includes information collected in the field, such as the presence and condition of artificial riverbanks (Bernier *et al.*, 2021) or the generally well-known actively managed areas (urban areas, critical infrastructures). With regard to riparian vegetation, other indicators that can be extracted from a LiDAR point cloud include tree health and the number of dead trees (Kamińska *et al.*, 2021). Flow obstruction by woody vegetation could also be quantified by looking at the number or

distribution of LiDAR returns in the minor bed, following the method of Jalonen *et al.* (2015), who quantified the characteristic surface area of foliage and branches in the channel at tree scale and with terrestrial LiDAR.

6.2.2 **Use of tools by managers in an operational context**

The use of the methods presented in Chapters 3 to 5 of this thesis requires specific skills, which are not necessarily mastered by river managers. Nevertheless, many uses require little technological expertise and are available to professionals whose main activity is not the processing of geographic information.

In Wallonia, where the work for this thesis took place, many river managers regularly use orthophotos or LiDAR DTMs available on a regional scale. Nevertheless, these data remain under-utilized in relation to their potential. In addition to the need for appropriate training, tools, methods and data are not all available in the same place. Moreover, the sheer volume of data associated with high-resolution remote sensing can be daunting for managers, especially when they don't have access to sufficient computing power or storage facilities.

Several tools have been developed or compiled within toolboxes, such as the Fluvial Corridor Toolbox, which is embedded in the most common GIS programs and facilitates geoprocessing in the context of rivers (Dunesme *et al.*, 2021). Other examples include the RCAT and BRAT models dedicated to assessing the ecological status of riparian zones (Macfarlane *et al.*, 2018). However, it's worth mentioning that the ease of use, documentation and maintenance of these tools is uneven.

The growing availability of OpenSource and interoperable data and tools makes it possible to design tailor-made training courses, adapted to the needs of field operators and sometimes backed up by research projects. For example, at the request of river managers, we have designed a GIS training course including an analysis of the limitations of each remote sensing technique (e.g. the behavior of LiDAR beams or photogrammetric models in water) and the implementation of a number of flexible approaches specific to the river context. Course material can be obtained on request from the author.

In the following paragraphs, we first consider challenges relative to the volume of datasets similar to those dealt with in this thesis. We then present considerations relating to the tools available to river managers for diagnosing erosion and mapping riparian vegetation.

6.2.2.1 Data volume

Table 20 presents data volumes associated with different sources of data used in this thesis, for a reference study area corresponding to 200 km of rivers. The use of UAV images generates important data volumes but is rare at such scale. Data volume is considerably larger (about ten times) when images or point clouds cover the whole watershed, compared to when only tiles relative to the river and its floodplain are selected. However, it is clear that data storage facilities (volume and prompt availability, for example through SSD storage or appropriate network) can be limiting in some institutions to work comfortably with high resolution remote

sensing data over large areas. This is particularly true for dense LiDAR datasets, with up to 1000 GB that must be processed (from .las format) to cover 200 km of rivers with 40 pulses/m². Thus, one must consider the costs and benefits of acquiring such large datasets depending on the intended use. In this thesis, considerably less dense LiDAR datasets (4 pulses/m²) seemed to give comparable performances for the classification of species composition (see Chapter 4 and Appendix 1), and we argue that similar or slightly higher densities would be satisfying for most applications regarding riparian forest or riverbank erosion.

Table 20: Indicative volumes associated to different sources of data used to map a reference study area of 200 km of rivers with their associated floodplain. Alternatively, datasets cover associated watersheds of 2000 km². Such a study area corresponds approximately to that used in Chapter 3 relative to riparian biomass. File sizes related to LiDAR point clouds were presented in the compressed format .laz (used for storage) and .las (preferentially used during processing). Individual file size corresponds to the size of tiles or images, as specified in brackets in the "format" column.

Type of data	Format	Size (Gb)	Individual file size (mb)
UAV images, 2 cm GSD	60.000 photographs	420	7
	Orthophotomosaic (200 X 1 km-long surveys)	200	1000
Satellite images, 3 m res., 8 bands	4 X 600 km² images	8	2000
Aerial images, 0,3 m res., 4 bands	Orthophotomosaic (200 X 1 km² tiles)	8	40
	Orthophotomosaic (associated 2000 km² watershed)	80	80.000
LiDAR data, 1 pulse/m²	LAZ point cloud (50 X 4 km² tiles)	2	40
	LAS point cloud (50 X 4 km² tiles)	12	240
	1 m res. DTM (20 X 4 km² tiles)	1	20
	1 m res. DTM (associated 2000 km² watershed)	10	10.000
LiDAR data, 4 pulses/m²	LAZ point cloud (200 X 1 km² tiles)	8	40
	LAS point cloud (200 X 1 km² tiles)	48	240
	0,5 m res. DTM (200 X 1 km² tiles)	4	20
	0,5 m res. DTM (associated 2000 km² watershed)	40	40.000
LiDAR data, 40 pulses/m²	LAZ point cloud (800 X 0,25 km² tiles)	200	250
	LAS point cloud (800 X 0,25 km² tiles)	1000	1250
	0,15 m res. DTM (800 X 0,25 km² tiles)	40	50
	0,15 m res. DTM (associated 2000 km² watershed)	400	400.000

However, the use of high resolution data can be further limited by processing time, as processing facilities are relatively expansive as compared to data storage. As processing time highly depends on optimization and hardware, it is difficult to set an indicative time for a particular process. With an adequate, relatively powerful desktop computer (i.e. 32 GB RAM a 6-core 4Ghz CPU), one can assume that normalizing a point cloud from .las files in the lidr environment should take the order of 5 s/km² for a LiDAR dataset with 1 pulse/m² (15 minutes for the 200 km long study area) and 200 s/km² for a LiDAR dataset with 40 pulses/m² (10 hours for the 200 km long study area). It is thus clear that high data volumes penalize availability for managers, and processing high resolution data requires adequate hardware, habits and skills (e.g. tiling, code optimization, running processes at night or on distinct computers).

6.2.2.2 Erosion diagnosis

As we saw in Chapter 5, remote sensing data can be used to detect or quantify changes in river morphology. Several data sources can be used to diagnose the extent of erosion. The first reflex is usually to consult historical aerial images. This technique makes it possible to go back in time and identify erosion of at least one meter. Quantification is difficult, except in the case of major erosions or erosions occurring over long periods of time. In the presence of tree cover, the technique is ineffective.

A second reflex is to carry out a conventional topographic survey, for comparison with an existing survey. Alternatively, two topographic surveys can be carried out in succession. This is a well-established technique, where the emphasis can be placed on acquiring the information required (sedimentation of a sandbar, lateral bank erosion, stream incision). Nevertheless, the diagnosis is carried out on discrete profiles, a problematic feature for many scenarios (localized erosion between two profiles, search for low points on a levee, profiles not exactly taken at the same point for streams with highly variable cross-sections). In addition, there may be a pronounced operator effect, linked in particular to the choice and density of measurement points, or to the definition of the bottom when the latter is soft or composed of coarse sediments.

Alternatively, when two LiDAR DTMs are available, comparing them can help diagnosing erosion. It can distinguish bank retreats of the same order as the resolution of the coarser DTM. For local diagnosis, unlike automatic processing over a large area (see 5.2.2.2), human intelligence can be mobilized to a certain extent to differentiate noise from information (Figure 59). Under these conditions, advanced GIS skills are not required to operate two LiDAR surveys. Nevertheless, the frequency of surveys is generally not controlled by the river manager, which is a major limitation for diagnosing recent erosion.

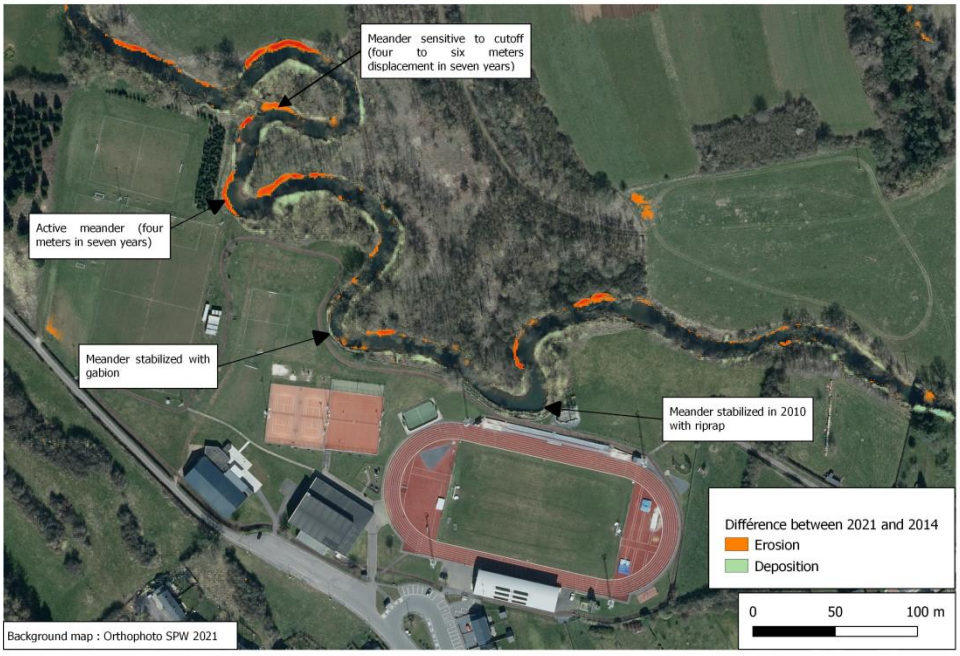

Figure 59: The figure shows a case study for monitoring erosion on the Ton at Virton. The town's sports facilities were built in the 1970s in an area with intense lateral erosion. Two digital terrain models from 2021 and 2014 were compared to highlight areas of erosion (orange) and deposition (blue-green). The part of the watercourse submerged in 2014 was masked, as were differences in elevation of less than 50 cm. Two meanders have been stabilized. Two other meanders have experienced recent activity, with forthcoming damage to infrastructure and meander cutoff. The erosion-deposition map helps to diagnose the extent and spatial structure of river movements.

Finally, UAV photogrammetric surveys can be carried out (Figure 60). These provide accurate, spatially continuous results (see section 5.3.1) and can be used in areas where no aerial imagery or LiDAR coverage is available. Nevertheless, they require specialized skills and are applicable in a limited range of situations. Although the marginal cost of these acquisitions is low, the fixed costs (particularly for acquiring the necessary skills) are relatively high. This approach only makes sense in the context of sufficiently large organizations, where a limited number of people can specialize in GIS and remote sensing.

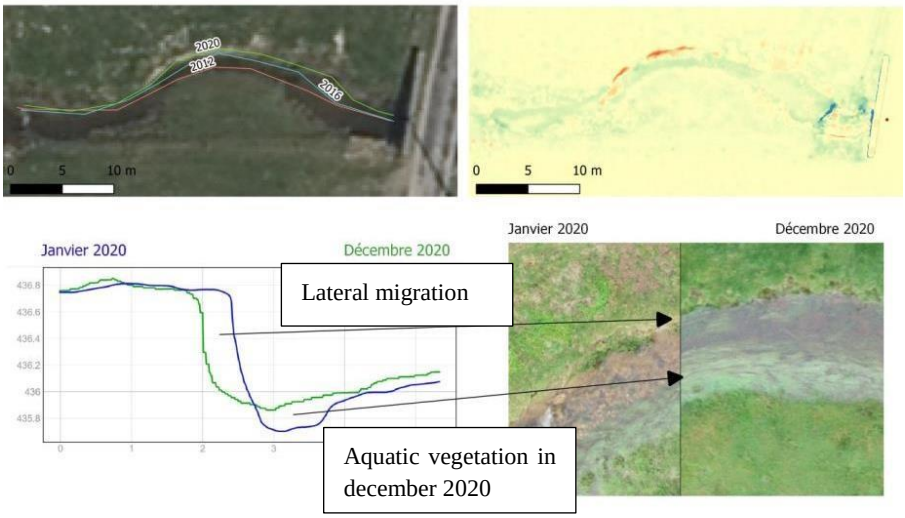

Figure 60 : Study of the erosion of a meander of the Lhomme river using different methods. From left to right and top to bottom: use of orthophotos acquired by plane between 2012 and 2020 to delimit the location of the right bank, use of a differential photogrammetric DSM for the beginning and end of 2020, comparison of bank profiles from photogrammetric DSMs, overlay of orthophotos produced using drones.

Irrespective of the technique chosen, the results of these different methods need to be cross-checked and critically interpreted, as cartographic products produced on the basis of remotely sensed data are not always free from artifacts (distortions in a photogrammetric model, interpolations in a LiDAR DTM, etc.).

6.2.2.3 Vegetation mapping

Two approaches to vegetation mapping have been described in Chapters 3 and 4 of this thesis. These approaches require a significant investment in know-how, field data and development before they can be deployed. In comparison, structured photointerpretation approaches are available to the widest possible audience and offer maximum flexibility for vegetation mapping. To achieve this, the following steps are carried out:

- Extract a hydrographic network of interest to be mapped;
- Geoprocess the lines into stretches 200 m long and 12 m wide;
- Interpret the orthophotos on each stretch to describe the riparian vegetation according to an interpretation grid (an example grid is shown in Table 21);
- Visualize riparian development indicators using a suitable symbology (Figure 61).

Table 21: Multicriteria grid for describing riparian vegetation with regional orthophotos

Criteria	0	1	2	3	4
Tree size	Tree absence	Diameter of tree crowns mostly < 6 m	Diameter of tree crowns mostly between 6 m and 12 m	Diameter of tree crowns mostly between 12 m and 18 m	Diameter of tree crowns mostly over 18 m
Canopy cover	Tree absence	Trees on < 1/3 of length	Trees on 1/3 to 2/3 of length	Discontinuous cover over more than 2/3 of length	Continuous tree cover
Senescence and potential for flow obstruction	Tree absence	Absence of fallen, overhanging or dead trees	A few dead or overhanging trees	Many dead or overhanging trees, big fallen trees	
Diversity of species or strata	Tree absence	1 species or strata (all tree crowns look alike)	2 to 4 species or strata can be distinguished	More than 4 species or strata can be distinguished	
Width of riparian buffer	Vegetation absence	Riparian strip with spontaneous vegetation < 12 m on either side of the river with adjacent intensive land use (crop, road, buildings)	Riparian strip with spontaneous vegetation < 12 m on either side of the river with adjacent extensive land use (grassland)	Riparian strip with spontaneous vegetation > 12 m on either side of the river (forest or wetland)	

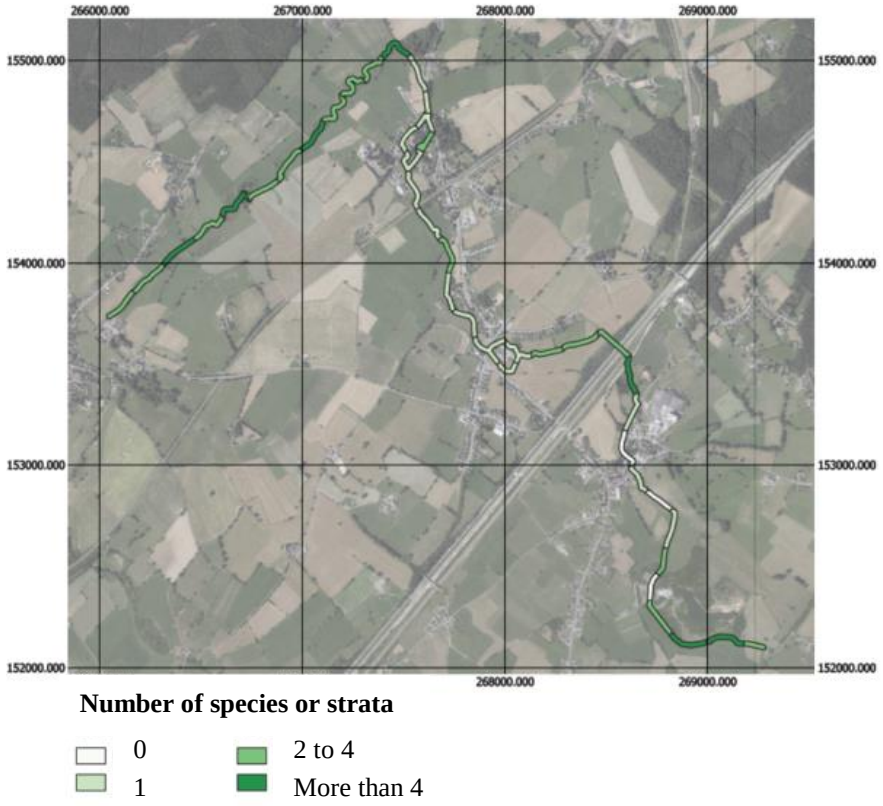

Figure 61 : Photointerpretation map of riparian species diversity and strata along a ten-kilometer stretch of river. On this river, diversity is lower in the immediate vicinity of urbanized areas.

Depending on the images available, different criteria can be interpreted. For example, interpretation of the age of the riparian vegetation requires several historical images, but can be carried out using orthophotos with a resolution of one meter. Such an approach was deployed in Chapter 3 of this thesis: its application on the floodplain of 230 km of rivers (i.e. 900 hectares of riparian vegetation) was achieved in a week by a well-trained operator. Identifying dominant species on the basis of orthophotos is more difficult. Even with images of centimetric resolution (UAV images), it is necessary to gather species by group and to have training data. A season of acquisition that takes advantage of the singular look of certain species at a given phenological stage, or the use of multispectral images, can help differentiate between riparian species (Figure 62).

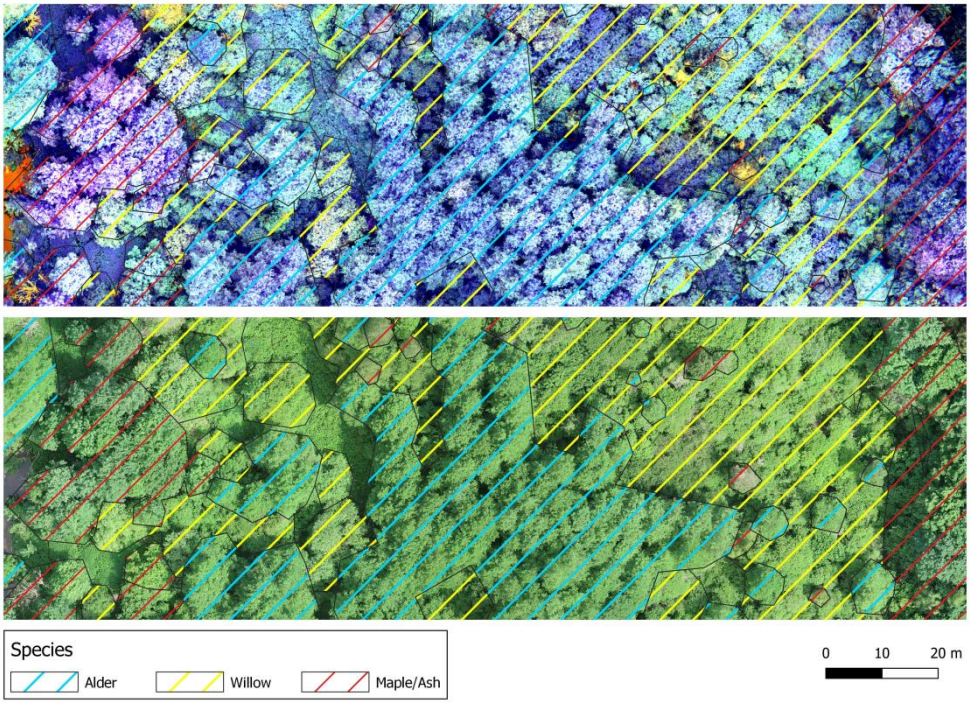

Figure 62 : Orthophotos obtained using a multispectral camera (top, blue-green-near infrared color composition) and a conventional camera (bottom, red-green-blue composition) mounted on a commercial UAV. In this image, maple and ash trees stand out for their rough canopy and predominantly blue color. Alder trees stand out for their near-infrared dominance, and willows for their green dominance.

Similar approaches can be deployed using 3D models derived from LiDAR or mixed LiDAR-photogrammetric data (Michez *et al.*, 2020). Some indicators, such as riparian height or canopy proportion, can be obtained automatically using simple aggregations of pixel values within predefined units. We have reproduced the approach presented in section 6.2.1 for dead wood production, using only operations that can be performed within a GIS. Three risk factors were mapped and intersected: lateral bank erosion (see section 5.2.2), canopy cover and tree height. Woody vegetation was delineated using a 2021 LiDAR CHM, retaining only vegetation with a minimum height of 3 meters. Buildings were masked out using an auxiliary layer. This step can also be performed using morphological filters. The average height of the vegetation corresponds to the average height of the CHM within the "woody vegetation" envelope. The potential for deadwood production was approximated by the product of the three risk factors mapped separately. Four relative risk classes were thus defined (Figure 63). The risk map is broadly in line with the results of the detailed approach presented in section 6.2.1.

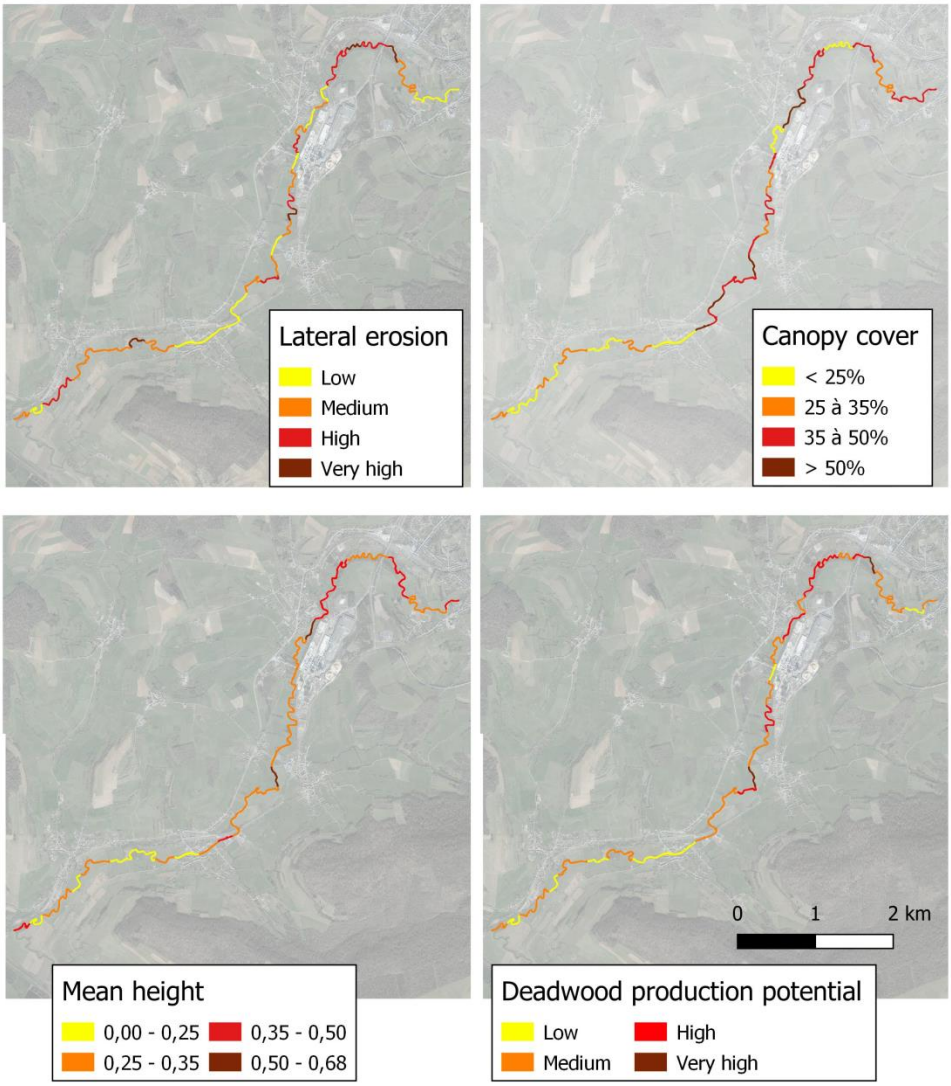

Figure 63 : Spatialized estimate for deadwood production potential along 12 km of the Ton downstream of Virton, using a simplified approach.

Thus, managers' approach to mapping riparian vegetation can be structured according to the following steps:

- define the objective (for example, to define a riparian vegetation regeneration plan);
- define the relevant indicators for this objective (e.g. proportion of vegetation cover, erosion intensity or land use);

- define the working scale (e.g. 100 m long stretches);
- define the indicator extraction method (photointerpretation of aerial images or automatic extraction of spatialized statistics) and translate this method into algorithmic form (photointerpretation grid or script);
- intersect the indicators to display spatial variation with an adequate level of contrast (for example, show areas of moderate erosion without riparian vegetation in grassland areas);
- interpret the map critically, confirming the information contained in the map by mobilizing field data or scheduling confirmation visits;
- exploit the data (draw up a plan of priority areas for planting or fencing).

6.3 Perspectives

Prospects for improvement of the tools developed or further studies using them have already been proposed in the various chapters. These include:

- The replication and comparison of biomass distribution studies in contrasting catchments, in order to identify how biomass drivers vary according to the geographic context (Chapter 3);
- The prediction of other biomass compartments (notably underground biomass), using allometry or soil models (Chapter 3);
- The improvement of species classification, notably with the use of high resolution multispectral images acquired at different times (but not merged) throughout the growing season (Chapter 4);
- The use of more complex distribution models for species compositon, allowing to distinguish which drivers operate at which scale (Chapter 4);
- A thorough assessment of the sensitivity of bank erosion estimates to varying conditions (river width and activity, bank height,…) (Chapter 5);
- The addition of new, complementary indicators in the model aiming to prioritize riparian maintenance operation (notably flow obstruction and tree health) (Chapter 6, section 6.2.1.).

These perspectives are not discussed further in this section. Instead, we focused on perspectives that relate to several chapters of this thesis. We structured this section according to the work of Rodriguez-Gonzalez *et al.* (2022), who identified 10 challenges to address in order to improve riparian science and management (Figure 64).

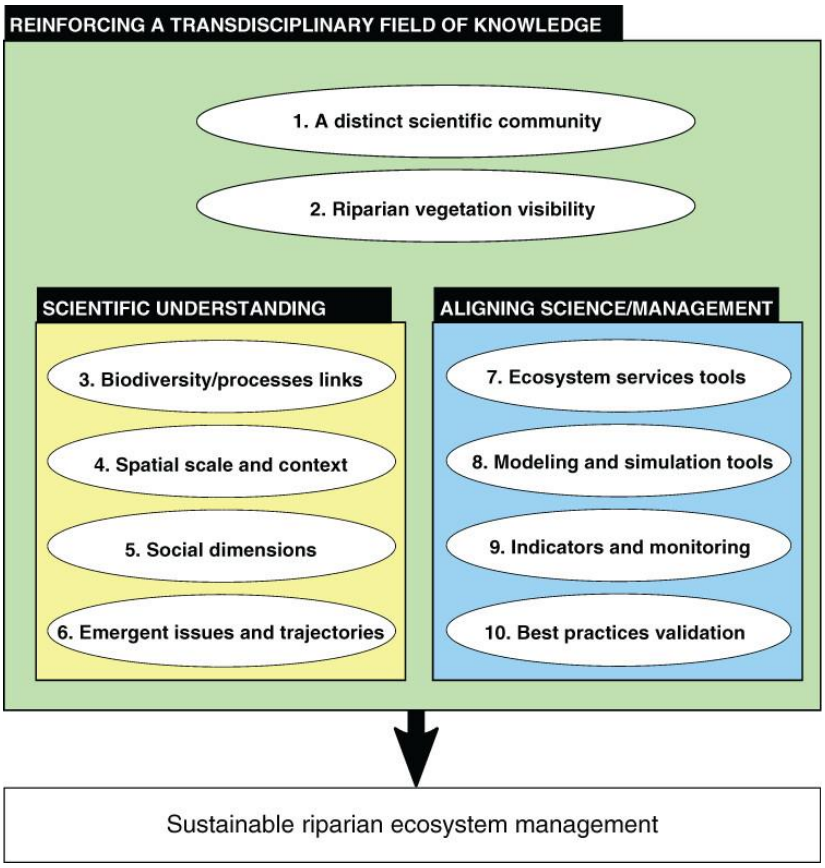

Figure 64: Ten challenges to enhance riparian vegetation science and management. From Rodriguez-Gonzalez *et al.* (2022).

A better integration of spatial scale and context was identified as a key challenge (challenge 4). Indeed, processes are mainly studied at the scale of a limited number of chosen river stretches. Yet these processes are often dependent on the local context, and management objectives often rely on the combination of these processes at watershed scale. The tools developed to map riparian forests using LiDAR data open up possibilities for better integrating this spatial dimension into thematic research on riparian ecosystems. This cross-cutting issue will be discussed through the contribution of our work to three other identified challenges, namely the study of emergent issues and trajectories (challenge 6), the improved modeling of riparian processes (challenge 8) and the improvement of monitoring and assessment protocols (challenge 9).

6.3.1 **Emerging issues and trajectories**

Our landscape-scale analyses of biomass and species compositon allowed us to better understand its spatial patterns and driving factors. Numerous studies have

studied the impact of land use and agricultural practices (e.g. Sawtschuk *et al.*, 2013, Fernandes *et al.*, 2011) or geomorphology, topography and soils on riparian forests (e.g. Rodriguez-Gonzalez *et al.*, 2010, Godfroy *et al.*, 2022). When the two types factors were integrated, one of two was often represented with a simple, monotonic gradient (e.g. Grijseels *et al.*, 2021, Bruno *et al.*, 2014). The inclusion of multi-directional gradients and more local drivers (e.g. soil type, proximal land use) for both types of factors has been far less common. In the studied rural catchments, we showed that both anthropogenic disturbance and geomorphological factors had to be taken into account. The impact of land use was stronger on biomass than on species composition, probably due to the fact that the latter responds more slowly to this factor (Sawtschuk *et al.*, 2013). Preliminary tests indicate that the inclusion of vegetation age (as computed for the biomass distribution model) could significantly improve the prediction of willow and other deciduous proportions, which could indicate succession mechanisms.

The diachronic analysis of riparian forest maps produced as part of our research can help us to interpret their trajectory in greater detail and propose appropriate management strategies. Such monitoring is relevant to understand changes affecting many watersheds such as channel incision (Godfroy *et al.*, 2023), biological invasions (Thomas *et al.*, 2015), climate change (Latella *et al.*, 2020) or changes in agricultural practices (Sawtschuk *et al.*, 2013). Altough unstudied to our knowledge, several drivers may have modified riparian forest dynamics over the last decades such as policy changes (rather ancient such as state takeover of vegetation management in the riverbed in 1950's or more recent with obligations to fence pastures along rivers), reservoir or hydroelectric dams, catastrophic floods (as 2021 floods in several catchments), tree dieback (alder and ash) or beaver recolonization.

Altough historical reference data are not available with comparable quality (especially regarding spatial coverage and location accuracy), trajectories can also be inferred from forest structure using contemporary data. In Chapters 3 and 4, biomass and composition were mapped separately and only total biomass was computed, irrespective of its distribution among size and species classes. However, the distribution of age classes can indicate forest dynamics such as regeneration, persistence of early successional species or senescence (Gonzalez *et al.*, 2010). In order to be fully operational for such purposes, the classification model should also be improved in order to distinguish other species such as *Fraxinus Exelsior*, or to encompass indicators of tree health. Tree structure could also be predicted from LiDAR data (e.g. single or multi-stemmed) as this characteristic can indicate clonal or sexual regeneration (Rodriguez-Gonzaez *et al.*, 2010).

6.3.2 **Improved modeling of riparian processes**

Riparian forests have an important but complex effect on erosion-deposition phenomena (Camporeale *et al.*, 2013). Roots have a stabilizing effect on the bank, but the stems generate additional weight which can provoke bank failure. In addition, flow diversification linked to vegetation or dead wood can stimulate erosion-deposition processes. The methods developed in this thesis could be used to

better understand how vegetation characteristics influence bank erosion processes under natural conditions and at the catchment scale. For example, a sediment model (e.g. SHETRAN, Jane *et al.* (2017)) could be calibrated over the study area on the basis of erosions estimated using LiDAR and hydrological data over the observation period. Variables related to the distribution of tree sizes (or biomass) by species could be calculated at the segment scale and subsequently added as explanatory variables to identify riparian vegetation characteristics influencing lateral bank erosion.

Maps of species composition, biomass and erosion could also be relevant to model wood supply to rivers. While the approach developed in section 6.2.1 is simple and only gives an indication of wood supply potential, spatially explicit models have been developed to predict it quantitatively. These models use data on fluvial processes (topography, discharge, erosion, etc.), forest characteristics and reference data on wood supply to calibrate the model (Steeb *et al.*, 2023). The descriptive maps of riparian vegetation produced in this thesis can provide local riparian forest characteristics (senescence, exposure to erosion and resistance to uprooting) that could help spatialize inputs at any point in the hydrographic network.

6.3.3 **Improving monitoring and assessment protocols**

According to the Water Framework Directive, member states of the European Union must assess the hydromorphological status of all rivers. Such assessment is currently heavily reliant on field-based data and expert opinion. Bizzi *et al.* (2016) identified an opportunity in the use of remote sensing to provide replicable indicators of river hydromorphological quality. Those remotely-sensed indicators can be integrated in a multi-scale framework such as the River Hierarchical Framework, that aims to understand processes occurring at multiple, nested scales (catchment, landscape unit, segment, reach, and geomorphic unit) (Gurnell at al., 2016).

Gonzalez de Tanago *et al.* (2021) point out that riparian vegetation is poorly characterized in most hydromorphological assessment schemes, being mostly assessed with simple indicators such as presence/absence or percentage of cover along rivers. With such indicators, the importance and indicator power of vegetation-related processes for the good ecological functioning of rivers is disregarded.

Vegetation-related indicators that were produced in this thesis (as well as riverbank erosion estimates) can be adequate to assess hydromorphological quality at multiple scales. At the catchment scale, ecological quality could be defined by the area covered by indigenous riparian vegetation or the continuity of riparian forest, as assessed by Michez *et al.* (2017). However, other indicators would be more adequate for assessing proper functioning at the segment and reach scale. Such indicators could include the diversity and typicity of riparian tree species, the age (or biomass) classes per species (indicating regeneration and self-sustainability or riparian tree populations), biogeomorphological coupling (for example, presence of pioneer

species saplings on exposed bars), or the presence of large trees (that provide unique habitats for certain species according to Pollock & Beechie, 2014).

The Figure 65 shows an example of visualization of riparian forests that could be relevant for assessing ecological integrity. Quantitative metrics may be automatically computed to reflect aforementioned indicators of good functioning. These quantitative metrics could in turn be compared to reference values extracted in sites with little disturbance to comply with WFD standards. However, before integrating such indicators in routine assessment, further studies would be needed to identify best variables, scales of observation, reference values and thresholds for good functioning (e.g. Van Looy & Piffady, 2017) on a variety of rivers.

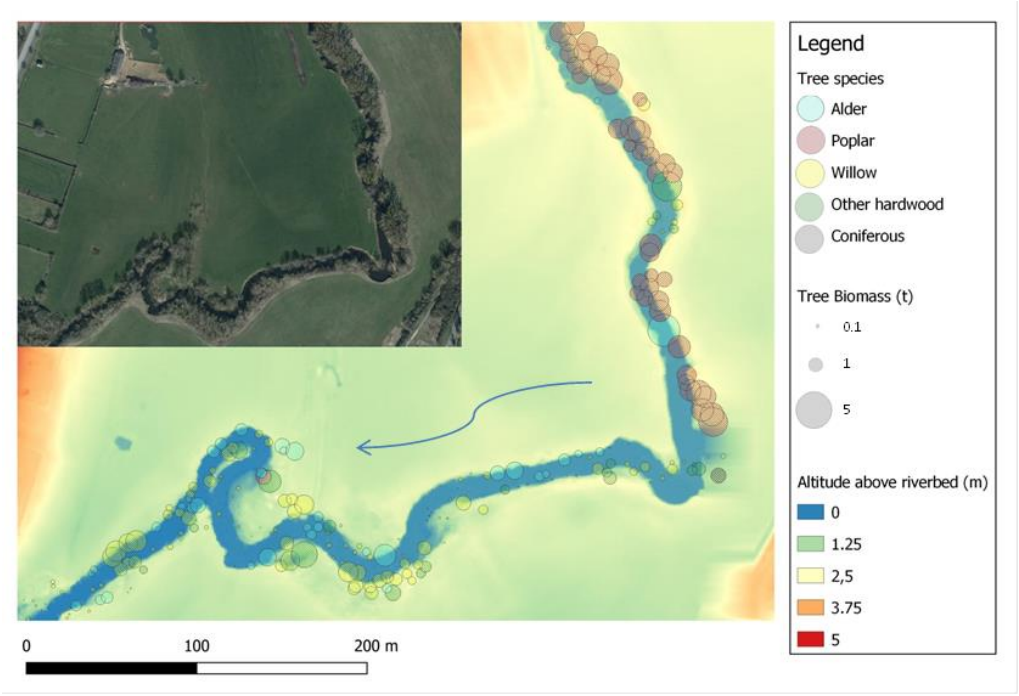

Figure 65: Visualization of riparian vegetation on a relative DEM. Trees are represented as discs, with color corresponding to tree species and size to tree biomass. The upper part of the river stretch (flowing in southward direction, in the right on the map), riparian vegetation is composed almost exclusively of planted poplars of similar, large size. River channel topography shows little diversity and sinuosity. Downstream (bottom of the map), channel is more sinuous and active. Alders, willows and other hardwoods are present in various dimensions. Willow saplings can be observed in the inner side of meanders, indicating biogeomorphic coupling.

7

Conclusion

7.1 Characterize riparian vegetation

The first objective of the thesis was to develop innovative approaches to map riparian vegetation. We reviewed the existing literature. More recently available data (LiDAR and high-resolution multispectral images) are mainly deployed on a local scale, and rarely as part of multi-temporal monitoring. For structural characteristics, LiDAR data are often preferred, while specific composition and physiological processes are mostly described using spectral data. The increasing availability of high-resolution data, regional or global datasets (hydrographic networks, floodplains) and processing tools opens up new prospects for monitoring vegetation over large areas, in lesser-known regions or with greater spatial (resolution) or thematic (variables studied) detail. These prospects can benefit both research and operational applications.

We then developed an approach for mapping riparian vegetation biomass at the scale of a watershed comprising 230 km of rivers and their floodplains (Semois-Chiers basin). This is a tree-centric approach based on a simple allometric relationship, fed by variables derived from the LiDAR point cloud or alternatively from a CHM. Individual tree biomasses are then summed by 3000 m² vegetation units, with an error of around 22% on average for the best model.

Specific composition was also characterized on the scale of a 155 km stretch of the Semois river and its associated floodplain. This is again a tree-centric approach with subsequent aggregation, based on a Random Forest algorithm and variables derived from a LiDAR point cloud and multispectral images. Trees were classified according to a limited number of species groups sharing similar ecological characteristics. The impact of the size of the aggregation unit or the number of classes on accuracy was assessed. For a simple four-class model, accuracy ranged from 80 to 90%, depending on the performance indicator and the size of the aggregation unit considered.

These "tree-centric" approaches offer great flexibility when aggregating trees into larger units. Here, they yielded reliable results on the scale of watersheds comprising around a hundred kilometers of watercourses, for both biomass and specific composition.

Spatial distributions of biomass and specific composition were analyzed in relation to edaphic, geomorphological, topographical, historical and human activity factors. The riparian landscape studied is marked by anthropogenic disturbances, particularly regarding biomass. Other factors, mainly related to waterlogging or topographical position, continue to exert a major influence on specific composition, and a more discreet influence on biomass.

Tools for mapping riparian vegetation must be complemented by tools for characterizing the physical component of the minor bed, as it has a major impact on riparian vegetation and its management. Several techniques for mapping the minor bed and its evolution have been tested. Techniques based on the photogrammetry of UAV images provide remarkable accuracy in both emerged and submerged parts of

the bed, but are only applicable in a limited range of conditions (limited vegetation cover, visible bottom). Conversely, LiDAR technology, which is generally coarser (lower resolution and lack of information on submerged parts), offers considerable potential for scaling up and generalizing the mapping of lateral bank mobility.

7.2 Support riparian management using remote sensing methods

The second sub-objective was to identify the applicative potential of remote sensing tools to support the management of riparian ecosystems.

Remote sensing can be used to produce spatialized indicators of the state of riparian ecosystems. These indicators can in turn be used for monitoring or planning riparian interventions. Approaches for mapping biomass, specific composition and lateral bank mobility were deployed in a watershed comprising some 50 km of watercourses. The results were used to generate a map of deadwood production potential (linked to bank erosion and vegetation senescence). This can be used as part of a planning process for riparian interventions, to target priority areas for management.

A number of tools are now available to help managers carry out GIS operations or process and even acquire remote sensing data. In addition, high-resolution remote sensing data and other associated data (hydrographic networks, DTM, land use maps) are increasingly available and of growing quality. In this context, it is essential to provide managers with robust, interoperable data and tools. In addition, personalized synthesis and training to these tools is still required, so that managers who so wish can appropriate these techniques.

Finally, the tools developed in this thesis can help better integrate scale issues in riparian research through the interpretation of trajectories, process modeling or improved monitoring and assessment or riparian vegetation.

8

References

Agrawal, S. & Gupta, R. D. (2017). Web GIS and its architecture: a review. *Arabian Journal of Geosciences, 10* (23). https://doi.org/10.1007/s12517-017-3296-2.

Ahmadi, K.,, Alavi, S.J. & Kouchaksaraei, M.T. (2017). Constructing site quality curves and productivity assessment for uneven-aged and mixed stands of oriental beech (Fagus Oriental Lipsky) in Hyrcanian Forest, Iran. *Forest Science and Technology, 13*(1): 41–46. https://doi.org/10.1080/21580103.2017.1292959.

Akasaka, T., Akasaka, M. & Yanagawa, H. (2010). Relative importance of the environmental factors at site and landscape scales for bats along the riparian zone. *Landscape and Ecological Engineering, 6*(2): 247–55. https://doi.org/10.1007/s11355-010-0105-4.

Alaibakhsh, M., Emelyanova, I., Barron, O., Sims, N., Khiadani, M. & Mohyeddin, A. (2016). Delineation of riparian vegetation from landsat multi-temporal imagery using PCA. *Hydrological Processes, 31*(4): 800–810. https://doi.org/10.1002/hyp.11054.

Alber, A. & Piégay, H. (2011). Spatial disaggregation and aggregation procedures for characterizing fluvial features at the network-scale: application to the Rhône basin (France). *Geomorphology, 125*(3): 343–60. https://doi.org/10.1016/j.geomorph.2010.09.009.

Alonso, A.,, Pérez, J., Monroy, S., López-Rojo, N., Basaguren, A., Bosch & J., Boyero, L. (2021). Loss of key riparian plant species impacts stream ecosystem functioning. *Ecosystems, 24*(6): 1436–49. https://doi.org/10.1007/s10021-020-00592-7.

Amiri, N., Heurich, M., Krzystek, P., & Skidmore, A. K. (2018). Feature relevance assessment of multispectral airborne LiDAR data for tree species classification. The International Archives of the Photogrammetry, Remote Sensing and Spatial Information Sciences, 42(3), 31-34. https://doi.org/10.5194/isprs-archives-XLII-3-31-2018.

Amlin, N. M. & Rood, S. B. (2003). Drought stress and recovery of riparian cottonwoods due to water table alteration along willow creek, Alberta. *Trees, 17*(4): 351–58. https://doi.org/10.1007/s00468-003-0245-3.

Anderson, K. & Gaston, K. J. (2013). Lightweight unmanned aerial vehicles will revolutionize spatial ecology. *Frontiers in Ecology and the Environment, 11*(3): 138–46. https://doi.org/10.1890/120150.

Antonarakis, A. S., Richards, K. S., & Brasington, J. (2008). Object-based land cover classification using airborne LiDAR. *Remote Sensing of Environment, 112*(6): 2988–98. https://doi.org/10.1016/j.rse.2008.02.004.

Arroyo, L. A., Johansen, K., Armston, J., & Phinn, S. (2010). Integration of LiDAR and Quickbird imagery for mapping riparian biophysical parameters and land cover types in australian tropical savannas. *Forest Ecology and Management, 259*(3): 598–606. https://doi.org/10.1016/j.foreco.2009.11.018.

Ashraf, S., Brabyn, L., Hicks, B. J., & Collier, K. (2010). Satellite remote sensing for mapping vegetation in New Zealand freshwater environments: a review. *New Zealand Geographer*, *66*(1): 33–43. https://doi.org/10.1111/j.1745-7939.2010.01168.x.

Ba, A., Laslier, M., Dufour, S., & Hubert-Moy, L. (2020). Riparian trees genera identification based on leaf-on/leaf-off airborne laser scanner data and machine learning classifiers in northern France. *International Journal of Remote Sensing*, *41* (5): 1645–67. https://doi.org/10.1080/01431161.2019.1674457.

Baggs Sargood, M., Cohen, T. J., Thompson, C. J., & Croke, J. (2015). Hitting rock bottom: morphological responses of bedrock-confined streams to a catastrophic flood. *Earth Surface Dynamics*, *3*(2), 265-279. https://doi.org/10.5194/esurf-3-265-2015.

Bailly, J. S., Kinzel, P. J., Allouis, T., Feurer, D., & Le Coarer, Y. (2012). Airborne LiDAR methods applied to riverine environments. In *Fluvial Remote Sensing for Science and Management*, 141–161. https://doi.org/10.1002/9781119940791.ch7.

Balian, E. V., & Naiman, R. J. (2005). Abundance and production of riparian trees in the lowland floodplain of the Queets river, Washington. *Ecosystems*, *8*(7): 841–61. https://doi.org/10.1007/s10021-005-0043-4.

Baskerville, G. L. 1972. Use of logarithmic regression in the estimation of plant biomass. *Canadian Journal of Forest Research*, *2*(1): 49–53. https://doi.org/10.1139/x72-009.

Beechie, T., Pess, G., Roni, P., & Giannico, G. (2008). Setting river restoration priorities: a review of approaches and a general protocol for identifying and prioritizing actions. *North American Journal of Fisheries Management*, *28*(3): 891–905. https://doi.org/10.1577/m06-174.1.

Belcore, E., Pittarello, M., Lingua, A. M., & Lonati, M. (2021). Mapping riparian habitats of Natura 2000 network (91e0*, 3240) at individual tree level using uav multi-temporal and multi-spectral data. *Remote Sensing*, *13*(9). https://doi.org/10.3390/rs13091756.

Belletti, B., Dufour, S., & Piégay, H. (2015). What is the relative effect of space and time to explain the braided river width and island patterns at a regional scale. *River Research and Applications*, *31*(1): 1–15. https://doi.org/10.1002/rra.2714.

Belluco, E., Camuffo, M., Ferrari, S., Modenese, L., Silvestri, S., Marani, A., & Marani, M. (2006). Mapping salt-marsh vegetation by multispectral and hyperspectral remote sensing. *Remote Sensing of Environment*, *105*(1): 54–67. https://doi.org/10.1016/j.rse.2006.06.006.

Benda, L., Hassan, M. A., Church, M., & May, C. L. (2005). Geomorphology of steepland headwaters: the transition from hillslopes to channels. *Journal of the American Water Resources Association*, *41*(4): 835–51. https://doi.org/10.1111/j.1752-1688.2005.tb04466.x.

Bendix, J. (1999). Stream power influence on southern californian riparian vegetation. *Journal of Vegetation Science*, *10*(2): 243–52. https://doi.org/10.2307/3237145.

Bendix, J., & Stella, J. C. (2013). Riparian vegetation and the fluvial environment: a biogeographic perspective. In *Treatise on Geomorphology*, 1-14: 53–74. https://doi.org/10.1016/b978-0-12-374739-6.00322-5.

Bernier, J. F., Chassiot, L., & Lajeunesse, P. (2021). Assessing bank erosion hazards along large rivers in the Anthropocene : a geospatial framework from the St. Lawrence fluvial system. *Geomatics, Natural Hazards and Risk*, *12*(1): 1584–1615. https://doi.org/10.1080/19475705.2021.1935333.

Bertoldi, W., Drake, N., & Gurnell, A. M. (2011). Interactions between river flows and colonizing vegetation on a braided river: exploring spatial and temporal dynamics in riparian vegetation cover using satellite data. *Earth Surface Processes and Landforms*, *36*(11): 1474–86. https://doi.org/10.1002/esp.2166.

Beumer, V., van Wirdum, G., Beltman, B., Griffioen, J., Grootjans, A. P., & Verhoeven, J. T. (2008). Geochemistry and flooding as determining factors of plant species composition in dutch winter-flooded riverine grasslands. *Science of the Total Environment*, *402*(1): 70–81. https://doi.org/10.1016/j.scitotenv.2008.03.044.

Biron, P. M., Choné, G., Buffin-Bélanger, T., Demers, S., & Olsen, T. (2013). Improvement of streams hydro-geomorphological assessment using LiDAR DEMs. *Earth Surface Processes and Landforms*, *38*(15): 1808–21. https://doi.org/10.1002/esp.3425.

Bizzi, S., Demarchi, L., Grabowski, R. C., Weissteiner, C. J., & Van de Bund, W. J. A. S. (2016). The use of remote sensing to characterise hydromorphological properties of European rivers. *Aquatic sciences*, *78*, 57-70.

Bolyn, C., Lejeune, P., Michez, A., & Latte, N. (2022). Mapping tree species proportions from satellite imagery using spectral–spatial deep learning. *Remote Sensing of Environment*, *280*: 113205. https://doi.org/10.1016/j.rse.2022.113205.

Bowler, D. E., Mant, R., Orr, H., Hannah, D. M., & Pullin, A. S. (2012). What are the effects of wooded riparian zones on stream temperature. *Environmental Evidence*, *1*(1): 1-9. https://doi.org/10.1186/2047-2382-1-3.

Brändle, M., & Brandl, R. (2001). Species richness of insects and mites on trees: expanding southwood. *Journal of Animal Ecology*, *70*(3): 491–504. https://doi.org/10.1046/j.1365-2656.2001.00506.x.

Bren, L. J. (1993). Riparian zone, stream, and floodplain issues: a review. *Journal of Hydrology*, 150(2-4), 277-299. https://doi.org/10.1016/0022-1694(93)90113-N.

Brogna, D., Dufrêne, M., Michez, A., Latli, A., Jacobs, S., Vincke, C., & Dendoncker, N. (2018). Forest cover correlates with good biological water quality. insights from a regional study (Wallonia, Belgium). *Journal of Environmental Management*, *211*: 9–21. https://doi.org/10.1016/j.jenvman.2018.01.017.

Bruno, D., Belmar, O., Sánchez-Fernández, D., & Velasco, J. (2014). Environmental determinants of woody and herbaceous riparian vegetation patterns in a semi-arid mediterranean basin. *Hydrobiologia*, *730*, 45-57.

Bucha, T., & Slávik, M. (2013). Improved methods of classification of multispectral aerial photographs: evaluation of floodplain forests in the inundation area of the Danube. *Folia Forestalia Polonica*, *55*(2): 58–71. https://doi.org/10.2478/ffp-2013-0007.

Budei, B. C., St-Onge, B., Hopkinson, C., & Audet, F. A. (2018). Identifying the genus or species of individual trees using a three-wavelength airborne LiDAR system. *Remote Sensing of Environment*, *204*: 632–47. https://doi.org/10.1016/j.rse.2017.09.037.

Bunn, S. E., Abal, E. G., Smith, M. J., Choy, S. C., Fellows, C. S., Harch, B. D., ... & Sheldon, F. (2010). Integration of science and monitoring of river ecosystem health to guide investments in catchment protection and rehabilitation. *Freshwater Biology*, *55*: 223–40. https://doi.org/10.1111/j.1365-2427.2009.02375.x.

Burmeier, S., Eckstein, R. L., Donath, T. W., & Otte, A. (2011). Plant pattern development during early post-restoration succession in grasslands-a case study of Arabis Nemorensis. *Restoration Ecology*, *19*(5): 648–59. https://doi.org/10.1111/j.1526-100X.2010.00668.x.

Cadol, D., & Wine, M. L. (2017). Geomorphology as a first order control on the connectivity of riparian ecohydrology. *Geomorphology*, *277*: 154–70. https://doi.org/10.1016/j.geomorph.2016.06.022.

Caissie, D. (2006). The thermal regime of rivers : A Review. *Freshwater Biology*, *51*(8): 1389–1406. https://doi.org/10.1111/j.1365-2427.2006.01597.x.

Camporeale, C., & Ridolfi, L. (2010). Interplay among river meandering, discharge stochasticity and riparian vegetation. *Journal of Hydrology*, *382*(1): 138–44. https://doi.org/10.1016/j.jhydrol.2009.12.024.

Camporeale, C., Perucca, E., Ridolfi, L., & Gurnell, A. M. (2013). Modeling the interactions between river morphodynamics and riparian vegetation. Reviews of Geophysics, 51(3), 379-414.

Cao, L., Coops, N. C., Innes, J. L., Dai, J., Ruan, H., & She, G. (2016). Tree species classification in subtropical forests using small-footprint full-waveform LiDAR data. *International Journal of Applied Earth Observation and Geoinformation*, *49*: 39–51. https://doi.org/10.1016/j.jag.2016.01.007.

Capon, S. J., & Pettit, N. E. (2018). Turquoise is the new green: restoring and enhancing riparian function in the Anthropocene. *Ecological Management & Restoration*, *19*(S1): 44–53. https://doi.org/10.1111/emr.12326.

Caponi, F., Koch, A., Bertoldi, W., Vetsch, D. F., & Siviglia, A. (2019). When does vegetation establish on gravel bars? observations and modeling in the alpine Rhine river. *Frontiers in Environmental Science*, *7*: 1–18. https://doi.org/10.3389/fenvs.2019.00124.

Carbonneau, P.E. & Piégay, H. (2012). Fluvial remote sensing for science and management. https://doi.org/10.1002/9781119940791.

Carli, C. M., & Bayley, S. E. (2015). River connectivity and road crossing effects on floodplain vegetation of the Upper Columbia River, Canada. *Écoscience*, *22*(2–4): 97–107. https://doi.org/10.1080/11956860.2015.1121705.

Cartisano, R., Mattioli, W., Corona, P., Mugnozza, G. S., Sabatti, M., Ferrari, B., ... & Giuliarelli, D. (2013). Assessing and mapping biomass potential productivity from poplar-dominated riparian forests: a case study. *Biomass and Bioenergy*, *54*: 293–302. https://doi.org/10.1016/j.biombioe.2012.10.023.

Cavalcanti, G. G., & Lockaby, B. G. (2006). Effects of sediment deposition on aboveground net primary productivity, vegetation composition, and structure in riparian forests. *Wetlands*, *26*(2): 400–409. https://doi.org/10.1672/0277-5212(2006)26[400:eosdoa]2.0.co;2.

Chaulagain, S., Stone, M. C., Dombroski, D., Gillihan, T., Chen, L., & Zhang, S. (2022). An investigation into remote sensing techniques and field observations to model hydraulic roughness from riparian vegetation. *River Research and Applications*, *38*(10): 1730–45. https://doi.org/https://doi.org/10.1002/rra.4053.

Chazette, P., Totems, J., Hespel, L., & Bailly, J. S. (2016). Principle and physics of the LiDAR measurement. *Optical Remote Sensing of Land Surface: Techniques and Methods*, 201–47. https://doi.org/10.1016/B978-1-78548-102-4.50005-3.

Chirici, G., McRoberts, R. E., Fattorini, L., Mura, M., & Marchetti, M. (2016). Comparing echo-based and canopy height model-based metrics for enhancing estimation of forest aboveground biomass in a model-assisted framework. *Remote Sensing of Environment*, *174*: 1–9. https://doi.org/10.1016/j.rse.2015.11.010.

Cienciala, P. (2021). Vegetation and geomorphic connectivity in mountain fluvial systems. *Water*, *13*(5). https://doi.org/10.3390/w13050593.

Cierjacks, A., Kleinschmit, B., Babinsky, M., Kleinschroth, F., Markert, A., Menzel, M., ... & Lang, F. (2010). Carbon stocks of soil and vegetation on Danubian floodplains. *Journal of Plant Nutrition and Soil Science*, *173*(5): 644–53. https://doi.org/10.1002/jpln.200900209.

Claeson, S. M., & Bisson, P. A. (2013). Passive reestablishment of riparian vegetation following removal of invasive knotweed (Polygonum). *Invasive Plant Science and Management*, *6*(2): 208–18. https://doi.org/10.1614/ipsm-d-12-00070.1.

Claessens, H., Oosterbaan, A., Savill, P., & Rondeux, J. (2010). A review of the characteristics of Black Alder (Alnus Glutinosa (L.) Gaertn.) and their implications for silvicultural practices. *Forestry*, *83*(2): 163–75. https://doi.org/10.1093/forestry/cpp038.

Claessens, H., Rondeux, J., Debruxelles, N., Burton, C., & Lejeune, P. (2009). Le suivi des bandes riveraines des cours d'eau de Wallonie. *Revue Forestière Française*, *61*(6): 595–610.

Claggett, P. R., Okay, J. A., & Stehman, S. V. (2010). Monitoring regional riparian forest cover change using stratified sampling and multiresolution imagery. *JAWRA Journal of the American Water Resources Association*, *46*(2): 334–43. https://doi.org/10.1111/j.1752-1688.2010.00424.x.

Clawson, R. G., Lockaby, B. G., & Rummer, B. (2001). Changes in production and nutrient cycling across a wetness gradient within a floodplain forest. *Ecosystems*, *4*(2): 126–38. https://doi.org/10.1007/s100210000063.

Clerici, N., Weissteiner, C. J., Paracchini, M. L., Boschetti, L., Baraldi, A., & Strobl, P. (2013). Pan-european distribution modelling of stream riparian zones based on multi-source earth observation data. *Ecological Indicators*, *24*: 211–23. https://doi.org/10.1016/j.ecolind.2012.06.002.

Comiti, F., Lucía, A., & Rickenmann, D. (2016). Large wood recruitment and transport during large floods: a review. *Geomorphology*, *269*: 23-39. https://doi.org/10.1016/j.geomorph.2016.06.016.

Congalton, R. (2010). Remote Sensing: An Overview. *GIScience and Remote Sensing*, *47*(4): 443–59. https://doi.org/10.2747/1548-1603.47.4.443.

Congalton, R. G., Birch, K., Jones, R., & Schriever, J. (2002). Evaluating remotely sensed techniques for mapping riparian vegetation. *Computers and Electronics in Agriculture*, *37*(1-3), 113-126. https://doi.org/10.1016/s0168-1699(02)00108-4.

Coomes, D. A., Dalponte, M., Jucker, T., Asner, G. P., Banin, L. F., Burslem, D. F., ... & Qie, L. (2017). Area-based vs tree-centric approaches to mapping forest carbon in Southeast Asian forests from airborne laser scanning data. *Remote Sensing of Environment*, *194*, 77-88. https://doi.org/10.1016/j.rse.2017.03.017.

Corenblit, D., Steiger, J., Gurnell, A. M., Tabacchi, E., & Roques, L. (2009). Control of sediment dynamics by vegetation as a key function driving biogeomorphic succession within fluvial corridors. *Earth Surface Processes and Landforms: The Journal of the British Geomorphological Research Group*, *34*(13), 1790-1810.

Corral-Rivas, S., Álvarez-González, J. G., Crecente-Campo, F., & Corral-Rivas, J. J. (2014). Local and generalized height-diameter models with random parameters for mixed, uneven-aged forests in Northwestern Durango, Mexico. *Forest Ecosystems*, *1*(1), 1-9. https://doi.org/10.1186/2197-5620-1-6.

Cronk, Q., Ruzzier, E., Belyaeva, I., & Percy, D. (2015). Salix transect of Europe: latitudinal patterns in willow diversity from Greece to arctic Norway. *Biodiversity data journal*, *3*. https://doi.org/10.3897/BDJ.3.e6258.

Cunningham, S. C., Griffioen, P., White, M. D., & Mac Nally, R. (2018). Assessment of ecosystems: A system for rigorous and rapid mapping of floodplain forest condition for Australia's most important river. *Land Degradation & Development*, *29*(1), 127-137. https://doi.org/10.1002/ldr.2845.

Curran, J. C., & Hession, W. C. (2013). Vegetative Impacts on Hydraulics and Sediment Processes across the Fluvial System. *Journal of Hydrology 505*: 364–76. https://doi.org/10.1016/j.jhydrol.2013.10.013.

Cushnie, J. L. (1987). The interactive effect of spatial resolution and degree of internal variability within land-cover types on classification accuracies. *International Journal of Remote Sensing*, *8*(1), 15-29. https://doi.org/10.1080/01431168708948612.

da Silva, R. L., Leite, M. F. A., Muniz, F. H., de Souza, L. A. G., de Moraes, F. H. R., & Gehring, C. (2017). Degradation impacts on riparian forests of the lower Mearim river, eastern periphery of Amazonia. *Forest Ecology and Management*, *402*, 92-101. https://doi.org/10.1016/j.foreco.2017.07.019.

Dagnelie, P., Palm, R., Rondeux, J. (2013). Cubage des Arbres et des Peuplements Forestiers. Tables et *É*quations. *Presses Agronomiques de Gembloux*.

Dahm, C. N., Cleverly, J. R., Allred Coonrod, J. E., Thibault, J. R., McDonnell, D. E., & Gilroy, D. J. (2002). Evapotranspiration at the land/water interface in a semi-arid drainage basin. *Freshwater Biology*, *47*(4), 831-843. https://doi.org/10.1046/j.1365-2427.2002.00917.x.

Dalponte, M., & Coomes, D. A. (2016). Tree-centric mapping of forest carbon density from airborne laser scanning and hyperspectral data. *Methods in ecology and evolution*, *7*(10), 1236-1245. https://doi.org/10.1111/2041-210X.12575.

Dauwalter, D. C., Fesenmyer, K. A., & Bjork, R. (2015). Using aerial imagery to characterize redband trout habitat in a remote desert landscape. *Transactions of the American Fisheries Society*, *144*(6), 1322-1339. https://doi.org/10.1080/00028487.2015.1088471.

De Rose**,** R. C., & Basher, L. R. (2011). Measurement of river bank and cliff erosion from sequential LIDAR and historical aerial photography. *Geomorphology*, *126*(1-2), 132-147. https://doi.org/10.1016/j.geomorph.2010.10.037.

Debruxelles, N, & Claessens, H. (2008). Le Monitoring Des Cours d ' Eau : Une Vitrine Du Réseau Hydrographique Wallon. *Parc et Réserves*, 63: 12–18.

Debruxelles, N., Claessens, H., Lejeune, P., & Rondeux, J. (2009). Design of a watercourse and riparian strip monitoring system for environmental management. *Environmental monitoring and assessment*, *156*, 435-450. https://doi.org/10.1007/s10661-008-0496-y.

Décamps, H. (2001). How a riparian landscape finds form and comes alive. *Landscape and Urban Planning*, *57*(3-4), 169-175. https://doi.org/10.1016/s0169-2046(01)00202-x.

Deiller, A. F., Walter, J. M. N., & Trémolières, M. (2001). Effects of flood interruption on species richness, diversity and floristic composition of woody regeneration in the upper Rhine alluvial hardwood forest. *Regulated Rivers: Research & Management: an International Journal Devoted to River Research and Management*, *17*(4-5), 393-405. https://doi.org/10.1002/rrr.649.

Deng, S., Katoh, M., Yu, X., Hyyppä, J., & Gao, T. (2016). Comparison of tree species classifications at the individual tree level by combining ALS data and RGB images using different algorithms. *Remote Sensing*, *8*(12), 1034. https://doi.org/10.3390/rs8121034.

Dian, R., Li, S., Sun, B., & Guo, A. (2021). Recent advances and new guidelines on hyperspectral and multispectral image fusion. *Information Fusion*, *69*, 40-51. https://doi.org/10.1016/j.inffus.2020.11.001.

Dietrich, J. T. (2017). Bathymetric structure-from-motion: Extracting shallow stream bathymetry from multi-view stereo photogrammetry. *Earth Surface Processes and Landforms*, *42*(2), 355-364. https://doi.org/10.1002/esp.4060.

Dixon, S. J., Sear, D. A., Odoni, N. A., Sykes, T., & Lane, S. N. (2016). The effects of river restoration on catchment scale flood risk and flood hydrology. *Earth Surface Processes and Landforms*, *41*(7), 997-1008. https://doi.org/10.1002/esp.3919.

Doody, T. M., Lewis, M., Benyon, R. G., & Byrne, G. (2014). A method to map riparian exotic vegetation (Salix spp.) area to inform water resource management. *Hydrological Processes*, *28*(11), 3809-3823. https://doi.org/10.1002/hyp.9916.

Dosskey, M. G., Vidon, P., Gurwick, N. P., Allan, C. J., Duval, T. P., & Lowrance, R. (2010). The role of riparian vegetation in protecting and improving chemical water quality in streams 1. *JAWRA Journal of the American Water Resources Association*, *46*(2), 261-277. https://doi.org/10.1111/j.1752-1688.2010.00419.x.

Dufour, S., & Piégay, H. (2006). Forêts riveraines des cours d'eau et ripisylves: spécificités, fonctions et gestion. *Revue forestière française*, *58*(4), 339-350.

Dufour, S., & Piégay, H. (2008). Geomorphological controls of Fraxinus excelsior growth and regeneration in floodplain forests. *Ecology*, *89*(1), 205-215. https://doi.org/10.1890/06-1768.1.

Dufour, S., & Piégay, H. (2009). From the myth of a lost paradise to targeted river restoration: forget natural references and focus on human benefits. *River research and applications*, *25*(5), 568-581. https://doi.org/10.1002/rra.1239.

Dufour, S., Bernez, I., Betbeder, J., Corgne, S., Hubert-Moy, L., Nabucet, J., ... & Trollé, C. (2013). Monitoring restored riparian vegetation: how can recent developments in remote sensing sciences help?. *Knowledge and Management of Aquatic Ecosystems*, (410), 10. https://doi.org/10.1051/kmae/2013068.

Dufour, S., Muller, E., Straatsma, M., & Corgne, S. (2012). Image utilisation for the study and management of riparian vegetation: overview and applications. In *Fluvial remote sensing for science and management*, 215-239. https://doi.org/10.1002/9781119940791.ch10.

Dufour, S., Rinaldi, M., Piégay, H., & Michalon, A. (2015). How do river dynamics and human influences affect the landscape pattern of fluvial corridors?

Lessons from the Magra River, Central–Northern Italy. *Landscape and Urban Planning*, *134*, 107-118. https://doi.org/10.1016/j.landurbplan.2014.10.007.

Dufour, S., Rodríguez-González, P. M., & Laslier, M. (2019). Tracing the scientific trajectory of riparian vegetation studies: Main topics, approaches and needs in a globally changing world. *Science of the total environment*, *653*, 1168-1185. https://doi.org/10.1016/j.scitotenv.2018.10.383.

Dufour, S., Urbanîc, G., Politti, E. (2020). Managers' views on riparian vegetation management in France. Report, COST Action CA16208 CONVERGES 13 p.

Duncanson, L., & Dubayah, R. (2018). Monitoring individual tree-based change with airborne lidar. *Ecology and evolution*, *8*(10), 5079-5089. https://doi.org/10.1002/ece3.4075.

Dunesme, C., Rousson; S. (2020). Fluvial Corridor Toolbox QGIS Plugin. https://doi.org/10.5281/zenodo.4317225.

Dunesme, S., Rousson, C., & Piégay, H. (2021). An open platform version of the Fluvial Corridor Toolbox with new functionalities to map nested floodplain envelops at the network scale. In *EGU General Assembly Conference Abstracts* (pp. EGU21-8771).

Dunford, R., Michel, K., Gagnage, M., Piégay, H., & Trémelo, M. L. (2009). Potential and constraints of Unmanned Aerial Vehicle technology for the characterization of Mediterranean riparian forest. *International Journal of Remote Sensing*, *30*(19), 4915-4935. https://doi.org/10.1080/01431160903023025.

Durning, L. E., Sankey, J. B., Yackulic, C. B., Grams, P. E., Butterfield, B. J., & Sankey, T. T. (2021). Hydrologic and geomorphic effects on riparian plant species occurrence and encroachment: Remote sensing of 360 km of the Colorado River in Grand Canyon. *Ecohydrology*, *14*(8), e2344. https://doi.org/10.1002/eco.2344.

Dutta, D., Wang, K., Lee, E., Goodwell, A., Woo, D. K., Wagner, D., & Kumar, P. (2016). Characterizing vegetation canopy structure using airborne remote sensing data. *IEEE Transactions on Geoscience and Remote Sensing*, *55*(2), 1160-1178. https://doi.org/10.1109/tgrs.2016.2620478.

Dybala, K. E., Matzek, V., Gardali, T., & Seavy, N. E. (2019a). Carbon sequestration in riparian forests: A global synthesis and meta-analysis. *Global Change Biology*, *25*(1), 57-67. https://doi.org/10.1111/gcb.14475.

Dybala, K. E., Steger, K., Walsh, R. G., Smart, D. R., Gardali, T., & Seavy, N. E. (2019b). Optimizing carbon storage and biodiversity co-benefits in reforested riparian zones. *Journal of Applied Ecology*, *56*(2), 343-353. https://doi.org/10.1111/1365-2664.13272.

Egels, Y. (2011). La photogrammétrie, principes généraux et terminologie. *Collection EDYTEM. Cahiers de géographie*, *12*(1), 41-50.

ElMasry, G., & Sun, D. W. (2010). Principles of hyperspectral imaging technology. In *Hyperspectral imaging for food quality analysis and control* (pp. 3-43). Academic Press. https://doi.org/10.1016/B978-0-12-374753-2.10001-2.

Fairhead, J., & Leach, M. (1998). Reconsidering the extent of deforestation in twentieth century West Africa. *UNASYLVA-FAO-*, 38-46.

Fassnacht, F. E., Hartig, F., Latifi, H., Berger, C., Hernández, J., Corvalán, P., & Koch, B. (2014). Importance of sample size, data type and prediction method for remote sensing-based estimations of aboveground forest biomass. *Remote Sensing of Environment*, *154*, 102-114. https://doi.org/10.1016/j.rse.2014.07.028.

Fassnacht, F. E., Latifi, H., Stereńczak, K., Modzelewska, A., Lefsky, M., Waser, L. T., ... & Ghosh, A. (2016). Review of studies on tree species classification from remotely sensed data. *Remote sensing of environment*, *186*, 64-87. https://doi.org/10.1016/j.rse.2016.08.013.

Fausch, K. D., Torgersen, C. E., Baxter, C. V., & Li, H. W. (2002). Landscapes to riverscapes: bridging the gap between research and conservation of stream fishes: a continuous view of the river is needed to understand how processes interacting among scales set the context for stream fishes and their habitat. *BioScience*, *52*(6), 483-498. https://doi.org/10.1641/0006-3568(2002)052[0483:ltrbtg]2.0.co;2.

Fédération des Conservatoires d'espaces naturels (2018). Les nouvelles technologies dans l'étude des milieux humides : exemples d'applications. *Fédération des Conservatoires d'espaces naturels*, 20 p.

Fernandes, M. R., Aguiar, F. C., & Ferreira, M. T. (2011). Assessing riparian vegetation structure and the influence of land use using landscape metrics and geostatistical tools. *Landscape and Urban Planning*, *99*(2), 166-177.

Fernandes, M. R., Aguiar, F. C., Ferreira, M. T., & Pereira, J. M. C. (2013a). Spectral separability of riparian forests from small and medium-sized rivers across a latitudinal gradient using multispectral imagery. *International journal of remote sensing*, *34*(7), 2375-2401. https://doi.org/10.1080/01431161.2012.744491.

Fernandes, M. R., Aguiar, F. C., Martins, M. J., Rico, N., Ferreira, M. T., & Correia, A. C. (2020). Carbon stock estimations in a mediterranean riparian forest: A case study combining field data and UAV imagery. *Forests*, *11*(4), 376. https://doi.org/10.3390/f11040376.

Fernandes, M. R., Aguiar, F. C., Silva, J. M., Ferreira, M. T., & Pereira, J. M. (2014). Optimal attributes for the object based detection of giant reed in riparian habitats: A comparative study between Airborne High Spatial Resolution and WorldView-2 imagery. *International Journal of Applied Earth Observation and Geoinformation*, *32*, 79-91. https://doi.org/10.1016/j.jag.2014.03.026.

Fernandes, M. R., Aguiar, F. C., Silva, J. M., Ferreira, M. T., & Pereira, J. M. (2013b). Spectral discrimination of giant reed (Arundo donax L.): A seasonal study in riparian areas. *ISPRS journal of photogrammetry and remote sensing*, *80*, 80-90. https://doi.org/10.1016/j.isprsjprs.2013.03.007.

Ferry, B., Morneau, F., Bontemps, J. D., Blanc, L., & Freycon, V. (2010). Higher treefall rates on slopes and waterlogged soils result in lower stand biomass and productivity in a tropical rain forest. *Journal of ecology*, *98*(1), 106-116. https://doi.org/10.1111/j.1365-2745.2009.01604.x.

Feurer, D. (2009). Géométrie 3D des lits de rivière par stéréophotogrammétrie à travers l'eau. *Unpublished doctoral thesis*.

Filippi, A. M., Güneralp, İ., & Randall, J. (2014). Hyperspectral remote sensing of aboveground biomass on a river meander bend using multivariate adaptive regression splines and stochastic gradient boosting. *Remote Sensing Letters*, *5*(5), 432-441. https://doi.org/10.1080/2150704x.2014.915070.

Forget, G., Carreau, C., Le Coeur, D., & Bernez, I. (2013). Ecological restoration of headwaters in a rural landscape (Normandy, France): a passive approach taking hedge networks into account for riparian tree recruitment. *Restoration Ecology*, *21*(1), 96-104. https://doi.org/10.1111/j.1526-100X.2012.00868.x.

Forzieri, G. (2012). Satellite retrieval of woody biomass for energetic reuse of riparian vegetation. *Biomass and bioenergy*, *36*, 432-438. https://doi.org/10.1016/j.biombioe.2011.10.036.

Forzieri, G., Castelli, F., & Preti, F. (2012). Advances in remote sensing of hydraulic roughness. *International journal of remote sensing*, *33*(2), 630-654. https://doi.org/10.1080/01431161.2010.531788.

Forzieri, G., Tanteri, L., Moser, G., & Catani, F. (2013). Mapping natural and urban environments using airborne multi-sensor ADS40–MIVIS–LiDAR synergies. *International Journal of Applied Earth Observation and Geoinformation*, *23*, 313-323. https://doi.org/10.1016/j.jag.2012.10.004.

Francalanci, S., Paris, E., & Solari, L. (2020). On the vulnerability of woody riparian vegetation during flood events. *Environmental Fluid Mechanics*, *20*, 635-661. https://doi.org/10.1007/s10652-019-09726-5.

Frazier, A. E., & Hemingway, B. L. (2021). A technical review of planet smallsat data: Practical considerations for processing and using planetscope imagery. *Remote Sensing*, *13*(19), 3930. https://doi.org/10.3390/rs13193930.

Fullerton, A. H., Beechie, T. J., Baker, S. E., Hall, J. E., & Barnas, K. A. (2006). Regional patterns of riparian characteristics in the interior Columbia River basin, Northwestern USA: applications for restoration planning. *Landscape Ecology*, *21*, 1347-1360. https://doi.org/10.1007/s10980-006-0017-8.

Fussell, J., Rundquist, D., & Harrington, J. A. (1986). On defining remote sensing. *Photogrammetric Engineering and Remote Sensing*, *52*(9), 1507-1511.

Garcia, M., Saatchi, S., Ferraz, A., Silva, C. A., Ustin, S., Koltunov, A., & Balzter, H. (2017). Impact of data model and point density on aboveground forest biomass estimation from airborne LiDAR. *Carbon balance and management*, *12*(1), 1-18. https://doi.org/10.1186/s13021-017-0073-1.

Genuer, R., Poggi, J. M., & Tuleau-Malot, C. (2015). VSURF: an R package for variable selection using random forests. *The R Journal*, *7*(2), 19-33.

Georges, B., Brostaux, Y., Claessens, H., Degré, A., Huylenbroeck, L., Lejeune, P., ... & Michez, A. (2020). Can water level stations be used for thermal assessment

in aquatic ecosystem? *River Research and Applications*, *36*(6), 960-973. https://doi.org/10.1002/rra.3520.

Gergel, S. E., Stange, Y., Coops, N. C., Johansen, K., & Kirby, K. R. (2007). What is the value of a good map? An example using high spatial resolution imagery to aid riparian restoration. *Ecosystems*, *10*, 688-702. https://doi.org/10.1007/s10021-007-9040-0.

Giese, L. A., Aust, W. M., Kolka, R. K., & Trettin, C. C. (2003). Biomass and carbon pools of disturbed riparian forests. *Forest Ecology and Management*, *180*(1-3), 493-508. https://doi.org/10.1016/s0378-1127(02)00644-8.

National Research Council (2002). Riparian areas: functions and strategies for management. *National Academies Press*.

Gob, F., Houbrechts, G., Hiver, J. M., & Petit, F. (2005). River dredging, channel dynamics and bedload transport in an incised meandering river (the River Semois, Belgium). *River Research and Applications*, *21*(7), 791-804. https://doi.org/10.1002/rra.883.

Godfroy, J., Lejot, J., Demarchi, L., Bizzi, S., Michel, K., & Piégay, H. (2022). Combining Hyperspectral, LiDAR, and Forestry Data to Characterize Riparian Forests along Age and Hydrological Gradients. *Remote Sensing*, *15*(1), 17. https://doi.org/10.3390/rs15010017.

Goetz, W.E., 2002. Developing a Predictive Model for Identifying Riparian Communities at an Ecoregion Scale in Idaho and Wyoming. *Unpublished master thesis*.

Goetz, S. J. (2006). Remote sensing of riparian buffers: past progress and future prospects 1. *JAWRA Journal of the American Water Resources Association*, *42*(1), 133-143. https://doi.org/10.1111/j.1752-1688.2006.tb03829.x.

Goetz, S., & Dubayah, R. (2011). Advances in remote sensing technology and implications for measuring and monitoring forest carbon stocks and change. *Carbon Management*, *2*(3), 231-244. https://doi.org/10.4155/cmt.11.18.

Gong, P., Wang, J., Yu, L., Zhao, Y., Zhao, Y., Liang, L., ... & Chen, J. (2013). Finer resolution observation and monitoring of global land cover: First mapping results with Landsat TM and ETM+ data. *International Journal of Remote Sensing*, *34*(7), 2607-2654. https://doi.org/10.1080/01431161.2012.748992.

Gong, Z., Cui, T., Pu, R., Lin, C., & Chen, Y. (2015). Dynamic simulation of vegetation abundance in a reservoir riparian zone using a sub-pixel Markov model. *International Journal of Applied Earth Observation and Geoinformation*, *35*, 175-186. https://doi.org/10.1016/j.jag.2014.09.004.

González del Tánago, M., & García de Jalón, D. (2011). Riparian Quality Index (RQI): A methodology for characterising and assessing the environmental conditions of riparian zones. *Limnetica*, *30*(2), 0235-254. https://doi.org/10.23818/limn.30.18.

Gonzàlez del Tánago, M., Bejarano, M. D., de Jalón, D. G., & Schmidt, J. C. (2015). Biogeomorphic responses to flow regulation and fine sediment supply in

Mediterranean streams (the Guadalete River, southern Spain). *Journal of Hydrology*, *528*, 751-762.

Gonzàlez del Tánago, M.., Martínez-Fernández, V., Aguiar, F. C., Bertoldi, W., Dufour, S., de Jalón, D. G., ... & Rodríguez-González, P. M. (2021). Improving river hydromorphological assessment through better integration of riparian vegetation: Scientific evidence and guidelines. *Journal of Environmental Management*, *292*, 112730. https://doi.org/10.1016/j.jenvman.2021.112730.

González, E., González-Sanchis, M., Cabezas, Á., Comín, F. A., & Muller, E. (2010). Recent changes in the riparian forest of a large regulated Mediterranean river: implications for management. *Environmental Management*, *45*, 669-681. https://doi.org/10.1007/s00267-010-9441-2.

González, E., Sher, A. A., Tabacchi, E., Masip, A., & Poulin, M. (2015). Restoration of riparian vegetation: a global review of implementation and evaluation approaches in the international, peer-reviewed literature. *Journal of Environmental Management*, *158*, 85-94. https://doi.org/10.1016/j.jenvman.2015.04.033.

Goodbody, T. R., Tompalski, P., Coops, N. C., Hopkinson, C., Treitz, P., & van Ewijk, K. (2020). Forest inventory and diversity attribute modelling using structural and intensity metrics from multi-spectral airborne laser scanning data. *Remote Sensing*, 12(13), 2109. https://doi.org/10.3390/rs12132109.

Grabska, E., Hostert, P., Pflugmacher, D., & Ostapowicz, K. (2019). Forest stand species mapping using the Sentinel-2 time series. *Remote Sensing*, *11*(10), 1197. https://doi.org/10.3390/rs11101197.

Grijseels, N. H., Buchert, M., Brooks, P. D., & Pataki, D. E. (2021). Using LiDAR to assess transitions in riparian vegetation structure along a rural-to-urban land use gradient in western North America. *Ecohydrology*, *14*(1), e2259. https://doi.org/10.1002/eco.2259.

Groemping, U., & Lehrkamp, M. (2018). Relaimpo: Relative Importance of Regressors in Linear Models. R package, version 2.2-3.

Groeneveld, D. P., & Watson, R. P. (2008). Near-infrared discrimination of leafless saltcedar in wintertime Landsat TM. *International Journal of Remote Sensing*, *29*(12), 3577-3588. https://doi.org/10.1080/01431160701711078.

Grove, J. R., Croke, J., & Thompson, C. (2013). Quantifying different riverbank erosion processes during an extreme flood event. *Earth Surface Processes and Landforms*, *38*(12), 1393-1406. https://doi.org/10.1002/esp.3386.

Gumiero, B., Mant, J., Hein, T., Elso, J., & Boz, B. (2013). Linking the restoration of rivers and riparian zones/wetlands in Europe: Sharing knowledge through case studies. *Ecological Engineering*, *56*, 36-50. https://doi.org/10.1016/j.ecoleng.2012.12.103.

Gurnell, A. M. (2003). Wood storage and mobility. In *American Fisheries Society Symposium* (pp. 75-92). American Fisheries Society.

Gurnell, A. M., Corenblit, D., García de Jalón, D., González del Tánago, M., Grabowski, R. C., O'hare, M. T., & Szewczyk, M. (2016). A conceptual model of vegetation–hydrogeomorphology interactions within river corridors. *River research and applications*, *32*(2), 142-163. https://doi.org/10.1002/rra.2928.

Gurnell, A. M., Rinaldi, M., Belletti, B., Bizzi, S., Blamauer, B., Braca, G., ... & Ziliani, L. (2016). A multi-scale hierarchical framework for developing understanding of river behaviour to support river management. *Aquatic sciences*, *78*, 1-16.

Guth, P. L., Van Niekerk, A., Grohmann, C. H., Muller, J. P., Hawker, L., Florinsky, I. V., ... & Strobl, P. (2021). Digital elevation models: terminology and definitions. *Remote Sensing*, *13*(18), 3581. https://doi.org/10.3390/rs13183581.

Hakula, A., Ruoppa, L., Lehtomäki, M., Yu, X., Kukko, A., Kaartinen, H., ... & Hyyppä, J. (2023). Individual tree segmentation and species classification using high-density close-range multispectral laser scanning data. ISPRS Open Journal of Photogrammetry and Remote Sensing, 9, 100039. https://doi.org/10.1016/j.ophoto.2023.100039.

Hall, A. A., Rood, S. B., & Higgins, P. S. (2011). Resizing a river: A downscaled, seasonal flow regime promotes riparian restoration. *Restoration Ecology*, *19*(3), 351-359. https://doi.org/10.1111/j.1526-100X.2009.00581.x.

Hamandawana, H., & Chanda, R. (2013). Environmental change in and around the Okavango Delta during the nineteenth and twentieth centuries. *Regional Environmental Change*, *13*, 681-694. https://doi.org/10.1007/s10113-012-0367-5.

Hamshaw, S. D., Engel, T., Rizzo, D. M., O'Neil-Dunne, J., & Dewoolkar, M. M. (2019). Application of unmanned aircraft system (UAS) for monitoring bank erosion along river corridors. *Geomatics, Natural Hazards and Risk*, *10*(1), 1285-1305. https://doi.org/10.1080/19475705.2019.1571533.

Hartling, S., Sagan, V., Sidike, P., Maimaitijiang, M., & Carron, J. (2019). Urban tree species classification using a WorldView-2/3 and LiDAR data fusion approach and deep learning. *Sensors*, *19*(6), 1284. https://doi.org/10.3390/s19061284.

Harwell, E. (2000). Remote sensibilities: discourses of technology and the making of Indonesia's natural disaster. *Development and Change*, *31*(1), 307-340. https://doi.org/10.1111/1467-7660.00156.

Heinzel, J., & Koch, B. (2011). Exploring full-waveform LiDAR parameters for tree species classification. *International Journal of Applied Earth Observation and Geoinformation*, *13*(1), 152-160. https://doi.org/10.1016/j.jag.2010.09.010.

Henshaw, A. J., Gurnell, A. M., Bertoldi, W., & Drake, N. A. (2013). An assessment of the degree to which Landsat TM data can support the assessment of fluvial dynamics, as revealed by changes in vegetation extent and channel position, along a large river. *Geomorphology*, *202*, 74-85. https://doi.org/10.1016/j.geomorph.2013.01.011.

Hering, D., Borja, A., Carstensen, J., Carvalho, L., Elliott, M., Feld, C. K., ... & van de Bund, W. (2010). The European Water Framework Directive at the age of 10: a critical review of the achievements with recommendations for the future. *Science of the total Environment*, *408*(19), 4007-4019. https://doi.org/10.1016/j.scitotenv.2010.05.031.

Hill, D. J., & Babbar-Sebens, M. (2019). Promise of UAV-assisted adaptive management of water resources systems. *Journal of Water Resources Planning and Management*, *145*(7), 02519001. https://doi.org/10.1061/(asce)wr.1943-5452.0001081.

Hill, D. J., Tarasoff, C., Whitworth, G. E., Baron, J., Bradshaw, J. L., & Church, J. S. (2017). Utility of unmanned aerial vehicles for mapping invasive plant species: a case study on yellow flag iris (Iris pseudacorus L.). *International Journal of Remote Sensing*, *38*(8-10), 2083-2105. https://doi.org/10.1080/01431161.2016.1264030.

Holmes, P. M., Richardson, D. M., Esler, K. J., Witkowski, E. T. F., & Fourie, S. (2005). A decision-making framework for restoring riparian zones degraded by invasive alien plants in South Africa. *South African Journal of Science*, *101*(11), 553-564.

Holmgren, J., Nilsson, M., & Olsson, H. (2003). Simulating the effects of lidar scanning angle for estimation of mean tree height and canopy closure. *Canadian Journal of Remote Sensing*, *29*(5), 623-632. https://doi.org/10.5589/m03-030.

Holmgren, J., Persson, Å., & Söderman, U. (2008). Species identification of individual trees by combining high resolution LiDAR data with multi-spectral images. *International Journal of Remote Sensing*, *29*(5), 1537-1552. https://doi.org/10.1080/01431160701736471.

Honey-Rosés, J., Acuña, V., Bardina, M., Brozović, N., Marcé, R., Munné, A., ... & Schneider, D. W. (2013). Examining the demand for ecosystem services: the value of stream restoration for drinking water treatment managers in the Llobregat River, Spain. *Ecological Economics*, *90*, 196-205. https://doi.org/10.1016/j.ecolecon.2013.03.019.

Hough-Snee, N., Roper, B. B., Wheaton, J. M., & Lokteff, R. L. (2015). Riparian vegetation communities of the American Pacific Northwest are tied to multi-scale environmental filters. *River research and applications*, *31*(9), 1151-1165. https://doi.org/10.1002/rra.2815.

Hooke, J. M., & Yorke, L. (2010). Rates, distributions and mechanisms of change in meander morphology over decadal timescales, River Dane, UK. *Earth Surface Processes and Landforms*, *35*(13), 1601-1614. https://doi.org/10.1002/esp.2079.

Hortobágyi, B., Corenblit, D., Steiger, J., & Peiry, J. L. (2018). Niche construction within riparian corridors. Part I: Exploring biogeomorphic feedback windows of three pioneer riparian species (Allier River, France). *Geomorphology*, *305*, 94-111. https://doi.org/10.1016/j.geomorph.2017.08.048.

Huck, J. (2020). QGIS plugin, version 0.6.

Hughes, F. M., Gonzalez del Tánago, M., & Mountford, J. O. (2012). Restoring floodplain forests in Europe. *A goal-oriented approach to forest landscape restoration*, 393-422. https://doi.org/10.1007/978-94-007-5338-9_15.

Hughes, M. L., McDowell, P. F., & Marcus, W. A. (2006). Accuracy assessment of georectified aerial photographs: implications for measuring lateral channel movement in a GIS. *Geomorphology*, *74*(1-4), 1-16. https://doi.org/10.1016/j.geomorph.2005.07.001.

Hupp, C. R. (1992). Riparian vegetation recovery patterns following stream channelization: a geomorphic perspective. *Ecology*, *73*(4), 1209-1226. https://doi.org/10.2307/1940670.

Husson, E., Lindgren, F., & Ecke, F. (2014). Assessing biomass and metal contents in riparian vegetation along a pollution gradient using an unmanned aircraft system. *Water, Air, & Soil Pollution*, *225*, 1-14. https://doi.org/10.1007/s11270-014-1957-2.

Huylenbroeck, L., Laslier, M., Dufour, S., Georges, B., Lejeune, P., & Michez, A. (2020). Using remote sensing to characterize riparian vegetation: A review of available tools and perspectives for managers. *Journal of environmental management*, *267*, 110652. https://doi.org/10.1016/j.jenvman.2020.110652.

Huylenbroeck, L., Latte, N., Lejeune, P., Georges, B., Claessens, H., & Michez, A. (2021). What factors shape spatial distribution of biomass in riparian forests? Insights from a LiDAR survey over a large area. *Forests*, *12*(3), 371. https://doi.org/10.3390/f12030371.

Huylenbroeck, L., Michez, A., & Claessens, H. (2019). Guide de gestion des ripisylves. *SPW Editions*.

Hyyppä, J., Hyyppä, H., Leckie, D., Gougeon, F., Yu, X., & Maltamo, M. (2008). Review of methods of small-footprint airborne laser scanning for extracting forest inventory data in boreal forests. *International Journal of Remote Sensing*, *29*(5), 1339-1366. https://doi.org/10.1080/01431160701736489.

Iglhaut, J., Cabo, C., Puliti, S., Piermattei, L., O'Connor, J., & Rosette, J. (2019). Structure from motion photogrammetry in forestry: A review. *Current Forestry Reports*, *5*, 155-168. https://doi.org/10.1007/s40725-019-00094-3.

Jalonen, J., Järvelä, J., Virtanen, J. P., Vaaja, M., Kurkela, M., & Hyyppä, H. (2015). Determining characteristic vegetation areas by terrestrial laser scanning for floodplain flow modeling. *Water*, *7*(2), 420-437. https://doi.org/10.3390/w7020420.

Jansen, B.J.M., Backx, J.J.G.M. (1998). Biologische Monitoring Zoete Rijkswateren : Ecotopenkartering Rijntakken-Oost 1997, RIZA rapport;98.054. RIZA, Lelystad.

Janssen, P., Stella, J. C., Piégay, H., Räpple, B., Pont, B., Faton, J. M., ... & Evette, A. (2020). Divergence of riparian forest composition and functional traits from natural succession along a degraded river with multiple stressor legacies.

Science of the Total Environment, *721*, 137730. https://doi.org/10.1016/j.scitotenv.2020.137730.

Jensen, J.R. (2015). Introductory Digital Image Processing: A Remote Sensing Perspective, 4th ed. *Pearson Prentice Hall Press*.

Johansen, K., Phinn, S., & Witte, C. (2010). Mapping of riparian zone attributes using discrete return LiDAR, QuickBird and SPOT-5 imagery: Assessing accuracy and costs. *Remote Sensing of Environment*, *114*(11), 2679-2691. https://doi.org/10.1016/j.rse.2010.06.004.

Johansen, K., Phinn, S., Dixon, I., Douglas, M., & Lowry, J. (2007). Comparison of image and rapid field assessments of riparian zone condition in Australian tropical savannas. *Forest Ecology and Management*, *240*(1-3), 42-60. https://doi.org/10.1016/j.foreco.2006.12.015.

Jolley, R. L., Lockaby, B. G., & Cavalcanti, G. G. (2009). Productivity of ephemeral headwater riparian forests impacted by sedimentation in the southeastern United States coastal plain. *Journal of Environmental Quality*, *38*(3), 965-979. https://doi.org/10.2134/jeq2008.0206.

Kalliola, R., & Puhakka, M. (1988). River dynamics and vegetation mosaicism: a case study of the River Kamajohka, northernmost Finland. Journal of Biogeography, 703-719. https://doi.org/10.2307/2845334.

Kamińska, A., Lisiewicz, M., & Stereńczak, K. (2021). Single tree classification using multi-temporal ALS data and CIR imagery in mixed old-growth forest in Poland. *Remote Sensing*, *13*(24), 5101. https://doi.org/10.3390/rs13245101.

Karrenberg, S., Edwards, P. J., & Kollmann, J. (2002). The life history of Salicaceae living in the active zone of floodplains. *Freshwater Biology*, *47*(4), 733-748. https://doi.org/10.1046/j.1365-2427.2002.00894.x.

Kashani, A. G., Olsen, M. J., Parrish, C. E., & Wilson, N. (2015). A review of LiDAR radiometric processing: From ad hoc intensity correction to rigorous radiometric calibration. *Sensors*, *15*(11), 28099-28128. https://doi.org/10.3390/s151128099.

Keeton, W. S., Kraft, C. E., & Warren, D. R. (2007). Mature and old-growth riparian forests: structure, dynamics, and effects on Adirondack stream habitats. *Ecological Applications*, *17*(3), 852-868. https://doi.org/10.1890/06-1172.

Kennedy, R. E., Townsend, P. A., Gross, J. E., Cohen, W. B., Bolstad, P., Wang, Y. Q., & Adams, P. (2009). Remote sensing change detection tools for natural resource managers: Understanding concepts and tradeoffs in the design of landscape monitoring projects. *Remote sensing of environment*, *113*(7), 1382-1396. https://doi.org/10.1016/j.rse.2008.07.018.

Kessler, A. C., Gupta, S. C., Dolliver, H. A. S., & Thoma, D. P. (2012). Lidar quantification of bank erosion in Blue Earth County, Minnesota. *Journal of Environmental Quality*, *41*(1), 197-207. https://doi.org/10.2134/jeq2011.0181.

Klein, L. R., Hendrix, W. G., Lohr, V. I., Kaytes, J. B., Sayler, R. D., Swanson, M. E., ... & Reganold, J. P. (2015). Linking ecology and aesthetics in sustainable agricultural landscapes: Lessons from the Palouse region of Washington, USA. *Landscape and Urban Planning*, *134*, 195-209. https://doi.org/10.1016/j.landurbplan.2014.10.019.

Koenig, K., & Höfle, B. (2016). Full-waveform airborne laser scanning in vegetation studies—a review of point cloud and waveform features for tree species classification. Forests, 7(9), 198.

Kominoski, J. S., Shah, J. J. F., Canhoto, C., Fischer, D. G., Giling, D. P., González, E., ... & Tiegs, S. D. (2013). Forecasting functional implications of global changes in riparian plant communities. *Frontiers in Ecology and the Environment*, *11*(8), 423-432. https://doi.org/10.1890/120056.

Korpela, I., Ørka, H. O., Maltamo, M., Tokola, T., & Hyyppä, J. (2010). Tree species classification using airborne LiDAR–effects of stand and tree parameters, downsizing of training set, intensity normalization, and sensor type. *Silva Fennica*, *44*(2), 319-339. https://doi.org/10.14214/sf.156.

Kramer, K., Vreugdenhil, S. J., & Van Der Werf, D. C. (2008). Effects of flooding on the recruitment, damage and mortality of riparian tree species: A field and simulation study on the Rhine floodplain. *Forest Ecology and Management*, *255*(11), 3893-3903. https://doi.org/10.1016/j.foreco.2008.03.044.

Kreuzwieser, J., Papadopoulou, E., & Rennenberg, H. (2004). Interaction of flooding with carbon metabolism of forest trees. *Plant Biology*, *6*(03), 299-306. https://doi.org/10.1055/s-2004-817882.

Kui, L., Stella, J. C., Shafroth, P. B., House, P. K., & Wilcox, A. C. (2017). The long-term legacy of geomorphic and riparian vegetation feedbacks on the dammed Bill Williams River, Arizona, USA. *Ecohydrology*, *10*(4), e1839. https://doi.org/10.1002/eco.1839.

Kukkonen, M., Maltamo, M., Korhonen, L., & Packalen, P. (2019). Multispectral airborne LiDAR data in the prediction of boreal tree species composition. *IEEE Transactions on Geoscience and Remote Sensing*, *57*(6), 3462-3471. https://doi.org/10.1109/TGRS.2018.2885057.

Lague, D., & Feldmann, B. (2020). Topo-bathymetric airborne LiDAR for fluvial-geomorphology analysis. In *Developments in earth surface processes* (Vol. 23, pp. 25-54). Elsevier. https://doi.org/10.1016/B978-0-444-64177-9.00002-3.

Lallias-Tacon, S., Liébault, F., & Piégay, H. (2014). Step by step error assessment in braided river sediment budget using airborne LiDAR data. *Geomorphology*, *214*, 307-323. https://doi.org/10.1016/j.geomorph.2014.02.014.

Lallias-Tacon, S., Liébault, F., & Piégay, H. (2017). Use of airborne LiDAR and historical aerial photos for characterising the history of braided river floodplain morphology and vegetation responses. *Catena*, *149*, 742-759. https://doi.org/10.1016/j.catena.2016.07.038.

Lamar, W. R., McGraw, J. B., & Warner, T. A. (2005). Multitemporal censusing of a population of eastern hemlock (Tsuga canadensis L.) from remotely sensed imagery using an automated segmentation and reconciliation procedure. *Remote Sensing of Environment*, *94*(1), 133-143. https://doi.org/10.1016/j.rse.2004.09.003.

Landon, N., Piégay, H., & Bravard, J. P. (1998). The Drôme river incision (France): from assessment to management. *Landscape and Urban Planning*, *43*(1-3), 119-131. https://doi.org/10.1016/s0169-2046(98)00046-2.

Laslier, M. (2018). *Suivi des impacts d'un arasement de barrage sur la végétation riveraine par télédétection à très haute résolution spatiale et temporelle* (Doctoral dissertation, Université Rennes 2).

Laslier, M., Hubert-Moy, L., & Dufour, S. (2019a). Mapping riparian vegetation functions using 3D bispectral LiDAR data. *Water*, *11*(3), 483. https://doi.org/10.3390/w11030483.

Laslier, M., Hubert-Moy, L., Corpetti, T., & Dufour, S. (2019b). Monitoring the colonization of alluvial deposits using multitemporal UAV RGB-imagery. *Applied Vegetation Science*, *22*(4), 561-572. https://doi.org/10.1111/avsc.12455.

Latte, N., & Lejeune, P. (2020). PlanetScope radiometric normalization and sentinel-2 super-resolution (2.5 m): A straightforward spectral-spatial fusion of multi-satellite multi-sensor images using residual convolutional neural networks. *Remote Sensing*, *12*(15), 2366. https://doi.org/10.3390/RS12152366.

Latte, N., Colinet, G., Fayolle, A., Lejeune, P., Hébert, J., Claessens, H., & Bauwens, S. (2013). Description of a new procedure to estimate the carbon stocks of all forest pools and impact assessment of methodological choices on the estimates. *European Journal of Forest Research*, *132*, 565-577. https://doi.org/10.1007/s10342-013-0701-6.

Latella, M., Bertagni, M. B., Vezza, P., & Camporeale, C. (2020). An integrated methodology to study riparian vegetation dynamics: From field data to impact modeling. *Journal of Advances in Modeling Earth Systems*, *12*(8), e2020MS002094. https://doi.org/10.1029/2020MS002094.

Lattin, P. D., Wigington Jr, P. J., Moser, T. J., Peniston, B. E., Lindeman, D. R., & Getter, D. R. (2004). Influence of remote sensing imagery source on quantification of riparian land cover/land use. *Jawra Journal of the American Water Resources Association*, *40*(1), 215-227. https://doi.org/10.1111/j.1752-1688.2004.tb01020.x.

Le Lay, Y. F., & Piégay, H. (2007). Le bois mort dans les paysages fluviaux français: éléments pour une gestion renouvelée. *Espace géographique*, *36*(1), 51-64. https://doi.org/10.3917/eg.361.0051.

Lee, P., Smyth, C., & Boutin, S. (2004). Quantitative review of riparian buffer width guidelines from Canada and the United States. *Journal of Environmental Management*, *70*(2), 165-180. https://doi.org/10.1016/j.jenvman.2003.11.009.

Legendre, P., Oksanen, J., & ter Braak, C. J. (2011). Testing the significance of canonical axes in redundancy analysis. *Methods in Ecology and Evolution*, *2*(3), 269-277. https://doi.org/10.1111/j.2041-210X.2010.00078.x.

Legleiter, C. J. (2012). Remote measurement of river morphology via fusion of LiDAR topography and spectrally based bathymetry. *Earth Surface Processes and Landforms*, *37*(5), 499-518. https://doi.org/10.1002/esp.2262.

Lindeman, R. H., Merenda, P. F., & Gold, R. Z. (1980). Introduction to bivariate and multivariate analysis. Scott Foresman & Co., Glenview.

Lisein, J., Pierrot-Deseilligny, M., Bonnet, S., & Lejeune, P. (2013). A photogrammetric workflow for the creation of a forest canopy height model from small unmanned aerial system imagery. *Forests*, *4*(4), 922-944. https://doi.org/10.3390/f4040922.

Lisein, J., Michez, A., Claessens, H., & Lejeune, P. (2015). Discrimination of deciduous tree species from time series of unmanned aerial system imagery. *PLoS One*, *10*(11), e0141006. https://doi.org/10.1371/journal.pone.0141006.

Liu, J., Skidmore, A. K., Jones, S., Wang, T., Heurich, M., Zhu, X., & Shi, Y. (2018). Large off-nadir scan angle of airborne LiDAR can severely affect the estimates of forest structure metrics. *ISPRS journal of photogrammetry and remote sensing*, *136*, 13-25. https://doi.org/10.1016/j.isprsjprs.2017.12.004.

Lobón-Cerviá, J., Mazzoni, R., & Rezende, C. F. (2016). Effects of riparian forest removal on the trophic dynamics of a Neotropical stream fish assemblage. *Journal of Fish Biology*, *89*(1), 50-64. https://doi.org/10.1111/jfb.12973.

Loicq, P., Moatar, F., Jullian, Y., Dugdale, S. J., & Hannah, D. M. (2018). Improving representation of riparian vegetation shading in a regional stream temperature model using LiDAR data. *Science of the total environment*, *624*, 480-490. https://doi.org/10.1016/j.scitotenv.2017.12.129.

Longley, P. A., Goodchild, M. F., Maguire, D. J., & Rhind, D. W. (2015). *Geographic information science and systems*. John Wiley & Sons.

Longuetaud, F., Santenoise, P., Mothe, F., Kiessé, T. S., Rivoire, M., Saint-André, L., ... & Deleuze, C. (2013). Modeling volume expansion factors for temperate tree species in France. *Forest Ecology and Management*, *292*, 111-121. https://doi.org/10.1016/j.foreco.2012.12.023.

Löwe, P., Anguix Alfaro, Á., Antonello, A., Baumann, P., Carrera, M., Durante, K., ... & Wessel, P. (2022). Open Source–GIS. In *Springer Handbook of Geographic Information* (pp. 807-843). Cham: Springer International Publishing.

Lu, D. (2006). The potential and challenge of remote sensing-based biomass estimation. *International journal of remote sensing*, *27*(7), 1297-1328. https://doi.org/10.1080/01431160500486732.

Lü, G., Batty, M., Strobl, J., Lin, H., Zhu, A. X., & Chen, M. (2019). Reflections and speculations on the progress in Geographic Information Systems (GIS): a

geographic perspective. *International journal of geographical information science*, *33*(2), 346-367. https://doi.org/10.1080/13658816.2018.1533136.

Łubek, A., Kukwa, M., Czortek, P., & Jaroszewicz, B. (2020). Impact of Fraxinus excelsior dieback on biota of ash-associated lichen epiphytes at the landscape and community level. *Biodiversity and Conservation*, *29*, 431-450. https://doi.org/10.1007/s10531-019-01890-w.

Lucas, C. M., Schöngart, J., Sheikh, P., Wittmann, F., Piedade, M. T., & McGrath, D. G. (2014). Effects of land-use and hydroperiod on aboveground biomass and productivity of secondary Amazonian floodplain forests. *Forest ecology and management*, *319*, 116-127. https://doi.org/10.1016/j.foreco.2014.02.008.

Mac Nally, R., Cunningham, S. C., Baker, P. J., Horner, G. J., & Thomson, J. R. (2011). Dynamics of Murray-Darling floodplain forests under multiple stressors: The past, present, and future of an Australian icon. *Water Resources Research*, *47*(12). https://doi.org/10.1029/2011wr010383.

Macfarlane, W. W., Gilbert, J. T., Gilbert, J. D., Saunders, W. C., Hough-Snee, N., Hafen, C., ... & Bennett, S. N. (2018). What are the conditions of riparian ecosystems? Identifying impaired floodplain ecosystems across the western US using the Riparian Condition Assessment (RCA) tool. *Environmental management*, *62*, 548-570. https://doi.org/10.1007/s00267-018-1061-2.

Macfarlane, W. W., McGinty, C. M., Laub, B. G., & Gifford, S. J. (2017). High-resolution riparian vegetation mapping to prioritize conservation and restoration in an impaired desert river. *Restoration Ecology*, *25*(3), 333-341. https://doi.org/10.1111/rec.12425.

Maillard, P., & Alencar-Silva, T. (2013). A method for delineating riparian forests using region-based image classification and depth-to-water analysis. *International journal of remote sensing*, *34*(22), 7991-8010. https://doi.org/10.1080/01431161.2013.827847.

Maliene, V., Grigonis, V., Palevičius, V., & Griffiths, S. (2011). Geographic information system: Old principles with new capabilities. *Urban Design International*, *16*, 1-6. https://doi.org/10.1057/udi.2010.25.

Mandlburger, G., Hauer, C., Höfle, B., Habersack, H., & Pfeifer, N. (2009). Optimisation of LiDAR derived terrain models for river flow modelling. *Hydrology and Earth System Sciences*, *13*(8), 1453-1466. https://doi.org/10.5194/hess-13-1453-2009.

Manfreda, S., McCabe, M. F., Miller, P. E., Lucas, R., Pajuelo Madrigal, V., Mallinis, G., ... & Toth, B. (2018). On the use of unmanned aerial systems for environmental monitoring. *Remote sensing*, *10*(4), 641. https://doi.org/10.3390/rs10040641.

Manfreda, S., Dvorak, P., Mullerova, J., Herban, S., Vuono, P., Arranz Justel, J. J., & Perks, M. (2019). Assessing the accuracy of digital surface models derived from optical imagery acquired with unmanned aerial systems. *Drones*, *3*(1), 15. https://doi.org/10.3390/drones3010015.

Manners, R., Schmidt, J., & Wheaton, J. M. (2013). Multiscalar model for the determination of spatially explicit riparian vegetation roughness. *Journal of Geophysical Research: Earth Surface*, *118*(1), 65-83. https://doi.org/10.1029/2011jf002188.

Marçais, B., Husson, C., Godart, L., & Cael, O. (2016). Influence of site and stand factors on Hymenoscyphus fraxineus-induced basal lesions. *Plant Pathology*, *65*(9), 1452-1461. https://doi.org/10.1111/ppa.12542.

Marcus, W. A., & Fonstad, M. A. (2008). Optical remote mapping of rivers at sub-meter resolutions and watershed extents. *Earth Surface Processes and Landforms: The Journal of the British Geomorphological Research Group*, *33*(1), 4-24. https://doi.org/10.1002/esp.1637.

Marks, C. O., Yellen, B. C., Wood, S. A., Martin, E. H., & Nislow, K. H. (2020). Variation in tree growth along soil formation and microtopographic gradients in riparian forests. *Wetlands*, *40*, 1909-1922. https://doi.org/10.1007/s13157-020-01363-9.

Martin, F. M., Müllerová, J., Borgniet, L., Dommanget, F., Breton, V., & Evette, A. (2018). Using single-and multi-date UAV and satellite imagery to accurately monitor invasive knotweed species. *Remote Sensing*, *10*(10), 1662. https://doi.org/10.3390/rs10101662.

Martin, H., Monnet, J. M., De Boisvilliers, M., Chevalier, R., & Villar, M. (2020). Remote sensing of american maple in alluvial forests: a case study in an island complex of the Loire valley (France). *iForest-Biogeosciences and Forestry*, *13*(5), 409. https://doi.org/10.3832/ifor3237-013.

Maruthi Sridhar, B. B., Vincent, R. K., Clapham, W. B., Sritharan, S. I., Osterberg, J., Neale, C. M., & Watts, D. R. (2010). Mapping saltcedar (Tamarix ramosissima) and other riparian and agricultural vegetation in the Lower Colorado River region using multi-spectral Landsat TM imagery. *Geocarto International*, *25*(8), 649-662. https://doi.org/10.1080/10106049.2010.521857.

Matsuura, T., & Suzuki, W. (2013). Analysis of topography and vegetation distribution using a digital elevation model: case study of a snowy mountain basin in northeastern Japan. *Landscape and ecological engineering*, *9*, 143-155. https://doi.org/10.1007/s11355-012-0187-2.

Matzek, V., Lewis, D., O'Geen, A., Lennox, M., Hogan, S. D., Feirer, S. T., ... & Tate, K. W. (2020). Increases in soil and woody biomass carbon stocks as a result of rangeland riparian restoration. *Carbon balance and management*, *15*, 1-15. https://doi.org/10.1186/s13021-020-00150-7.

Matzek, V., Stella, J., & Ropion, P. (2018). Development of a carbon calculator tool for riparian forest restoration. *Applied vegetation science*, *21*(4), 584-594. https://doi.org/10.1111/avsc.12400.

Megonigal, J. P., Conner, W. H., Kroeger, S., & Sharitz, R. R. (1997). Aboveground production in southeastern floodplain forests: a test of the subsidy–

stress hypothesis. *Ecology*, *78*(2), 370-384. https://doi.org/10.1890/0012-9658(1997)078[0370:apisff]2.0.co;2.

Meinen, B. U., & Robinson, D. T. (2020). Mapping erosion and deposition in an agricultural landscape: Optimization of UAV image acquisition schemes for SfM-MVS. *Remote Sensing of Environment*, *239*, 111666. https://doi.org/10.1016/j.rse.2020.111666.

Mendez-Estrella, R., Romo-Leon, J. R., & Castellanos, A. E. (2017). Mapping changes in carbon storage and productivity services provided by riparian ecosystems of semi-arid environments in Northwestern Mexico. *ISPRS International Journal of Geo-Information*, *6*(10), 298. https://doi.org/10.3390/ijgi6100298.

Mertens, P. (2011). Diversité des milieux de développement pour les saules indigènes. *Forêt Wallonne*, 112: 21–28.

Miao, X., Patil, R., Heaton, J. S., & Tracy, R. C. (2011). Detection and classification of invasive saltcedar through high spatial resolution airborne hyperspectral imagery. *International Journal of Remote Sensing*, *32*(8), 2131-2150. https://doi.org/10.1080/01431161003674618.

Michałowska, M., & Rapiński, J. (2021). A review of tree species classification based on airborne LiDAR data and applied classifiers. *Remote Sensing*, *13*(3), 353. https://doi.org/10.3390/rs13030353.

Michez, A. (2016). Caractérisation multi-échelle des bandes riveraines des cours d'eau wallons par télédétection active et passive. *Unpublished doctoral thesis*. https://doi.org/10.13140/RG.2.2.17433.62569.

Michez, A., Huylenbroeck, L., Bolyn, C., Latte, N., Bauwens, S., & Lejeune, P. (2020). Can regional aerial images from orthophoto surveys produce high quality photogrammetric Canopy Height Model? A single tree approach in Western Europe. *International Journal of Applied Earth Observation and Geoinformation*, *92*, 102190. https://doi.org/10.1016/j.jag.2020.102190.

Michez, A., Piégay, H., Lisein, J., Claessens, H., & Lejeune, P. (2016a). Mapping of riparian invasive species with supervised classification of Unmanned Aerial System (UAS) imagery. *International Journal of Applied Earth Observation and Geoinformation*, *44*, 88-94. https://doi.org/10.1016/j.jag.2015.06.014.

Michez, A., Piégay, H., Lejeune, P., & Claessens, H. (2017). Multi-temporal monitoring of a regional riparian buffer network (> 12,000 km) with LiDAR and photogrammetric point clouds. *Journal of environmental management*, *202*, 424-436. https://doi.org/10.1016/j.jenvman.2017.02.034.

Michez, A., Piégay, H., Lisein, J., Claessens, H., & Lejeune, P. (2016b). Classification of riparian forest species and health condition using multi-temporal and hyperspatial imagery from unmanned aerial system. *Environmental monitoring and assessment*, *188*, 1-19. https://doi.org/10.1007/s10661-015-4996-2.

Mitchard, E. T., Saatchi, S. S., White, L. J., Abernethy, K. A., Jeffery, K. J., Lewis, S. L., ... & Meir, P. (2012). Mapping tropical forest biomass with radar and

spaceborne LiDAR in Lopé National Park, Gabon: overcoming problems of high biomass and persistent cloud. *Biogeosciences*, *9*(1), 179-191. https://doi.org/10.5194/bg-9-179-2012.

Morgan, J. L., Gergel, S. E., & Coops, N. C. (2010). Aerial photography: a rapidly evolving tool for ecological management. *BioScience*, *60*(1), 47-59. https://doi.org/10.1525/bio.2010.60.1.9.

Muhadi, N. A., Abdullah, A. F., Bejo, S. K., Mahadi, M. R., & Mijic, A. (2020). The use of LiDAR-derived DEM in flood applications: A review. *Remote Sensing*, *12*(14), 2308. https://doi.org/10.3390/rs12142308.

Muller, E., Decamps, H., & Dobson, M. K. (1993). Contribution of space remote sensing to river studies. *Freshwater Biology*, *29*(2), 301-312. https://doi.org/10.1111/j.1365-2427.1993.tb00766.x.

Munné, A., Prat, N., Solà, C., Bonada, N., & Rieradevall, M. J. A. C. M. (2003). A simple field method for assessing the ecological quality of riparian habitat in rivers and streams: QBR index. *Aquatic conservation: marine and freshwater ecosystems*, *13*(2), 147-163. https://doi.org/10.1002/aqc.529.

Nadal-Sala, D., Hartig, F., Gracia, C. A., & Sabaté, S. (2019). Global warming likely to enhance black locust (Robinia pseudoacacia L.) growth in a Mediterranean riparian forest. *Forest Ecology and Management*, *449*, 117448. https://doi.org/10.1016/j.foreco.2019.117448.

Næsset, E. (2004). Effects of different flying altitudes on biophysical stand properties estimated from canopy height and density measured with a small-footprint airborne scanning laser. *Remote Sensing of Environment*, *91*(2), 243-255. https://doi.org/10.1016/j.rse.2004.03.009.

Nagler, P. L., Brown, T., Hultine, K. R., Bean, D. W., Dennison, P. E., Murray, R. S., & Glenn, E. P. (2012). Regional scale impacts of Tamarix leaf beetles (Diorhabda carinulata) on the water availability of western US rivers as determined by multi-scale remote sensing methods. *Remote Sensing of Environment*, *118*, 227-240. https://doi.org/10.1016/j.rse.2011.11.011.

Nagler, P. L., Doody, T. M., Glenn, E. P., Jarchow, C. J., Barreto-Muñoz, A., & Didan, K. (2016). Wide-area estimates of evapotranspiration by red gum (Eucalyptus camaldulensis) and associated vegetation in the Murray–Darling River Basin, Australia. *Hydrological Processes*, *30*(9), 1376-1387. https://doi.org/10.1002/hyp.10734.

Naiman, R. J., & Decamps, H. (1997). The ecology of interfaces: riparian zones. *Annual review of Ecology and Systematics*, *28*(1), 621-658. https://doi.org/10.1146/annurev.ecolsys.28.1.621.

Naiman, R. J., Decamps, H., & McClain, M. E. (2005). *Riparia: ecology, conservation, and management of streamside communities*. Elsevier.

Naiman, R. J., Decamps, H., & Pollock, M. (1993). The role of riparian corridors in maintaining regional biodiversity. *Ecological applications*, *3*(2), 209-212. https://doi.org/10.2307/1941822.

Nardi, F., Annis, A., Di Baldassarre, G., Vivoni, E. R., & Grimaldi, S. (2019). GFPLAIN250m, a global high-resolution dataset of Earth's floodplains. *Scientific data*, *6*(1), 1-6. https://doi.org/10.1038/sdata.2018.309.

Nardi, L., & Rinaldi, M. (2015). Spatio-temporal patterns of channel changes in response to a major flood event: the case of the Magra River (central–northern Italy). *Earth Surface Processes and Landforms*, *40*(3), 326-339. https://doi.org/10.1002/esp.3636.

Navratil, O., Brekenfeld, N., Puijalon, S., Sabastia, M., Boyer, M., Pella, H., ... & Piola, F. (2021). Distribution of Asian knotweeds on the Rhône River basin, France: A multi-scale model of invasibility that combines biophysical and anthropogenic factors. *Science of the Total Environment*, *763*, 142995. https://doi.org/10.1016/j.scitotenv.2020.142995.

Narumalani, S., Mishra, D. R., Wilson, R., Reece, P., & Kohler, A. (2009). Detecting and mapping four invasive species along the floodplain of North Platte River, Nebraska. *Weed Technology*, *23*(1), 99-107. https://doi.org/10.1614/wt-08-007.1.

Nilsson, C., Brown, R. L., Jansson, R., & Merritt, D. M. (2010). The role of hydrochory in structuring riparian and wetland vegetation. *Biological Reviews*, *85*(4), 837-858. https://doi.org/10.1111/j.1469-185X.2010.00129.x.

Norbury, M., Phillips, H., Macdonald, N., Brown, D., Boothroyd, R., Wilson, C., ... & Shaw, D. (2021). Quantifying the hydrological implications of pre-and post-installation willowed engineered log jams in the Pennine Uplands, NW England. *Journal of Hydrology*, *603*, 126855. https://doi.org/10.1016/j.jhydrol.2021.126855.

Notebaert, B., Verstraeten, G., Govers, G., & Poesen, J. (2009). Qualitative and quantitative applications of LiDAR imagery in fluvial geomorphology. *Earth Surface Processes and Landforms*, *34*(2), 217-231. https://doi.org/10.1002/esp.1705.

Odum, E. P., Finn, J. T., & Franz, E. H. (1979). Perturbation theory and the subsidy-stress gradient. *Bioscience*, *29*(6), 349-352. https://doi.org/10.2307/1307690.

Oksanen, J., Blanchet, F. G., Friendly, M., Kindt, R., Legendre, P., Mcglinn, D., ... & Maintainer, H. W. (2020). Package "vegan" title community ecology package. R package, version 2.5-7.

Ose, K., Corpetti, T., & Demagistri, L. (2016). Multispectral satellite image processing. In *Optical remote sensing of land surface* (pp. 57-124). Elsevier. https://doi.org/10.1016/B978-1-78548-102-4.50002-8.

Pace, G., Gutiérrez-Cánovas, C., Henriques, R., Boeing, F., Cássio, F., & Pascoal, C. (2021). Remote sensing depicts riparian vegetation responses to water stress in a

humid Atlantic region. *Science of The Total Environment*, *772*, 145526. https://doi.org/10.1016/j.scitotenv.2021.145526.

Palmquist, E. C., Ralston, B. E., Merritt, D. M., & Shafroth, P. B. (2018). Landscape-scale processes influence riparian plant composition along a regulated river. *Journal of Arid Environments*, *148*, 54-64. https://doi.org/10.1016/j.jaridenv.2017.10.001.

Papanicolaou, A. T., Wilson, C. G., Tsakiris, A. G., Sutarto, T. E., Bertrand, F., Rinaldi, M., ... & Langendoen, E. (2017). Understanding mass fluvial erosion along a bank profile: using PEEP technology for quantifying retreat lengths and identifying event timing. *Earth Surface Processes and Landforms*, *42*(11), 1717-1732. https://doi.org/10.1002/esp.4138.

Parent, J. R., Volin, J. C., & Civco, D. L. (2015). A fully-automated approach to land cover mapping with airborne LiDAR and high resolution multispectral imagery in a forested suburban landscape. *ISPRS Journal of Photogrammetry and Remote Sensing*, *104*, 18-29. https://doi.org/10.1016/j.isprsjprs.2015.02.012.

Pautasso, M., Aas, G., Queloz, V., & Holdenrieder, O. (2013). European ash (Fraxinus excelsior) dieback–A conservation biology challenge. *Biological conservation*, *158*, 37-49. https://doi.org/10.1016/j.biocon.2012.08.026.

Peerbhay, K., Mutanga, O., Lottering, R., & Ismail, R. (2016). Mapping Solanum mauritianum plant invasions using WorldView-2 imagery and unsupervised random forests. *Remote Sensing of Environment*, *182*, 39-48. https://doi.org/10.1016/j.rse.2016.04.025.

Penning, E. (2018). Interactions between flow and vegetation: Translating knowledge from academic research to daily water management. In *E3S Web of Conferences* (Vol. 40, p. 01001). EDP Sciences. https://doi.org/10.1051/e3sconf/20184001001.

Petts, G. E., & Amoros, C. (1996). The fluvial hydrosystem. In *The Fluvial Hydrosystems* (pp. 1-12). Dordrecht: Springer Netherlands. https://doi.org/10.1007/978-94-009-1491-9_1.

Peuquet, D. J., & Marble, D. F. (Eds.). (1990). *Introductory readings in geographic information systems*. CRC Press.

Piégay, H., & Landon, N. (1997). Promoting ecological management of riparian forests on the Drôme River, France. *Aquatic conservation: marine and freshwater ecosystems*, *7*(4), 287-304. https://doi.org/10.1002/(SICI)1099-0755(199712)7:4<287::AID-AQC247>3.0.CO;2-S.

Piégay, H., Arnaud, F., Belletti, B., Bertrand, M., Bizzi, S., Carbonneau, P., ... & Slater, L. (2020). Remotely sensed rivers in the Anthropocene: State of the art and prospects. *Earth Surface Processes and Landforms*, *45*(1), 157-188. https://doi.org/10.1002/esp.4787.

Pierrot-Deseilligny, M., & Clery, I. (2011). Évolutions récentes en photogrammétrie et modélisation 3D par photo des milieux naturels. *Collection*

EDYTEM. Cahiers de géographie, *12*(1), 51-66. https://doi.org/10.3406/edyte.2011.1177.

Pisek, J., Diaz-Pines, E., Matteucci, G., Noe, S., & Rebmann, C. (2022). On the leaf inclination angle distribution as a plant trait for the most abundant broadleaf tree species in Europe. *Agricultural and Forest Meteorology*, *323*, 109030. https://doi.org/10.1016/j.agrformet.2022.109030.

Ploton, P., Mortier, F., Réjou-Méchain, M., Barbier, N., Picard, N., Rossi, V., ... & Pélissier, R. (2020). Spatial validation reveals poor predictive performance of large-scale ecological mapping models. *Nature communications*, *11*(1), 4540.

Poff, B., Koestner, K. A., Neary, D. G., & Henderson, V. (2011). Threats to riparian ecosystems in Western North America: an analysis of existing literature 1. *JAWRA Journal of the American Water Resources Association*, *47*(6), 1241-1254. https://doi.org/10.1111/j.1752-1688.2011.00571.x.

Politti, E., Bertoldi, W., Gurnell, A., & Henshaw, A. (2018). Feedbacks between the riparian Salicaceae and hydrogeomorphic processes: A quantitative review. *Earth-Science Reviews*, *176*, 147-165. https://doi.org/10.1016/j.earscirev.2017.07.018.

Pollock, M. M., & Beechie, T. J. (2014). Does riparian forest restoration thinning enhance biodiversity? The ecological importance of large wood. *JAWRA Journal of the American Water Resources Association*, 50(3), 543-559.

Pontius Jr, R. G., & Millones, M. (2011). Death to Kappa: birth of quantity disagreement and allocation disagreement for accuracy assessment. *International Journal of Remote Sensing*, *32*(15), 4407-4429. https://doi.org/10.1080/01431161.2011.552923.

Poole, G. C., & Berman, C. H. (2001). An ecological perspective on in-stream temperature: natural heat dynamics and mechanisms of human-causedthermal degradation. *Environmental management*, *27*, 787-802. https://doi.org/10.1007/s002670010188.

Racine, E. B., Coops, N. C., Bégin, J., & Myllymäki, M. (2021). Tree species, crown cover, and age as determinants of the vertical distribution of airborne LiDAR returns. *Trees*, *35*(6), 1845-1861. https://doi.org/10.1007/s00468-021-02155-2.

Radoux, J., Bourdouxhe, A., Coos, W., Dufrêne, M., & Defourny, P. (2019). Improving ecotope segmentation by combining topographic and spectral data. *Remote Sensing*, *11*(3), 354. https://doi.org/10.3390/rs11030354.

Radoux, J., Bourdouxhe, A., Coppée, T., De Vroey, M., Dufrêne, M., & Defourny, P. (2022). A consistent land cover map time series at 2 m spatial resolution—the LifeWatch 2006-2015-2018-2019 Dataset for Wallonia. *Data*, *8*(1), 13.

Rajão, R. (2013). Representations and discourses: the role of local accounts and remote sensing in the formulation of Amazonia's environmental policy. *Environmental Science & Policy*, *30*, 60-71. https://doi.org/10.1016/j.envsci.2012.07.019.

Rapinel, S., Mony, C., Lecoq, L., Clément, B., Thomas, A., & Hubert-Moy, L. (2019). Evaluation of Sentinel-2 time-series for mapping floodplain grassland plant communities. *Remote sensing of environment*, *223*, 115-129. https://doi.org/10.1016/j.rse.2019.01.018.

Richardson, D. M., Holmes, P. M., Esler, K. J., Galatowitsch, S. M., Stromberg, J. C., Kirkman, S. P., ... & Hobbs, R. J. (2007). Riparian vegetation: degradation, alien plant invasions, and restoration prospects. *Diversity and distributions*, *13*(1), 126-139. https://doi.org/10.1111/j.1366-9516.2006.00314.x.

Richardson, J. J., Moskal, L. M., & Kim, S. H. (2009). Modeling approaches to estimate effective leaf area index from aerial discrete-return LIDAR. *Agricultural and Forest Meteorology*, *149*(6-7), 1152-1160. https://doi.org/10.1016/j.agrformet.2009.02.007.

Richardson, J. J., Torgersen, C. E., & Moskal, L. M. (2019). Lidar-based approaches for estimating solar insolation in heavily forested streams. *Hydrology and Earth System Sciences*, *23*(7), 2813-2822. https://doi.org/10.5194/hess-23-2813-2019.

Richter, R., Reu, B., Wirth, C., Doktor, D., & Vohland, M. (2016). The use of airborne hyperspectral data for tree species classification in a species-rich Central European forest area. *International journal of applied earth observation and geoinformation*, *52*, 464-474. https://doi.org/10.1016/j.jag.2016.07.018.

Riedler, B., Pernkopf, L., Strasser, T., Lang, S., & Smith, G. (2015). A composite indicator for assessing habitat quality of riparian forests derived from Earth observation data. *International Journal of Applied Earth Observation and Geoinformation*, *37*, 114-123. https://doi.org/10.1016/j.jag.2014.09.006.

Riis, T., Kelly-Quinn, M., Aguiar, F. C., Manolaki, P., Bruno, D., Bejarano, M. D., ... & Dufour, S. (2020). Global overview of ecosystem services provided by riparian vegetation. *BioScience*, *70*(6), 501-514. https://doi.org/10.1093/biosci/biaa041.

Rijkswaterstaat (2014). Vegetatielegger : instrument voor veilige en natuurlijke uiterwaarden.

Rivaes, R. P., Rodriguez-Gonzalez, P. M., Ferreira, M. T., Pinheiro, A. N., Politti, E., Egger, G., ... & Frances, F. (2014). Modeling the evolution of riparian woodlands facing climate change in three European rivers with contrasting flow regimes. *PLoS One*, *9*(10), e110200. https://doi.org/10.1371/journal.pone.0110200.

Rodríguez-González, P. M., Stella, J. C., Campelo, F., Ferreira, M. T., & Albuquerque, A. (2010). Subsidy or stress? Tree structure and growth in wetland forests along a hydrological gradient in Southern Europe. *Forest Ecology and Management*, *259*(10), 2015-2025. https://doi.org/10.1016/j.foreco.2010.02.012.

Rodríguez-González, P. M., Abraham, E., Aguiar, F., Andreoli, A., Baležentienė, L., Berisha, N., ... & Dufour, S. (2022). Bringing the margin to the focus: 10 challenges for riparian vegetation science and management. Wiley Interdisciplinary Reviews: Water, 9(5), e1604. https://doi.org/10.1002/wat2.1604

Rommel, E., Giese, L., Fricke, K., Kathöfer, F., Heuner, M., Mölter, T., ... & Baschek, B. (2022). Very high-resolution imagery and machine learning for detailed mapping of riparian vegetation and substrate types. *Remote Sensing*, *14*(4), 954. https://doi.org/10.3390/rs14040954.

Rood, S. B., Braatne, J. H., & Goater, L. A. (2010). Responses of obligate versus facultative riparian shrubs following river damming. *River Research and Applications*, *26*(2), 102-117.

Roussel, J. R., Auty, D., Coops, N. C., Tompalski, P., Goodbody, T. R., Meador, A. S., ... & Achim, A. (2020). lidR: An R package for analysis of Airborne Laser Scanning (ALS) data. *Remote Sensing of Environment*, *251*, 112061. https://doi.org/https://doi.org/10.1016/j.rse.2020.112061.

Rubol, S., Ling, B., & Battiato, I. (2018). Universal scaling-law for flow resistance over canopies with complex morphology. *Scientific reports*, *8*(1), 4430. https://doi.org/10.1038/s41598-018-22346-1.

Rutherford, J. C., Meleason, M. A., & Davies-Colley, R. J. (2018). Modelling stream shade: 2. Predicting the effects of canopy shape and changes over time. *Ecological Engineering*, *120*, 487-496. https://doi.org/10.1016/j.ecoleng.2018.07.008.

Sá, C., & Grieco, J. (2016). Open data for science, policy, and the public good. *Review of Policy Research*, *33*(5), 526-543. https://doi.org/10.1111/ropr.12188.

Saccone, P., Girel, J., Pages, J. P., Brun, J. J., & Michalet, R. (2013). Ecological resistance to Acer negundo invasion in a European riparian forest: relative importance of environmental and biotic drivers. *Applied vegetation science*, *16*(2), 184-192. https://doi.org/10.1111/j.1654-109X.2012.01227.x.

Salinas, M. J., & Guirado, J. (2002). Riparian plant restoration in summer-dry riverbeds of southeastern Spain. *Restoration Ecology*, *10*(4), 695-702. https://doi.org/10.1046/j.1526-100X.2002.01050.x.

Sawtschuk, J., Delisle, M., Mesmin, X., & Bernez, I. (2014). How past riparian management practices can affect composition and structure of vegetation for headwater ecological restoration projects. *Acta botanica gallica*, 161(3), 309-320. https://doi.org/10.1080/12538078.2014.933362.

Sankey, T. T., Sankey, J. B., Horne, R., & Bedford, A. (2016). Remote sensing of tamarisk biomass, insect herbivory, and defoliation: novel methods in the Grand Canyon Region, Arizona. *Photogrammetric Engineering & Remote Sensing*, *82*(8), 645-652. https://doi.org/10.14358/pers.82.8.645.

Sanz-Ablanedo, E., Chandler, J. H., Rodríguez-Pérez, J. R., & Ordóñez, C. (2018). Accuracy of unmanned aerial vehicle (UAV) and SfM photogrammetry survey as a function of the number and location of ground control points used. *Remote Sensing*, *10*(10), 1606. https://doi.org/10.3390/rs10101606.

Schifman, L. A., Stella, J. C., Volk, T. A., & Teece, M. A. (2012). Carbon isotope variation in shrub willow (Salix spp.) ring-wood as an indicator of long-term water

status, growth and survival. *biomass and bioenergy*, *36*, 316-326. https://doi.org/10.1016/j.biombioe.2011.10.042.

Schilling, E. B., & Lockaby, B. G. (2006). Relationships between productivity and nutrient circulation within two contrasting southeastern US floodplain forests. *Wetlands*, *26*(1), 181-192. https://doi.org/10.1672/0277-5212(2006)26[181:rbpanc]2.0.co;2.

Schnitzler, A. (1995). Successional status of trees in gallery forest along the river Rhine. *Journal of Vegetation Science*, *6*(4), 479-486. https://doi.org/10.2307/3236346.

Scorpio, V., Crema, S., Marra, F., Righini, M., Ciccarese, G., Borga, M., ... & Comiti, F. (2018). Basin-scale analysis of the geomorphic effectiveness of flash floods: A study in the northern Apennines (Italy). *Science of the Total Environment*, *640*, 337-351. https://doi.org/10.1016/j.scitotenv.2018.05.252.

Scott, M. L., Nagler, P. L., Glenn, E. P., Valdes-Casillas, C., Erker, J. A., Reynolds, E. W., ... & Jones, C. L. (2009). Assessing the extent and diversity of riparian ecosystems in Sonora, Mexico. *Biodiversity and Conservation*, *18*, 247-269. https://doi.org/10.1007/s10531-008-9473-6.

Scown, M., Thoms, M. C., & De Jager, N. R. (2016). Measuring spatial patterns in floodplains: A step towards understanding the complexity of floodplain ecosystems. *River science: Research and management for the 21st century*, 103-131.

Seddon, J. A., Zerger, A., Doyle, S. J., & Briggs, S. V. (2007). The extent of dryland salinity in remnant woodland and forest within an agricultural landscape. *Australian Journal of Botany*, *55*(5), 533-540. https://doi.org/10.1071/bt06100.

Seena, S., Carvalho, F., Cássio, F., & Pascoal, C. (2017). Does the developmental stage and composition of riparian forest stand affect ecosystem functioning in streams? *Science of the Total Environment*, *609*, 1500-1511. https://doi.org/10.1016/j.scitotenv.2017.07.252.

Service Public de Wallonie (2008). Occupation et utilisation du sol en Wallonie – COSW 2007. https://geoportail.wallonie.be.

Service Public de Wallonie (2014). Nuage de points LIDAR 2013-2014. https://geoportail.wallonie.be.

Service Public de Wallonie (2015). Carte Numérique Des Sols de Wallonie. https://geoportail.wallonie.be.

Service Public de Wallonie (2018). Orthophotos 2018. https://geoportail.wallonie.be.

Service Public de Wallonie (2020). Réseau Hydrographique Wallon. https://geoportail.wallonie.be.

Service Public de Wallonie (2021). Cartographies Des Zones Inondables (En Vigueur) – Directive Inondation 2007/60/CE. https://geoportail.wallonie.be.

Service Public de Wallonie (2022). Projet de Programmes d'Actions sur les Rivières par une Approche Intégrée et Sectorisée 2022-2027. *Moniteur belge*, 12/10/2023, p. 85788.

Service Public de Wallonie (2023). Relevé des débits de la sation limnimétrique de Membre sur la Semois. Accessed October 9, 2023. https://hydrometrie.wallonie.be/.

Shendryk, I., Broich, M., Tulbure, M. G., McGrath, A., Keith, D., & Alexandrov, S. V. (2016). Mapping individual tree health using full-waveform airborne laser scans and imaging spectroscopy: A case study for a floodplain eucalypt forest. *Remote Sensing of Environment*, *187*, 202-217. https://doi.org/10.1016/j.rse.2016.10.014.

Shi, Y., Wang, T., Skidmore, A. K., & Heurich, M. (2018). Important LiDAR metrics for discriminating forest tree species in Central Europe. *ISPRS journal of photogrammetry and remote sensing*, *137*, 163-174. https://doi.org/10.1016/j.isprsjprs.2018.02.002.

Shields Jr, F. D., Coulton, K. G., & Nepf, H. (2017). Representation of vegetation in two-dimensional hydrodynamic models. *Journal of Hydraulic Engineering*, *143*(8), 02517002. https://doi.org/10.1061/(asce)hy.1943-7900.0001320.

Sims, N. C., & Colloff, M. J. (2012). Remote sensing of vegetation responses to flooding of a semi-arid floodplain: Implications for monitoring ecological effects of environmental flows. *Ecological Indicators*, *18*, 387-391. https://doi.org/10.1016/j.ecolind.2011.12.007.

Singer, M. B., Stella, J. C., Dufour, S., Piégay, H., Wilson, R. J., & Johnstone, L. (2013). Contrasting water-uptake and growth responses to drought in co-occurring riparian tree species. *Ecohydrology*, *6*(3), 402-412. https://doi.org/10.1002/eco.1283.

Solins, J. P., Thorne, J. H., & Cadenasso, M. L. (2018). Riparian canopy expansion in an urban landscape: Multiple drivers of vegetation change along headwater streams near Sacramento, California. *Landscape and Urban Planning*, *172*, 37-46. https://doi.org/10.1016/j.landurbplan.2017.12.005.

Sondheim, M., Gardels, K., & Buehler, K. (1999). GIS interoperability. *Geographical information systems*, *1*, 347-358.

Spiekermann, R., Betts, H., Dymond, J., & Basher, L. (2017). Volumetric measurement of river bank erosion from sequential historical aerial photography. *Geomorphology*, *296*, 193-208. https://doi.org/10.1016/j.geomorph.2017.08.047.

Staben, G. W., & Evans, K. G. (2008). Estimates of tree canopy loss as a result of Cyclone Monica, in the Magela Creek catchment northern Australia. *Austral Ecology*, *33*(4), 562-569. https://doi.org/10.1111/j.1442-9993.2008.01911.x.

Starkey, E.N. (2016). Upper Columbia Basin Network stream channel characteristics and riparian condition annual report 2013: John Day Fossil Beds National Monument (JODA). Natural Resource Data Series NPS/UCBN/NRDS—2015/808. National Park Service, Fort Collins, Colorado.

Steeb, N., Ruiz-Villanueva, V., Badoux, A., Rickli, C., Mini, A., Stoffel, M., & Rickenmann, D. (2023). Geospatial modelling of large-wood supply to rivers: a state-of-the-art model comparison in Swiss mountain river catchments. *Earth Surface Dynamics*, *11*(3), 487-509. https://doi.org/10.5194/esurf-11-487-2023.

Steiniger, S., & Hay, G. J. (2009). Free and open source geographic information tools for landscape ecology. *Ecological informatics*, *4*(4), 183-195. https://doi.org/10.1016/j.ecoinf.2009.07.004.

Stella, J. C., & Bendix, J. (2019). Multiple stressors in riparian ecosystems. In *Multiple stressors in river ecosystems* (pp. 81-110). Elsevier. https://doi.org/10.1016/b978-0-12-811713-2.00005-4.

Stöcker, C., Bennett, R., Nex, F., Gerke, M., & Zevenbergen, J. (2017). Review of the current state of UAV regulations. *Remote sensing*, *9*(5), 459. https://doi.org/10.3390/rs9050459.

Stoffel, M., Corona, C., Ballesteros-Cánovas, J. A., & Bodoque, J. M. (2013). Dating and quantification of erosion processes based on exposed roots. *Earth-Science Reviews*, *123*, 18-34. https://doi.org/10.1016/j.earscirev.2013.04.002.

Stohlgren, T. J., Bull, K. A., Otsuki, Y., Villa, C. A., & Lee, M. (1998). Riparian zones as havens for exotic plant species in the central grasslands. *Plant Ecology*, *138*, 113-125. https://doi.org/10.1023/A:1009764909413.

Straatsma, M. W., & Baptist, M. J. (2008). Floodplain roughness parameterization using airborne laser scanning and spectral remote sensing. *Remote Sensing of Environment*, *112*(3), 1062-1080. https://doi.org/10.1016/j.rse.2007.07.012.

Straatsma, M. W., & Kleinhans, M. G. (2018). Flood hazard reduction from automatically applied landscaping measures in RiverScape, a Python package coupled to a two-dimensional flow model. *Environmental Modelling & Software*, *101*, 102-116. https://doi.org/10.1016/j.envsoft.2017.12.010.

Straatsma, M. W., Fliervoet, J. M., Kabout, J. A., Baart, F., & Kleinhans, M. G. (2019). Towards multi-objective optimization of large-scale fluvial landscaping measures. *Natural Hazards and Earth System Sciences*, *19*(6), 1167-1187. https://doi.org/10.5194/nhess-19-1167-2019.

Strahler, A. H., Woodcock, C. E., & Smith, J. A. (1986). On the nature of models in remote sensing. *Remote sensing of environment*, *20*(2), 121-139. https://doi.org/10.1016/0034-4257(86)90018-0.

Strasser, T., & Lang, S. (2015). Object-based class modelling for multi-scale riparian forest habitat mapping. *International Journal of Applied Earth Observation and Geoinformation*, *37*, 29-37. https://doi.org/10.1016/j.jag.2014.10.002.

Strasser, T., Lang, S., Riedler, B., Pernkopf, L., & Paccagnel, K. (2013). Multiscale object feature library for habitat quality monitoring in riparian forests. *IEEE geoscience and remote sensing letters*, *11*(2), 559-563. https://doi.org/10.1109/LGRS.2013.2278335.

Strnadová, V., Černý, K., Holub, V., & Gregorová, B. (2010). The effects of flooding and Phytophthora alni infection on black alder. *Journal of Forest Science*, *56*(1), 41-46. https://doi.org/10.17221/67/2009-jfs.

Suchenwirth, L., Stümer, W., Schmidt, T., Förster, M., & Kleinschmit, B. (2014). Large-scale mapping of carbon stocks in riparian forests with self-organizing maps and the k-nearest-neighbor algorithm. *Forests*, *5*(7), 1635-1652. https://doi.org/10.3390/f5071635.

Sun, M., Cui, L., Park, J., García, M., Zhou, Y., Silva, C. A., ... & Zhao, K. (2022). Evaluation of NASA's GEDI Lidar Observations for Estimating Biomass in Temperate and Tropical Forests. *Forests*, *13*(10), 1686. https://doi.org/10.3390/f13101686.

Sutfin, N. A., Wohl, E. E., & Dwire, K. A. (2016). Banking carbon: a review of organic carbon storage and physical factors influencing retention in floodplains and riparian ecosystems. *Earth Surface Processes and Landforms*, *41*(1), 38-60. https://doi.org/10.1002/esp.3857.

Szabó, Z., Tóth, C. A., Tomor, T., & Szabó, S. (2017). Airborne LiDAR point cloud in mapping of fluvial forms: A case study of a Hungarian floodplain. *GIScience & Remote Sensing*, *54*(6), 862-880. https://doi.org/10.1080/15481603.2017.1339987.

Tabacchi, E., Correll, D. L., Hauer, R., Pinay, G., Planty-Tabacchi, A. M., & Wissmar, R. C. (1998). Development, maintenance and role of riparian vegetation in the river landscape. *Freshwater biology*, *40*(3), 497-516. https://doi.org/10.1046/j.1365-2427.1998.00381.x.

Thévenet, A, Citterio, A. and Haury, J. (2003). Ripisylves et Populations Piscicoles. In *Les forêts riveraines des cours d'eau : Écologie, fonctions et gestion*, IDF, 170–86.

Thomas, L. K., Mosner, E., & Leyer, I. (2015). River dynamics and invasion: distribution patterns of native and invasive woody vegetation at the Río Negro, Argentina. *Riparian Ecology and Conservation*, *2*(1), 45-57. https://doi.org/10.1515/remc-2015-0001.

Tillack, A., Clasen, A., Kleinschmit, B., & Förster, M. (2014). Estimation of the seasonal leaf area index in an alluvial forest using high-resolution satellite-based vegetation indices. *Remote Sensing of Environment*, *141*, 52-63. https://doi.org/10.1016/j.rse.2013.10.018.

Tockner, K., & Stanford, J. A. (2002). Riverine flood plains: present state and future trends. *Environmental conservation*, *29*(3), 308-330.

Tompalski, P., Coops, N. C., White, J. C., Wulder, M. A., & Yuill, A. (2017). Characterizing streams and riparian areas with airborne laser scanning data. *Remote sensing of environment*, *192*, 73-86. https://doi.org/10.1016/j.rse.2017.01.038.

Tomsett, C., & Leyland, J. (2019). Remote sensing of river corridors: A review of current trends and future directions. *River Research and Applications*, *35*(7), 779-803. https://doi.org/10.1002/rra.3479.

Tonkin, J. D., Merritt, D. M., Olden, J. D., Reynolds, L. V., & Lytle, D. A. (2018). Flow regime alteration degrades ecological networks in riparian ecosystems. *Nature ecology & evolution*, *2*(1), 86-93. https://doi.org/10.1038/s41559-017-0379-0.

Tormos, T., Kosuth, P., Durrieu, S., Villeneuve, B., & Wasson, J. G. (2011). Improving the quantification of land cover pressure on stream ecological status at the riparian scale using High Spatial Resolution Imagery. *Physics and Chemistry of the Earth, Parts A/B/C*, *36*(12), 549-559. https://doi.org/10.1016/j.pce.2010.07.012.

Toth, C., & Jóźków, G. (2016). Remote sensing platforms and sensors: A survey. *ISPRS Journal of Photogrammetry and Remote Sensing*, *115*, 22-36. https://doi.org/10.1016/j.isprsjprs.2015.10.004.

Tournadre, V.; Pierrot-Deseilligny, M.; Faure, P.H. UAV linear photogrammetry. Int. Arch. Photogramm. Remote Sens. Spat. Inf. Sci. ISPRS Arch. 2015, 40, 327–333. https://doi.org/10.5194/isprsarchives-XL-3-W3-327-2015.

Townsend, P. A. (2002). Relationships between forest structure and the detection of flood inundation in forested wetlands using C-band SAR. *International Journal of Remote Sensing*, *23*(3), 443-460. https://doi.org/10.1080/01431160010014738.

Townsend, P. A., & Walsh, S. J. (2001). Remote sensing of forested wetlands: application of multitemporal and multispectral satellite imagery to determine plant community composition and structure in southeastern USA. *Plant Ecology*, *157*, 129-149. https://doi.org/10.1023/a:1013999513172.

Tufekcioglu, A., Raich, J. W., Isenhart, T. M., & Schultz, R. C. (2003). Biomass, carbon and nitrogen dynamics of multi-species riparian buffers within an agricultural watershed in Iowa, USA. *Agroforestry systems*, *57*, 187-198. https://doi.org/10.1023/a:1024898615284.

Turner, M. D., & Taylor, P. J. (2003). Critical reflections on the use of remote sensing and GIS technologies in human ecological research. *Human Ecology*, *31*(2), 177-182. https://doi.org/10.1023/a:1023958712140.

Turner, W., Rondinini, C., Pettorelli, N., Mora, B., Leidner, A. K., Szantoi, Z., ... & Woodcock, C. (2015). Free and open-access satellite data are key to biodiversity conservation. *Biological Conservation*, *182*, 173-176. https://doi.org/10.1016/j.biocon.2014.11.048.

Urbanič, G., Politti, E., Rodríguez-González, P. M., Payne, R., Schook, D., Alves, M. H., ... & Dufour, S. (2022). Riparian Zones—From Policy Neglected to Policy Integrated. *Frontiers in Environmental Science*, *10*, 868527. https://doi.org/10.3389/fenvs.2022.868527.

van Coller, A. L., Rogers, K. H., & Heritage, G. L. (2000). Riparian vegetation-environment relationships: complimentarity of gradients versus patch hierarchy approaches. *Journal of Vegetation Science*, *11*(3), 337-350.

Van Looy, K., & Piffady, J. (2017). Metapopulation modelling of riparian tree species persistence in river networks under climate change. *Journal of Environmental Management*, 202, 437-446. https://doi.org/10.1016/j.jenvman.2016.11.019.

Vande Kamp, K. V., Rigge, M., Troelstrup Jr, N. H., Smart, A. J., & Wylie, B. (2013). Detecting channel riparian vegetation response to best-management-practices implementation in ephemeral streams with the use of spot high-resolution visible imagery. *Rangeland Ecology & Management*, *66*(1), 63-70. https://doi.org/10.2111/rem-d-11-00153.1.

Vanden Borre, J., Paelinckx, D., Mücher, C. A., Kooistra, L., Haest, B., De Blust, G., & Schmidt, A. M. (2011). Integrating remote sensing in Natura 2000 habitat monitoring: prospects on the way forward. *Journal for Nature Conservation*, *19*(2): 116–25. https://doi.org/10.1016/j.jnc.2010.07.003.

Vandendaele, B. (2022). Amélioration de l'inventaire forestier à l'aide de nuages de points à haute densité acquis par drone lidar et lidar mobile: étude de cas en forêts feuillues tempérées. *Unpublished doctoral thesis*.

Varga, K., Dévai, G., & Tóthmérész, B. (2013). Land use history of a floodplain area during the last 200 years in the Upper-Tisza region (Hungary). *Regional Environmental Change*, *13*, 1109-1118. https://doi.org/10.1007/s10113-013-0424-8.

Vaz, A. S., Alcaraz-Segura, D., Campos, J. C., Vicente, J. R., & Honrado, J. P. (2018). Managing plant invasions through the lens of remote sensing: A review of progress and the way forward. *Science of the Total Environment*, *642*, 1328-1339. https://doi.org/10.1016/j.scitotenv.2018.06.134.

Verry, E. S., Dolloff, C. A., & Manning, M. E. (2004). Riparian ecotone: a functional definition and delineation for resource assessment. *Water, air and soil pollution: focus*, *4*, 67-94. https://doi.org/10.1023/b:wafo.0000012825.77300.08.

Vivier, A., Breton, L., Grivel, S., Melun, G., Piégay, H., Demarchi, L., …, & Dupont, P. (2018). Actes de la journée technique "Avancées, apports et perspectives de la télédétection pour la caractérisation physique des corridors fluviaux."

Vollmer, D., Prescott, M. F., Padawangi, R., Girot, C., & Grêt-Regamey, A. (2015). Understanding the value of urban riparian corridors: considerations in planning for cultural services along an Indonesian river. *Landscape and Urban Planning*, *138*, 144-154. https://doi.org/10.1016/j.landurbplan.2015.02.011.

Wagner-Lücker, I., Lanz, E., Förster, M., Janauer, G. A., & Reiter, K. (2013). Knowledge-based framework for delineation and classification of ephemeral plant communities in riverine landscapes to support EC Habitat Directive assessment. *Ecological informatics*, *14*, 44-47. https://doi.org/10.1016/j.ecoinf.2012.11.003.

Wallace, C. S., Villarreal, M. L., & van Riper III, C. (2013). Influence of monsoon-related riparian phenology on yellow-billed cuckoo habitat selection in Arizona. *Journal of Biogeography*, *40*(11), 2094-2107. https://doi.org/10.1111/jbi.12167.

Wan, Y., Wan, C., & Hedgepeth, M. (2015). Elucidating multidecadal saltwater intrusion and vegetation dynamics in a coastal floodplain with artificial neural networks and aerial photography. *Ecohydrology*, *8*(2), 309-324. https://doi.org/10.1002/eco.1509.

Wang, L., Silván-Cárdenas, J. L., Yang, J., & Frazier, A. E. (2013). Invasive saltcedar (Tamarisk spp.) distribution mapping using multiresolution remote sensing imagery. *The Professional Geographer*, *65*(1), 1-15. https://doi.org/10.1080/00330124.2012.679440.

Wasser, L., Chasmer, L., Day, R., & Taylor, A. (2015). Quantifying land use effects on forested riparian buffer vegetation structure using LiDAR data. *Ecosphere*, *6*(1), 1-17. https://doi.org/10.1890/es14-00204.1.

Wawrzyniak, V., Allemand, P., Bailly, S., Lejot, J., & Piégay, H. (2017). Coupling LiDAR and thermal imagery to model the effects of riparian vegetation shade and groundwater inputs on summer river temperature. *Science of the Total Environment*, *592*, 616-626. https://doi.org/10.1016/j.scitotenv.2017.03.019.

Weissteiner, C. J., Ickerott, M., Ott, H., Probeck, M., Ramminger, G., Clerici, N., ... & De Sousa, A. M. R. (2016). Europe's green arteries—A continental dataset of riparian zones. *Remote Sensing*, *8*(11), 925. https://doi.org/10.3390/rs8110925.

White, J. C., Coops, N. C., Wulder, M. A., Vastaranta, M., Hilker, T., & Tompalski, P. (2016). Remote sensing technologies for enhancing forest inventories: A review. *Canadian Journal of Remote Sensing*, *42*(5), 619-641. https://doi.org/10.1080/07038992.2016.1207484.

Willaarts B., Ballesteros Olza, M., Hernandez-Mora-Nuria. 2014. Ten years of the Water Framework Directive in Spain: An overview of the ecological and chemical status of surface water bodies. In *Integrated Water Resources Management in the 21st Century: Revisiting the paradigm*, CRC Press, 99–120.

Wohl, E. (2017). Bridging the gaps: An overview of wood across time and space in diverse rivers. *Geomorphology*, *279*, 3-26. https://doi.org/10.1016/j.geomorph.2016.04.014.

Wohl, E., Bledsoe, B. P., Fausch, K. D., Kramer, N., Bestgen, K. R., & Gooseff, M. N. (2016). Management of large wood in streams: an overview and proposed framework for hazard evaluation. *JAWRA Journal of the American Water Resources Association*, *52*(2), 315-335. https://doi.org/10.1111/1752-1688.12388.

Wohl, E., Dwire, K., Sutfin, N., Polvi, L., & Bazan, R. (2012). Mechanisms of carbon storage in mountainous headwater rivers. *Nature communications*, *3*(1), 1263. https://doi.org/10.1038/ncomms2274.

Wondzell, S. M., Diabat, M., & Haggerty, R. (2019). What matters most: are future stream temperatures more sensitive to changing air temperatures, discharge, or riparian vegetation?. *JAWRA Journal of the American Water Resources Association*, *55*(1), 116-132. https://doi.org/10.1111/1752-1688.12707.

Woodget, A. S., Carbonneau, P. E., Visser, F., & Maddock, I. P. (2015). Quantifying submerged fluvial topography using hyperspatial resolution UAS imagery and structure from motion photogrammetry. *Earth surface processes and landforms*, *40*(1), 47-64. https://doi.org/10.1002/esp.3613.

Woodget, A. S., Dietrich, J. T., & Wilson, R. T. (2019). Quantifying below-water fluvial geomorphic change: The implications of refraction correction, water surface elevations, and spatially variable error. *Remote Sensing*, *11*(20), 2415. https://doi.org/10.3390/rs11202415.

Wright, M. N., & Ziegler, A. (2017). ranger: A Fast Implementation of Random Forests for High Dimensional Data in C++ and R. *Journal of Statistical Software*, *77*(1), 1–17. https://doi.org/10.18637/jss.v077.i01

Wulder, M. A., White, J. C., Nelson, R. F., Næsset, E., Ørka, H. O., Coops, N. C., ... & Gobakken, T. (2012). Lidar sampling for large-area forest characterization: A review. *Remote sensing of environment*, *121*, 196-209. https://doi.org/10.1016/j.rse.2012.02.001.

Yang, X. (2007). Integrated use of remote sensing and geographic information systems in riparian vegetation delineation and mapping. *International journal of remote sensing*, *28*(2), 353-370. https://doi.org/10.1080/01431160600726763.

Yousefi, S., Mirzaee, S., Keesstra, S., Surian, N., Pourghasemi, H. R., Zakizadeh, H. R., & Tabibian, S. (2018). Effects of an extreme flood on river morphology (case study: Karoon River, Iran). *Geomorphology*, *304*, 30-39. https://doi.org/10.1016/j.geomorph.2017.12.034.

Yu, X., Litkey, P., Hyyppä, J., Holopainen, M., & Vastaranta, M. (2014). Assessment of low density full-waveform airborne laser scanning for individual tree detection and tree species classification. *Forests*, *5*(5), 1011-1031. https://doi.org/10.3390/f5051011.

Yu, X., Hyyppä, J., Litkey, P., Kaartinen, H., Vastaranta, M., & Holopainen, M. (2017). Single-sensor solution to tree species classification using multispectral airborne laser scanning. Remote Sensing, 9(2), 108. https://doi.org/10.3390/rs9020108.

Zahidi, I., Yusuf, B., Cope, M., Ahmed Mohamed, T., & Mohd Shafri, H. Z. (2018). Effects of depth-varying vegetation roughness in two-dimensional hydrodynamic modelling. *International Journal of River Basin Management*, *16*(4), 413-426. https://doi.org/10.1080/15715124.2017.1394313.

Zaimes, G. N., Gounaridis, D., & Symenonakis, E. (2019). Assessing the impact of dams on riparian and deltaic vegetation using remotely-sensed vegetation indices and Random Forests modelling. *Ecological indicators*, *103*, 630-641. https://doi.org/10.1016/j.ecolind.2019.04.047.

Zaimes, G. N., Schultz, R. C., & Isenhart, T. M. (2004). Stream bank erosion adjacent to riparian forest buffers, row-crop fields, and continuously-grazed pastures along Bear Creek in central Iowa. *Journal of Soil and Water Conservation*, *59*(1), 19-27.

Zanne, A., Lopez-Gonzalez, G., Coomes, D., Ilic, J., Jansen, S., Lewis, S.,…, & Chave, J. (2009). Data from: Towards a worldwide wood economics spectrum. *Dryad Digit Repos*. https://doi.org/10.5061/dryad.234.

Zhao, K., Suarez, J. C., Garcia, M., Hu, T., Wang, C., & Londo, A. (2018). Utility of multitemporal lidar for forest and carbon monitoring: Tree growth, biomass dynamics, and carbon flux. *Remote Sensing of Environment*, *204*, 883-897. https://doi.org/10.1016/j.rse.2017.09.007.

Zianis, D., Muukkonen, P., Mäkipää, R., Mencuccini, M. (2005). Biomass and Stem Volume Equations for Tree Species in Europe. *Finnish Society of Forest Science*.

Zogaris, S., Markogianni, V., Özeren, S. C., & Dimitriou, E. (2015). Assessment of Riparian zone and river Island conditions in a Trans-boundary greenbelt: The Evros/Meriç river (Greece-Turkey). *Fresenius Environmental Bulletin*, *24*(1), 269-277.

Zolkos, S. G., Goetz, S. J., & Dubayah, R. (2013). A meta-analysis of terrestrial aboveground biomass estimation using lidar remote sensing. *Remote sensing of environment*, *128*, 289-298. https://doi.org/10.1016/j.rse.2012.10.017.

Appendix 1: Methods and results for mapping specific composition and biomass on the Ton watershed (section 6.2.1)

Methods

For species mapping, five species groups were considered: willow, alder, poplar, conifer and other deciduous. The Random Forest model was trained on a dataset comprising 62 trees from each group. The proportions of the surface area occupied by the crowns of each group were aggregated at the scale of stretches 300 m long and 12 m wide on either side of the watercourse.

Biomass was estimated using the first model calibrated in Chapter 3 of the thesis, applied to the segmented LiDAR tree crowns of 2021. The model is based solely on crown dimension and 90th height quantile, variables considered to have little dependence on the characteristics of the LiDAR used. The biomasses calculated in 2014 and 2021 were compared at the scale of 300-meter stretches as follows:

$$\Delta AGB\ (\%) = \frac{AGB2021 - AGB2014}{AGB\ 2021 + AGB\ 2014} * 2 * 100\%$$

Results

The internal accuracy of the species mapping model at the tree crown scale is 81%, which is very close to that obtained for a four-class model in chapter 4 of this thesis (Table 22). Given the larger scale of aggregation (around 7000 m² compared with 900 m² for the study presented in Chapter 4), it is expected that the accuracy on 300 m units will be at least equal to that obtained in Chapter 4.

Table 22: Confusion matrix for species classification at tree level

	Alder	Other deciduous	Poplar	Conifer	Willows	User's accuracy (%)
Alder	50	4	0	2	6	80,6
Other deciduous	8	42	2	2	7	68,9
Poplar	1	3	54	0	3	88,5
Conifer	0	0	1	61	0	98,4
Willows	10	8	0	0	42	70,0
Producer's accuracy (%)	72,5	73,7	94,7	93,8	72,4	81,3

Biomass estimates have not been validated. Nevertheless, given that the method employed, the geographical context and the aggregation area are comparable to the

study presented in chapter 3 of this thesis, a similar accuracy can be expected, i.e. of the order of 27% mean relative error for the 300 m long stretches.

The maps describing the riparian vegetation at basin scale are shown in Figure 66 and Figure 67. In terms of specific composition, the willow group is the most represented (Figure 66). Upstream of the watershed (Chavratte, Vire and Ton upstream of its confluence with the Vire), the riparian vegetation is composed of willows, alders and other deciduous trees in equal proportions. In rivers downstream of the basin (Ton downstream of its confluence with the Vire and Chiers rivers), willow becomes dominant, often representing over 50% of the canopy. Biomass distribution is largely influenced by the urbanization of valley bottoms, with lower biomass in the Signeulx, Lamorteau and Virton crossings (Figure 67). Biomass is also low downstream of Lamorteau.

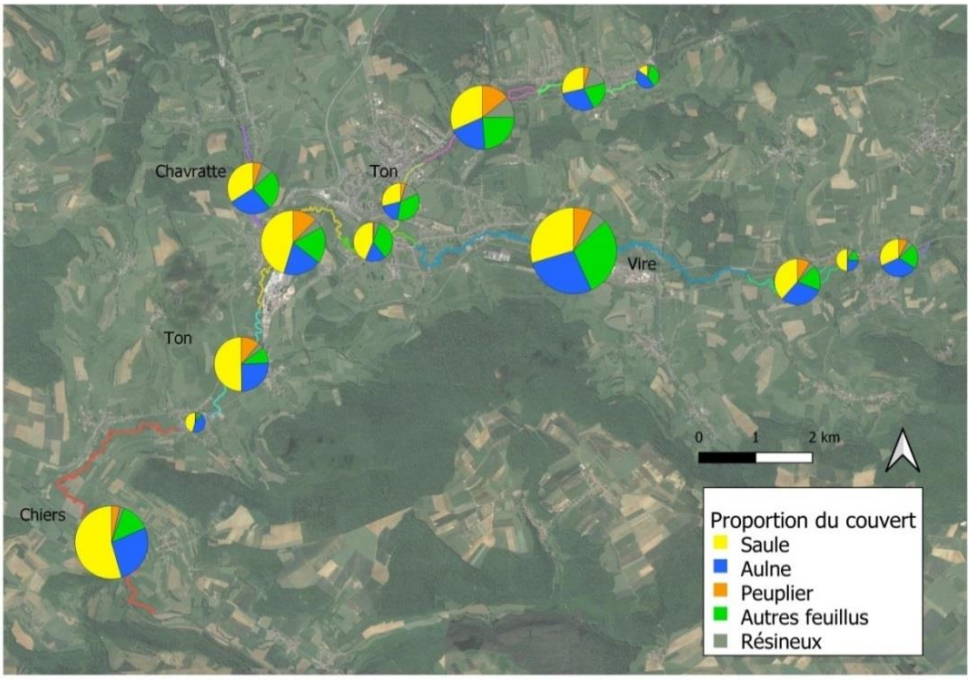

Figure 66: Specific composition map at management sector scale. The diameter of the pie charts is proportional to the length of the sector considered.

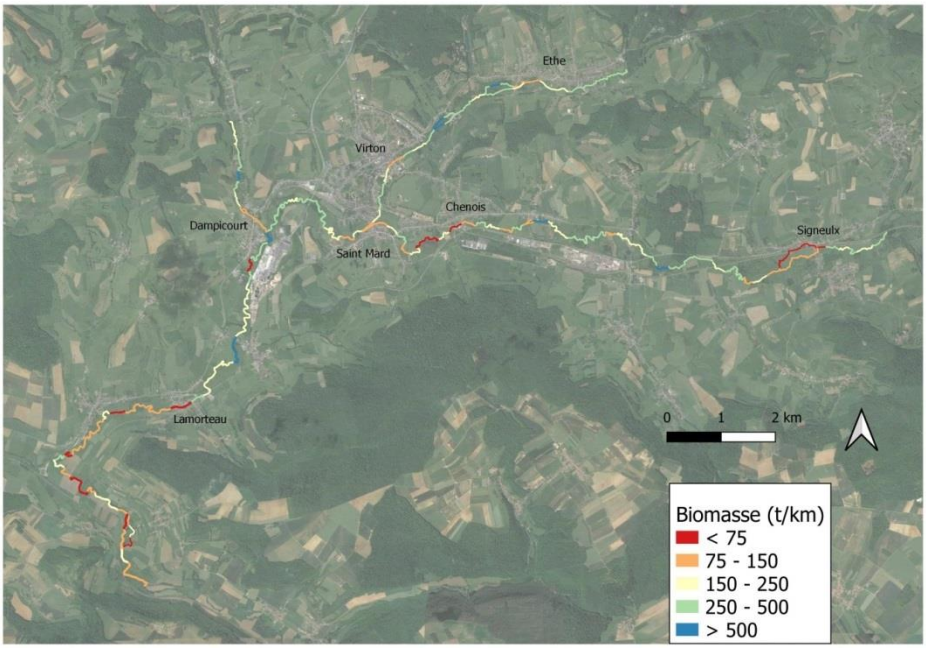

Figure 67: Biomass map at the scale of 300-metre-long stretches.

Finally, the relative difference between biomass calculated in 2021 and 2014 is shown in Figure 68. Overall, the riparian forest is capitalizing, with an average increase in biomass of 15%. The areas where biomass has decreased correspond for the most part to areas where vegetation maintenance work was carried out during the period under consideration, essentially on the Vire river, where flooding issues are concentrated.

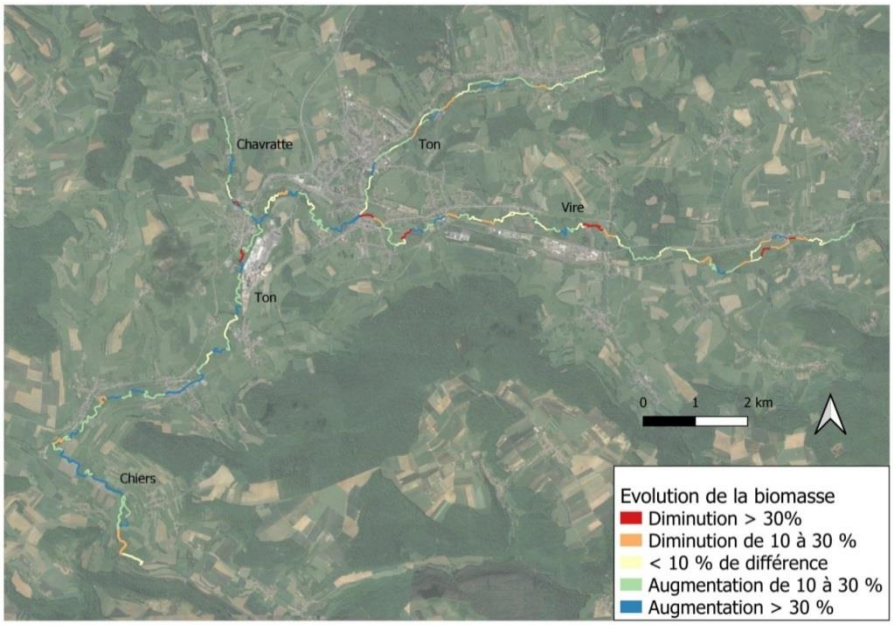

Figure 68: Map of biomass evolution at the scale of 300-meter-long stretches, between 2014 and 2021